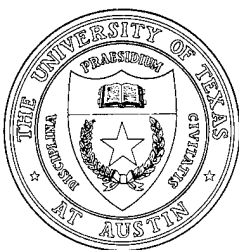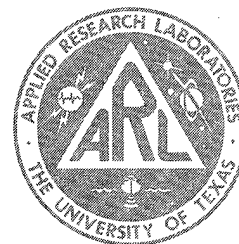# Linear and Nonlinear Acoustic Bloch Wave Propagation in Periodic Waveguides
Technical Report under Grant N00014-89-J-1109

Charles E. Bradley

Applied Research Laboratories
The University of Texas at Austin
P. O. Box 8029   Austin, TX 78713-8029

26 May 1994

Technical Report

Approved for public release: Distribution unlimited.

DTIC QUALITY INSPECTED 4

19970319 209

UNCLASSIFIED

REPORT DOCUMENTATION PAGE	Form Approved OMB No. 0704-0188

Public reporting burden for this collection of information is estimated to average 1 hour per response, including the time for reviewing instructions, searching existing data sources, gathering and maintaining the data needed, and completing and reviewing the collection of information. Send comments regarding this burden estimate or any other aspect of this collection of information, including suggestions for reducing this burden, to Washington Headquarters Services, Directorate for Information Operations and Reports, 1215 Jefferson Davis Highway, Suite 1204, Arlington, VA 22202-4302, and to the Office of Management and Budget, Paperwork Reduction Project (0704-0188), Washington, DC 20503.

1. AGENCY USE ONLY (Leave blank)	2. REPORT DATE 26 May 1994	3. REPORT TYPE AND DATES COVERED technical

4. TITLE AND SUBTITLE	5. FUNDING NUMBERS
Linear and Nonlinear Acoustic Bloch Wave Propagation in Periodic Waveguides, Technical Report under Grant N00014-89-J-1109	PE 61153N G N00014-89-J-1109 TA 3126317

6. AUTHOR(S)

Charles E. Bradley

7. PERFORMING ORGANIZATION NAMES(S) AND ADDRESS(ES)	8. PERFORMING ORGANIZATION REPORT NUMBER
Applied Research Laboratories The University of Texas at Austin P.O. Box 8029 Austin, Texas 78713-8029	ARL-TR-94-10

9. SPONSORING/MONITORING AGENCY NAME(S) AND ADDRESS(ES)	10. SPONSORING/MONITORING AGENCY REPORT NUMBER
Office of Naval Research ONR 331 800 North Quincy Street Arlington, VA 22217-5660	

11. SUPPLEMENTARY NOTES

Ph.D. Dissertation of Charles E. Bradley

12a. DISTRIBUTION/AVAILABILITY STATEMENT	12b. DISTRIBUTION CODE
Approved for public release: Distribution unlimited.	

13. ABSTRACT (Maximum 200 words)

Propagation of acoustic waves (linear and nonlinear, time-harmonic and pulsed) in a broad class of periodically nonuniform wave guides is investigated theoretically and experimentally. It is shown that the linear, time-harmonic solution wave functions are Bloch wave functions. Expressions for parameters characterizing Bloch waves (such as the Bloch wave number) are derived and the features of their band-structure determined. Propagation of linear Bloch wave pulses is investigated using the standard dispersion integral. Several new dispersive pulse solutions exhibiting highly unusual behavior (such as acceleration, carrier frequency shifting, and near-infinite group velocity) are found. In the case of nonlinear time-harmonic Bloch wave propagation, a forward traveling fundamental Bloch wave generates both forward and backward traveling second harmonic Bloch waves, the amplitudes of which oscillate with distance. An effective coefficient of nonlinearity for Bloch waves is identified and found to be, dependent upon frequency, either larger or smaller than that of the host fluid. The dispersion associated with Bloch waves provides an effective means of suppressing the waveform distorting effect of nonlinearity. These findings are verified with measurements made in an air-filled, rectangular aluminum duct loaded with a periodic array of scattering side branches.

14. SUBJECT TERMS		15. NUMBER OF PAGES 285
acoustics group velocity Bloch waves finite-amplitude dispersion waveguides		16. PRICE CODE

17. SECURITY CLASSIFICATION OF REPORT UNCLASSIFIED	18. SECURITY CLASSIFICATION OF THIS PAGE UNCLASSIFIED	19. SECURITY CLASSIFICATION OF ABSTRACT UNCLASSIFIED	20. LIMITATION OF ABSTRACT

NSN 7540-01-280-5500

Standard Form 298 (Rev. 2-89)
Prescribed by ANSI Std. 239-18
298-102

This page intentionally left blank.

Table of Contents

List of Figures

xiii

Preface

This report is adapted from the doctoral dissertation of the same title by Charles E. Bradley. Mr. Bradley began his graduate studies in the Department of Mechanical Engineering in September 1987. The research for his master's degree, which was completed in December 1990, was an introductory study of Bloch wave propagation in a periodic waveguide [Technical Report ARL-TR-91-19, Applied Research Laboratories, The University of Texas at Austin, 24 July 1991 (ADA 244068)]. The work reported here grew out of the earlier investigation.

Mr. Bradley's current address is Berkeley Actuator and Sensor Center, Department of Electrical Engineering, 497 Cory Hall, University of California, Berkeley, California 94720.

David T. Blackstock
Supervisor

This page intentionally left blank.

Chapter 1

Introduction

Bloch waves, the very unusual wave-like disturbances that occur in periodic media, have been studied extensively in the context of nearly every species of wave. The catalog of work spans the disciplines of acoustics, radio, microwave and optical frequency electromagnetics, solid mechanics, quantum mechanics, and others. The primary reason for the interdisciplinary interest in Bloch waves is the unusual dispersion that is characteristic of Bloch waves. With the introduction of some sort of periodic structure into a wave medium, the frequency axis becomes divided into an alternating series of frequency bands called passbands and stopbands. Passband frequency Bloch waves propagate freely and stopband frequency Bloch waves are exponentially attenuated, much like an evanescent wave. The so-called "band structure" of the Bloch wave dispersion relation is the property of Bloch waves that is most often exploited in applications.

The moniker "Bloch wave" came about following the seminal doctoral work of Nobel laureate Felix Bloch in 1928. It was he who showed that the quantum mechanical matter wave solutions of the Schrödinger equation that governs the dynamics of electrons in a crystal lattice are of a particular form, that which today is known as a Bloch wave function. This work forms the basis of the quantum mechanical "band theory" of electrical conductivity and semi-conductivity in solids (e.g., Kittel, 1986). If the frequency of the matter waves that represent the conduction electrons lie in a passband, then the electrons

"propagate" and the material is a conductor.[1] If the electron frequency lies in a stopband, the electrons are immobile and the material is an insulator. If the frequency lies in a stopband near the edge of a passband, then energy supplied to the electron by an electric field (i.e., an applied voltage) may increase the electron energy to a sufficient degree that the electron frequency is pushed into the passband and the electron becomes mobile. Such materials are semi-conductors.

Since the time of Bloch's work, knowledge of the interesting behavior of Bloch waves has gradually leaked from the condensed matter physics community into other disciplines. Much of the interest is due to the band structure: a periodic medium acts as a traveling wave filter. A classic microwave filter design is simply a section of waveguide that is loaded with a periodic array of scatterers (e.g., Collin, 1960). Such filters are likewise used in the case of optical waveguides (Flanders, 1976) and surface acoustic wave devices (Tancrell, 1974). While the filtration property is probably that which is most frequently made use of, other unusual properties of Bloch waves are similarly exploited. It is the so-called "slow wave" property of Bloch waves that allows the exchange of energy between a microwave field and a charged particle in the linear particle accelerator (Slater, 1948; Slater, 1950) and in the electron beam traveling wave amplifier (e.g., Collin, 1960). The near-unit reflectivity of periodic media at stopband frequencies is exploited to create extremely high Q surface acoustic wave oscillators (Bell and Li, 1976) as well as distributed feedback lasing cavities (Kogelnik and Shank, 1972). Owing to the dispersion associated with passband frequency Bloch waves, periodic media are at times referred to as "artificial dielectrics" and are used for phase correction (Bloembergen and Sievers, 1970).

The subject of this dissertation is the propagation of acoustic waves in a periodic waveguide. The investigation is both theoretical and experimental. The objectives are to (1) show that the solutions to a broad class of periodic

---

[1]The frequency of the matter wave is proportional to the energy of the electron. As electrons are fermionic, the energy of the most energetic electrons (i.e., the conduction electrons) is dependent upon the entire electronic population of the solid and is therefore characteristic of the solid.

acoustic waveguide problems are Bloch waves, (2) characterize the properties of the Bloch waves in both the time-harmonic and the transient case, and (3) investigate the effect of nonlinearity in the propagation of the Bloch waves. The original motivation for the work was an interest in nonlinear dispersive conventional wave propagation. The hallmark of nonlinearity in the propagation of acoustic waves in a nondispersive system is a steadily increasing distortion of the waveform with propagation distance. If the acoustic field is sufficiently intense, the waveform may eventually distort to the point of shock formation. In *dispersive* nonlinear wave systems, the dispersion is, in some cases, able to disrupt the nonlinear distortion process and prevent the formation of shocks. As Bloch waves are dispersive, it was conjectured that the introduction of some sort of periodic structure into an otherwise uniform waveguide would be a means of preventing not only shock formation, but perhaps *any* significant nonlinear distortion.

While a significant portion of the present work is dedicated to the problem of nonlinear Bloch wave propagation, most of the work addresses the linear problem. There are two reasons for this. First, it was found that the foundations of even the linear theory are weak. As an example, it had not previously been shown for anything other than gradually varying waveguides that the solution wave functions are indeed Bloch wave functions. It had likewise not been shown that the Bloch wave formalism holds in the presence of dissipative mechanisms. The first several chapters of this dissertation are therefore dedicated to the development of a fundamental theory for Bloch waves in a broad class of periodic waveguides. The second reason for the large portion of linear work is that the findings are quite unusual and therefore interesting! While most of the findings apply only to Bloch waves, several of the findings apply to dissipative, dispersive conventional waves in general.

1.1 Past Work

The previous work on wave propagation in periodic media may be divided into two categories: (1) that which specifically addresses the problem of acoustic waves in periodic waveguides, and (2) all other work. While the only *directly* relevant previous work is that of the former category, several works

that belong to the latter do have some degree of relevance. The former category represents a fairly small body of work that may readily be reviewed here. The latter category, however, is composed of virtually innumerable works, and only several of the most relevant are discussed here.

1.1.1 Past Work on Periodic Acoustic Waveguides

Previous work on acoustic waves in periodic waveguides has addressed two types of periodic waveguide: waveguides with periodically nonuniform boundaries, and uniform waveguides that contain a periodic array of scattering inclusions. Two basic solution approaches have been used on these problems. In the first approach, it is either shown or assumed that the solution wave functions are Bloch wave functions. Expressions for the parameters that characterize the Bloch waves, such as the Bloch dispersion relation, are then derived. In the second approach, a perturbation approach, no mention is made of the possibility of Bloch wave solutions. The periodic deviation from uniformity is taken to be small and its effect on the propagation of waves is investigated to leading order. While the Bloch wave approach has been applied to both categories of waveguide problem, the perturbation approach has been applied only to the periodically nonuniform boundary problem.

In past works in which the solutions are *shown* to be Bloch wave functions, the system is modeled with an equation to which the Floquet theorem is directly applicable. The Floquet theorem is applicable to ordinary differential equations with periodic coefficients (e.g., Ince, 1956) and shows that the solution functions $\psi(z)$ have the property

$$\psi(z + h) = e^{jqh}\psi(z),$$

or, equivalently, are of the form

$$\psi(z) = \Phi(z)e^{jqz}, \tag{1.1}$$

where h is the periodicity of the coefficients, $\Phi(z + h) = \Phi(z)$, and q is the Bloch wave number. These function are known as Bloch wave functions. Bai and Keller (1987), who treat a scattering inclusion problem, model the system

with the Webster horn equation (see, for example, Morse, 1976)

$$\frac{\partial^2\psi}{\partial z^2} + \frac{A'(z)}{A(z)}\frac{\partial\psi}{\partial z} - \frac{1}{c_0^2}\frac{\partial^2\psi}{\partial t^2} = 0,$$

which is valid when the changes in cross-sectional area of the duct $A(z)$ are sufficiently gradual. In the time-harmonic case the Webster horn equation becomes a second order ordinary differential equation with periodic coefficients, to which the Floquet theorem is applicable. Note that the Floquet theorem only tells us the *form* of the solution and not the solution itself, which is found by use of a strained parameter perturbation approach: the standard wave number k is strained to yield the Bloch wave number q. It should be noted that for the waveguide geometry treated, the validity of the analysis at frequencies above the second stopband frequency is doubtful,[2] although the results are reported for higher frequencies. Drumheller (1989), who treats a periodically nonuniform boundary problem (which accounts for periodic inhomogeneity as well), models the system with a periodically inhomogeneous Helmholtz-like equation

$$\frac{d^2\psi}{dz^2} + K^2\psi = 0. \tag{1.2}$$

This is a Helmholtz equation in which the effective wave number K is a periodic function of position. The Floquet theorem is applicable to this equation as well. The periodic deviation from uniformity is taken to be discrete and the piecewise solution in each uniform section of waveguide is found. The condition that the piecewise solution be consistent with a Bloch wave solution places a condition on $q(\omega)$. This condition is the Bloch dispersion relation.

The Bloch waves/piecewise solution approach also appears in two other works (Barnes and Kirkwood, 1972; Morse and Ingard, 1986), although in both it is *assumed* that the solution functions are Bloch wave functions. In the work of Barnes and Kirkwood (1972), who treat a periodically nonuniform boundary problem, the assumption that the solutions are Bloch wave functions

---

[2]For the waveguide geometry treated, the scatterers couple the zeroth and second higher order waveguide modes, which are cut on above the second stopband frequency. The Webster horn equation is not valid for the case of multi-mode propagation.

is implicit in their assumption that the impedance is periodic. Morse and Ingard (1986), who solve a scattering inclusion problem, simply state that the solution is expected to be in the form of a Bloch wave function. The piecewise solution is found in the (low frequency) lumped element approximation, which is valid when the free-medium wavelength is much larger than a period of the waveguide. The treatment of Morse and Ingard is, to the author's knowledge, the only one that includes dissipation (the lumped element model includes a resistance).

As was pointed out above, past works in which the second approach, the perturbation approach, is taken are all periodically nonuniform boundary type waveguide problems (Samuels, 1958; Salant, 1973; Nayfeh, 1974; Nayfeh, 1975). In these works the possibility of Bloch wave solutions is not addressed. The deviation from uniformity in the waveguide boundary is assumed small and the boundary condition is expanded about the mean waveguide surface. To zeroth order the waveguide is uniform and the solution, owing to the source boundary condition, is a forward traveling wave that consists of a single wave-guide mode. To first order, the zeroth order forward traveling wave is coupled to both a second forward traveling wave and a backward traveling wave. Although these secondary waves propagate in the same waveguide mode, they differ in spatial frequency. None of the cited works was done in the context of Bloch wave propagation, and the secondary waves were not recognized as simply the first higher order components in the traveling wave spectral representation of a Bloch wave function (a spatial frequency decomposition of Eq.1.1):

$$p(z) = \sum_{n=-\infty}^{+\infty} C_n e^{j(q+2\pi n/h)z}. \tag{1.3}$$

The Webster horn equation is a valid model equation for these problems and may be used, in conjunction with the Floquet theorem, to show that the solutions are indeed Bloch wave functions. It is expected, therefore, that the continuation of the perturbation series used in the aforementioned papers beyond leading order would eventually fill in the values of C_n in Eq. 1.3.

With one exception, the aforementioned work is all purely theoretical. Drumheller (1989) measured the response of his periodic waveguide to a very wideband (nearly impulsive) excitation. When displayed in spectral form, his

data show the theoretically predicted scalloping due to passband/stopband filtration, which is a qualitative confirmation of the stopband structure of Bloch wave dispersion.

In conclusion, the Bloch wave form of the solution is acknowledged in about half of the previous work. When the Bloch wave solution is used, in only two papers (Bai and Keller, 1987; Drumheller, 1989) is it *shown* that the solutions are indeed Bloch wave functions. In both cases, a fairly restrictive model equation is used in the proof. In only one case is dissipation included in the model (Morse and Ingard, 1986), and then only in an *ad hoc* fashion. In the only experimental work (Drumheller, 1989) the investigation is limited to a qualitative confirmation of the stopband structure. To the author's knowledge, no work has been done on the problems of narrowband pulse propagation (short or long range), energy transport, or nonlinear propagation in periodic acoustic waveguides.

1.1.2   Other Relevant Past Work

Some other relevant work in the general area of waves in periodic media, but which does not address acoustic waveguides, is also of interest here. The problem of energy transport in a periodic waveguide is treated by Collin (1960) for the case of a microwave waveguide. He uses the same approach that is used here in the derivation of *one* of the two energy transport velocities that are of interest. He fails, however, to recognize the existence of a second significant energy transport velocity.

The problem of nonlinear wave propagation in periodically inhomogeneous media was first treated by Bloembergen and Sievers (1970) for the optical case and, later, in more detail by Tang and Bey (1973) for the optical case and by Akhmanov *et al.* (1975) and Lanina *et al.* (1978) for the acoustical case. In all cases both the fundamental and the second harmonic fields are expressed in the traveling wave spectral representation, which are then approximated by a truncated series. This approximate representation of a Bloch wave field, however, is valid only in the weak dispersion (nearly uniform medium) limit. In this dissertation the *full* Bloch wave field is taken into account and the findings are therefore valid when the dispersion is arbitrarily strong.

It is also worth noting that the approaches outlined in the last section are also used in periodic medium problems that do not involve acoustic waveguides. The Bloch waves/piecewise solution approach was used by Achenbach and Kittahara (1987) for the problem of waves in an elastic solid with a three-dimensional, periodic array of scattering inclusions. Their analysis is interesting in that for the frequency range treated, the problem is equivalent to that of a uniform, fluid-filled waveguide with a periodic array of scattering inclusions along its axis. The Bloch waves/piecewise solution approach has also been applied to the problem of wave propagation in a periodically inhomogeneous medium (Brekhovskikh, 1980). The medium is modeled with a periodically inhomogeneous Helmholtz-type equation as described earlier (Eq. 1.2), and Bloch wave solutions are found. Probably the best known application of the Bloch waves/piecewise solution method is in the determination of the quantum mechanical electronic energy structure for a Kronig-Penney solid (e.g., Kittel, 1986). The perturbation approach that is outlined in the last section is likewise applicable to the periodically inhomogeneous medium problem. Though the author could find no such work, it is expected that the result is the same traveling wave spectral series found in the periodically nonuniform waveguide problem.

It should also be pointed out that this dissertation is the continuation of the work performed by the author for his Masters research (Bradley, 1991). In that work, which treats a periodically nonuniform waveguide problem, the Bloch waves/piecewise solutions approach is used and the Bloch dispersion relation derived. Measurements of the Bloch wave dispersion are made, and are found to compare well with the theory.

1.2 Outline of This Work

The work presented in this dissertation may be divided into four parts: (1) linear, time harmonic Bloch wave propagation, (2) linear Bloch wave pulse propagation, (3) Bloch wave energy transport, and (4) nonlinear, time harmonic Bloch wave propagation.

Linear, time harmonic Bloch wave propagation is the subject of three chapters. In Chap. 2 we show that for a very broad class of periodic wave-

uides, the solutions are Bloch wave functions. The approach taken is to show that the Floquet theorem is applicable to a much broader class of problems than ordinary differential equations with periodic coefficients. In this way, the limitations inherent in modeling the system with an equation such as the Webster horn equation (for which the changes in cross-sectional area must be gradual) are avoided. The approach also allows us to treat the dissipative case. We show that the Bloch wave formalism holds even when the waveguide is filled with a viscous, thermally conducting fluid. In Chap. 3 the properties of the Bloch waves are investigated both theoretically and experimentally. Theoretical expressions for the Bloch dispersion relation and wave functions are derived and compared with measurements. It is shown that reciprocity places significant constraints on how the forward and backward traveling Bloch waves may differ. In Chap. 4 systems with finite sections of periodic waveguide are considered. Bloch wave reflection and transmission relations are derived, and a general method of solution for such systems is outlined.

The problem of Bloch wave pulse propagation is addressed in two chapters. In Chap. 5 the Bloch wave dispersion integral is derived and its solutions considered. It is shown that the solution of the Bloch wave dispersion integral may be found by application of a recovery operator to the solution of a conventional wave dispersion integral. The conventional wave dispersion integral is considered in the light of a set of characteristic pulse distortion distances. In this way the ranges of validity of several classic and several new solutions of the conventional wave dispersion integral are made clear. Novel pulse distortion effects such as pulse frequency shifting and pulse acceleration are found in the analysis as well as in measurement. In Chap. 6 the asymptotic behavior of linear Bloch wave pulses is considered. Owing to the highly characteristic form of the Bloch dispersion curve, the properties of the pulse may be found for a wide variety of initial pulses.

The problem of energy transport by linear Bloch waves is taken up in Chap. 7. Expressions for the intensity, power, and energy density of time-harmonic Bloch waves are derived. These expressions are then used to calculate the energy transport velocity, and there are found to be two. This apparent inconsistency is reconciled by consideration of the difference between mobile and stagnant energy and the findings confirmed by measurement of the energy

transport velocity.

Chapter 8 is devoted to nonlinear, time harmonic Bloch wave propagation. More specifically, the generation of the second harmonic component of the distortion field is considered. A discrete Green's function approach to the solution is developed and it is found that a forward traveling fundamental Bloch wave results in a bidirectional excitation of second harmonic Bloch waves. This approach allows us to account for the *full Bloch wave representations* of the fundamental and second harmonic fields. In the approaches used in the past these fields have been approximately represented by truncated traveling wave spectral series (see Eq. 1.3), an approximation that is valid in the weak dispersion (i.e., nearly uniform waveguide) limit. With the discrete Green's function method such approximations are avoided, and the results consequently valid in the case of arbitrarily strong dispersion. It is found that the introduction of periodicity into a waveguide is a very effective means of disrupting waveform distortion caused by nonlinearity. Measurements of the second harmonic amplitude show good agreement with the theory and verify the disruption of the nonlinear waveform distortion.

1.3   The System Under Study

In this study we consider a very broad class of periodic waveguides. While a number of substantial results may be obtained for such a system, the results are made much more tangible when they are expressed explicitly for a particular system. For this reason, we consider not only the class of periodic waveguides but two specific periodic waveguides as well. These two periodic waveguides are also those for which the measurements are made.

1.3.1   The Theoretical System

The class of periodic waveguides under study is defined as follows. The waveguide is a rigid, impenetrable, isothermal tube that is continuous (i.e., holes in the waveguide wall are not allowed) and periodic. It is allowed to contain an arbitrary periodic array of scattering inclusions, which are similarly rigid, impenetrable, and isothermal. The only restriction on the shape of the
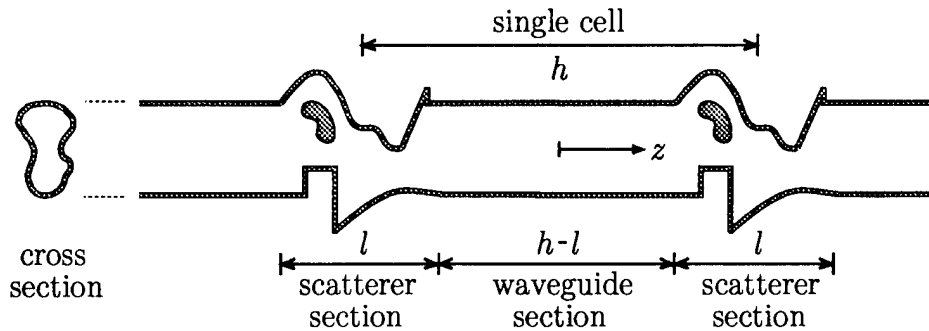
Figure 1.1: An example of the class of waveguide under study.

waveguide is that each cycle must include at least one arbitrarily short section of inclusion-free uniform duct, the cross-section of which is arbitrary. The waveguide is assumed to be filled with an arbitrary viscous and heat-conducting fluid.

An example of the waveguide is shown in Fig. 1.1. The sections of uniform, inclusion-free duct are referred to as "waveguide sections," and the intervening sections of deformed and/or inclusion containing duct are referred to as "scattering sections" or simply "scatterers." The axial coordinate z is centered on a waveguide section and the translated axial coordinate $\xi = z - h/2$ is centered on a scattering section, where h is the periodicity of the waveguide. The length of the scattering sections is l and that of the waveguide sections is $h-l$. A section of the periodic waveguide of length h that is centered on a waveguide section (such as the section $-h/2 < z < h/2$) is referred to as a "cell." If the scatterers are symmetric under reversal of the axial coordinate ($\xi \to -\xi$), then the periodic waveguide itself exhibits the same symmetry. Such waveguides are, for obvious reasons, termed isotropic periodic waveguides. If on the other hand the scatterers are asymmetric, then the waveguide has directional properties. These waveguides are termed anisotropic periodic waveguides.

In order to express the results of the analysis as applied to specific periodic waveguides, two are considered. One is isotropic and the other is anisotropic. These two periodic waveguides are also those in which measurements are made. Both waveguides consist of a rectangular duct (of transverse dimensions $a \times b$) that is loaded by a set of rigidly terminated rectangular side
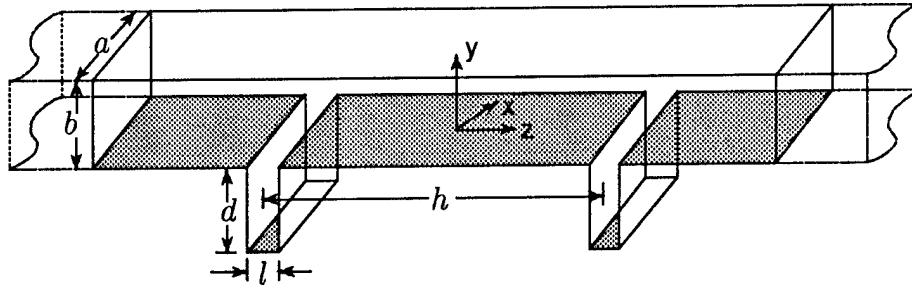
Figure 1.2: Two cycles of the isotropic periodic side branch waveguide. Each scatterer is composed of a single side branch.

branches (of transverse dimensions a x l). The side branch or collection of side branches that loads each cycle of the waveguide acts as a scatterer. Each cycle of the isotropic waveguide is loaded by a single side branch of depth d as shown in Fig. 1.2.

The scatterers are symmetric under axial reversal and the resultant waveguide is therefore isotropic. Each cycle of the anisotropic waveguide is loaded by a *pair* of side branches, one of depth d and the other of depth $d/2$ (see Fig. 1.3(b)). Each scatterer is therefore composed of an asymmetric pair of side branches and is *not* symmetric under axial reversal. The resultant waveguide is therefore anisotropic. The two waveguides are referred to as the isotropic and the anisotropic periodic side branch waveguides.
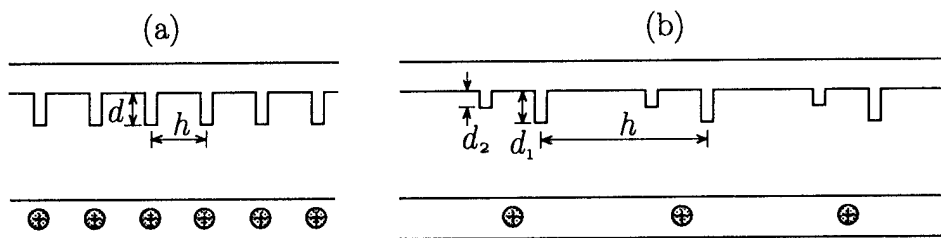
Figure 1.3: The isotropic (a) and the anisotropic (b) periodic side branch waveguides. Below each waveguide is shown a schematic representation to illustrate the locations of the scatterers.

1.3.2 The Experimental System
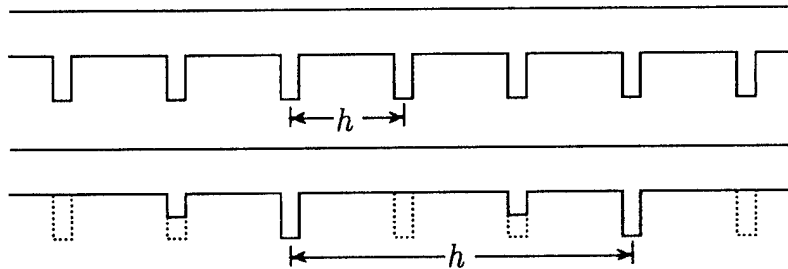
Figure 1.4: The isotropic periodic side branch waveguide may be converted into the anisotropic waveguide by selectively filling and half filling side branches.

The measurements are made in the two periodic side branch waveguides described in the last section. Both are made of aluminum and are air filled. One is a 48 cycle section of the isotropic periodic waveguide and the other is a 16 cycle section of the anisotropic periodic waveguide. Figure 1.4 shows that the isotropic waveguide may be transformed into the anisotropic waveguide simply by selectively filling and half filling the side branches. Owing to this transformation, which obviates the need to build two separate waveguides, the isotropic waveguide has, by a factor of three, a greater number of cycles than the anisotropic waveguide. The periodic waveguides are driven at one end by a compression driver and terminated at the other end, as shown in Fig. 1.5. The termination is a length of uniform waveguide that is loaded with an anechoic fiberglass wedge. This section of uniform waveguide is rectangular and of the same transverse dimensions as the rectangular duct; i.e., it is simply a side branch-free extension of the periodic waveguide. The acoustic pressure
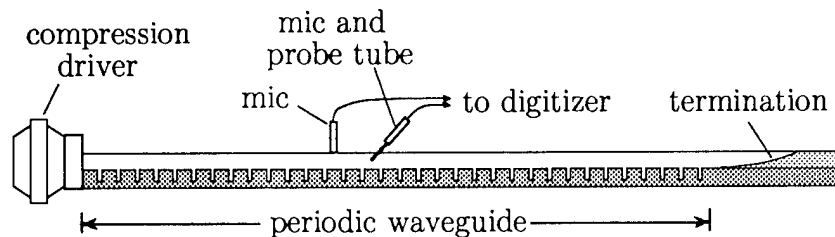
Figure 1.5: The periodic waveguide system in which the measurements are made.

field is measured with a condenser microphone in one of two configurations. In the first configuration, the microphone is mounted with its diaphragm flush with the inner surface of the waveguide wall. The field is not disturbed and yet a measure of the acoustic pressure field at the waveguide wall is obtained. In the second configuration, the condenser microphone is connected to the probe tube, which is inserted into the volume of the waveguide. Further details of the waveguide construction and the measurement techniques are included in Appendix E.

Chapter 2

The Floquet Theorem and the Time Harmonic Bloch Wave Solutions

In this chapter it is shown that the mathematical system of partial differential equations and boundary conditions that describes linear, dissipative acoustic wave propagation in the periodic waveguide under consideration is of a class that has Bloch wave solutions. In order to show that Bloch wave functions are solutions of the system, we show that the Floquet theorem may be applied to the mathematical system under the assumption of time-harmonicity. While the Floquet theorem is penned so as to apply to a class of ordinary differential equations, it is shown here that it is more generally applicable to a *system* composed of *partial* differential equations and boundary conditions provided (1) the system is invariant under a translation operation, and (2) the system has two linearly independent solutions. It is found that for sufficiently low frequencies, the Floquet theorem is indeed applicable to the system and the solutions are indeed Bloch wave functions. The Bloch wave functions are determined by an eigenvalue problem. In this way we are able to accomplish what we set out to prove (that the solutions are Bloch wave functions) and establish a connection between our system and those of earlier works in which the Floquet theorem is used directly to show that the solutions of a system are Bloch wave functions. There are, however, two problems with the approach. First, the proof is valid only for low frequencies and, second, the eigenvalue problem that determines the Bloch wave functions is prohibitively complicated. For these reasons a sec-

ond, more fundamental proof of the existence of the Bloch wave solutions is presented. While the Bloch wave solutions are again given by an eigenvalue problem, it is a much simpler eigenvalue problem. Its simplicity is exploited at length in Chapter 3 to determine many of the characteristics of the Bloch waves. It is also found that the more fundamental proof may be applied even when the frequency restriction is lifted. In such a case the solutions are found to be Bloch waves of higher order.

2.1 The System of Equations and its Invariance Under Translation

The system of linearized equations that describes the dynamics of a viscous, heat conducting, homogeneous fluid consists of three conservation equations and two constitutive relations. The field variables that appear in these equations are $\hat{P} = P_0 + p$, $\hat{u} = u$, $\hat{\rho} = \rho_0 + \rho$, $\hat{T} = T_0 + T$, and $\hat{s} = s_0 + s$, which represent pressure, fluid velocity, mass density, temperature, and entropy, respectively. The total variable value (denoted by a hat) is expressed as the sum of the ambient value (subscripted with a zero) and the acoustic or fluctuating value. The linearized equations of conservation of mass, momentum, and entropy are (e.g., Pierce, 1981)

$$\frac{\partial \rho}{\partial t} + \rho_0 \nabla \cdot u = 0, \tag{2.1}$$

$$\rho_0 \frac{\partial u}{\partial t} = -\nabla p + \mu \nabla^2 u + (\mu_B + \mu/3)\nabla(\nabla \cdot u), \tag{2.2}$$

and

$$\rho_0 T_0 \frac{\partial s}{\partial t} = \kappa \nabla^2 T, \tag{2.3}$$

respectively, where μ and μ_B are the coefficients of shear and bulk viscosity and κ is the coefficient of thermal conductivity. The constitutive relations are taken to be the two equilibrium thermodynamic relations $\hat{\rho} = \hat{\rho}(\hat{P}, \hat{s})$ and $\hat{T} = \hat{T}(\hat{P}, \hat{s})$. Linearized expansions of these relations may be written

$$\rho = \left(\frac{1}{c_0^2}\right)p - \left(\frac{\rho_0 \beta T_0}{C_P}\right)s, \tag{2.4}$$

and

$$T = \left(\frac{\beta T_0}{\rho_0 C_P}\right) p + \left(\frac{T_0}{C_P}\right) s, \tag{2.5}$$

where c_0 is the small-signal lossless sound speed, β is the coefficient of thermal expansion, and C_P is the specific heat at constant pressure, all evaluated at the ambient condition. Because both the waveguide boundary and any inclusions, if present, are assumed to be rigid and isothermal, the boundary conditions are

$$\mathbf{u}|_S = 0 \qquad T|_S = 0, \tag{2.6}$$

where S is the surface of the waveguide.

Because the fluid is homogeneous and linear, each of the coefficients that multiplies the various differential operators in the system of equations (such as ρ_0, T_0, and κ) is a constant. Each of the operators that appears in the system is invariant under the set of arbitrary spatial translations

$$\mathbf{r} \rightarrow \mathbf{r} + \Delta\mathbf{r}.$$

The system of equations is therefore invariant under arbitrary spatial translations. The boundary conditions, however, owing to the spatial dependence of the surface of evaluation S, are invariant under the more restricted set of translations

$$\mathbf{r} \rightarrow \mathbf{r} + nh\hat{\mathbf{e}}_z,$$

where n is an integer and $\hat{\mathbf{e}}_z$ is the axial unit vector. The *total system* then, composed of the system of equations and the boundary conditions, is invariant under the set of translations $\mathbf{r} \rightarrow \mathbf{r} + nh\hat{\mathbf{e}}_z$. It it worth noting that the system would exhibit the same invariance if the fluid were periodically inhomogeneous with the same periodicity as the waveguide surface.

2.2 The Global and Local Fields

We now find an expression for the acoustic pressure field in the waveguide sections. It is shown that the representation of the field may be simplified with the identification of what is referred to here as the "global" component of the field: that which carries all the pertinent information as to the cell-to-cell

structure of the field. The remainder field, the "local" field, may be discarded without consequence. We begin with a consideration of the acoustic field in the vicinity of a single scatterer in an otherwise uniform waveguide. It is also assumed that the fluid is nondissipative. The solution of this simplified system leads simply to the solution of the periodic waveguide system. The effect of dissipation may then be accounted for.

In the nondissipative limit, the system of equations may be reduced to the classical wave equation in the acoustic pressure. Under the assumption of time-harmonic fields, the wave equation becomes the Helmholtz equation

$$\nabla^2 p + k^2 p = 0,$$

where $k^2 = (\omega/c_0)^2$. Likewise, in the absence of dissipation the boundary condition becomes the standard normal pressure gradient restriction

$$\nabla p \cdot \hat{n}|_S = 0,$$

where $\hat{n}$ is the unit vector normal to the waveguide surface S. The solution in the waveguides on either side of the scatterer is composed of incident and scattered fields, both of which may be represented as sums over the discrete set of allowed waveguide modes. It is assumed that the frequency is below the cut-on frequency of the first higher order waveguide mode, and that the fields incident upon the scatterer are purely zeroth order. The total field, then, is composed of a propagating component (the incident and scattered zeroth order waves) and an evanescent component (the scattered higher order modal field), which is confined to the near-vicinity of the scatterer. The total solution in the waveguides may be expressed

$$
\begin{aligned}
p(\mathbf{r}_\perp, \xi) = A_0 e^{jk\xi} \quad &+ \quad (S_{11}A_0 + S_{12}B_0)e^{-jk\xi} \\
&+ \quad \sum_{n=1}^{\infty} A_n \phi_n(\mathbf{r}_\perp) e^{|k_{z,n}(\xi+l/2)|} \quad \xi < -l/2 \\
p(\mathbf{r}_\perp, \xi) = B_0 e^{-jk\xi} \quad &+ \quad (S_{21}A_0 + S_{22}B_0)e^{jk\xi} \\
&+ \quad \sum_{n=1}^{\infty} B_n \phi_n(\mathbf{r}_\perp) e^{-|k_{z,n}(\xi-l/2)|} \quad \xi > l/2, \qquad (2.7)
\end{aligned}
$$

where A_0 and B_0 are the pressure amplitudes of the waves incident upon the scatterer from $\xi < 0$ and $\xi > 0$, respectively, and the S_{ij} are zeroth order scattering matrix elements. The transverse mode functions $\phi_n(\mathbf{r}_\perp)$ and wave numbers $k_{\perp n}$ are the solutions of the transverse component of the uniform waveguide

problem; i.e., they are the solutions of the system $\nabla_\perp^2 \phi_n(\mathbf{r}_\perp) + k_{\perp n}^2 \phi_n(\mathbf{r}_\perp) = 0$, where $\nabla_\perp \phi_n \cdot \hat{\mathbf{n}}|_S = 0$, $\nabla_\perp = \nabla - \hat{\mathbf{e}}_z \partial/\partial z$, and $\mathbf{r} = \mathbf{r}_\perp + z\hat{\mathbf{e}}_z$. The axial wave numbers are given by $k_{z,n} = [(\omega/c_0)^2 - k_{\perp n}^2]^{1/2}$. A schematic representation of the field structure is shown in Fig. 2.1.
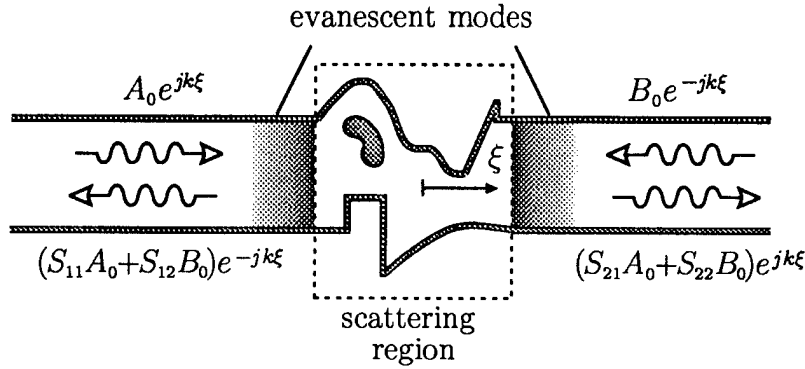
Figure 2.1: The incident and scattered waves in the vicinity of a scatterer.

The single-scatterer solution (Eqs. 2.7) may be used to describe the field in the vicinity of a scatterer in the periodic waveguide provided the field incident upon each scatterer is purely zeroth order. In order for this to be the case, the evanescent modes generated at the neighboring scatterers must decay to a negligibly small amplitude over the distance $h - l$. Such a requirement leads to the frequency constraint

$$\omega \ll c_0[k_{\perp 1}^2 - (h - l)^{-2}]^{1/2}. \qquad (2.8)$$

Under this constraint, *the higher order modal fields are confined to the near vicinity of each scatterer.* They extend some distance into the waveguide on either side of the scatterers, but the only *extended* field is the zeroth order field. The evanescent field is simply a *localized perturbation* to the zeroth order field and has no consequence with respect to the global behavior of the system. Such a field structure suggests the decomposition of the exact, three-dimensional field into global and local components:

$$p(\mathbf{r}) = p_{\text{global}}(z) + p_{\text{local}}(\mathbf{r}), \qquad (2.9)$$

where $p_{\text{global}}(z)$ is the global, purely zeroth order field component and $p_{\text{local}}(\mathbf{r})$ is the local, "remainder" field that is significant only in the near-vicinity of

the scatterers. By this line of reasoning, we may neglect the local field contribution and consider only the global field, which carries all the information necessary to reconstruct the exact field. Once the global field is determined, the local field and therefore the exact, three-dimensional total field is, in principle, determined. In the nth cell, the global solution is simply

$$p_{\text{global}}(z) = C_n^{(+)} e^{jkz_n} + C_n^{(-)} e^{-jkz_n} \qquad |z_n| < h/2, \qquad (2.10)$$

where $z_n = z - nh$ is a shifted axial coordinate centered on the nth cell. A schematic representation of this global field is shown in Fig. 2.2. From this point on, a reference to the acoustic pressure field is, unless otherwise stated, a reference to the global component of the acoustic pressure field only.
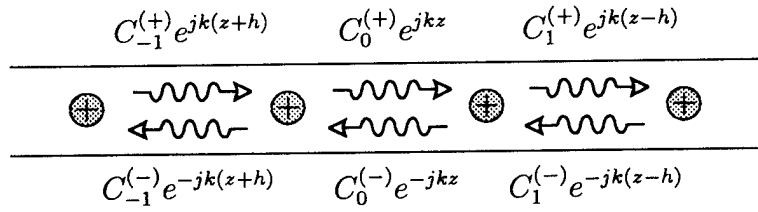
AS-94-723

Figure 2.2: A schematic representation of the conventional wave structure of a periodic waveguide solution. The amplitudes shown are those of the traveling waves at the center of each cell.

In the dissipative case the same line of reasoning may be used to justify the use of the zeroth order field alone. That is, under the frequency constraint Eq. 2.8, the evanescent higher order modes are simply localized perturbations to the zeroth order field and need not be accounted for. In fact, the evanescent modes *do* dissipate some energy and therefore represent an energy sink to the zeroth order field, which maintains their level. These losses, however, are accounted for intrinsically in the definition of the scattering matrix elements.

The dissipative global solution is given by Eq. 2.10 with the nondissipative wave number $k = \omega/c_0$ replaced by the well known (e.g., Pierce, 1981)

dissipative wave number

$$k = \omega/c_0 + (1+j)\frac{1}{\sqrt{2}R_{\mathrm{H}}}\left[\left(\frac{\mu}{\rho_0 c_0^2}\right)^{1/2} + (\gamma - 1)\left(\frac{\kappa/C_p}{\rho_0 c_0^2}\right)^{1/2}\right]\omega^{1/2}, \quad (2.11)$$

where R_{H} is the hydraulic radius (twice the cross-sectional area divided by the circumference) of the waveguide sections. This wave number is valid over a broad range of frequency in which the so-called ω^2 or free field thermoviscous losses are negligible compared to the $\omega^{1/2}$ or thermoviscous acoustic boundary layer losses.

2.3   The Linearly Independent Solutions

We now present a very general form of the solution of the system. The system has, by way of a frequency constraint (Eq. 2.8) and the global/local field decomposition (Eq. 2.9), effectively been reduced to an infinite sequence of coupled one-dimensional wave cells of length h. It is seen in Eq. 2.10 that each cell has two linearly independent solutions, but what of the *system* of coupled cells? It is easily shown using a T-matrix (transmission matrix) approach that the entire system has two linearly independent solutions as well.

While the S-matrix relates the scattered field to the incident field in the vicinity of a scatterer, the T-matrix relates the fields on either side of the scatterer (these matrices are defined in Appendix B). The zeroth order wave amplitudes in the centers of the nth and the $(n+1)^{\mathrm{th}}$ cells are related by the transmission relation

$$\begin{bmatrix} C_{n+1}^{(+)} \\ C_{n+1}^{(-)} \end{bmatrix} = \frac{1}{S_{21}}\begin{bmatrix} -|S|e^{jkh} & S_{22} \\ -S_{11} & e^{-jkh} \end{bmatrix}\begin{bmatrix} C_n^{(+)} \\ C_n^{(-)} \end{bmatrix} = \mathbf{T}^{\mathrm{C}}\begin{bmatrix} C_n^{(+)} \\ C_n^{(-)} \end{bmatrix}, \quad (2.12)$$

where $|S|$ is the determinant of the scattering matrix and $\mathbf{T}^{\mathrm{C}}$ is the T-matrix associated with transmission across the cell. Given the two traveling wave amplitudes in the nth cell, we are able to derive the traveling wave amplitudes in *any other cell of the structure* by repeated application of Eq. 2.12 or its inverse. The wave function of the entire system may therefore be expressed in terms of only the two constants $C_n^{(+)}$ and $C_n^{(-)}$. These two constants are the

two arbitrary constants associated with the general solution to a system that has two linearly independent solutions.

A very general pair of linearly independent solutions may be defined in the nth cell as

$$F_1(z) = C_n^{(+)} e^{jkz_n} + C_n^{(-)} e^{-jkz_n}$$

$$F_2(z) = D_n^{(+)} e^{jkz_n} + D_n^{(-)} e^{-jkz_n}. \tag{2.13}$$

Outside of the nth cell, the constants $C^{(+)}$, $C^{(-)}$, $D^{(+)}$, and $D^{(-)}$ may be found by repeated applications of the transmission matrix (Eq. 2.12) or its inverse. The Wronskian of $F_1(z)$ and $F_2(z)$ is

$$W(z) = 2jk \left[C_n^{(-)} D_n^{(+)} - C_n^{(+)} D_n^{(-)} \right],$$

which is constant in any cell and is nonzero if

$$C_n^{(-)}/C_n^{(+)} \neq D_n^{(-)}/D_n^{(+)}.$$

In other words, $F_1(z)$ and $F_2(z)$ are linearly independent as long as they are not the same function.

2.4 The Floquet Theorem and the Associated Eigenvalue Problem

In this section the Floquet theorem is applied to show that the solutions of the system are Bloch wave functions. As it appears in the literature, the Floquet theorem applies only to ordinary differential equations (e.g., Ince, 1956), and may not be applied *directly* to our partial differential system. It is shown here, however, that because (1) the system exhibits an invariance under the set of translation operations $\mathbf{r} \rightarrow \mathbf{r} + nh\hat{\mathbf{e}}_z$, and (2) there are two linearly independent solutions of the system, the Floquet theorem may indeed be applied to the system. As a result, the solutions are shown to be Bloch wave functions.

Consider the arbitrary pair of linearly independent solution functions defined in Eq. 2.13. An arbitrary solution function must be expressible as a linear superposition of $F_1(z)$ and $F_2(z)$ as these functions form a linearly

independent basis. Because the system is invariant under axial translations of h, the functions $F_1(z + h)$ and $F_2(z + h)$ must also be solutions and must therefore be expressible in terms of the basis:

$$F_1(z + h) = J_{11}F_1(z) + J_{12}F_2(z)$$

$$F_2(z + h) = J_{21}F_1(z) + J_{22}F_2(z), \qquad (2.14)$$

or, equivalently,

$$|F(z + h)\rangle = \mathbf{J}|F(z)\rangle, \qquad (2.15)$$

where

$$|F(z)\rangle = \begin{bmatrix} F_1(z) \\ F_2(z) \end{bmatrix}$$

is the basis vector[1] and $\mathbf{J}$ is the matrix composed of the constants J_{ij}.

Note that, in general, the basis $|F(z)\rangle$ is such that upon translation (i.e., propagation), the basis wave functions "mix". That is, in order to express the translated solution wave function $F_1(z + h)$ we must use both $F_1(z)$ and $F_2(z)$. We now look for a particular pair of basis functions that exhibit an independence (i.e., do not "mix") under the translation operation. In other words, we seek a basis for which $J_{12} = J_{21} = 0$, in which case we have a pair of traveling wave type solutions that diagonalize the translation operation. The elements of the basis we seek have the property

$$\mathcal{T}\Gamma(z) = \Gamma(z + h) = s\Gamma(z), \qquad (2.16)$$

which we recognize as the eigenvalue problem associated with $\mathcal{T}$, the unit cell translation operator.

Because $\Gamma(z)$ is a solution of the system, it may be expressed as a linear combination of the basis wave functions:

$$\Gamma(z) = \beta_1 F_1(z) + \beta_2 F_2(z) = \langle \beta | F(z) \rangle.$$

---

[1]The so-called bracket linear algebraic notation, in which $|\cdot\rangle$ denotes a column vector and $\langle\cdot|$ denotes a row vector, is described in the book by Arfken (1985).

The shifted function $\Gamma(z + h)$ may therefore be expressed

$$\Gamma(z + h) = \beta_1 F_1(z + h) + \beta_2 F_2(z + h) = \langle \beta | F(z + h) \rangle. \qquad (2.17)$$

With the introduction of Eq. 2.15, Eq. 2.17 may be written

$$\Gamma(z + h) = \langle \beta | \mathbf{J} | F(z) \rangle.$$

The eigenvalue problem (Eq. 2.16) therefore becomes $\langle \beta | \mathbf{J} | F(z) \rangle = s \langle \beta | F(z) \rangle$, or equivalently

$$\mathbf{J}^T | \beta \rangle = s | \beta \rangle, \qquad (2.18)$$

where the superscript T denotes the transpose. Note that Eq. 2.18 is the state vector representation of the eigenvalue problem associated with the translation operator $\mathcal{T}$, where the state is defined in terms of the basis $|F(z)\rangle$. The solution eigenvectors, here labeled $|\beta^{(\pm)}\rangle$, yield the eigenfunctions

$$F^{(\pm)}(z) = \langle \beta^{(\pm)} | F(z) \rangle$$

and the associated eigenvalues yield the desired independent or "non-mixing" translation property of the eigenfunctions

$$F^{(\pm)}(z + h) = s^{(\pm)} F^{(\pm)}(z). \qquad (2.19)$$

Equation 2.19 is a statement of the essential result of the Floquet theorem: that there does indeed exist a pair of basis wave functions that exhibit the desired independence under translation. Equation 2.18 is the eigenvalue problem that generates the wave functions, the eigenfunctions $F^{(\pm)}(z)$, which are the Bloch wave functions. The Bloch wave functions are simply a particularly judicious choice of linearly independent solution functions in terms of which we may express other solutions. We will see, however, that it is not always straightforward to determine which of the solution functions is the forward traveling Bloch wave function $F^{(+)}(z)$ and which is the backward traveling Bloch wave function $F^{(-)}(z)$.

2.5 The Underlying Eigenvalue Problem

While the eigenvalue problem associated with the Floquet theorem leads us to the desired result (a translationally independent basis), there is an underlying eigenvalue problem that carries the same information as Eq. 2.18 but is much more fundamental. This "nested" eigenvalue problem is found by taking the same steps as in the last section, but with the basis functions $|F(z)\rangle$ expressed in terms of the exponential functions that were used to define them (see Eq. 2.13). Equation 2.13 may be expressed

$$F_1(z) = \langle C_n | e(z) \rangle \qquad F_2(z) = \langle D_n | e(z) \rangle,$$

where $|C_n\rangle = [C_n^{(+)} \ C_n^{(-)}]^T$, $|D_n\rangle = [D_n^{(+)} \ D_n^{(-)}]^T$, and

$$|e(z)\rangle = \begin{bmatrix} e^{+jkz_n} \\ e^{-jkz_n} \end{bmatrix}.$$

As before, we express the solution function $\Gamma(z)$ in terms of the basis $|F(z)\rangle$, which we in turn express in terms of the exponential "basis" functions[2]:

$$\begin{aligned}
\Gamma(z) &= \langle \beta | F(z) \rangle \\
&= \beta_1 \langle C_n | e(z) \rangle + \beta_2 \langle D_n | e(z) \rangle \\
&= \langle \sigma_n | e(z) \rangle,
\end{aligned}$$

where

$$|\sigma_n\rangle = \beta_1 |C_n\rangle + \beta_2 |D_n\rangle = [|C_n\rangle |D_n\rangle] |\beta\rangle$$

is a vector composed of the traveling wave amplitudes at the center of the nth cell. The shifted function $\Gamma(z + h)$ may also be expressed in terms of the exponential functions:

$$\begin{aligned}
\Gamma(z + h) &= \langle \beta | F(z + h) \rangle \\
&= \beta_1 \langle C_{n+1} | e(z) \rangle + \beta_2 \langle D_{n+1} | e(z) \rangle \\
&= \langle \sigma_{n+1} | e(z) \rangle.
\end{aligned} \qquad (2.20)$$

---

[2]The exponential functions do not form a basis in the true sense as they are not solutions of the system.

From Eq. 2.12 we have $|C_{n+1}\rangle = \mathbf{T}^C|C_n\rangle$ and $|D_{n+1}\rangle = \mathbf{T}^C|D_n\rangle$, and Eq. 2.20 may be written

$$\Gamma(z + h) = \langle \sigma_n|(\mathbf{T}^C)^T|e(z)\rangle.$$

The eigenvalue problem (Eq. 2.16) therefore becomes

$$\mathbf{T}^C|\sigma_n\rangle = s|\sigma_n\rangle. \tag{2.21}$$

The resultant eigenvectors yield the eigenfunctions (the Bloch wave functions)

$$F^{(\pm)}(z) = \langle \sigma_n^{(\pm)}|e(z)\rangle \tag{2.22}$$

and the eigenvalues $s^{(\pm)}$ yield the translation relations as shown in Eq. 2.19.

The exponential basis approach has considerable advantages over the standard Floquet approach. While both methods result in the same eigenfunctions and translation relations, the eigenvalue problem found in terms of the exponential basis is much more fundamental than the other, a fact that is exploited at length in Chapter 3 to determine the characteristics of the Bloch wave functions for various waveguide geometries. The difference between the two approaches lies in the translation operator. In the $|F(z)\rangle$ basis, the translation operator $\mathbf{J}$ is specific to whichever particular basis is chosen. We first choose a particular $F_1(z)$ and $F_2(z)$ (i.e., choose complex values for $C_n^{(+)}$, $C_n^{(-)}$, $D_n^{(+)}$, and $D_n^{(-)}$). Equation 2.14 may then be inverted (using Eqs. 2.12 and 2.13) to solve for the elements of $\mathbf{J}$:

$$\mathbf{J} = \frac{j}{||C_n\rangle|D_n\rangle|} \begin{bmatrix} -\langle D_n|\mathbf{s_2}|\mathbf{T}^C|C_n\rangle & \langle C_n|\mathbf{s_2}|\mathbf{T}^C|C_n\rangle \\ -\langle D_n|\mathbf{s_2}|\mathbf{T}^C|D_n\rangle & \langle C_n|\mathbf{s_2}|\mathbf{T}^C|D_n\rangle \end{bmatrix},$$

where $\mathbf{s_2}$, defined as

$$\mathbf{s_2} = \begin{bmatrix} 0 & -j \\ j & 0 \end{bmatrix},$$

is the second Pauli spin matrix (e.g., Arfken, 1985). The eigenvalue problem (Eq. 2.18) may then be solved and the Bloch wave functions found. In the $|e(z)\rangle$ basis, the translation operator is $\mathbf{T}^C$, which has no dependence on which particular functions $F_1(z)$ and $F_2(z)$ we started with. The operator $\mathbf{T}^C$ is a *fundamental characterization of the scatterers* dependent only upon the waveguide geometry. The cell T-matrix eigenvalue problem is therefore a much more fundamental statement of the problem.

2.6 Higher Order Bloch Wave Modes

Up to this point we have worked under the frequency restriction (Eq. 2.8) that ensures that only one mode is significant after propagation over the distance between scatterers. In other words, it has been assumed that the global field is composed only of the zeroth order waveguide mode. It is now shown that this assumption, which was made in order to simplify the derivation, need not have been made. The exponential basis version of the Floquet theorem may be extended and used to show that in the arbitrary frequency case, in which an arbitrary number of waveguide modes are cut on, the solutions are still Bloch wave functions.

We consider the case in which m modes are significant after propagation through a waveguide section. The frequency constraint for this case is

$$\omega \ll c_0 [k_{\perp m}^2 - (h - l)^{-2}]^{1/2},$$

where $k_{\perp m}$ is the transverse wave number associated with the mth mode. It may be the case that all m modes are cuton or that some are evanescent yet significant. The global solution in the nth cell is now composed of m forward and m backward traveling wave modes, and may be expressed

$$p_{\text{global}}(\mathbf{r}) = \sum_{i=0}^{m-1} \left[C_n^{(i+)} \phi_i(\mathbf{r}_\perp) e^{jk_i z_n} + C_n^{(i-)} \phi_i(\mathbf{r}_\perp) e^{-jk_i z_n} \right],$$

where n is the cell number associated with $\mathbf{r}$ and $\phi_i(\mathbf{r}_\perp)$ is the transverse field function associated with the ith mode. The system now has $2m$ linearly independent solution functions, the lth of which may be expressed

$$F_l(\mathbf{r}) = \sum_{i=0}^{m-1} \left[C_{n,l}^{(i+)} \phi_i(\mathbf{r}_\perp) e^{jk_i z_n} + C_{n,l}^{(i-)} \phi_i(\mathbf{r}_\perp) e^{-jk_i z_n} \right].$$

The calculation of the Wronskian of this set of solution functions (holding $\mathbf{r}_\perp$ constant) indeed shows that they are linearly independent as long as no two of the functions are related by a multiplicative constant. Extending the earlier approach, we define the state vector as

$$|C_{n,l}\rangle = \begin{bmatrix} C_{n,l}^{(0+)} & C_{n,l}^{(0-)} & \cdots & C_{n,l}^{(m-1+)} & C_{n,l}^{(m-l-)} \end{bmatrix}^T$$

and set of exponential basis functions

$$|e(\mathbf{r})\rangle = \begin{bmatrix} e^{jk_0 z_n} & e^{-jk_0 z_n} & \cdots & \phi_{m-1}(\mathbf{r}_\perp)e^{jk_{m-1}z_n} & \phi_{m-1}(\mathbf{r}_\perp)e^{-jk_{m-1}z_n} \end{bmatrix}^T.$$

In this notation, we have by definition

$$F_l(\mathbf{r}) = \langle C_{n,l}|e(\mathbf{r})\rangle$$

and

$$F_l(\mathbf{r} + h\hat{\mathbf{e}}_z) = \langle C_{n+1,l}|e(\mathbf{r})\rangle.$$

The set of basis functions are defined

$$|F(\mathbf{r})\rangle = [F_1(\mathbf{r}) \quad \cdots \quad F_{2m}(\mathbf{r})]^T,$$

and the $2m$ x $2m$ translation matrix is such that

$$|C_{n+1,l}\rangle = \mathbf{T}^C|C_{n,l}\rangle.$$

We may now proceed as in the $m = 1$ case. An arbitrary solution and the arbitrary solution translated by a period are $\Gamma(\mathbf{r}) = \langle \sigma_n|e(\mathbf{r})\rangle$ and $\Gamma(\mathbf{r} + h\hat{\mathbf{e}}_z) = \langle \sigma_{n+1}|e(\mathbf{r})\rangle$, where $|\sigma_{n+1}\rangle = \mathbf{T}^C|\sigma_n\rangle$. We again look for solutions with the translational independence $\Gamma(\mathbf{r} + h\hat{\mathbf{e}}_z) = s\Gamma(\mathbf{r})$, which again leads to the eigenvalue problem

$$\mathbf{T}^C|\sigma_n\rangle = s|\sigma_n\rangle.$$

The eigenvalue problem is now a $2m$ x $2m$ problem, resulting in m forward traveling and m backward traveling Bloch wave modes. As the transverse dimensions of the waveguide become large (compared to a free-space wavelength) or the waveguide sections become short (compared to the largest characteristic evanescent mode decay length), the value of m increases and the problem becomes more difficult. From this point on, only the $m = 1$ case is considered.

Chapter 3

The Eigenvalue Problem and the Bloch Wave Functions

In this chapter we investigate the properties of time harmonic Bloch waves. The structure of these Bloch waves is determined by the eigenvalues $s^{(\pm)}$ and the eigenvectors $|\sigma_n^{(\pm)}\rangle$ of the eigenvalue problem

$$\mathbf{T}^C|\sigma_n\rangle = s|\sigma_n\rangle.$$

It turns out that we may learn a great deal about the properties of Bloch waves simply by consideration of the properties of the eigenvalue problem. That is, information about many of the interesting properties of the Bloch waves, such as the band structure of the Bloch dispersion relation, may be deduced by direct investigation of the general eigenvalue problem. The findings are valid for any periodic waveguide that is of the very general class described in the introduction.[1]

We begin by making some observations as to the general structure of the Bloch waves and the roles of the eigenvalues and eigenvectors in the determination of that structure. We then look at the equations that determine

---

[1]While this approach is very powerful (we are able to gain a great deal of information about a very general system), it is also somewhat abstract. An earlier publication of the author's (Bradley, 1991) contains a very different, less general, more explicit, and therefore more digestable treatment of the problem.

$s^{(\pm)}(\omega)$ and $|\sigma_n^{(\pm)}(\omega)\rangle$ to investigate the banded structure of these functions of frequency. The forward and backward traveling Bloch wave functions are compared and their similarities and differences noted. The multivaluedness of the Bloch wave number and the difficulties it causes in the identification of propagation direction is discussed. Finally, a new functional representation of the Bloch wave function is presented. This representation turns out to be valuable in much of the subsequent work, particularly that presented in Chapter 8 on nonlinear Bloch wave propagation.

3.1 The General Structure of the Bloch Waves

It will soon become evident that the Bloch wave functions, which we have shown are themselves composed of collections of conventional waves, exhibit distinctly wave-like behavior. For this reason it is appropriate (as well as traditional) to use the alternative expression for the eigenvalues

$$s^{(\pm)} = e^{jq^{(\pm)}h},$$

where $q^{(\pm)}$ is the (generally complex) Bloch wave number. Given such a definition, the translation relation (Eq. 2.19)

$$F^{(\pm)}(z + h) = e^{jq^{(\pm)}h} F^{(\pm)}(z),$$

appears more explicitly as a *propagation* relation. The solution of the eigenvalue problem results in (1) $s^{(\pm)}(\omega)$, from which we find $q^{(\pm)}(\omega)$, the Bloch wave dispersion relation, and (2) $|\sigma_n^{(\pm)}(\omega)\rangle$, which carries the information as to the conventional wave makeup of the Bloch wave functions.

Surprisingly, prior to the actual solution of the eigenvalue problem, several substantial observations about the qualitative nature of the solution functions may be made. Equation 2.22 shows that the Bloch wave functions are composed of collections of conventional waves. The components of $|\sigma_n\rangle$ are simply the amplitudes of these component waves in the nth cell. The state vector eigenvalue problem (Eq. 2.21) may be written

$$\begin{aligned}
\mathbf{T}^C |\sigma_n^{(\pm)}\rangle &= |\sigma_{n+1}^{(\pm)}\rangle \\
&= e^{jq^{(\pm)}h} |\sigma_n^{(\pm)}\rangle.
\end{aligned} \tag{3.1}$$

We see that the component wave amplitudes in the $n + 1^{\text{th}}$ cell are identical to those in the nth cell up to a factor of $e^{jq^{(\pm)}h}$. The factor $e^{jq^{(\pm)}h}$ represents a shift in phase (and a magnitude adjustment if $q^{(\pm)}$ is complex) of the pair of component waves. The *relative* amplitude of the component waves, however, *is constant in all cells of the structure.* This is most clearly shown by combining Eqs. 2.22 and 3.1 to express the Bloch wave function as

$$F^{(\pm)}(z) = \langle \sigma_0^{(\pm)} | e(z) \rangle e^{jnq^{(\pm)}h}, \tag{3.2}$$

where, again, n is the cell number associated with z. The Bloch wave is simply composed of a string of essentially identical compound wave fields. The eigenvalue $s^{(\pm)}$ (or equivalently, $q^{(\pm)}$) accounts for the cell-to-cell structure or *macrostructure* of the Bloch waves, and the eigenvector $|\sigma_0^{(\pm)}\rangle$ accounts for the structure *within* the cell, the *microstructure* of the Bloch waves. It may be anticipated at this point that a parameter that characterizes the (complex) relative amplitude of the component waves will serve as a useful characterization of the Bloch wave microstructure.

3.2 The Eigenvalues and Bloch Wave Dispersion

In this section we consider the eigenvalues of Eq. 2.21 and the characteristics of the resultant Bloch dispersion relation. Various features of the banded structure of the dispersion relation are derived directly from the eigenvalue problem. In addition to the usual Bragg stopbands, a new species of stopband associated with resonance of the scatterer is identified. Measurements of Bloch wave dispersion made in both isotropic and anisotropic periodic side branch waveguides is found to verify the theoretical findings.

3.2.1 The Bloch Dispersion Relation

To find an expression for the Bloch wave numbers (i.e., a Bloch dispersion relation), the characteristic equation for the eigenvalues must be solved:

$$\begin{vmatrix} T_{11}^{\text{C}} - s & T_{12}^{\text{C}} \\ T_{21}^{\text{C}} & T_{22}^{\text{C}} - s \end{vmatrix} = s^2 - s(T_{11}^{\text{C}} + T_{22}^{\text{C}}) + |T^{\text{C}}| = 0. \tag{3.3}$$

The two solutions $s^{(+)}$ and $s^{(-)}$ of the quadratic characteristic equation are the eigenvalues associated with $F^{(+)}(z)$ and $F^{(-)}(z)$, respectively. If it is assumed that $s^{(+)}$ is a solution, then it follows that $s^{(-)} = |T^C|/s^{(+)}$ is the second solution. According to the principle of reciprocity, however, $|T^C| = 1$ (see Appendix B), and the two eigenvalues are $s^{(+)}$ and $s^{(-)} = 1/s^{(+)}$. The Bloch wave numbers, therefore, are simply $q^{(+)}$ and $q^{(-)} = -q^{(+)} + 2\pi m/h$, where m is an integer. We now define $q = q^{(+)}$ and the translation relations become[2]

$$F^{(\pm)}(z + h) = e^{\pm jqh} F^{(\pm)}(z). \tag{3.4}$$

We see that the two Bloch wave functions have the form of a forward and a backward traveling wave, both of (generally complex) spatial frequency q. In other words, *reciprocity disallows birefringence*.[3] Although the system is generally anisotropic as the scatterers are generally asymmetric, in terms of q, the Bloch wave functions are symmetric. The advance in phase and decrease in amplitude that occurs in the $+z$ direction for the $(+)$ Bloch wave is identical to those that occur in the $-z$ dirction for the $(-)$ Bloch wave. In other words, in terms of the macrostructure, the forward and backward traveling Bloch waves are identical.

The usual form of the Bloch dispersion relation is found by first rewriting the characteristic equation as $s + 1/s = T^C_{11} + T^C_{22}$, and then substituting e^{jqh} for s to find

$$\cos(qh) = \frac{1}{2}(T^C_{11} + T^C_{22}). \tag{3.5}$$

This is the Bloch dispersion relation. Recall that the elements of $\mathbf{T}^C$ are associated with propagation across the entire cell and not just past the scatterer. The elements of $\mathbf{T}^C$ (and therefore q) will therefore depend upon frequency in two distinct ways: (1) through waveguide propagation factors containing $k(\omega)$, and (2) through the frequency dependence of the scatterer. The Bloch wave

---

[2]Note that we have made no decision yet as to *which* of the two values of q is to be called $q^{(+)}$ and which is to be called $q^{(-)}$.

[3]In a one-dimensional birefringent wave system, the wave numbers for the forward and backward traveling waves are not related simply by $k^{(-)} = -k^{(+)}$, as they are for most wave systems (e.g., Jackson, 1975).

number therefore has both a direct and a nested dependence upon frequency: $q = q[k(\omega), \omega]$.

The structure of the dispersion relation is most simply investigated by the consideration of a nondissipative system. In such a case we have $T_{22}^{\mathrm{C}} = T_{11}^{\mathrm{C}*}$ (see Appendix B), and the Bloch dispersion relation becomes simply

$$\cos(qh) = \mathrm{Re}\{T_{11}^{\mathrm{C}}\} = \gamma(\omega). \tag{3.6}$$

Because Eq. 3.6 is real, the inverse cosine function involved in the evaluation of q may be broken into parts:

$$qh = \begin{cases} n_{\mathrm{e}}\pi \pm j\cosh^{-1}(\gamma) & \gamma > 1 \\ \pm \cos^{-1}(\gamma) & -1 \leq \gamma \leq 1 \\ n_{\mathrm{o}}\pi \pm j\cosh^{-1}(|\gamma|) & \gamma < -1 \end{cases}, \tag{3.7}$$

where n_{e} and n_{o} are even and odd integers, respectively. The multivaluedness of q is addressed later; the point of interest here is that for $|\mathrm{Re}\{T_{11}^{\mathrm{C}}\}| \leq 1$, q is real and for $|\mathrm{Re}\{T_{11}^{\mathrm{C}}\}| > 1$ q is complex. The spectral regions in which q is real are associated with propagating Bloch waves and are known as passbands. The intervening spectral regions, in which q is complex, are associated with exponentially attenuated Bloch waves and are referred to as stopbands.

A great deal may be learned about the band structure of the dispersion relation by considering the case wherein the scattering is caused by a reactive shunt load of acoustic impedance jX_{La} in an otherwise uniform waveguide of acoustic impedance $Z_{0\mathrm{a}} = \rho_0 c_0 / A_{\mathrm{wg}}$, where A_{wg} is the cross-sectional area of the waveguide. In such a case, $T_{11}^{\mathrm{C}} = (1 + \frac{1}{2}jZ_{0\mathrm{a}}/X_{\mathrm{La}})e^{jkh}$ and the Bloch dispersion relation becomes

$$\cos(qh) = \cos(kh) - \frac{1}{2}\frac{Z_{0\mathrm{a}}}{X_{\mathrm{La}}}\sin(kh). \tag{3.8}$$

In this form we see that there are two conditions under which a stopband is likely occur:

- When the frequency is such that $kh \simeq n\pi$. Because $\cos(n\pi) = (-1)^n$, the magnitude of the right-hand side of Eq. 3.8 is likely to exceed unity, which is the stopband condition. As this set of frequencies are those that satisfy the Bragg condition, these stopbands are referred to as Bragg stopbands, the nth of which is called the "$n\pi$" stopband.

- When the frequency is at or near a resonance frequency of the load. In such a case the load reactance goes to zero and the magnitude of the right-hand side of Eq. 3.8 exceeds unity, causing a stopband. These stopbands are referred to here as scatterer resonance stopbands.

In the Bragg stopbands, the magnitude of the right-hand side of Eq. 3.8 exceeds unity but does not change signs. It therefore follows (see Eq. 3.7) that the following are characteristic of Bragg stopbands:

$$\text{Re}\{qh\} = \text{constant} = n\pi \qquad \text{and} \qquad |\text{Im}\{qh\}| > 0 \quad \text{(but finite)}.$$

In the scatterer resonance stopbands, the right-hand side of Eq. 3.8 diverges to infinity and flips sign at $\omega = \omega_r$, the scatterer resonance frequency. It therefore follows (see Eq. 3.7) that it is characteristic of scatterer resonance stopbands that $\text{Re}\{qh\}$ is discontinuous at the resonance frequency:

$$\lim_{\omega \to \omega_r^+} \text{Re}\{qh\} = n_e\pi \qquad \text{and} \qquad \lim_{\omega \to \omega_r^-} \text{Re}\{qh\} = n_o\pi$$

or

$$\lim_{\omega \to \omega_r^+} \text{Re}\{qh\} = n_o\pi \qquad \text{and} \qquad \lim_{\omega \to \omega_r^-} \text{Re}\{qh\} = n_e\pi,$$

where n_e is an even integer, n_o is an odd integer, and the limit $\lim_{\omega \to \omega_r^\pm}$ denotes the approach to the resonance frequency from the $\pm$ side. It also follows that, at the scatterer resonance frequency,

$$\lim_{\omega \to \omega_r} |\text{Im}\{qh\}| \to \infty.$$

In the dissipative case the right-hand side of Eq. 3.5, and therefore q as well, is generally complex at all frequencies. In other words, the imaginary part of the Bloch wave number becomes, owing to the effects of dissipation, nonzero in the passbands as well as in the stopbands. Unless the dissipation is very large, such as when the characteristic length associated with dissipation in the uniform waveguide is small compared to the structure periodicity ($1/\text{Im}\{k\} \ll h$), the band structure is evident in the dispersion.

3.2.2 The Periodic side branch Waveguides

The Bloch dispersion relation for a particular periodic waveguide is found by substituting the expressions for the elements of the cell T-matrix into Eq. 3.5. The cell T-matrix elements associated with scattering by a side branch are derived in Appendix D (see Eq. D.2). The substitution of these expressions into Eq. 3.5 yields

$$\cos(qh) = \cos(kh) - \frac{A_{\text{sb}}}{2A_{\text{wg}}} \tan(k_{\text{sb}}\hat{d}) \sin(kh), \tag{3.9}$$

where k_{sb} is the wave number associated with the waves in the side branch and $\hat{d}$ is the end-corrected side branch depth (see Appendix D). Equation 3.9 is the Bloch dispersion relation for the isotropic periodic side branch waveguide. In Fig. 3.1 is shown a plot of this Bloch dispersion relation for the nondissipative case. As predicted, Bragg stopbands occur at $\omega h/c_0 = \pi$ and $\omega h/c_0 = 2\pi$ and a scatterer resonance stopband occurs at the resonance frequency of the side branch, as indicated in the column on the right margin of the figure. In addition, it is clear that the real part of q is discontinuous and the imaginary part of q singular at the resonance frequency of the scatterer. Also included in Fig. 3.1 is the dispersion curve for the dissipative case. As might be expected, the dissipation tends to smooth out the sharply cusped features that occur at the boundaries of the stopbands and at the scatterer resonance frequency. The real part of q is no longer discontinuous and the imaginary part of q is no longer singular at the scatterer resonance frequency.

The measurement of the Bloch wave dispersion for the isotropic periodic side branch waveguide is outlined as follows. The real part of q is measured by monitoring the phase of the Bloch wave (at the cell centers) as a function of distance, and the imaginary part of q is measured by monitoring the amplitude (also at the cell centers) as a function of distance. Recall that the Bloch wave, when sampled only at intervals of h, is indistinguishable from a conventional wave of wave number q. As is true of conventional waves, therefore, the rate of increase of phase with distance is $\text{Re}\{q\}$, and the rate of decrease of the (log) amplitude with distance is $\text{Im}\{q\}$. The amplitude and phase of the acoustic pressure field was detected at 22 cell centers along the waveguide for 455 frequencies between 200 Hz and 4.0 kHz. The rate of increase of the phase and
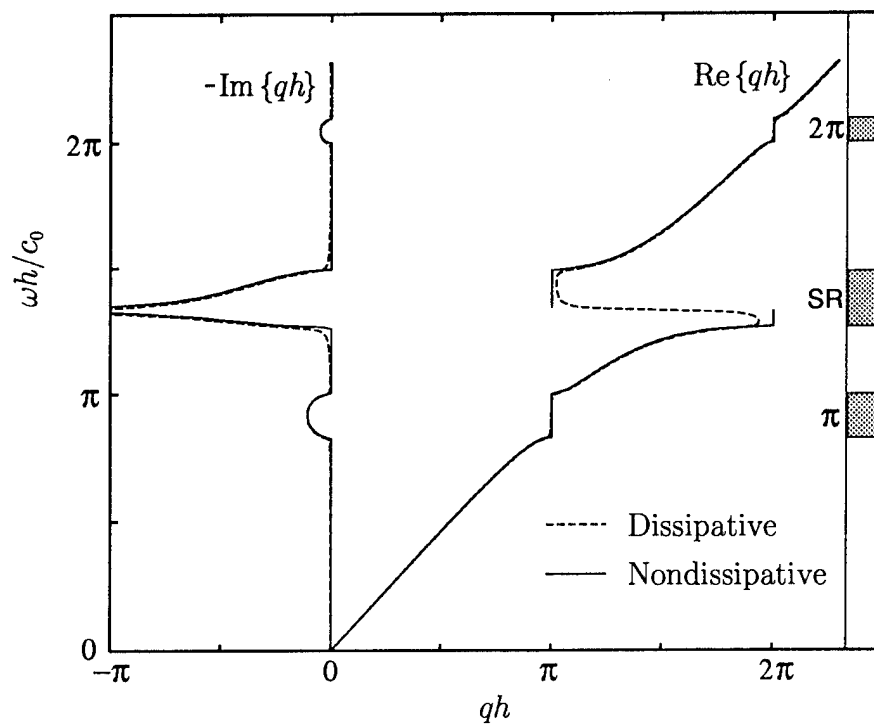
Figure 3.1: The Bloch dispersion for the isotropic periodic side branch waveguide. The π and 2π Bragg stopbands and the scatterer resonance stopband (SR) are so indicated in the column on the right margin.

the rate of decrease of the (log) amplitude were found by performing linear regressions of the set of field measurements for each frequency. The details of the measurements are discussed in Appendix E.

Figures 3.2 and 3.3 show the experimental values of the Bloch wave number for the isotropic periodic waveguide as compared to values from the dissipative theory. Both the real and imaginary parts of the Bloch wave number show very good agreement with the theory. The features of the π and 2π Bragg stopbands and the first scatterer resonance stopband are clearly evident in the measurements. The predicted characteristics of the scatterer resonance stopband, most notably the sharply spiked Im$\{q\}$ and the nearly discontinuous Re$\{q\}$, are verified. Figure 3.4 shows the theoretical and experimental values of the imaginary part of the Bloch wave number on an expanded scale. That the dissipative theory predicts the nonzero passband value of the attenuation very well serves to support the theoretical postulate that the Bloch wave formalism holds in the presence of dissipation. The nondissipative theory, on the other hand, predicts zero passband attenuation.

While the dispersion measurement in the isotropic periodic side branch waveguide consisted of the measurement of only a single Bloch wave number, in the anisotropic waveguide we must measure two (both $q^{(+)}$ and $q^{(-)}$). In this way we are able to experimentally verify the theoretical finding that $q^{(-)} = -q^{(+)}$. We must therefore measure the dispersion in the waveguide with one orientation, and then repeat the measurement with the waveguide reversed. The details of this measurement are outlined in Appendix E.

The measured values of the wave numbers for both the forward and the backward traveling Bloch waves in the anisotropic periodic waveguide are shown in Fig. 3.5. Included in the plots are the values from the dissipative theory. It should be noted that we have plotted $-q^{(-)}$ instead of $q^{(-)}$ for the sake of comparison with $q^{(+)}$. The agreement between theory and experiment is quite good except at the high frequency end of the measurement range, where the theoretical and experimental curves diverge. It is believed that the divergence is due to our inability to accurately predict the frequencies of the scatterer resonance stopbands. A scatterer resonance stopband is predicted to occur at a frequency near 2.0 kHz, just beyond the high frequency end of the range of measurements shown in Fig. 3.5. The measurements show
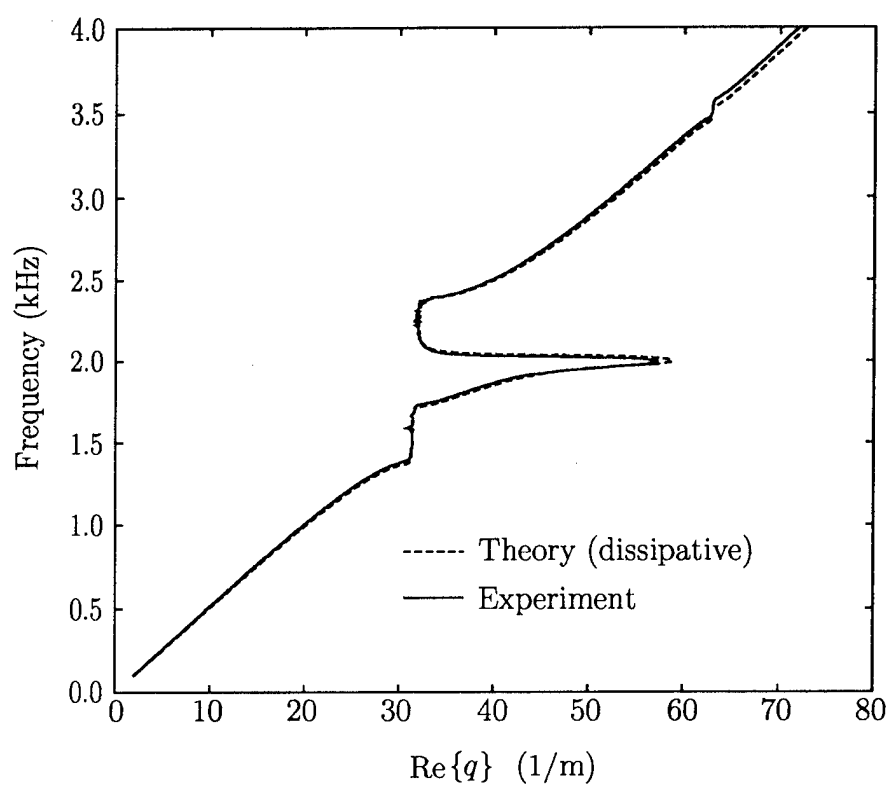
Figure 3.2: Theoretical and experimental values of the real part of the Bloch wave number for the isotropic periodic side branch waveguide. The theoretical values are from the dissipative theory.
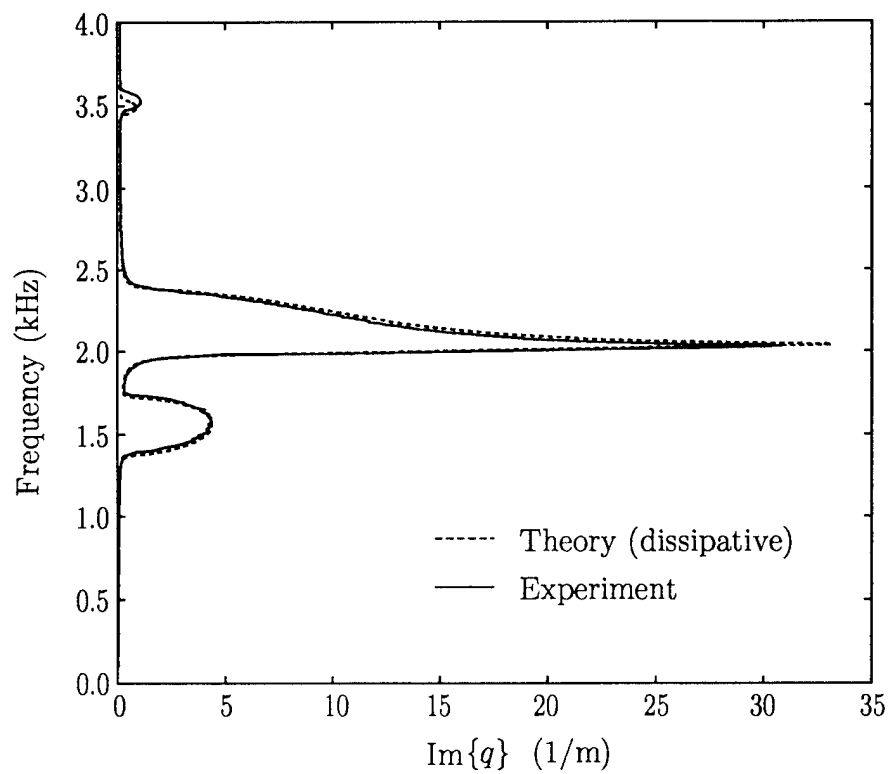
Figure 3.3: Theoretical and experimental values of the imaginary part of the Bloch wave number for the isotropic periodic side branch waveguide. The theoretical values are from the dissipative theory.
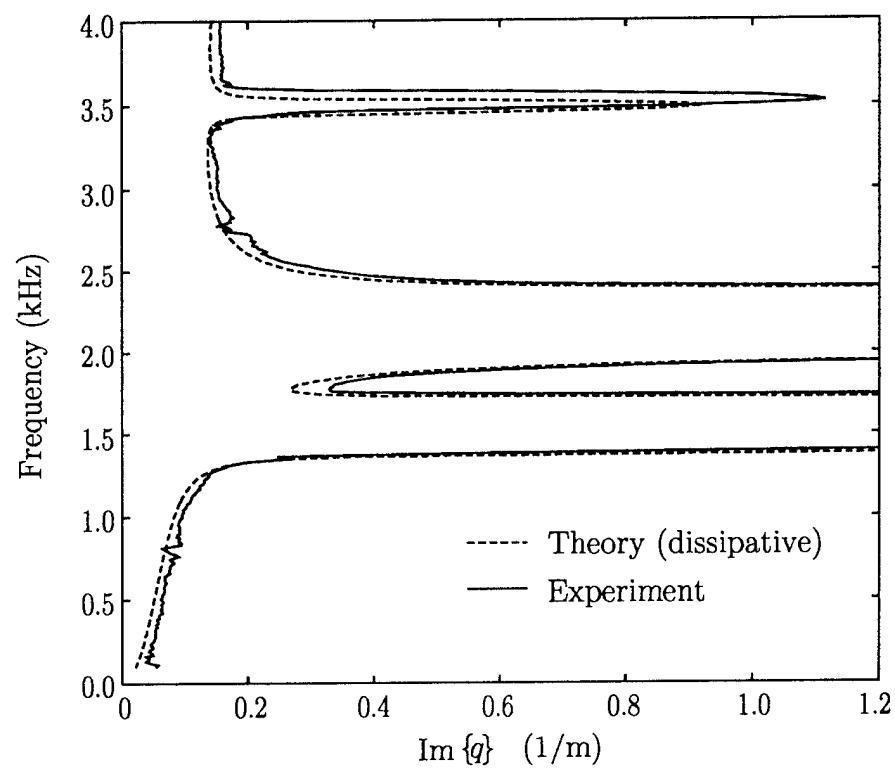
Figure 3.4: Experimental values of the imaginary part of the Bloch wave number for the isotropic periodic side branch waveguide on an expanded scale (this data is also shown in Fig. 3.3). Also included are values from the dissipative theory.
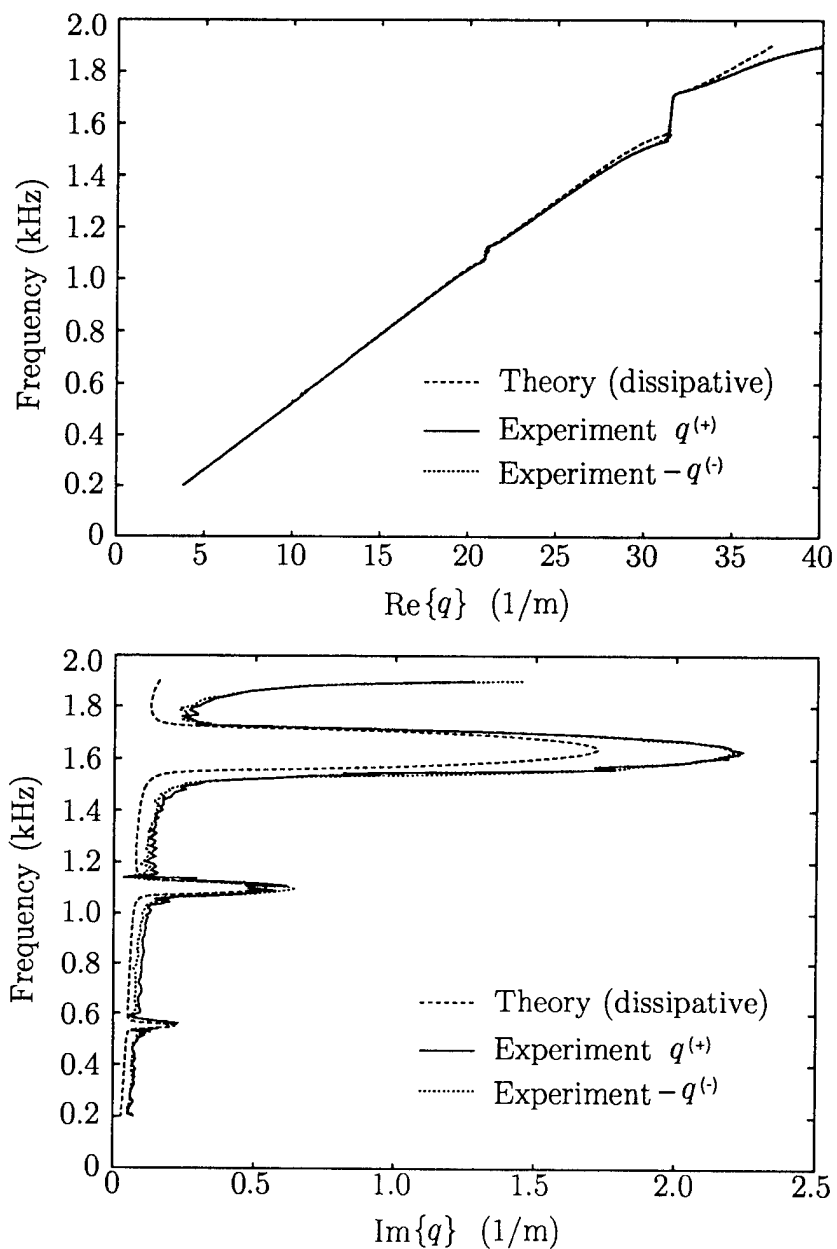
Figure 3.5: Experimental values of the Bloch wave number for both forward and backward traveling Bloch waves in the anisotropic periodic side branch waveguide. Also included are values from the dissipative theory, for which $q^{(-)} = -q^{(+)}$.
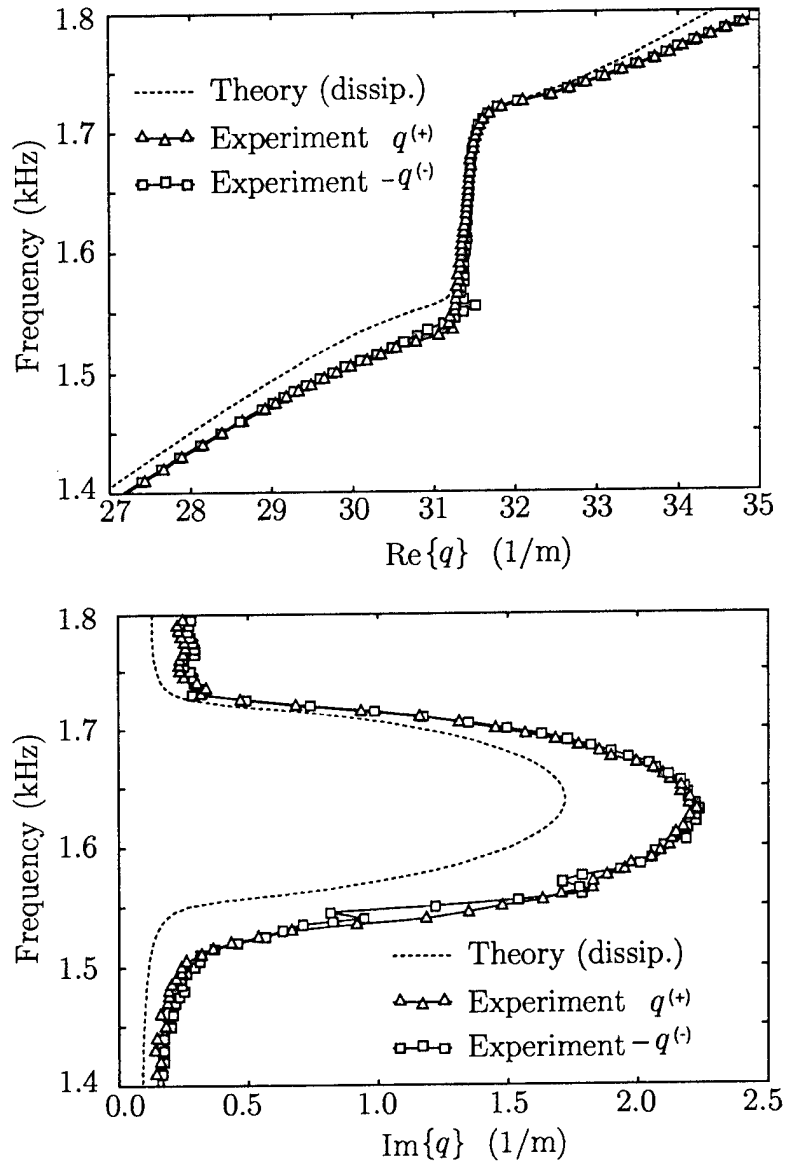
Figure 3.6: The theoretical and experimental values of $q^{(+)}$ and $q^{(-)}$ shown in Fig. 3.5 expanded about the 3π stopband. The theoretical values are from the dissipative theory.

marked increases in both the real and the imaginary parts of the Bloch wave number as the frequency approaches 2.0 kHz, where the theory predicts more gradual increases. Evidently, the theory predicts the frequency of occurence of the scatterer resonance stopband to be higher than what the measurements indicate. This may be due to the use of the circular tube end correction to approximate the effective depth of the side branches (see Appendix D).

Although the agreement between the theoretical and the measured values of the Bloch wave number is not as good as it is for the isotropic waveguide, it appears quite conclusively that the measured values of $q^{(+)}$ and $-q^{(-)}$ are equal. Figure 3.6, which shows the data from Fig. 3.5 on a scale expanded about the 3π stopband, serves to support this conclusion. The measurements therefore support the theoretical prediction that, even for an anisotropic waveguide, the forward and backward traveling Bloch wave numbers are related by $q^{(-)} = -q^{(+)}$.

3.3 The Eigenvectors and the Component Wave Structure of the Bloch Waves

In this section we consider the eigenvectors of Eq. 2.21 and the characteristics of the resultant conventional wave structure of the Bloch waves. As in the case of the Bloch dispersion relation, various features of the component wave structure may be derived directly from the eigenvalue problem. Measurements of the component wave amplitudes made in both isotropic and anisotropic periodic waveguides are shown and found to verify the theoretical findings.

3.3.1 The Bloch Wave Parameter g/f

It was pointed out earlier that the eigenvectors are the source of information as to the conventional wave makeup of the Bloch wave function. Because the relative amplitude of the component waves is identical in each cell of the structure (see Eq. 3.2), we need only find the eigenvector associated with

a single cell. The eigenvalue problem for the zeroth cell is

$$
\begin{bmatrix} T_{11}^{\mathrm{C}} - s & T_{12}^{\mathrm{C}} \\ T_{21}^{\mathrm{C}} & T_{22}^{\mathrm{C}} - s \end{bmatrix} \begin{bmatrix} \sigma_{01} \\ \sigma_{02} \end{bmatrix} = \begin{bmatrix} 0 \\ 0 \end{bmatrix}, \quad \text{where} \quad |\sigma_0\rangle = \begin{bmatrix} \sigma_{01} \\ \sigma_{02} \end{bmatrix}. \tag{3.10}
$$

Because the eigenvector has two components it is simply characterized, up to an arbitrary constant, by the ratio σ_{02}/σ_{01}. From Eq. 3.10 we find that the equation that determines σ_{02}/σ_{01} may be written

$$
T_{12}^{\mathrm{C}}(\sigma_{02}/\sigma_{01})^2 + (T_{11}^{\mathrm{C}} - T_{22}^{\mathrm{C}})(\sigma_{02}/\sigma_{01}) - T_{21}^{\mathrm{C}} = 0. \tag{3.11}
$$

Equation 3.11 characterizes the eigenvectors and therefore the conventional wave structure of the Bloch wave. For this reason Eq. 3.11 is referred to as the microstructure equation (see the discussion following Eq. 3.2).

We may now proceed as we did in the investigation of the properties of the Bloch wave numbers. The two solutions of the quadratic microstructure equation are labeled $(\sigma_{02}/\sigma_{01})^{(+)}$ and $(\sigma_{02}/\sigma_{01})^{(-)}$. One substantial relationship between these two solutions may be found right away. If it is found that $(\sigma_{02}/\sigma_{01})^{(+)}$ is one solution, then it follows that

$$
(\sigma_{02}/\sigma_{01})^{(-)} = \left[(-T_{12}^{\mathrm{C}}/T_{21}^{\mathrm{C}})(\sigma_{02}/\sigma_{01})^{(+)} \right]^{-1} \tag{3.12}
$$

is the second solution.

As in the case of the Bloch wave dispersion, it is most straightforward to further investigate the characteristics of $\sigma_{02}/\sigma_{01}^{(\pm)}$ by consideration of the nondissipative case. In the absence of dissipation we have $T_{21}^{\mathrm{C}} = T_{12}^{\mathrm{C*}}$ and $T_{22}^{\mathrm{C}} = T_{11}^{\mathrm{C*}}$ (see Appendix B), and Eq. 3.11 becomes

$$
T_{12}^{\mathrm{C}}(\sigma_{02}/\sigma_{01})^2 + 2j\mathrm{Im}\{T_{11}^{\mathrm{C}}\}(\sigma_{02}/\sigma_{01}) - T_{21}^{\mathrm{C*}} = 0.
$$

The two solutions of this equation are simply

$$
\sigma_{02}/\sigma_{01}^{(\pm)} = \frac{-j\mathrm{Im}\{T_{11}^{C}\} \mp \left[|T_{12}^{C}|^2 - \mathrm{Im}\{T_{11}^{C}\}^2 \right]^{1/2}}{T_{12}^{C}}. \tag{3.13}
$$

The reasoning behind the choice of labels is made clear in Sec. 3.4. It was pointed out in the discussion that follows Eq. 3.7 that the condition for the

occurrence of a stopband is $|\mathrm{Re}\{T_{11}^C\}| > 1$. From the conservation of energy we have $\mathrm{Re}\{T_{11}^C\}^2 - 1 = |T_{12}^C|^2 - \mathrm{Im}\{T_{11}^C\}^2$ (see Appendix B), and the stopband condition may be expressed $|T_{12}^C|^2 - \mathrm{Im}\{T_{11}^C\}^2 > 0$. In the stopbands, therefore, the argument of the square root in Eq. 3.13 is positive and real, and the magnitude of that equation becomes simply

$$|\sigma_{02}/\sigma_{01}^{(\pm)}| = 1. \tag{3.14}$$

In the passbands, the argument of the square root is negative and real, and the magnitude of Eq. 3.13 is

$$|\sigma_{02}/\sigma_{01}^{(\pm)}| = \frac{|\mathrm{Im}\{T_{11}^C\}|}{|T_{12}^C|}\left[1 \mp \left(1 - \frac{|T_{12}^C|^2}{\mathrm{Im}\{T_{11}^C\}^2}\right)^{1/2}\right]. \tag{3.15}$$

From the stopband condition, we have $0 \leq |T_{12}^C|/|\mathrm{Im}\{T_{11}^C\}| \leq 1$, and therefore

$$0 \leq \left(1 - \frac{|T_{12}^C|^2}{\mathrm{Im}\{T_{11}^C\}^2}\right)^{1/2} \leq 1 \tag{3.16}$$

in the passbands. From Eq. 3.15 and the passband condition (Eq. 3.16), it follows that in the passbands

$$|\sigma_{02}/\sigma_{01}^{(-)}| > 1 \qquad \text{and} \qquad |\sigma_{02}/\sigma_{01}^{(+)}| < 1. \tag{3.17}$$

Note that the labeling is such that energy is transported in the $+z$ direction by the $(+)$ Bloch wave and in the $-z$ direction by the $(-)$ Bloch wave.

Another passband relationship between $\sigma_{02}/\sigma_{01}^{(+)}$ and $\sigma_{02}/\sigma_{01}^{(-)}$ may be found by consideration of Eq. 3.13. In the passband we have

$$\sigma_{02}/\sigma_{01}^{(\pm)} = \frac{-j\mathrm{Im}\{T_{11}^C\} \mp j\left[\mathrm{Im}\{T_{11}^C\}^2 - |T_{12}^C|^2\right]^{1/2}}{T_{12}^C}, \tag{3.18}$$

where the argument of the square root is real and positive. Using the relations $\sigma_{02}/\sigma_{01}^{(-)} = [-(T_{12}^C/T_{21}^C)\sigma_{02}/\sigma_{01}^{(+)}]^{-1}$ (from the discussion following Eq. 3.11) and $T_{21}^C = T_{12}^{C*}$ (from Appendix B), we find

$$\sigma_{02}/\sigma_{01}^{(-)} = \frac{T_{12}^{C*}}{j\mathrm{Im}\{T_{11}^C\} + j\left[\mathrm{Im}\{T_{11}^C\}^2 - |T_{12}^C|^2\right]^{1/2}}. \tag{3.19}$$

The multiplication of the (+) case of Eq. 3.18 and the complex conjugate of Eq. 3.19 verifies that

$$[\sigma_{02}/\sigma_{01}^{(+)}][\sigma_{02}/\sigma_{01}^{(-)*}] = 1. \tag{3.20}$$

In order to simplify comparisons between the two Bloch wave functions, we redefine the components of the eigenvectors:

$$|\sigma_0^{(+)}\rangle = \begin{bmatrix} f^{(+)} \\ g^{(+)} \end{bmatrix} \qquad |\sigma_0^{(-)}\rangle = \begin{bmatrix} g^{(-)} \\ f^{(-)} \end{bmatrix}. \tag{3.21}$$

From Eqs. 3.2 and 3.4, the Bloch wave functions are then

$$F^{(\pm)}(z) = (f^{(\pm)}e^{\pm jk(z-nh)} + g^{(\pm)}e^{\mp jk(z-nh)})e^{\pm jnqh}, \tag{3.22}$$

where n is the cell number associated with z. A schematic representation of the two Bloch waves in terms of their component wave makeup is shown in Fig. 3.7. The component wave that travels in the direction of propagation of the Bloch wave is here termed the "f-wave" and the other the "g-wave". Given these definitions, we have the relations

$$g/f^{(+)} = \sigma_{02}/\sigma_{01}^{(+)} \quad \text{and} \quad g/f^{(-)} = [\sigma_{02}/\sigma_{01}^{(-)}]^{-1}, \tag{3.23}$$

which, together with Eq. 3.12, lead to the relation

$$(g/f)^{(-)} = (-T_{12}^{C}/T_{21}^{C})(g/f)^{(+)} \quad . \tag{3.24}$$

The f-wave/g-wave makeup is *different for the two Bloch waves*. Recall that in terms of q, which accounts for the cell-to-cell or macrostructure of the Bloch waves, the Bloch waves are symmetric. Here, however, we see that in terms of g/f, which accounts for the Bloch wave structure within the cell, the Bloch waves are generally *asymmetric*: $g/f^{(-)} \neq g/f^{(+)}$. *The macrostructure of the Bloch waves is symmetric yet the microstructure is generally asymmetric.* Note that if the waveguide is isotropic, then $-T_{12}^{C}/T_{21}^{C} = 1$ (see Appendix B) and we have $g/f^{(-)} = g/f^{(+)}$: the two Bloch waves are simply reversed copies of one another, as they must be due to the axial reversal invariance of the waveguide. In the absence of dissipation we have $T_{21}^{C*} = T_{12}^{C}$ (see Appendix B), from which it follows that $|g/f^{(-)}| = |g/f^{(+)}|$ (see Eq. 3.24). In terms of the magnitude of g/f, the Bloch waves are symmetric. The *phase* of g/f, however, is generally
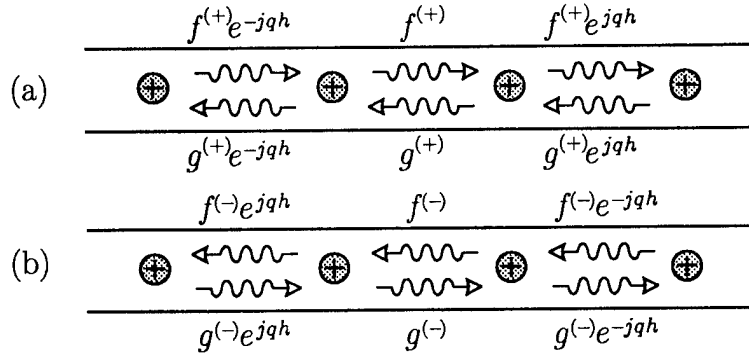
Figure 3.7: The f-wave/g-wave composition of (a) the forward traveling and (b) the backward traveling Bloch wave function.

different for the two Bloch waves. In other words, the Bloch wave asymmetry is manifest primarily in the *phase* of the microstructure. It is possible, in the dissipative case, that there be a *degree* of asymmetry in the magnitude of the microstructure, but generally very little.

The passband/stopband characteristics of $g/f^{(\pm)}$ may be found by consideration of those found for $\sigma_{02}/\sigma_{01}^{(\pm)}$. From Eqs. 3.14, 3.24 and the fact that $T_{21}^{C*} = T_{12}^{C}$ (see Appendix B), it is found that in the stopbands

$$|g/f^{(\pm)}| = 1.$$

In the stopbands, the f and g waves have equal magnitude; there is a *resonant, standing wave* condition and no net energy is transported. From Eqs. 3.17, 3.24 and the fact that $T_{21}^{C*} = T_{12}^{C}$ (see Appendix B), it is found that in the passbands

$$|g/f^{(\pm)}| < 1.$$

In the passbands the amplitude of the f-wave is larger than that of the g-wave. The component wave of larger amplitude propagates in the direction of propagation of the Bloch wave. It therefore follows that at passband frequencies energy is transported in the direction of propagation of the Bloch wave, as we might expect. The relation Eq. 3.20 also implies that in the passband

$$g/f^{(-)} = g/f^{(+)*}. \tag{3.25}$$

As was already pointed out, if the waveguide is isotropic as well as nondissipative, then $g/f^{(-)} = g/f^{(+)}$, and Eq. 3.25 implies $\text{Im}\{g/f^{(\pm)}\} = 0$. In other words, for an isotropic waveguide, we have the passband condition

$$\angle g/f = n\pi,$$

where $\angle$ denotes the phase.

3.3.2 The Periodic Side Branch Waveguides

In principle, an expression for g/f for a particular periodic waveguide is found by substituting the expressions for the elements of the cell T-matrix into Eq. 3.11, solving that quadratic and, by way of Eq. 3.23, converting the resultant expression for σ_{02}/σ_{01} into an expression for g/f. In practice, however, it is frequently less work to obtain the values of g/f from the expression for the Bloch acoustic impedance (see Sec. 4.1). The Bloch acoustic impedance, which is simply the acoustic impedance at the cell centers, may be found from Eq. 4.2. Equation 4.1 may be inverted to find an expression for g/f in terms of the Bloch acoustic impedance, for which we have an explicit expression. For the isotropic periodic side branch waveguide, for example, this approach yields an explicit expression for g/f:

$$
\begin{aligned}
g/f = {} & \left\{ \left[\frac{1}{2}(A_{\text{sb}}/A_{\text{wg}}) \tan(k_{\text{sb}}\hat{d})[\cos(kh) - 1] + \sin(kh) \right]^{1/2} \right. \\
& \left. - \left[\frac{1}{2}(A_{\text{sb}}/A_{\text{wg}}) \tan(k_{\text{sb}}\hat{d})[\cos(kh) + 1] + \sin(kh) \right]^{1/2} \right\} \\
& \div \left\{ \left[\frac{1}{2}(A_{\text{sb}}/A_{\text{wg}}) \tan(k_{\text{sb}}\hat{d})[\cos(kh) - 1] + \sin(kh) \right]^{1/2} \right. \\
& \left. + \left[\frac{1}{2}(A_{\text{sb}}/A_{\text{wg}}) \tan(k_{\text{sb}}\hat{d})[\cos(kh) + 1] + \sin(kh) \right]^{1/2} \right\} . \quad (3.26)
\end{aligned}
$$

For the anisotropic periodic side branch waveguide, however, values of $g/f^{(\pm)}$ must be obtained by way of Eqs. 3.11 and 3.23.

Each of the features of the parameter g/f outlined earlier is seen clearly in Figs. 3.8 and 3.9 for the isotropic and anisotropic periodic side branch
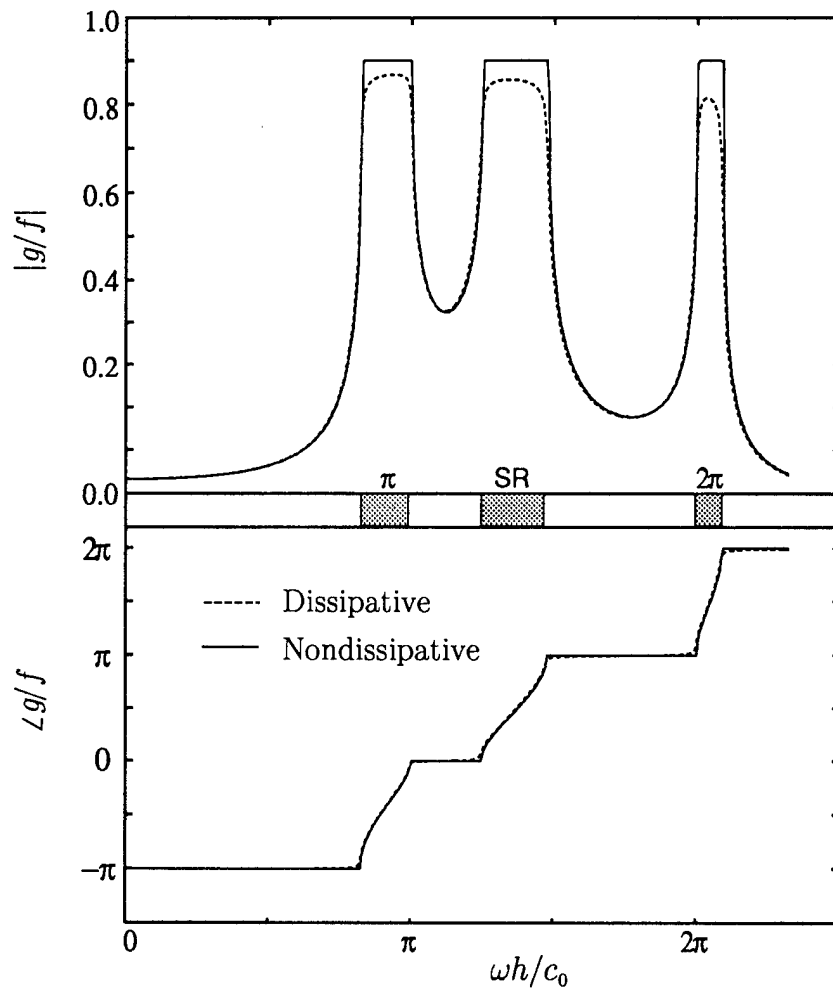
Figure 3.8: Theoretical values of the magnitude and phase of g/f for the isotropic periodic waveguide. The π and 2π Bragg stopbands and the scatterer resonance (SR) stopband are so indicated.
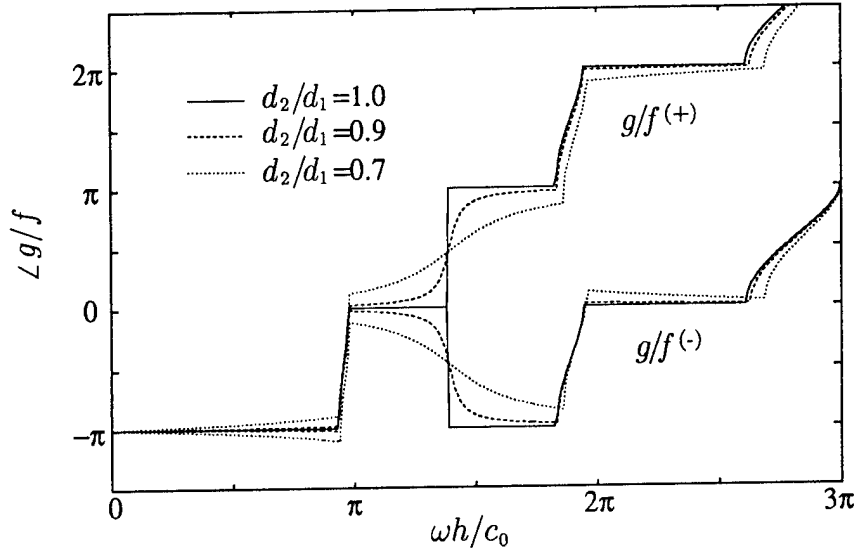
Figure 3.9: Theoretical values (from the nondissipative theory) of the phase of $g/f^{(+)}$ and $g/f^{(-)}$ for the anisotropic periodic side branch waveguide with three degrees of anisotropy. In the $d_2/d_1 = 1.0$ case, the waveguide is isotropic, and as d_2/d_1 decreases it becomes increasingly anisotropic (see Fig. 1.3(b)).

AS-94-732

waveguides. In the case of the nondissipative isotropic waveguide, Fig. 3.8 shows clearly that in the stopbands $|g/f| = 1$, and in the passbands $|g/f| < 1$ and $\angle g/f = n\pi$. As is the case for the dispersion curve, when dissipation is included the sharply cusped features are smoothed. Figure 3.9 shows $\angle g/f^{(\pm)}$ (according to the nondissipative theory) for the anisotropic waveguide with three different degrees of anisotropy.[4] When $d_1/d_2 = 1$, the waveguide is isotropic and $\angle g/f^{(\pm)} = n\pi$ in the stopbands, as we expect for an isotropic periodic waveguide in the absence of dissipation. Note also that $\angle g/f^{(+)} = \angle g/f^{(-)}$. When the waveguide becomes anisotropic, (the $d_1/d_2 = 0.9$ and $d_1/d_2 = 0.7$ cases), the phases of $g/f^{(+)}$ and $g/f^{(-)}$ differ, and in the passbands are split symmetrically about zero phase (in other words, $g/f^{(-)} = g/f^{(+)*}$).

The relative component wave amplitude g/f was measured in both

---

[4]The degree of anisotropy for the anisotropic periodic side branch waveguide may be adjusted by varying d_1, the depth of the shallower of the two side branches (see Fig. 1.3(b)).

the isotropic and anisotropic periodic side branch waveguides. In order to obtain enough information to resolve the relative amplitude and phase of the components of a compound wave field, measurements of the field must be taken at two or more different locations. In order to measure the relative component wave amplitude, therefore, the Bloch wave field was measured at two points in each cell. The details of this measurement are described in Appendix E.

In Fig. 3.10 is shown the theoretical and experimental values of $|g/f|$ and $\angle g/f$ for the isotropic periodic waveguide. Both the magnitude and the phase of the relative component wave amplitude show very good agreement with the dissipative theory. The predicted resonant, standing wave behavior of the component waves in the stopbands is verified by the nearly unit measured values of $|g/f|$. Likewise, the predicted nearly constant phase of g/f in the passbands is clearly evident (the nondissipative theory predicts *exactly* constant phase in the passband). Figures 3.11 and 3.12 show the real and imaginary parts, respectively, of $g/f^{(\pm)}$ for the anisotropic waveguide. The real and imaginary parts are shown instead of the magnitude and phase because there are spans of frequency in which $\mathrm{Im}\{g/f^{(\pm)}\} \simeq 0$. Any small jitter in the value of $\mathrm{Im}\{g/f^{(\pm)}\}$ in these ranges becomes artificially large jitter in the associated values of the phase. The agreement between theory and experiment is again quite good except at the high frequency end of the measurement range. As was found in the dispersion measurements, the theory evidently predicts the occurrence of the next stopband at a higher frequency than that at which it actually occurs. In Fig. 3.13 is shown the real parts of $g/f^{(+)}$ and $g/f^{(-)}$ and the imaginary parts of $g/f^{(+)}$ and $-g/f^{(-)}$ (both theoretical and experimental) on scales expanded about the 2π stopband. Clearly $g/f^{(+)}$ and $g/f^{(-)}$ are not equal (particularly in the stopbands), which indicates that the effect of anisotropy is present in the Bloch wave microstructure, as predicted. In the nondissipative theory, it was found that $g/f^{(+)} = g/f^{(-)*}$ in the passbands. Figure 3.13 shows that, as we expect of a mildly dissipative system, this is very nearly true: $\mathrm{Re}\{g/f^{(+)}\} \simeq \mathrm{Re}\{g/f^{(-)}\}$ and $\mathrm{Im}\{g/f^{(+)}\} \simeq -\mathrm{Im}\{g/f^{(-)}\}$ in the passbands.
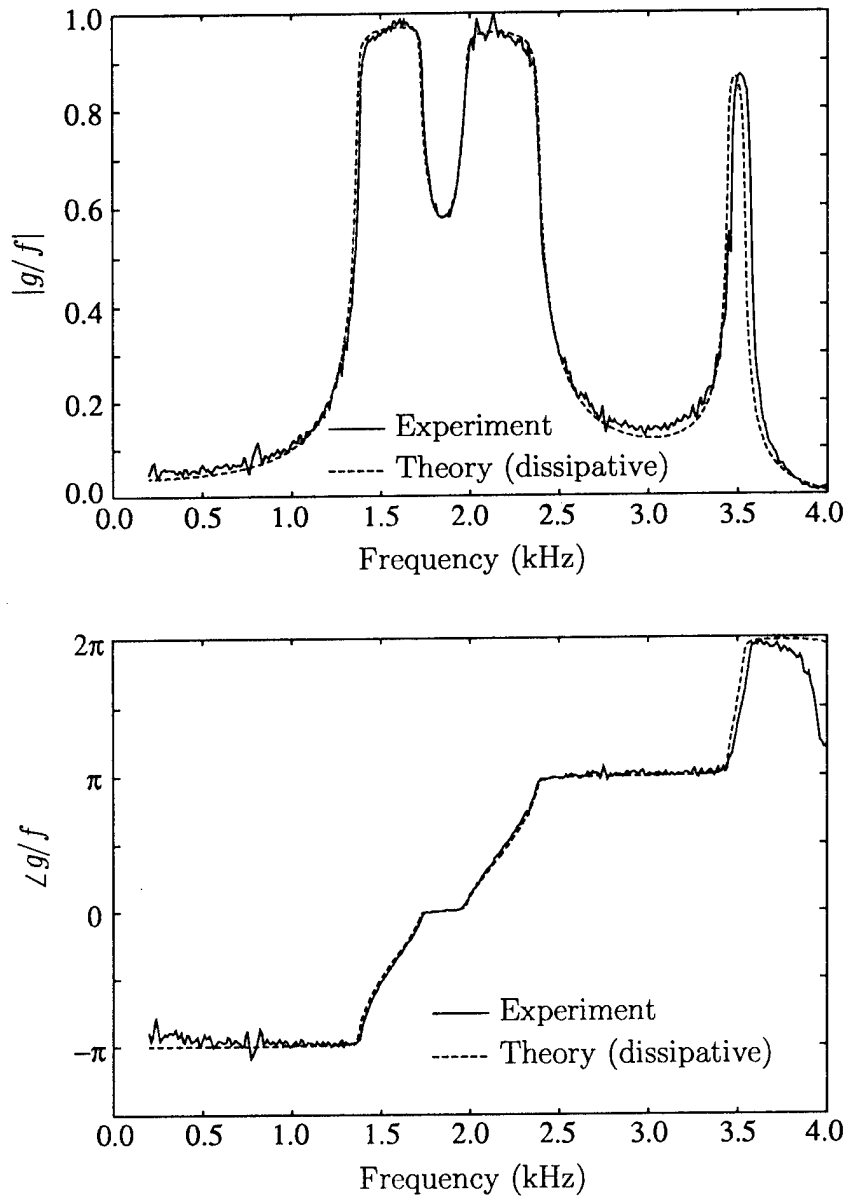
Figure 3.10: Theoretical and experimental values of the magnitude and phase of g/f for the isotropic periodic waveguide.

AS-94-733
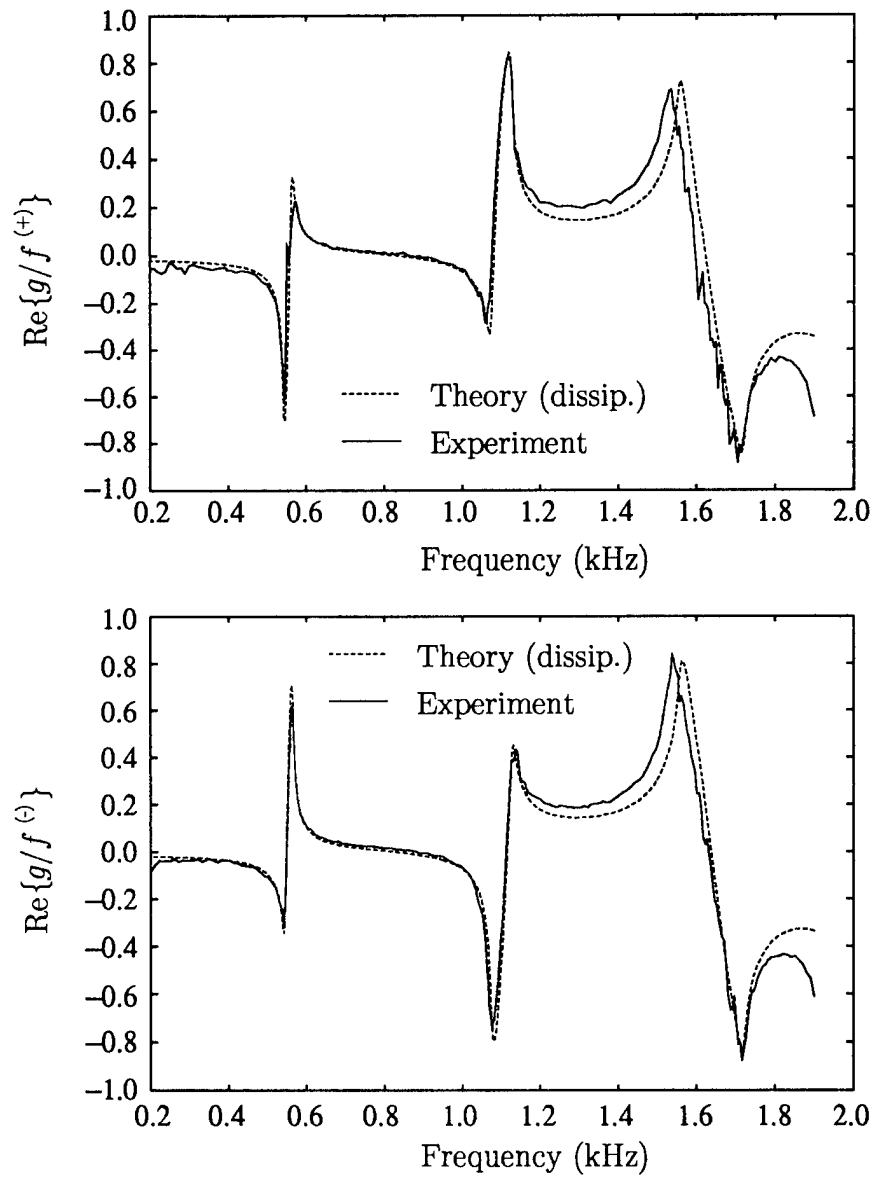
Figure 3.11: Theoretical and experimental values of the real part of $g/f^{(+)}$ and $g/f^{(-)}$ for the anisotropic periodic waveguide. The theoretical values are from the dissipative theory.
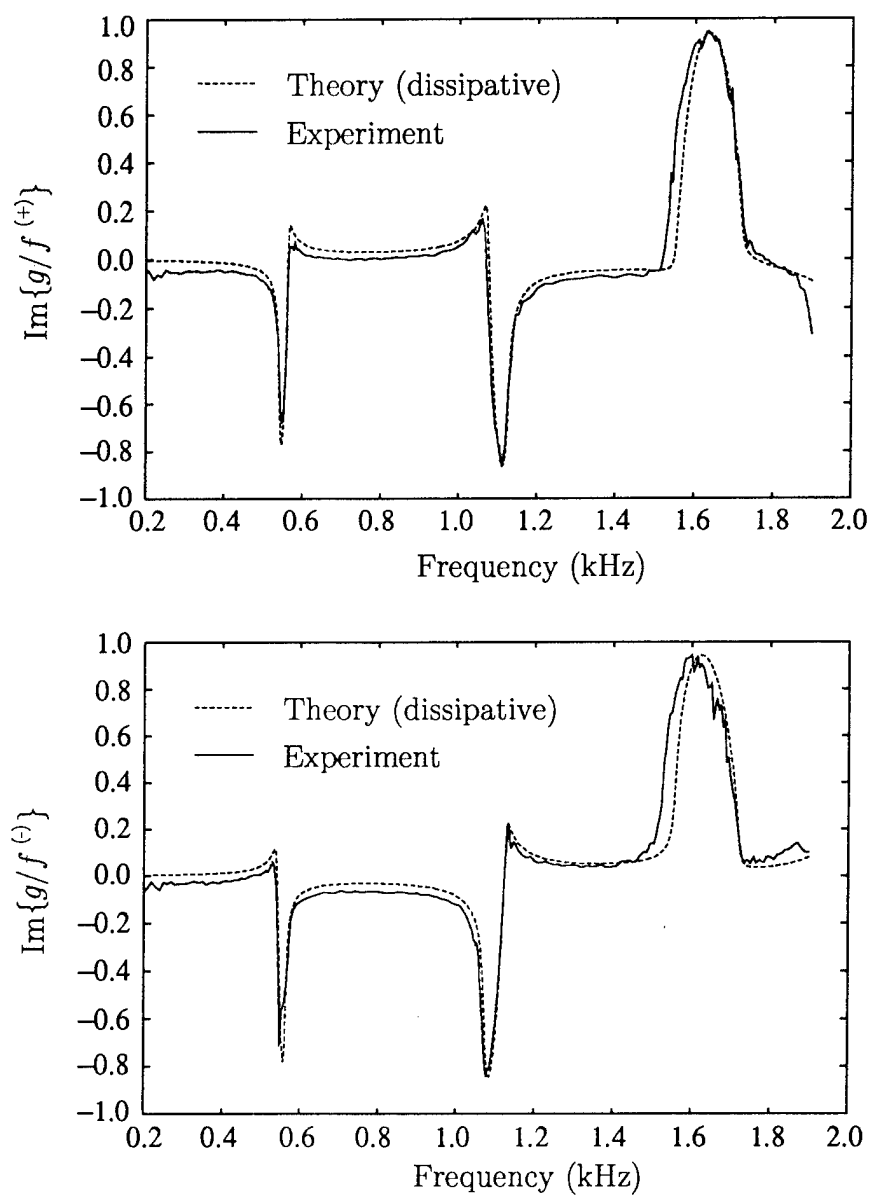
Figure 3.12: Theoretical and experimental values of the imaginary part of $g/f^{(+)}$ and $g/f^{(-)}$ for the anisotropic periodic waveguide. The theoretical values are from the dissipative theory.
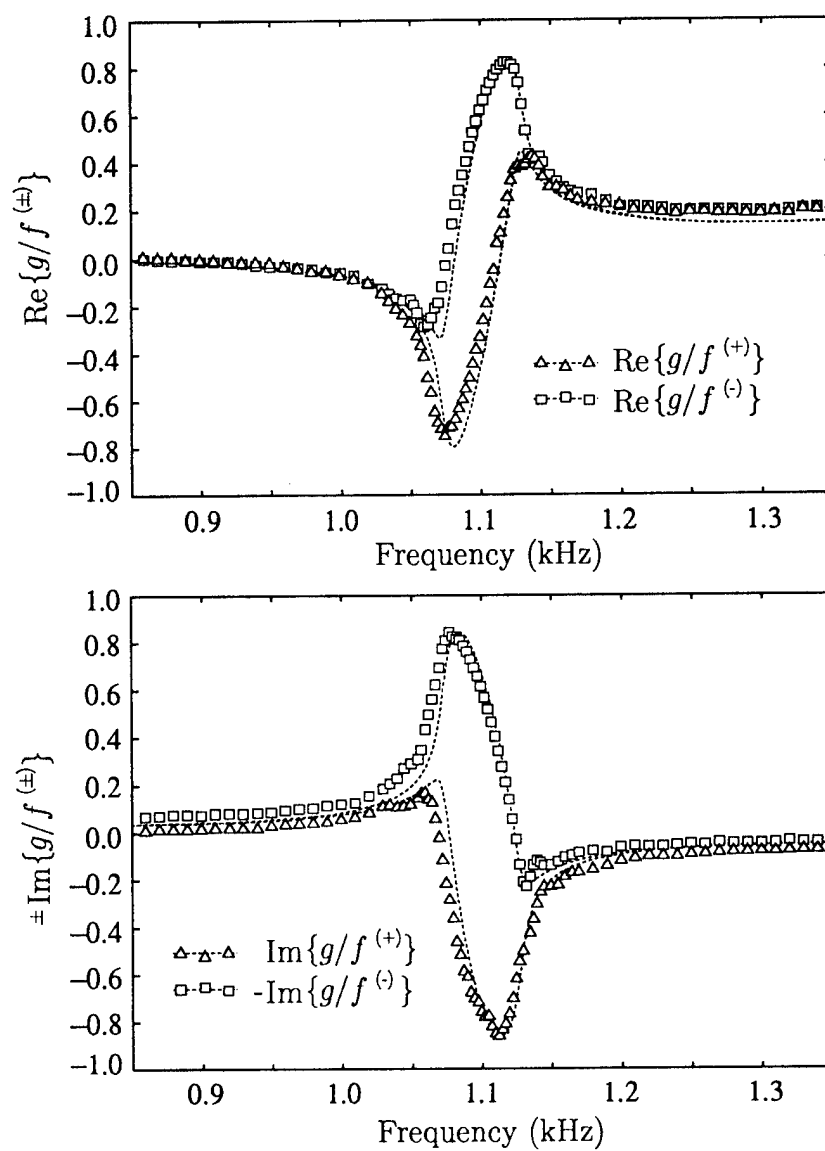
Figure 3.13: The measurements of the real and imaginary parts of $g/f^{(+)}$ and $g/f^{(-)}$ shown in Figs. 3.11 and 3.12 on a scale expanded about the 2π stopband. Also included are theoretical values from the dissipative theory.

3.4 The Multivalued Dispersion Relation and the Forward and Backward Propagating Bloch Waves

Two persistent sources of confusion concerning Bloch waves are the definitions of the propagation direction and the phase speed. The confusion occurs because the Bloch dispersion relation is multivalued. In this section it is shown that, while the concept of phase speed is inapplicable to a Bloch wave as a whole, the definition of propagation direction may be made on the basis of group velocity and attenuation.

While we have labeled the two Bloch wave solutions $(+)$ and $(-)$, and have referred to them as forward and backward traveling Bloch waves, we have not defined which is which. It was shown earlier (Eq. 3.4) that

$$F^{(\pm)}(z + h) = e^{\pm jq^{(+)}h}F^{(\pm)}(z).$$

It is tempting to draw the conclusion that if $\mathrm{Re}\{q^{(+)}\} > 0$, then $F^{(+)}$ is a forward traveling wave and $F^{(-)}$ is a backward traveling wave, both of phase speed $\omega/\mathrm{Re}\{q^{(+)}\}$. Such conclusions, which are based on our experience with conventional waves, are simply not valid for Bloch waves as the Bloch wave number is multivalued. A different (but equally valid) value of $q^{(+)}$ is associated with a different phase speed and possibly a different propagation direction. As a consequence of the multivaluedness of the dispersion relation, the notion of phase speed is meaningless in the context of Bloch waves. The usual definition of propagation direction, which is based on the sign of the phase velocity, is consequently inapplicable as well. In order to arrive at a reasonable definition of propagation direction, we must determine which combinations of $\mathrm{Re}\{q\}$ and $\mathrm{Im}\{q\}$ are allowed.

Mathematically, the dispersion relation is multivalued because its evaluation requires the evaluation of an inverse cosine function (see Eq. 3.5). As the cosine is periodic (with respect to the real part of its argument), it follows that if $q^{(1)}$ is a solution, then $q^{(1)} + 2\pi m_1/h$, where m_1 is an integer, is also a solution. Each of this infinite set of alternative values of wave number is a valid wave number for one of the Bloch wave solutions. Another characteristic of the inverse cosine is that if $q^{(1)}$ is one solution, then $q^{(2)} = -q^{(1)} + 2\pi m_2/h$

is another. As we saw earlier (the discussion following Eq. 3.3), this second set of wave numbers is that associated with the second Bloch wave solution. Neither of the Bloch wave solutions has a unique wave number, phase speed, or propagation direction.[5] Confusion occurs because Bloch waves are frequently represented as a sum over a discrete set of spatial frequency components (the traveling wave spectral representation, see Eq. 1.3 or Sec. 3.5). Each of the set of possible wave numbers associated with a Bloch wave corresponds to a component of the spatial frequency spectrum, and therefore has a valid interpretation. Likewise, the phase velocity associated with each Bloch wave number is the phase velocity of the corresponding component of the spatial frequency spectrum.

In order to arrive at a sensible definition of propagation direction for Bloch waves, we must consider quantities other than phase. From the relationship $q^{(2)} = -q^{(1)} + 2\pi m/h$, we find

$$\text{Im}\{q^{(2)}\} = -\text{Im}\{q^{(1)}\}$$

and

$$(\partial/\partial\omega)\text{Re}\{q^{(2)}\} = -(\partial/\partial\omega)\text{Re}\{q^{(1)}\}.$$

While the phase itself (i.e., $\text{Re}\{q\}$) is not unique, the attenuation and group velocity *are* unique. We must investigate which $\text{Im}\{q\}$ (positive or negative) belongs with which $(\partial/\partial\omega)\text{Re}\{q\}$ (positive or negative) and decide which combination should be those associated with $q^{(+)}$, the Bloch wave number associated with the forward propagating Bloch wave, and which should be those associated with $q^{(-)}$.

In order to find the correct pairing of $\text{Re}\{q\}$ and $\text{Im}\{q\}$, we define q_{r1} and q_{r2} to be the real parts of the two solutions such that $\partial q_{r1}/\partial\omega > 0$ and

---

[5]The infinite set of alternative wave numbers for each Bloch wave solution is simply an artifact of the wrap-around nature of phase. Recall that $\text{Re}\{qh\}$ is simply the cell-to-cell shift in phase associated with a Bloch wave. Clearly $\text{Re}\{(q + 2\pi m/h)h\} = \text{Re}\{qh\} + 2\pi m$ is an equally valid representation of the phase shift, so $q + 2\pi m/h$ is an equally valid Bloch wave number. This is simply a spatial aliasing effect. Note that the eigenvalue s is single-valued; the multivaluedness of q comes about as a consequence of the representation $s = e^{jqh}$.

$\partial q_{r2}/\partial \omega < 0$, and q_{i1} and q_{i2} to be the imaginary parts such that $q_{i1} > 0$ and $q_{i2} < 0$. Consider now the characteristics of the cosine of a complex argument:

$$\cos(-q^*h) = \cos(q^*h) = \cos(qh)^*.$$

In the nondissipative case we must solve $\cos(qh) = \gamma(\omega)$, where $\gamma(\omega)$ is real. If q is a solution, then q^* and $-q^*$ are also solutions. In other words, we are free to pair q_{r1} with either q_{i1} or q_{i2}; $q = \pm q_{r1} \pm j_{i1}$ are all valid solutions. This makes sense as in the nonsdissipative case $\mathrm{Im}\{q\} = 0$ in the passbands (i.e., $q_{i1} = q_{i2}$ so the sign doesn't matter) and in the stopbands $\partial q_{r1}/\partial \omega = \partial q_{r2}/\partial \omega$. In the dissipative case, however, $\gamma(\omega)$ is complex. If q is a solution, then q^* and $-q^*$ are *not* solutions. If $q_{r1} + jq_{i2}$ is a solution, then $q_{r1} + jq_{i1}$ is not. A simple way to find the correct pairing is to investigate the limit as the periodic waveguide degenerates to a uniform waveguide. In that limit we must have

$$\frac{\partial}{\partial \omega}\mathrm{Re}\{q^{(\pm)}\} \rightarrow \frac{\partial}{\partial \omega}\mathrm{Re}\{\pm k\} \quad \text{and} \quad \mathrm{Im}\{q^{(\pm)}\} \rightarrow \mathrm{Im}\{\pm k\}.$$

The necessary pairing is such that

$$\frac{\partial}{\partial \omega}\mathrm{Re}\{q^{(+)}\} > 0 \quad \text{and} \quad \mathrm{Im}\{q^{(+)}\} > 0$$

$$\frac{\partial}{\partial \omega}\mathrm{Re}\{q^{(-)}\} < 0 \quad \text{and} \quad \mathrm{Im}\{q^{(-)}\} < 0.$$

In other words, $q^{(+)} = q_{r1} + jq_{i1}$ and $q^{(-)} = q_{r2} + jq_{i2}$. This implies attenuation in the same direction as the group velocity, which makes sense. It should be noted, however, that it is still possible to have $\mathrm{Re}\{q^{(+)}\} < 0$ and $\mathrm{Re}\{q^{(-)}\} > 0$; The *family* of branches of the dispersion relation with $(\partial/\partial \omega)\mathrm{Re}\{q\} > 0$ is necessarily associated with $\mathrm{Im}\{q\} > 0$, but the particular branch chosen is still arbitrary.

The question as to which value of g/f is associated with $q^{(+)}$ and which is associated with $q^{(-)}$ may likewise be answered by consideration of the uniform waveguide limit. In that limit we must have

$$|\sigma_{02}/\sigma_{01}^{(+)}| \rightarrow 0 \quad \text{and} \quad |\sigma_{02}/\sigma_{01}^{(-)}| \rightarrow \infty.$$

It therefore must be the case that $g/f^{(+)} = \sigma_{02}/\sigma_{01}^{(+)}$ and $g/f^{(-)} = (\sigma_{02}/\sigma_{01}^{(-)})^{-1}$, where, as defined earlier, $\sigma_{02}/\sigma_{01}^{(+)}$ and $\sigma_{02}/\sigma_{01}^{(-)}$ are solutions to Eq. 3.11 such that $|\sigma_{02}/\sigma_{01}^{(+)}| < 1$ and $|\sigma_{02}/\sigma_{01}^{(-)}| > 1$.

It should be noted that these "rules" as to which parameter values are associated with a particular Bloch wave function are derived simply to aid in the understanding of what sorts of solutions are possible. The correct set of parameters associated with a particular solution is always selected by the mathematics. The solution of Eq. 3.5 always yields a correct pairing of $\text{Re}\{q\}$ and $\text{Im}\{q\}$. The appropriate value of g/f always results (via σ_{02}/σ_{01}) from the substitution of the value of q into Eq. 3.10: $\sigma_{02}/\sigma_{01} = (e^{jqh} - T_{11}^{C})/T_{12}^{C}$.
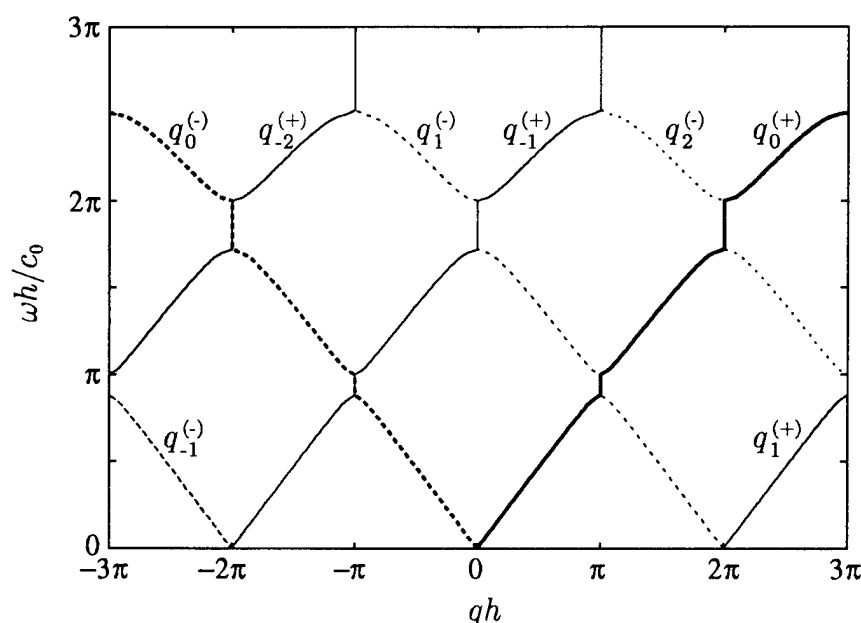
Figure 3.14: Several branches of the dispersion relation for the isotropic periodic side branch waveguide with $A_{\text{sb}}/A_{\text{wg}} = 1$ and $d/h = .14$. The branches associated with the forward traveling Bloch wave are indicated with solid lines and those associated with the backward traveling Bloch wave are indicated with dotted lines.

It is convenient to adopt, as convention, a single branch of the dispersion relation and refer to it only. The branch which, in the uniform waveguide limit, degenerates to the relation $q^{(\pm)} = \pm k$ will be denoted $q_0^{(\pm)}$ and will be referred to as the primary branch. Any other branch (say, the mth branch) is related to the primary branch by $q_m^{(\pm)} = q_0^{(\pm)} \pm 2\pi m/h$. We also make the definition $q_m = q_m^{(+)}$, so that $q_m^{(\pm)} = \pm q_m$. Several branches of the dispersion

curve are shown in Fig. 3.14 for an isotropic waveguide similar to that described in the introduction, but with the parameter values $A_{sb}/A_{wg} = 1$ and $d/h = .14$ (the different parameters are chosen to move the scatterer resonance frequency out of the range of the plot to avoid confusion). When no subscript is present, it is assumed that q is on the primary branch. In the language of condensed matter physics, a plot of the dispersion relation showing only the primary branch, such as that shown in Fig. 3.1, is referred to as the *extended zone scheme* of representation. In other presentations, *all* branches are shown (the periodic zone scheme, as shown in Fig. 3.14) or only the branches falling within the first Brillouin zone are shown (the reduced zone scheme).

3.5 The Bloch Wave Functions

While the earlier representations of Bloch wave functions (such as Eqs. 3.2 and 3.22) are certainly valid representations, they are not strictly explicit functional representations. As opposed to depending only upon z, there is a somewhat parametric dependence upon n, the cell number associated with z, as well. We will first show the two standard functional representations of Bloch wave functions, here called the quasiperiodic and the traveling wave spectral representations, in explicitly anisotropic form. In addition, a new functional representation that proves to be useful in the consideration of nonlinear effects is shown. Before these forms are shown, however, we will, as a matter of convenience, define the Bloch wave functions $F^{(\pm)}(z)$ with the normalization $F^{(\pm)}(0) \equiv 1$. The normalization renders the wave function dimensionless and of unit magnitude such that whatever coefficient multiplies the Bloch wave function is simply the value of the acoustic pressure at the center of the zeroth cell (i.e., at $z = 0$). This makes the Bloch wave functions $F^{(\pm)}(z)$ very strongly analogous to the conventional wave functions $e^{\pm jkz}$. The normalized Bloch wave functions are

$$F^{(\pm)}(z) = \left[\frac{f^{(\pm)}e^{\pm jkz_n} + g^{(\pm)}e^{\mp jkz_n}}{f^{(\pm)} + g^{(\pm)}} \right] e^{\pm jnq_m h}$$

$$= \left[\frac{e^{\pm jkz_n} + (g/f)^{(\pm)}e^{\mp jkz_n}}{1 + (g/f)^{(\pm)}} \right] e^{\pm jnq_m h} \qquad (3.27)$$

where n is the cell number associated with z.

In the quasiperiodic representation, the Bloch wave functions are written

$$F^{(\pm)}(z) = \Phi_{q_m}^{(\pm)}(z)e^{\pm jq_m z}, \tag{3.28}$$

where $\Phi_{q_m}^{(\pm)}(z)$ is periodic with period h. The subscript q_m shows that $\Phi_{q_m}^{(\pm)}(z)$ is dependent upon which branch of the dispersion relation is (arbitrarily) chosen: $\Phi_{q_m}^{(\pm)}(z) = \Phi_{q_0}^{(\pm)}(z)e^{\mp j2\pi m z/h}$. It is easily verified that Eq. 3.28 satisfies the translation relations (Eq. 3.4). In this form, that of a periodically modulated traveling wave, the Bloch wave function is seen to be the product of two periodic functions that are of generally incommensurate spatial frequencies. The Bloch wave functions are therefore quasiperiodic (and therefore aperiodic). From Eqs. 3.27 and 3.28 we find

$$\Phi_{q_m}^{(\pm)}(z) = \frac{e^{\pm j(k-q_m)z} + (g/f)^{(\pm)}e^{\mp j(k+q_m)z}}{1 + (g/f)^{(\pm)}} \quad |z| < h/2, \tag{3.29}$$

and $\Phi_{q_m}^{(\pm)}(z + h) = \Phi_{q_m}^{(\pm)}(z)$. If the scatterers are symmetric, then we have $\Phi_{q_m}^{(-)}(z) = \Phi_{q_m}^{(+)}(-z)$.

The second standard representation of the Bloch wave functions, here called the traveling wave spectral representation, is found by representing the periodic function $\Phi_{q_m}^{(\pm)}(z)$ as the Fourier series

$$\Phi_{q_m}^{(\pm)}(z) = \sum_{n=-\infty}^{+\infty} C_{m,n}^{(\pm)}e^{\pm 2\pi jnz/h} \quad \text{where} \quad C_{m,n}^{(\pm)} = \frac{1}{h}\int_{-h/2}^{h/2} \Phi_{q_m}^{(\pm)}(z)e^{\mp 2\pi jnz/h}dz. \tag{3.30}$$

The substitution of the series representation of $\Phi_{q_m}^{(\pm)}(z)$ into Eq. 3.28 results in

$$F^{(\pm)}(z) = \sum_{n=-\infty}^{+\infty} C_{m,n}^{(\pm)}e^{\pm j(q_m+2\pi n/h)z}, \tag{3.31}$$

which is seen to be a sum over a discrete spectrum of both forward and backward traveling conventional waves, the nth of which travels at a phase velocity $\omega/\text{Re}\{q_m + 2\pi n/h\}$. Note that each component of the traveling wave spectrum corresponds to a branch of the dispersion relation. This is a source of the confusion with respect to the phase velocity of Bloch waves. The traveling wave spectral *components* of a Bloch wave each has a well defined phase velocity, but

the Bloch wave as a whole does not. It is readily found that $C_{m,n}^{(\pm)} = C_{0,m+n}^{(\pm)}$, and Eq. 3.31 becomes $F^{(\pm)}(z) = \sum_n C_{0,n+m}^{(\pm)} e^{\pm j(q_0 + 2\pi(m+n)/h)z}$. That is, if instead of the primary branch q_0 we choose the mth dispersion branch q_m, the traveling wave spectral amplitudes $C_{m,n}^{(\pm)}$ are simply shifted by m. Note that both the quasiperiodic and the traveling wave spectral representation show a dependence upon the chosen branch of the dispersion relation.

While the quasiperiodic and the traveling wave spectral representations each reveal an interesting way to think of the composition of the Bloch wave functions, they both hide what is undoubtedly the simplest way of representing their composition: as a string of compound conventional wave fields (as is evident in the "parametric" representation of Eq. 3.22). We begin with the definition of the cell wave function, the wave function associated with the zeroth cell of the structure:

$$\psi^{(\pm)}(z) = \frac{e^{\pm jkz} + g/f^{(\pm)} e^{\mp jkz}}{1 + g/f^{(\pm)}} \qquad -h/2 < z \le h/2$$

$$\psi^{(\pm)}(z) = 0 \qquad\qquad\qquad\text{elsewhere.}$$

The field in the nth cell is simply $\psi^{(\pm)}(z - nh) = \psi^{(\pm)} * \delta(z - nh)$ multiplied by the translation factor $e^{\pm jq_m h}$, where $*$ denotes the convolution operation. The total function may therefore be written

$$F^{(\pm)}(z) = \psi^{(\pm)}(z) * \sum_{n=-\infty}^{+\infty} \delta(z - nh)e^{\pm jnqh}, \qquad (3.32)$$

where the convolution of $\psi^{(\pm)}(z)$ with the nth phase (and amplitude) weighted delta function in the lattice simply places an appropriately phased (and shaded) copy of $\psi^{(\pm)}(z)$ in the nth cell of the structure. Note that this representation shows *no dependence* on the chosen branch of the dispersion relation!

Although all three of the preceding functional representations of Bloch wave functions are derived for the global field alone, each may be extended to represent the full 3-dimensional field. As was noted when the global and local fields were defined, once the global field is determined in the vicinity of a scatterer, the local field at that scatterer is, in principal, determined. The full three-dimensional field associated with a single scatterer is dependent only upon

the incident field, which is, by definition, composed of the global component only. The global field on either side of a scatterer, and therefore the total incident field, is identical for every scatterer in the waveguide up to factors of e^{jqh}. The full 3-dimensional scattered field in the vicinity of the scatterer is therefore, up to factors of e^{jqh}, identical to that of every other scatterer in the waveguide. Equation 3.32 may therefore be generalized to

$$F^{(\pm)}(\mathbf{r}) = \psi^{(\pm)}(\mathbf{r}) * \sum_{n=-\infty}^{+\infty} \delta(z - nh)e^{\pm jnqh},$$

where $\psi^{(\pm)}(\mathbf{r})$ is the exact 3D field in the zeroth cell. Similarly, Eq. 3.28 may be generalized to become

$$F^{(\pm)}(\mathbf{r}) = \Phi_{q_m}^{(\pm)}(\mathbf{r})e^{\pm jq_m z},$$

where $\Phi_{q_m}^{(\pm)}(\mathbf{r} + h\hat{\mathbf{e}}_z) = \Phi_{q_m}^{(\pm)}(\mathbf{r})$ and in the zeroth cell $\Phi_{q_m}^{(\pm)}(\mathbf{r}) = \psi^{(\pm)}(\mathbf{r})e^{\mp jq_m z}$, and Eq. 3.31 may by be generalized to become

$$F^{(\pm)}(\mathbf{r}) = \sum_{n=-\infty}^{+\infty} C_{m,n}^{(\pm)}(\mathbf{r}_\perp)e^{\pm j(q_m + 2\pi n/h)z},$$

where

$$C_{m,n}^{(\pm)}(\mathbf{r}_\perp) = \frac{1}{h}\int_{-h/2}^{h/2} \Phi_{q_m}^{(\pm)}(\mathbf{r}_\perp + h\hat{\mathbf{e}}_z)e^{\mp 2\pi jhz/h}dz.$$

The translation relation associated with the full three-dimensional field is therefore given by

$$F^{(\pm)}(\mathbf{r} + h\hat{\mathbf{e}}_z) = F^{(\pm)}(\mathbf{r})e^{\pm jqh}.$$

This page intentionally left blank.

Chapter 4

Finite and Semi-Infinite Periodic Waveguides

In this chapter the work of the two preceding chapters is generalized so as to apply to finite and semi-infinite periodic waveguide systems. Recall that up to this point, the findings have all hinged upon the invariance of the system under translation, a property that occurs only in infinite systems. It is shown in this section that the solution in a periodic waveguide of *any* length (infinite, semi-infinite, or finite) may be represented in terms of the two Bloch wave functions. We begin with the definition of the Bloch acoustic impedance, which turns out to be a convenient quantity to work with. It is then shown that Bloch waves are able to meet an arbitrary terminating impedance type boundary condition. As in the conventional wave case, the particular combination of forward and backward traveling waves that meets the termination condition is best expressed in terms of reflection and transmission coefficients. Finally, a general approach to the solution of problems that involve a section or sections of periodic waveguide is outlined.

4.1 The Bloch Acoustic Impedance

Owing to the compound conventional wave composition of the Bloch waves, the impedance is a function of position. It appears, therefore, that we will not be able to identify a characteristic impedance for the periodic wave-

guide. The Bloch wave impedance, however, is found to be spatially periodic, with the same periodicity as the waveguide. As a consequence of the shared periodicity we are able to identify, with the adoption of a convention, a characteristic impedance.

In light of the translation relations (Eqs. 3.4), the acoustic impedance of a Bloch wave shows invariance under the unit translation operation:

$$Z_a(z+h) = \frac{p(z+h)}{A_{wg}u(z+h)} = \frac{p(z)e^{\pm jqh}}{A_{wg}u(z)e^{\pm jqh}} = \frac{p(z)}{A_{wg}u(z)} = Z_a(z).$$

One period of the waveguide transforms the impedance back into itself. For this reason, the impedance in a periodic medium is termed an *iterative* impedance (Brillouin, 1946). Because the structure is invariant under translations of h (there is no single preferred reference point along z), the impedance *must* repeat at intervals of h.

From Eq. 3.22, the acoustic impedance of a Bloch wave field is

$$Z_a^{(\pm)}(z) = \pm Z_{0a}\frac{e^{\pm jkz_n} + g/f^{(\pm)}e^{\mp jkz_n}}{e^{\pm jkz_n} - g/f^{(\pm)}e^{\mp jkz_n}} \quad |z| < h/2,$$

where $Z_{0a} = \rho_0 c_0/A_{wg}$. As the impedance repeats at intervals of h, the characteristic impedance may, as a convention, be taken to be the impedance at a particular reference point. The reference point is taken to be $z = 0$, and the resultant characteristic impedance, called the Bloch acoustic impedance,[1] is given by

$$Z_{Ba}^{(\pm)} = Z_a^{(\pm)}(0) = \pm Z_{0a}\frac{1 + g/f^{(\pm)}}{1 - g/f^{(\pm)}}. \tag{4.1}$$

When the waveguide is isotropic we have $g/f^{(+)} = g/f^{(-)}$ and Bloch acoustic impedances are such that $Z_{Ba}^{(-)} = -Z_{Ba}^{(+)}$, like the impedances of forward and backward traveling conventional waves. When the waveguide is anisotropic then we generally have $g/f^{(+)} \neq g/f^{(-)}$ and hence $Z_{Ba}^{(-)} \neq -Z_{Ba}^{(+)}$. A system

---

[1]The global pressure field most closely resembles the full three-dimensional field at the cell centers. The acoustic impedance associated with the global field alone is therefore most representative of the actual impedance.

with such anisotropy has some very unusual wave reflection properties, as is shown in Sec. 4.2.

As usual, the characteristics of the Bloch impedance are most readily found by examination of the nondissipative case. From Eqs. 3.25 and 4.1, it is found that in the passbands

$$Z_{\text{Ba}}^{(-)} = -Z_{\text{Ba}}^{(+)*}$$

and in the stopbands

$$\text{Re}\{Z_{\text{Ba}}^{(\pm)}\} = 0.$$

The Bloch acoustic impedance is reactive in the stopbands, as might be expected. If the waveguide is isotropic as well as nondissipative, then Eqs. 3.11 and 4.1 may be combined (using Eq. 3.21) to find

$$Z_{\text{Ba}}^{(\pm)} = \pm Z_{\text{0a}} \left[\frac{\text{Im}\{T_{11}^{\text{C}} - T_{12}^{\text{C}}\}}{\text{Im}\{T_{11}^{\text{C}} + T_{12}^{\text{C}}\}} \right]^{1/2}. \tag{4.2}$$

From the stopband conditions found in Appendix C, it is found that the argument of the square root in Eq. 4.2 is real and positive for passband frequencies and real and negative for stopband frequencies. The Bloch acoustic impedance, therefore, is resistive in the passbands and reactive in the stopbands. In Fig. 4.1 is shown the Bloch acoustic impedance for the isotropic periodic side branch waveguide. The plot shows the alternating resistive/reactive passband/stopband structure, and also that the impedance is a very wildly varying function of frequency. Such impedance structure makes the Bloch impedance extremely difficult to sythesize for waveguide termination purposes. As was found for the other Bloch wave parameters, the inclusion of dissipative mechanisms simply tends to smooth these sharply cusped transitions.

4.2 Bloch Wave Reflection and Transmission

Consider the case wherein a periodic waveguide occupies the half-space $z \leq 0$ and is terminated at $z = 0$ into an arbitrary termination of acoustic impedance Z_{Ta}. The forward and backward traveling Bloch wave solutions are known to meet the transverse boundary conditions (i.e., the waveguide wall
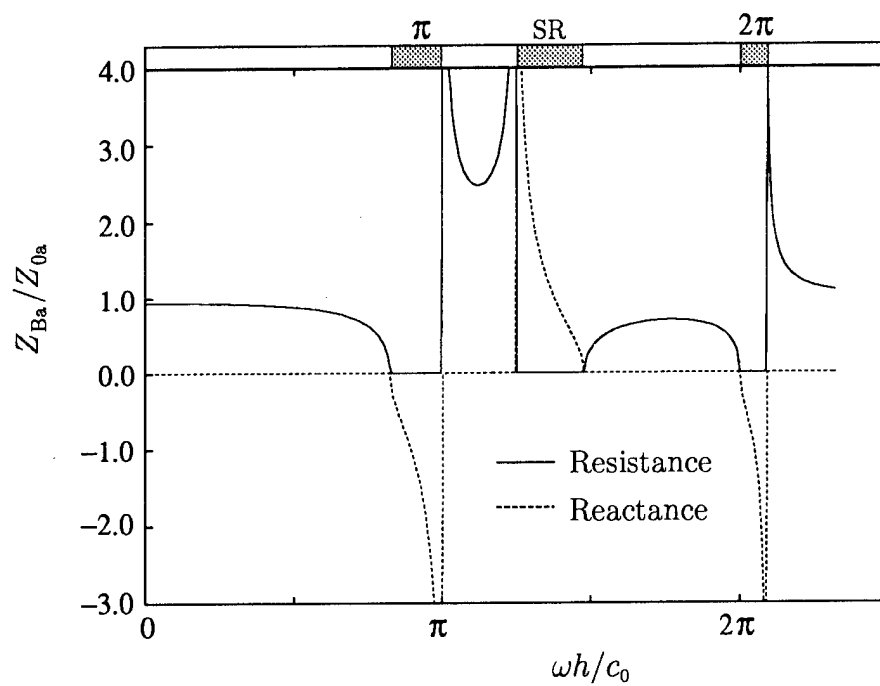
Figure 4.1: The (normalized) Bloch acoustic impedance for the isotropic periodic side branch waveguide. The π and 2π Bragg stopbands and the scatterer resonance (SB) stopband are so indicated.

boundary conditions). The question here is whether or not a combination of the forward and backward traveling Bloch wave solutions is able to meet the arbitrary termination boundary condition. If so, then the trial solutions are the finite waveguide solutions.

The trial solution is the compound Bloch wave field

$$p(z) = A^+ F^{(+)}(z) + A^- F^{(-)}(z) \qquad z \leq 0.$$

The acoustic impedance at the interface is

$$Z_\mathrm{a}|_{z=0} = \frac{A^+ + A^-}{A^+/Z_\mathrm{Ba}^{(+)} + A^-/Z_\mathrm{Ba}^{(-)}},$$

which must be equal to the termination impedance Z_Ta. As in the case of conventional waves, this requirement simply fixes the relationship between the forward and backward traveling Bloch wave amplitudes, and the trial solution is indeed the solution. In the usual manner, the solution is best expressed in terms of a reflection coefficient:

$$R_\mathrm{B} = \frac{A^-}{A^+} = -\frac{1/Z_\mathrm{Ba}^{(+)} - 1/Z_\mathrm{Ta}}{1/Z_\mathrm{Ba}^{(-)} - 1/Z_\mathrm{Ta}} = \frac{Z_\mathrm{Ta} - Z_\mathrm{Ba}^{(+)}}{\nu Z_\mathrm{Ta} + Z_\mathrm{Ba}^{(+)}}, \qquad (4.3)$$

where R_B is the Bloch wave reflection coeffient and

$$\nu = -Z_\mathrm{Ba}^{(+)}/Z_\mathrm{Ba}^{(-)}$$

is a measure of the anisotropy of the system. The compound Bloch wave field is able to satisfy the boundary condition in a manner that is strongly analogous to that of conventional wave fields. The only difference lies in the anisotropy term ν, which disappears from the expression for R_B when the scatterers are symmetric (i.e., when $\nu \to 1$). Note that if the terminating impedance is rigid ($Z_\mathrm{Ta} \to \infty$), then we have $R_\mathrm{B} \to 1/\nu$, which may be such that $|R_\mathrm{B}| > 1$! While a conventional wave reflection coefficient with greater than unit magnitude would violate energy conservation, for the Bloch wave case it is simply a consequence of an asymmetric impedance. The pressure and velocity fields associated with the forward traveling Bloch wave are simply distributed differently in the cell than those of the backward traveling Bloch

wave. Recall that the Bloch wave amplitude is defined in terms of the mid-cell pressure. If the reflected Bloch wave has a particularly small mid-cell particle velocity and/or a particularly large mid-cell acoustic pressure (compared to those of the incident Bloch wave), then it is likely that the amplitude of the reflected Bloch wave will be larger than that of the incident Bloch wave.

As is described in Appendix E, the least-squares approach to the measurements of q and g/f in the anisotropic periodic side branch waveguide entails, as a by product, a measurement of R_B as well. In the experimental system, the periodic waveguide is terminated into a termination impedance of $\rho_0 c_0/A_{\text{wg}}$. The magnitude of the Bloch reflection coefficient for this case is, in the 2π Bragg stopband, theoretically larger than unity. In Fig. 4.2 is shown the theoretical and experimental values of $|R_B|$ for the system in which $q^{(+)}$ and $g/f^{(+)}$ were measured (i.e., the system in which the deeper of the two side branches that comprises a scatterer is nearest the termination). The agreement between theory and experiment is less than perfect, but the large reflection amplitudes are clearly evident.

If the terminating medium is a source-free uniform waveguide of acoustic impedance Z_{Ta}, then the transmission coefficient is

$$T = \frac{a^+}{A^+} = \frac{1/Z_{\text{Ba}}^{(-)} + 1/Z_{\text{Ba}}^{(+)}}{1/Z_{\text{Ba}}^{(-)} + 1/Z_{\text{Ta}}} = \frac{Z_{\text{Ta}}(1+\nu)}{\nu Z_{\text{Ta}} + Z_{\text{Ba}}^{(+)}}, \qquad (4.4)$$

where the transmitted field is $p(z) = a^+ e^{jk_T z}$ and k_T is the wave number associated with the terminating waveguide.

If the problem geometry is reversed so that we have a conventional wave incident upon the interface, the trial field

$$p(z) = \begin{cases} a^+ e^{jkz} + a^- e^{-jkz} & z \leq 0 \\ A^+ F^{(+)}(z) & z > 0 \end{cases}$$

yields

$$R = \frac{a^-}{a^+} = \frac{Z_{\text{Ba}}^{(+)} - Z_{\text{Ia}}}{Z_{\text{Ba}}^{(+)} + Z_{\text{Ia}}} \qquad (4.5)$$

$$T_B = \frac{A^+}{a^+} = \frac{2 Z_{\text{Ba}}^{(+)}}{Z_{\text{Ba}}^{(+)} + Z_{\text{Ia}}}, \qquad (4.6)$$
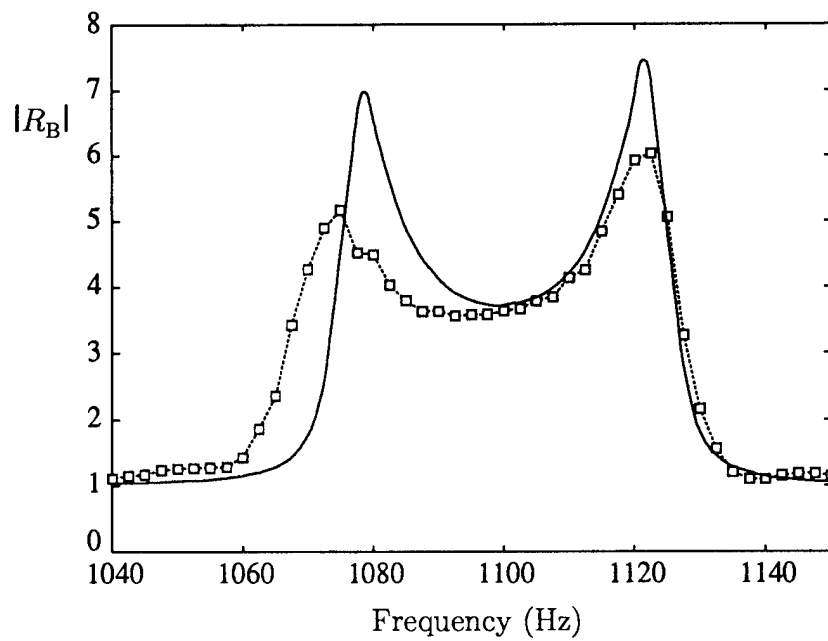
Figure 4.2: Theoretical and experimental values of $|R_B|$, the Bloch wave reflection coefficient, for the anisotropic periodic side branch waveguide terminated into a uniform waveguide of acoustic impedance $Z_{0a} = \rho_0 c_0 / A_{wg}$.

where Z_{Ia} is the acoustic impedance of the incident (conventional) wave medium. Note that the incident and reflected conventional waves could be those due to an incident and reflected Bloch wave; i.e., the incident wave medium could be another periodic waveguide.

If the periodic waveguide is terminated into a semi-infinite uniform waveguide that is identical to the periodic waveguide but without scatterers (i.e., if $Z_{\text{Ia}} = Z_{\text{Ta}} = \rho_0 c_0/A_{\text{wg}}$), then the reflection/transmission laws have a simple physical interpretation. The reflection and transmission coefficients then become

$$R_{\text{B}} = -g/f^+ \frac{1 + g/f^-}{1 + g/f^+} \rightarrow -g/f \qquad T = \frac{1 - g/f^- g/f^+}{1 + g/f^+} \rightarrow 1 - g/f$$

$$R = g/f^+ \rightarrow g/f \qquad T_{\text{B}} = 1 + g/f^+ \rightarrow 1 + g/f,$$

where the right-arrow denotes the case in which the waveguide degenerates to isotropy (i.e., $g/f^+ = g/f^- = g/f$). Note that the role of the reflected Bloch wave is to cancel the g^+ wave at the interface. That is, the forward traveling Bloch wave has a nonzero g^+ wave (of amplitude $A_{\text{F}} g/f^+/(1+g/f^+)$) at $z = 0$. In the absence of sources for $z > 0$, there can be no backward traveling conventional wave at $z = 0$. The amplitude of the reflected Bloch wave, therefore must be such that the f^- wave (of amplitude $A_{\text{B}}/(1 + g/f^-)$) cancels the g^+ wave at $z = 0$. The Bloch reflection coefficient shown above ensures exactly that cancellation, and the resultant conventional wave field at $z = 0$ is progressive, as it must be.

4.3 The Analogous Conventional Wave System

The findings of the preceeding section lead us to a convenient method of solution for systems that include finite or semi-infinite sections of periodic waveguide. We make use of what is here called the analogous conventional wave system, which is defined as follows. Imagine that each section of periodic waveguide is replaced by a section of uniform waveguide that is filled with such a fluid that the characteristic acoustic impedance of the section is equal to

the Bloch acoustic impedance and the dispersion is equal to the Bloch wave dispersion. The resultant, purely conventional wave system is the analogous conventional wave system. Each of the reflection and transmission relations of Eqs. 4.3-4.6 is identical to that of the corresponding analogous conventional wave system. While this is most obvious for the isotropic (i.e., $\nu = 1$) case, it holds for the anisotropic case as well (we must simply be consistent with the definition of impedance for an anisotropic system).

The solution of the analogous conventional wave system bears a very simple relationship to that of the original system. If a wave system includes a section of periodic waveguide that spans $z_1 < z < z_2$ (where $z = 0$ is a cell center), then the solution in this interval may be expressed (in the quasiperiodic representation) as

$$p(z) = A_{\mathrm{F}} F^{(+)}(z) + A_{\mathrm{B}} F^{(-)}(z) = A_{\mathrm{F}} \Phi_q^{(+)}(z) e^{jqz} + A_{\mathrm{B}} \Phi_q^{(-)}(z) e^{-jqz}.$$

In the corresponding span of the analogous conventional wave system, the solution is

$$p(z) = A_{\mathrm{F}} e^{jqz} + A_{\mathrm{B}} e^{-jqz}. \tag{4.7}$$

We see that the solution of the original system may be recovered from that of the analogous conventional wave system simply by multiplication of the forward and backward traveling components of Eq. 4.7 by $\Phi_q^{(+)}(z)$ and $\Phi_q^{(-)}(z)$, respectively. We may alternatively choose to recover the Bloch wave solution in the traveling wave spectral representation by multiplication of the components by $\sum C_n^{(+)} e^{2\pi j n z/h}$ and $\sum C_n^{(-)} e^{-2\pi j n z/h}$, or in the convolution representation by acting on the components with the operators $\psi^{(+)}(z) * \sum_n \delta(z - nh)$ and $\psi^{(-)}(z) * \sum_n \delta(z - nh)$, where the multiplication of the operand by the lattice takes place prior to the convolution. In other words, we may treat the sections of periodic waveguide as though they were simply some sort of "acoustic transmission line" with the Bloch acoustic impedance and the Bloch wave dispersion. If the field of the analogous conventional wave system is sampled at the locations corresponding to the cell centers in the original system, the result is indistinguishable from the sampling of the original system at the cell centers. If the entire field structure must be known, it may be recovered from the analogous conventional wave system solution via a simple operation.

This page intentionally left blank.

Chapter 5

Bloch Wave Pulse Propagation

Here we consider the propagation of the Bloch waves that arise from a source boundary condition that is not time harmonic. The approach taken is to derive and then solve a Bloch wave dispersion integral. In order to solve the Bloch dispersion integral, the similarity between the Bloch wave and the conventional wave dispersion integrals is exploited. It is shown that we may first solve a conventional wave dispersion integral, and then apply an operator to the solution to result in the solution of the Bloch dispersion integral.

In the first section the Bloch wave dispersion integral is derived and the "recovery operator" approach to its solution is introduced. In the second and third sections, we turn to the solution of the conventional wave dispersion integral. While there are several well known solutions of this integral, the validity of these erstwhile solutions has not, to the author's knowledge, been considered. It is shown in the second section that a set of characteristic pulse distortion distances exists, and that these distances are central in the determination of the ranges of validity of the various solutions of the conventional dispersion integral. In the third section, both the well known solutions and several new solutions are derived in the context of the characteristic distortion distances. In this way the validity of all of these solutions is firmly established. In the fourth and final section, the properties of the recovered Bloch wave pulse are considered.

5.1 The Bloch Wave Dispersion Integral and Its Solution

In this section the Bloch wave dispersion integral is derived and the general approach to its solution is presented. It is shown that when a polychromatic Bloch wave is represented as the superposition of a spectrum of time harmonic Bloch waves, it appears in the form of a dispersion integral. In order to solve this Bloch wave dispersion integral, the similarity between the Bloch wave and the conventional wave dispersion integrals is exploited. It is shown that we may first solve a conventional wave dispersion integral, and then apply a simple operator to the solution to obtain the solution of the Bloch dispersion integral.

5.1.1 Polychromatic Bloch Waves

The time harmonic results are made general in the usual manner. Consider a forward traveling Bloch wave that has a temporal frequency spectrum $\Lambda^{(+)}(\omega)$ at $z = 0$; i.e.,

$$\Lambda^{(+)}(\omega) = \int_{-\infty}^{+\infty} p(0,t)e^{j\omega t}dt.$$

Each frequency component, of differential amplitude $\Lambda^{(+)}(\omega)d\omega/2\pi$, is associated with the (differential) time harmonic Bloch wave

$$dp(z,t) = \left[\frac{\Lambda^{(+)}(\omega)d\omega}{2\pi}\right] F^{(+)}(z,\omega)e^{-j\omega t},$$

where the frequency dependence of $F^{(+)}$, the forward traveling time harmonic Bloch wave function, has been made explicit. The integration of all such frequency components results in an integral representation of a general forward traveling Bloch wave:

$$p(z,t) = \frac{1}{2\pi} \int_{-\infty}^{+\infty} \Lambda^{(+)}(\omega)F^{(+)}(z,\omega)e^{-j\omega t}d\omega.$$

A similar argument may be used to arrive at a similar representation of a general backward traveling Bloch wave, and the sum of the forward and the

backward traveling Bloch waves,

$$p(z,t) = \frac{1}{2\pi} \int_{-\infty}^{+\infty} \Lambda^{(+)}(\omega) F^{(+)}(z,\omega) e^{-j\omega t} d\omega$$

$$+ \frac{1}{2\pi} \int_{-\infty}^{+\infty} \Lambda^{(-)}(\omega) F^{(-)}(z,\omega) e^{-j\omega t} d\omega, \tag{5.1}$$

is a fully general integral representation of a compound Bloch wave field. The transformation of Eq. 5.1 into the frequency domain is trivial, and the general frequency domain solution is

$$P(z,\omega) = \Lambda^{(+)}(\omega) F^{(+)}(z,\omega) + \Lambda^{(-)}(\omega) F^{(-)}(z,\omega). \tag{5.2}$$

5.1.2 The Bloch Wave Dispersion Integral

Consider the following problem. A semi-infinite periodic waveguide contains a pressure source at $z = 0$ and is of infinite extent in the $+z$ direction. The boundary conditions are, (1) $p(z,t)|_{z=0} = p_0(t)$, and (2) a generalization of the Sommerfeld radiation condition that is appropriate for periodic media. In order for this generalized radiation condition to apply to a system, there must be (a), no sources in the system for $z > 0$, and (b), the system must be uniformly periodic. As nonuniformity in an otherwise periodic medium generally causes Bloch wave scattering, the Bloch wave radiation condition ensures that the solution has no backward traveling Bloch wave component. Boundary condition (2) therefore leads to $\Lambda^{(-)}(\omega) = 0$. Upon transformation to the temporal frequency domain, boundary condition (1) becomes

$$\Lambda^{(+)}(\omega) F^{(+)}(0,\omega) = P_0(\omega),$$

where $P_0(\omega) = \int p_0(t) e^{j\omega t} dt$. Because the normalization of the Bloch wave functions is such that $F^{(+)}(0,\omega) = 1$ (see Eq. 3.27), the forward traveling Bloch wave spectrum is $\Lambda^{(+)}(\omega) = P_0(\omega)$, and the frequency domain solution is

$$P(z,\omega) = P_0(\omega) F^{(+)}(z,\omega). \tag{5.3}$$

This solution, transformed into the time domain, is

$$p(z,t) = \frac{1}{2\pi} \int_{-\infty}^{+\infty} P_0(\omega) F^{(+)}(z,\omega) e^{-j\omega t} d\omega. \tag{5.4}$$

If instead of the acoustic pressure boundary condition we have the velocity boundary condition $u(z,t)|_{z=0} = u_0(t)$, then the spectrum of the forward traveling Bloch wave is $\Lambda^{(+)}(\omega) = U_0(\omega)A_{\text{wg}}Z_{\text{Ba}}^{(+)}(\omega)$, where $U_0(\omega) = \int u_0(t)e^{j\omega t}dt$, $Z_{\text{Ba}}^{(+)}$ is the Bloch acoustic impedance associated with the forward traveling Bloch wave, and A_{wg} is the cross-sectional area of the waveguide. In general, then, the equation to be solved is

$$p(z,t) = \frac{1}{2\pi} \int_{-\infty}^{+\infty} \Lambda(\omega)F(z,\omega)e^{-j\omega t}d\omega, \tag{5.5}$$

where for the pressure boundary condition $\Lambda(\omega) = P_0(\omega)$ and for the velocity boundary condition $\Lambda(\omega) = U_0(\omega)A_{\text{wg}}Z_{\text{Ba}}^{(+)}(\omega)$. As the problem under consideration admits only progressive Bloch wave solutions, the $(+)$ and $(-)$ subscripts have been dropped.

Equation 5.5 is the Bloch wave dispersion integral. The relationship between the conventional and the Bloch wave dispersion integral is most apparent when the Bloch wave function is expressed in the quasiperiodic representation. In such a case Eq. 5.5 becomes

$$p(z,t) = \frac{1}{2\pi} \int_{-\infty}^{+\infty} \Lambda(\omega)\Phi_q(z,\omega)e^{jq(\omega)z}e^{-j\omega t}d\omega, \tag{5.6}$$

which we see is the conventional wave dispersion integral with the additional factor $\Phi_q(z,\omega)$. If we are concerned only with the value of the pressure at the cell centers (i.e., at $z = nh$), then, because $\Phi_q(nh,\omega) = 1$, Eq. 5.6 becomes

$$p(z,t) = \frac{1}{2\pi} \int_{-\infty}^{+\infty} \Lambda(\omega)e^{jq(\omega)z}e^{-j\omega t}d\omega \quad \text{for} \quad z = nh. \tag{5.7}$$

Note that Eq. 5.7 is the conventional wave dispersion integral. Such a finding is not unexpected as it was found in the time harmonic case that a Bloch wave and a conventional wave of the same wave number are indistinguishable if sampled at intervals of h (see Sec. 3.1). Equation 5.7 shows that this is true of polychromatic Bloch waves as well. The point of interest is that if we are interested only in the value of the wave function at the cell centers, then the problem becomes a conventional wave dispersion problem. If we require a more general solution, then we must solve the more complicated Bloch dispersion integral (Eq. 5.5).

With a slightly different perspective, we find an interesting and straight-forward method of solution of the Bloch dispersion integral. Note first that not only is Eq. 5.7 the solution of the Bloch wave problem at the cell centers, but it is also the solution of the analogous conventional wave problem for *any* value of z. The analogous conventional wave problem is that in which the periodic waveguide is replaced by a conventional wave medium with dispersion and impedance equal to the Bloch wave dispersion and impedance (see Sec. 4.3). The solutions of the Bloch wave and the analogous conventional wave problem are identical at the cell centers; the cell-to-cell or macrostructure of the Bloch wave solution is identical to that of the analogous conventional wave problem. It is evident that in the solution of the analogous conventional wave problem, only information as to the cell-to-cell or macrostructure of the Bloch wave is retained. The intra-cellular structure or microstructure has effectively been discarded. It is shown in the following section that, as in the time harmonic case, the full Bloch wave solution may be recovered from the solution of the analogous conventional wave problem by means of a "recovery operation". We first solve the analogous conventional wave problem (i.e., Eq. 5.7) to find the macroscopic structure of the pulse. If we are then interested in the details of the wave structure within a cell, we may then operate on the conventional wave solution with the recovery operator.

5.1.3 The Recovery Operations

The recovery transformations are operations which, when acting on the solution of the analogous conventional wave problem, result in the solution of the Bloch wave problem. If $p(z,t)$ and $P(z,\omega)$ are the time and frequency domain solutions of the Bloch wave problem, respectively, and $p_c(z,t)$ and $P_c(z,\omega)$ are those of the analogous conventional wave problem, then we define a time domain recovery operator $\mathcal{R}_t$ and a frequency domain recovery operator $\mathcal{R}_\omega$ as follows:

$$p(z,t) = \mathcal{R}_t \left\{ p_c(z,t) \right\} \quad \text{and} \quad P(z,\omega) = \mathcal{R}_\omega \left\{ P_c(z,\omega) \right\}.$$

As we have three representations of the Bloch wave function, we have three recovery operations, each one of which recovers the Bloch wave solution in one of the three functional representations, and each one of which may be expressed

in either the time or the frequency domain. In terms of the above notation, the time and frequency domain solutions of the Bloch wave problem are

$$p(z,t) = \frac{1}{2\pi} \int_{-\infty}^{+\infty} \Lambda(\omega) F(z,\omega) e^{-j\omega t} d\omega, \tag{5.8}$$

and

$$P(z,\omega) = \Lambda(\omega) F(z,\omega), \tag{5.9}$$

respectively, and those of the analogous conventional wave problem are

$$p_c(z,t) = \frac{1}{2\pi} \int_{-\infty}^{+\infty} \Lambda(\omega) e^{jq(\omega)z} e^{-j\omega t} d\omega, \tag{5.10}$$

and

$$P_c(z,\omega) = \Lambda(\omega) e^{jq(\omega)z}. \tag{5.11}$$

The recovery operator that recovers the frequency domain Bloch wave solution, in the quasiperiodic representation, from the frequency domain conventional wave solution is simply the multiplicative operator $\Phi_q(z,\omega)$:

$$\begin{aligned}
\Phi_q(z,\omega) P_c(z,\omega) &= \Lambda(\omega) \Phi_q(z,\omega) e^{jq(\omega)z} \\
&= \Lambda(\omega) F(z,\omega) = P(z,\omega).
\end{aligned}$$

Similarly, the recovery operator for the traveling wave spectral representation is the multiplicative operator $\sum_n C_n(\omega) e^{j2\pi nz/h}$:

$$\begin{aligned}
\sum_n C_n(\omega) e^{j2\pi nz/h} P_c(z,\omega) &= \sum_n C_n(\omega) e^{j2\pi nz/h} \Lambda(\omega) e^{jq(\omega)z} \\
&= \Lambda(\omega) \sum_n C_n(\omega) e^{j(q+2\pi n/h)z} \\
&= \Lambda(\omega) F(z,\omega) = P(z,\omega).
\end{aligned}$$

The frequency domain recovery operator for the convolution representation may be written $\psi(z,\omega) *_z \sum_n \delta(z-nh)$, where the multiplication of the operand by the lattice precedes the spatial convolution, denoted $*_z$:

$$\begin{aligned}
\psi(z,\omega) *_z \sum_n \delta(z-nh) P_c(z,\omega) &= \psi(z,\omega) *_z \sum_n \delta(z-nh) \Lambda(\omega) e^{jq(\omega)z} \\
&= \Lambda(\omega) \psi(z,\omega) *_z \sum_n \delta(z-nh) e^{jnq(\omega)h} \\
&= \Lambda(\omega) F(z,\omega) = P(z,\omega).
\end{aligned}$$

The time domain expressions of the three frequency domain operators emerge naturally when the expression $P(z,\omega) = \mathcal{R}_\omega P_c(z,\omega)$ is Fourier transformed. The quasiperiodic recovery operation $P(z,\omega) = [\Phi_q(z,\omega)] P_c(z,\omega)$ becomes

$$
\begin{aligned}
p(z,t) &= \frac{1}{2\pi} \int_{-\infty}^{+\infty} \Phi_q(z,\omega) P_c(z,\omega) e^{-j\omega t} d\omega \\
&= \frac{1}{2\pi} \int_{-\infty}^{+\infty} \Phi_q(z,\omega) e^{-j\omega t} d\omega *_t \frac{1}{2\pi} \int_{-\infty}^{+\infty} P_c(z,\omega) e^{-j\omega t} d\omega \\
&= \phi_q(z,t) *_t p_c(z,t),
\end{aligned}
$$

where

$$
\phi_q(z,t) = \frac{1}{2\pi} \int_{-\infty}^{+\infty} \Phi_q(z,\omega) e^{-j\omega t} d\omega
$$

and $*_t$ denotes convolution with respect to time. The quasiperiodic time domain recovery operator is therefore

$$
\phi_q(z,t) *_t .
$$

Similarly, the traveling wave spectral transformation may be written

$$
P(z,\omega) = \left[\sum_n C_n(\omega) e^{j2\pi n z/h} \right] P_c(z,\omega),
$$

and yields

$$
\begin{aligned}
p(z,t) &= \frac{1}{2\pi} \int_{-\infty}^{+\infty} \sum_n C_n(\omega) e^{j2\pi n z/h} P_c(z,\omega) e^{-j\omega t} d\omega \\
&= \sum_n e^{j2\pi n z/h} c_n(t) *_t p_c(z,t),
\end{aligned}
$$

where

$$
c_n(t) = \frac{1}{2\pi} \int_{-\infty}^{+\infty} C_n(\omega) e^{-j\omega t} d\omega.
$$

The traveling wave spectral time domain recovery operator is therefore

$$
\sum_n e^{j2\pi n z/h} c_n(t) *_t .
$$

Finally, the transformation associated with the convolution representation, $P(z,\omega) = [\psi(z,\omega) *_z \sum_n \delta(z - nh)] P_c(z,\omega)$, becomes

$$
\begin{aligned}
p(z,t) &= \frac{1}{2\pi} \int_{-\infty}^{+\infty} \psi(z,\omega) *_z \sum_n \delta(z - nh) P_c(z,\omega) e^{-j\omega t} d\omega \\
&= \Psi(z,t) *_z *_t \sum_n \delta(z - nh) p_c(z,t),
\end{aligned}
$$

where

$$\Psi(z,t) = \frac{1}{2\pi} \int_{-\infty}^{+\infty} \psi(z,\omega) e^{-j\omega t} d\omega.$$

The convolution time domain recovery operator is therefore

$$\Psi(z,t) *_z *_t \sum_n \delta(z - nh).$$

It should be noted that the purpose of the above derivation of the recovery operators is simply to show that, in principle, the proposed solution approach is valid. It is shown in Sec. 5.4 that there are much more practically applicable, *differential* versions of the recovery operators. While the concept of the recovery operator is important here, the derivation of the practical forms must await the introduction of the pulse envelope formalism.

To conclude, the problem of solving the Bloch dispersion integral has been split into two sub-problems. We must first solve the conventional wave dispersion integral associated with the analogous conventional wave problem, and then apply the recovery operator of choice to the solution.

5.2 The Evolution of the Pulse Envelope and the Characteristic Distortion Distances

Thus far it has been shown that the Bloch dispersion integral may be solved by the application of a recovery operator to the solution of the analogous conventional wave dispersion integral. In this section the solution of the conventional dispersion integral is considered. Instead of proceeding directly to the pulse solution, however, we first recast the problem in terms of the pulse *envelope*. That is, we solve an envelope evolution integral instead of the conventional dispersion integral. While the pulse function and the envelope function are simply related, the problem becomes considerably less cluttered in envelope form. It is next shown that there exists a set of characteristic distances associated with the evolution of the pulse envelope, and that if we are concerned with the propagation of the pulse over a distance that is small compared to one of the characteristic distances, then the envelope evolution integral may be

simplified. Finally, the wave equation that governs the evolution of the envelope is derived and the significance of the characteristic distances with respect to the wave equation established.

5.2.1 The Envelope Evolution Integral

Just as the conventional dispersion integral (Eq. 5.7) governs the evolution of a wave pulse, we may derive another, slightly simpler integral that governs the evolution of the *envelope* of the pulse. The source boundary condition is taken to be

$$p(0,t) = a_0(t)e^{-j\omega_0 t}, \tag{5.12}$$

where $a_0(t)$ is the (real) envelope function of characteristic time scale $2\tau_0$ and ω_0 is the pulse carrier frequency. The envelope spectrum is

$$A_0(\omega) = \int_{-\infty}^{+\infty} a_0(t)e^{j\omega t}dt$$

and the pulse spectrum is

$$\Lambda(\omega) = \frac{1}{2\pi}\int_{-\infty}^{+\infty} a_0(t)e^{j(\omega-\omega_0)t}dt = A_0(\omega - \omega_0), \tag{5.13}$$

both of which have a characteristic bandwidth[1] of $4/\tau_0$. The substitution of Eq. 5.13 into Eq. 5.7 results in the dispersion integral

$$p(z,t) = \frac{1}{2\pi}\int_{-\infty}^{+\infty} A_0(\omega - \omega_0)e^{jq(\omega)z}e^{-j\omega t}d\omega, \tag{5.14}$$

where the subscript c for conventional wave has been dropped for simplicity. In anticipation of a solution in the envelope-carrier form

$$p(z,t) = a(z,t)e^{j[q(\omega_0)z - \omega_0 t]}, \tag{5.15}$$

where $a(z,t)$ is a carrier modulating envelope function (see Fig. 5.1), we rewrite the dispersion integral

$$p(z,t) = e^{j[q(\omega_0)z - \omega_0 t]}\frac{1}{2\pi}\int_{-\infty}^{+\infty} A_0(\omega - \omega_0)e^{j[q(\omega)-q(\omega_0)]z}e^{-j[\omega-\omega_0]t}d\omega$$

$$= e^{j[q(\omega_0)z - \omega_0 t]}\frac{1}{2\pi}\int_{-\infty}^{+\infty} A_0(\Omega)e^{jQ(\Omega)z}e^{-j\Omega t}d\Omega, \tag{5.16}$$

---

[1]The Gaussian envelope function $e^{-(t/\tau_0)^2}$ has a characteristic duration $2\tau_0$ and a spectrum proportional to $e^{-(\omega\tau_0/2)^2}$. The characteristic bandwidth is therefore $4/\tau_0$.

where $\Omega = \omega - \omega_0$ and $Q(\Omega) = q(\omega) - q(\omega_0)$. From Eqs. 5.15 and 5.16, we identify the envelope evolution integral

$$a(z,t) = \frac{1}{2\pi} \int_{-\infty}^{+\infty} A_0(\Omega) e^{jQ(\Omega)z} e^{-j\Omega t} d\Omega, \qquad (5.17)$$

where the form of the integral leads us to refer to Ω and $Q(\Omega)$ as the envelope frequency and envelope wave number, respectively. It should be noted that the pulse envelope function defined here differs from another that is occasionally encountered in the literature. This other envelope function is defined to be the real, positive definite function that envelopes the pulse (i.e., the magnitude of the pulse envelope function defined here).
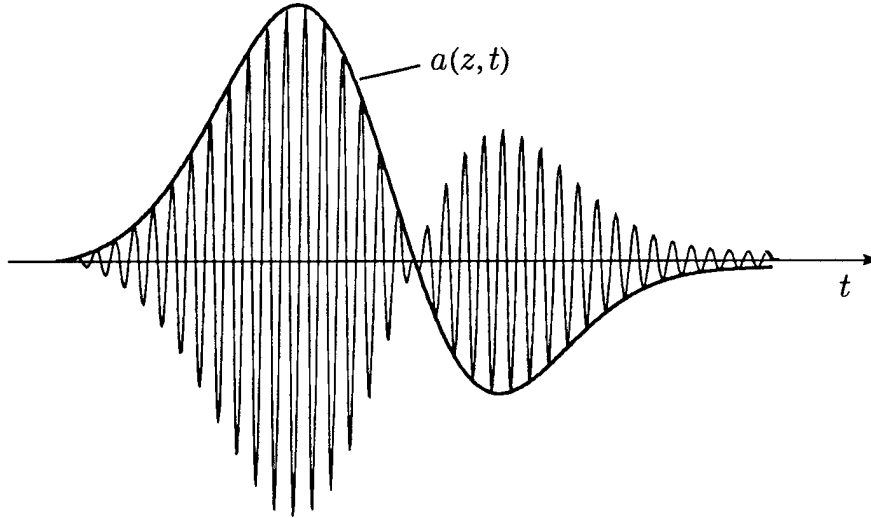
Figure 5.1: An example of a pulse and the associated (real) envelope function.

AS-94–740

5.2.2   The Characteristic Envelope Distortion Distances

Here it is shown that if the propagation distance is sufficiently short, then the envelope evolution integral may be simplified considerably and may, in some instances, be integrated analytically. As soon as we say that the propagation path is "short", we must ask, "short compared to what?" This is the question that is addressed here.

Because $a_0(t)$ is a function that is slowly varying on the scale of a carrier period (i.e., $2\pi/\omega_0 \ll \tau_0$), the signal spectrum is confined to a narrow band of frequencies near $\omega = \omega_0$. The envelope spectrum, which is simply the pulse spectrum shifted down in frequency, is therefore similarly confined to a narrow band of frequencies near $\Omega = 0$. Because the integrand of Eq. 5.17 is significant only near $\Omega = 0$, we need only be concerned with the behavior of $Q(\Omega)$ in this narrow frequency band. The Maclaurin expansion of $Q(\Omega)$ is

$$Q(\Omega)|_{\Omega \sim 0} = \sum_{n=0}^{\infty} \frac{1}{n!} Q^{(n)}(0) \Omega^n \tag{5.18}$$

$$= \sum_{n=1}^{\infty} \frac{1}{n!} \kappa_0^{(n)} \Omega^n + j \sum_{n=1}^{\infty} \frac{1}{n!} \alpha_0^{(n)} \Omega^n, \tag{5.19}$$

where we have used the definitions $Q(0) = 0$ and

$$Q^{(n)}(0) = \left. \frac{d^n Q}{d\Omega^n} \right|_{\Omega=0} = \left. \frac{d^n q}{d\omega^n} \right|_{\omega=\omega_0} = q^{(n)}(\omega_0) = q_0^{(n)} = \kappa_0^{(n)} + j\alpha_0^{(n)}.$$

The exponential term in the envelope evolution integral is therefore

$$e^{jQ(\Omega)z} = \left[e^{j\kappa_0^{(1)}\Omega z} e^{j\frac{1}{2}\kappa_0^{(2)}\Omega^2 z} e^{j\frac{1}{6}\kappa_0^{(3)}\Omega^3 z} \cdots \right] \left[e^{-\alpha_0^{(1)}\Omega z} e^{-\frac{1}{2}\alpha_0^{(2)}\Omega^2 z} e^{-\frac{1}{6}\alpha_0^{(3)}\Omega^3 z} \cdots \right]. \tag{5.20}$$

We see that the terms in the first set of brackets (those involving κ), which originated from the real part of the expansion of $Q(\Omega)$, are dispersive terms and those in the second set of brackets (those involving α), which originated from the imaginary part of the expansion, are attenuation terms.

Consider the function $e^{j\kappa_0^{(n)}\Omega^n z/n!}$, the nth term from the real part of the expansion. This function may in turn be expanded as

$$e^{j\kappa_0^{(n)}\Omega^n z/n!} = 1 + j\kappa_0^{(n)}\Omega^n z/n! + \cdots.$$

If $|\kappa_0^{(n)}\Omega^n z/n!| \ll 1$, then we have $e^{j\kappa_0^{(n)}\Omega^n z/n!} \simeq 1$ and the term may be neglected from the expansion shown in Eq. 5.20. Similarly, the nth term from the imaginary part of the expansion may be neglected provided $|\alpha_0^{(n)}\Omega^n z/n!| \ll 1$. Because the envelope spectrum is localized to within a range of $\sim 2/\tau_0$ of $\Omega = 0$, we know $\Omega = \mathcal{O}(2/\tau_0)$. The nth term of the real part of the expansion

may therefore be neglected provided $|\kappa_0^{(n)}(2/\tau_0)^n z/n!| \ll 1$, or, equivalently, provided

$$z \ll \left| \frac{n!}{2^n} \frac{\tau_0^n}{\kappa_0^{(n)}} \right|.$$

Similarly, the nth term of the imaginary part of the expansion may be neglected provided

$$z \ll \left| \frac{n!}{2^n} \frac{\tau_0^n}{\alpha_0^{(n)}} \right|.$$

In other words, each term in the expansion has a characteristic distance associated with it. If we are concerned with the propagation of the pulse over a distance that is very small compared to the characteristic distance associated with a particular term in the expansion, then that term may be neglected. It is not until the pulse nears a particular characteristic distance that the distorting effects of the associated term in the expansion become significant. We make the definitions

$$z_\kappa^{(n)}(\omega_0) = \frac{n!}{2^n} \frac{\tau_0^n}{\kappa_0^{(n)}} \tag{5.21}$$

$$z_\alpha^{(n)}(\omega_0) = \frac{n!}{2^n} \frac{\tau_0^n}{\alpha_0^{(n)}}, \tag{5.22}$$

which are the *characteristic distortion distances* associated with the nth term in the expansion. The real expansion terms (those arising from κ) are dispersive distortion terms, and the distances $z_\kappa^{(n)}(\omega_0)$ are the characteristic distances associated with dispersive distortion. The imaginary expansion terms (those arising from α) are attenuation distortion terms, and the distances $z_\alpha^{(n)}(\omega_0)$ are the characteristic distances associated with attenuation distortion. It should be noted that this method of determination of the importance of terms in the envelope evolution equation may be applied directly to the conventional dispersion integral (Eq. 5.7) as well. As might be expected, the characteristic distortion distances found in that case are the same as those found here.

The magnitudes of the characteristic distortion distances $z_\kappa^{(2)}$, $z_\kappa^{(3)}$, $z_\alpha^{(1)}$, and $z_\alpha^{(2)}$ are shown as functions of the dimensionless carrier frequency $\omega_0 h/c_0$ in Fig. 5.2. The distances shown are those for the isotropic periodic waveguide described in the introduction and for the case in which $\omega_0 \tau_0 = 8\pi$ (i.e., there are ~ 8 carrier cycles over the duration of the pulse). Near the

centers of the passbands, where the real part of the Bloch wave number is a nearly linear function of frequency and the imaginary part is nearly constant, the characteristic distortion distances are consequently very large. Near the stopbands, however, where both the real and the imaginary parts of the Bloch wave number have a strong dependence upon frequency, the characteristic distortion distances become quite small. In the vicinity of the stopband edges,
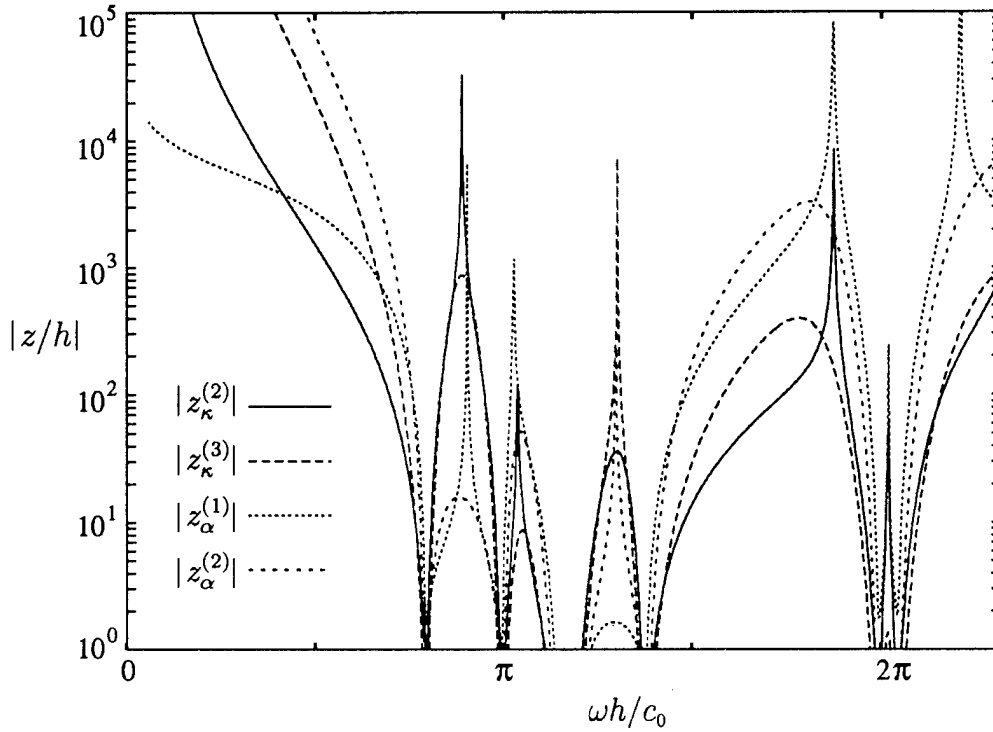
Figure 5.2: The magnitudes of the first four characteristic envelope distortion distances as functions of carrier frequency for a pulse with a duration of 8 cycles propagating in the isotropic periodic side branch waveguide.

AS-94-741

they become less than a structure period.

Equations 5.21 and 5.22 show that the characteristic pulse distortion distances are bandwidth dependent. For a given carrier frequency ω_0 and envelope function $a_0(t/\tau_0)$ of characteristic duration τ_0, Eqs. 5.21 and 5.22 give us a set of characteristic distances. If the carrier frequency and envelope function f

are held fixed, but the duration of the envelope is doubled ($\tau_0 \rightarrow 2\tau_0$), then the pulse bandwidth is reduced by a factor of 2 and the nth characteristic distortion distance is increased by a factor of 2^n. The narrower the pulse bandwidth is, the further the pulse propagates before a particular pulse distortion term begins to have a significant distorting influence on the pulse.

5.2.3 The Envelope Wave Equation

An alternative approach to the solution of the problem would be to derive and solve the *wave equation* that governs the evolution of the envelope. While the approach chosen here is to solve the envelope evolution integral, the envelope wave equation allows us to identify the relationship that exists between the present problem and several related problems, and is therefore of interest.

In order to arrive at the envelope wave equation we proceed backwards through the solution technique by which a spatial evolution type wave equation is solved via Fourier transforms. As the problem at hand is a boundary value problem, the dispersion relation $q = q(\omega)$ (or, equivalently, $Q = Q(\Omega)$) is of the boundary value form as opposed to the initial value form $\omega = \omega(q)$. Such a dispersion relation is the space-time Fourier transform of a partial differential equation of the form

$$\frac{\partial \psi}{\partial z} + \sum_n C_n \frac{\partial^n \psi}{\partial t^n} = 0, \tag{5.23}$$

which is the spatial evolution equation form, as opposed to

$$\frac{\partial \psi}{\partial t} + \sum_n C_n \frac{\partial^n \psi}{\partial z^n} = 0,$$

which is of the temporal evolution equation form associated with initial value problems. Upon transformation, Eq. 5.23 becomes the polynomial dispersion relation $q + \sum C_n (-j)^{n+1} \omega^n = 0$. We apply this solution technique in reverse to recover the envelope wave equation from the envelope dispersion relation.

The Fourier transform of the envelope function $a(z, t)$ is, from Eq. 5.17,

$$A(z, \Omega) = A_0(\Omega) e^{jQ(\Omega)z}. \tag{5.24}$$

Equation 5.24 is the envelope frequency domain solution of the envelope evolution problem. Operating on this solution with $\partial/\partial z$, we find

$$\frac{\partial A(z,\Omega)}{\partial z} = A_0(\Omega)jQ(\Omega)e^{jQ(\Omega)z} = jQ(\Omega)A(z,\Omega). \qquad (5.25)$$

The inverse Fourier transform of Eq. 5.25 is

$$\frac{1}{2\pi}\int_{-\infty}^{+\infty}\frac{\partial A}{\partial z}e^{-j\Omega t}d\Omega = \frac{j}{2\pi}\int_{-\infty}^{+\infty}Q(\Omega)A(z,\Omega)e^{-j\Omega t}d\Omega,$$

or

$$\frac{\partial}{\partial z}a(z,t) = \frac{j}{2\pi}\int_{-\infty}^{+\infty}Q(\Omega)A(z,\Omega)e^{-j\Omega t}d\Omega. \qquad (5.26)$$

With the introduction of the expansion of the envelope wave number (Eq. 5.18), Eq. 5.26 becomes

$$\frac{\partial}{\partial z}a(z,t) = j\sum_{n=1}^{\infty}\frac{1}{n!}Q^{(n)}(0)j^n\frac{1}{2\pi}\int_{-\infty}^{+\infty}(-j\Omega)^n A(z,\Omega)e^{-j\Omega t}d\Omega$$

$$= \sum_{n=1}^{\infty}\frac{1}{n!}j^{n+1}Q^{(n)}(0)\frac{\partial^n}{\partial t^n}a(z,t),$$

or, because $Q^{(n)}(0) = q^{(n)}(\omega_0) = q_0^{(n)}$,

$$\frac{\partial a}{\partial z} + \sum_{n=1}^{\infty}\frac{1}{n!}j^{n-1}q_0^{(n)}\frac{\partial^n a}{\partial t^n} = 0. \qquad (5.27)$$

Equation 5.27 is the progressive wave equation that governs the evolution of the pulse envelope. The method used to recover the wave equation from the integral solution, the inverse of the Fourier transform solution method, is simply a way of verifying the validity of the standard operator formalism for the envelope wave number and envelope frequency. In the standard operator formalism, a wave equation is recovered from a dispersion relation by replacing the wave number and frequency by their associated operators:

$$q \leftrightarrow -j\frac{\partial}{\partial z} \qquad \omega \leftrightarrow j\frac{\partial}{\partial t}. \qquad (5.28)$$

Here, we have shown that such formalism holds for the envelope quantities as well:

$$Q \leftrightarrow -j\frac{\partial}{\partial z} \qquad \Omega \leftrightarrow j\frac{\partial}{\partial t}.$$

If we begin with the expression for the envelope dispersion relation shown in Eq. 5.18 and replace the envelope wave number and frequency with their associated operators, Eq. 5.27 results.

The source boundary condition that the solution of Eq. 5.27 must meet is found via the pulse boundary condition shown in Eq. 5.12. By the definition of the envelope, $p(z,t) = a(z,t)e^{j[q_0 z - \omega_0 t]}$. We therefore have

$$p(0,t) = a(0,t)e^{-j\omega_0 t} = a_0(t)e^{-j\omega_0 t},$$

or

$$a(0,t) = a_0(t). \tag{5.29}$$

The significance of several of the terms in Eq. 5.27 becomes apparent when, using $q_0^{(n)} = \kappa_0^{(n)} + j\alpha_0^{(n)}$, the equation is rewritten as

$$\frac{\partial a}{\partial z} + \kappa_0^{(1)}\frac{\partial a}{\partial t} + \sum_{n=2}^{\infty}\frac{1}{n!}j^{n-1}\kappa_0^{(n)}\frac{\partial^n a}{\partial t^n} + j\sum_{n=1}^{\infty}\frac{1}{n!}j^{n-1}\alpha_0^{(n)}\frac{\partial^n a}{\partial t^n} = 0. \tag{5.30}$$

The first two terms we recognize as the linear, lossless, nondispersive, progressive wave equation in $a(z,t)$, the solution to which is $a(z,t) = a_0(t - \kappa_0^{(1)}z)$. In other words, the first two terms represent nondistorting propagation of the envelope at the group velocity

$$c_{g0} = 1/\kappa_0^{(1)} = \frac{d\omega}{d\mathrm{Re}\{q\}}\bigg|_{\omega=\omega_0}.$$

The remainder of the terms cause envelope distortion.

The relative importance of the envelope distortion terms may be investigated by the transformation of Eq. 5.27 into dimensionless form. Consider the propagation of a pulse of characteristic amplitude C_0 and characteristic duration τ_0 over a propagation distance z_p. The introduction of the dimensionless variables $\tilde{a} = a/C_0$, $\tilde{t} = 2t/\tau_0$, and $\tilde{z} = z/z_p$ into Eq. 5.27 results in

$$\frac{\partial \tilde{a}}{\partial \tilde{z}} + \sum_{n=1}^{\infty}j^{n-1}\left(\frac{z_p}{n!\tau_0^n/2^n\kappa_0^{(n)}}\right)\frac{\partial^n \tilde{a}}{\partial \tilde{t}^n} - j\sum_{n=1}^{\infty}j^{n-1}\left(\frac{z_p}{n!\tau_0^n/2^n\alpha_0^{(n)}}\right)\frac{\partial^n \tilde{a}}{\partial \tilde{t}^n} = 0.$$

As in the analysis of the dispersion and envelope evolution integrals, the nth real term is negligible provided $z_p \ll |n!\tau_0^n/2^n\kappa_0^{(n)}|$ and the nth imaginary term

is negligible provided $z_p \ll |n!\tau_0^n/2^n\alpha_0^{(n)}|$. Each term in the partial differential equation is associated with an exponential term in the envelope evolution integral. If we are interested in the pulse after having propagated a distance that is much less than the characteristic distance associated with a particular term, then that term may be neglected in both the wave equation and the integral solution. For example, the term $e^{j\kappa_0^{(n)}\Omega^n z}$ in Eq. 5.17 and the term $(1/n!)j^{n-1}\kappa_0^{(n)}\partial^n a/\partial t^n$ in Eq. 5.27 are both associated with the characteristic distortion distance $z_\kappa^{(n)}$. If we are interested only in propagation over distances $z \ll |z_\kappa^{(n)}|$, then both terms may be neglected.

It is worth noting that the envelope evolution equation may be derived directly from the dispersion integral without making use of the envelope frequency and wave number. We begin with the Taylor expansion of the dispersion relation about the carrier frequency. With the multiplication of both sides of the expansion by $p(z,t)$, and the replacement of q and ω by their associated operators, as shown in Eqs. 5.28, the expansion becomes

$$- \left(j\frac{\partial}{\partial z} + q_0 \right) p = \sum_{n=1}^{\infty} \frac{1}{n!} q_0^{(n)} \left(j\frac{\partial}{\partial z} - \omega_0 \right)^n p. \qquad (5.31)$$

With the introduction of the envelope-carrier form $p(z,t) = a(z,t)e^{j[q_0 z - \omega_0 t]}$, Eq. 5.31 becomes

$$- j\frac{\partial a}{\partial z}e^{j[q_0 z - \omega_0 t]} = \sum_{n=1}^{\infty} \frac{1}{n!} q_0^{(n)} \sum_{k=0}^{n} \binom{n}{k} j^k (-\omega_0)^{n-k} \frac{\partial^k}{\partial t^k} a(z,t)e^{j[q_0 z - \omega_0 t]}, \quad (5.32)$$

where $\binom{n}{k} = n!/(n-k)!k!$ is the binomial coefficient. The result of the differential operator $\partial^k/\partial t^k$ acting on the envelope-carrier form of the acoustic pressure field may similarly be expressed in terms of the binomial coefficients, and Eq. 5.32 may be written

$$- j\frac{\partial a}{\partial z} = \sum_{n=1}^{\infty} \frac{1}{n!} q_0^{(n)} \sum_{k=0}^{n} \binom{n}{k} j^k (-\omega_0)^{n-k} \sum_{l=0}^{k} \binom{k}{l} (-j\omega_0)^l \frac{\partial^{k-l} a}{\partial t^{k-l}},$$

or, equivalently,

$$- j\frac{\partial a}{\partial z} = \sum_{n=1}^{\infty} \frac{1}{n!} q_0^{(n)} \sum_{k=0}^{n} \sum_{i=0}^{k} \binom{n}{k}\binom{k}{i} (-1)^{k-i} (-\omega_0)^{n-i} j^{-i} \frac{\partial^i a}{\partial t^i}, \qquad (5.33)$$

where the index $i = k - l$ is flipped and shifted with respect to l. The double sum $\sum_{k=0}^{n} \sum_{i=0}^{k}$ may be rewritten $\sum_{i=0}^{n} \sum_{k=i}^{n}$, and the identity

$$\sum_{k=i}^{n} \binom{n}{k} \binom{k}{i} (-1)^{k-i} = \delta_{i,n},$$

where $\delta_{i,n}$ is the Kronecker delta function, may be used to express Eq. 5.33

$$\frac{\partial a}{\partial z} + \sum_{n=1}^{\infty} \frac{1}{n!} j^{n-1} q_0^{(n)} \frac{\partial^n a}{\partial t^n} = 0,$$

which is the envelope evolution equation found earlier.

5.3 Conventional Wave Pulse Envelope Solutions

We may now consider some solutions of the envelope evolution problem. These solutions determine the cell-to-cell or macrostructure of the Bloch wave pulse (the issue of the microstructure is addressed in Sec. 5.4). The reader should be reminded, however, that the envelope evolution integral determines the envelope function (and, by Eq. 5.15, the full pulse solution as well) for wave pulses that propagate in an arbitrary dissipative and/or dispersive conventional wave medium. As the problem to be solved here is generic, the results found here are likewise generic. The solutions serve not only to describe the macrostructure of the Bloch wave pulses that are of interest here, but serve also to describe the envelopes of pulses that propagate in an arbitrary dissipative and/or dispersive conventional wave medium as well.

While there are two "classic" solutions of the dispersive pulse propagation problem that appear in the literature (the "nondistorting pulse" solution shown in Sec. 5.3.1 and the "dispersive spreading" solution shown in Sec. 5.3.2), the conditions for the validity of these solutions is an issue that has not been addressed. As a consequence of the ill-defined validity of these solutions, the concept of group velocity, which becomes defined in the course of the aforementioned distortionless pulse solution, is likewise ill-defined in terms of conditions of validity. When the solutions are cast in terms of the characteristic distortion distances developed in Sec. 5.2.2, however, the validity of the

solutions becomes clearly defined. For this reason, the "nondistorting pulse" and "dispersive spreading" solutions are rederived here. In addition, several new solutions of the dispersive pulse propagation problem are presented. Novel dispersive distortion effects such as pulse carrier frequency shifting and pulse acceleration are found.

The pulse distortion effects may be categorized as being either of the AM type or the PM (or FM) type. The AM (amplitude modulation) distortion effects arise from distortion of the *magnitude* of the envelope function and PM (phase modulation) distortion effects arise from *phase* distortion of the envelope function. The magnitude of the envelope function is what is often considered to be the pulse envelope; it is the function that envelopes the pulse. As the magnitude of the envelope function evolves, so evolves the overall shape of the pulse. In other words, the magnitude of the envelope function carries the information as to the AM distortion effects. The phase of the envelope function, on the other hand, influences the pulse carrier. A net accumulation of phase in the envelope function at some value of z is reflected in a net phase shift of the pulse carrier. Time dependence in the envelope phase at some value of z causes phase modulation of the pulse carrier. The phase modulation may include net shifts in the carrier frequency or ramping of the carrier frequency. In other words, the phase of the envelope function carries information as to the FM distortion effects. Examples of AM and FM distortion are shown in Fig. 5.3.

5.3.1 Distortionless Pulse Propagation and the Bloch Wave Group Velocity

Consider the case in which the pulse propagates over a distance that is small compared to *any* of the characteristic pulse distortion distances. In other words, we have $z \ll |z_\kappa^{(n)}|$ for all $n \geq 2$, and $z \ll |z_\alpha^{(n)}|$ for all $n \geq 1$. We may therefore discard all envelope distortion terms in Eq. 5.30, and are left with only the first two terms. As is evident in the discussion following Eq. 5.30, the group velocity is $c_{\mathrm{gr}}(\omega) = 1/\kappa^{(1)}(\omega)$, and the group velocity evaluated at the carrier frequency is written $c_{\mathrm{g0}} = 1/\kappa^{(1)}(\omega_0) = 1/\kappa_0^{(1)}$. The envelope wave

(a) initial pulse

(b) AM distortion

(c) FM or PM distortion
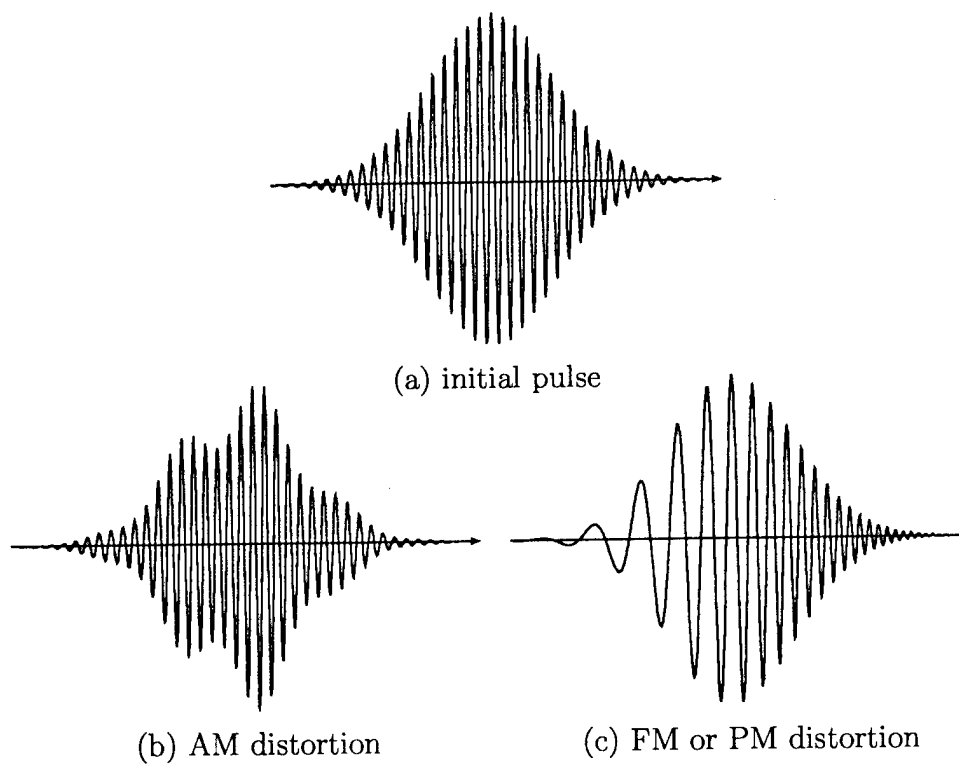
Figure 5.3: An example of an initial pulse and the pulse after having undergone AM and FM (or, equivalently, PM) distortion.

equation may therefore be written

$$\frac{\partial a}{\partial z} + \frac{1}{c_{g0}}\frac{\partial a}{\partial t} = 0, \tag{5.34}$$

which we recognize as the linear, lossless, progressive wave equation. If instead we choose the integral approach to the problem, we discard all envelope distortion terms in the envelope evolution integral (Eq. 5.17), and are left with

$$a(z,t) = \frac{1}{2\pi}\int_{-\infty}^{+\infty} A_0(\Omega)e^{j\kappa_0^{(1)}\Omega z}e^{-j\Omega t}d\Omega.$$

The effective dispersion relation is

$$q(\omega) = \kappa_0 + j\alpha_0 + \kappa_0^{(1)}(\omega - \omega_0).$$

The solution to the wave equation is simply $a(z,t) = a(t - z/c_{g0})$, or, with the application of the envelope boundary condition (Eq. 5.29), $a(z,t) = a_0(t - z/c_{g0})$. Similarly, the envelope evolution integral may easily be evaluated by rewriting it in the form of a Fourier transform:

$$a(z,t) = \frac{1}{2\pi}\int_{-\infty}^{+\infty} A_0(\Omega)e^{-j\Omega(t-z/c_{g0})}d\Omega = a_0(t - z/c_{g0}). \tag{5.35}$$

The pressure wave function, given by $p(z,t) = a(z,t)e^{j[q_0 z - \omega_0 t]}$, is therefore

$$p(z,t) = a_0(t - z/c_{g0})e^{-\alpha_0 z}e^{j[\kappa_0 z - \omega_0 t]}. \tag{5.36}$$

Equation 5.36 is the classic "nondistorting pulse" solution that is found in abundance in the literature. The carrier propagates at the phase velocity ω_0/κ_0 and decays exponentially at the decay rate α_0 (i.e., the carrier propagates as does the unmodulated carrier). The pulse envelope propagates without distortion at the group velocity c_{g0}. It is this solution that offers the most concrete definition of the group velocity.[2] *The pulse propagates at the group velocity over*

---

[2]The group velocity has other significant interpretations with regards to the velocity of energy transport, as shown in Sec. 7.3, and the asymptotic velocity of propagation of frequency information, as shown in Sec. 6.2.1

distances that are small compared to the smallest of the characteristic distortion distances. Beyond the smallest distortion distance, the pulse distorts and there is no generally applicable definition of the velocity of the pulse.

Both the dissipative and the nondissipative theoretical values of the group velocity for the isotropic waveguide described in the introduction are shown plotted in Fig. 5.4. In the passbands, the group velocity is less than
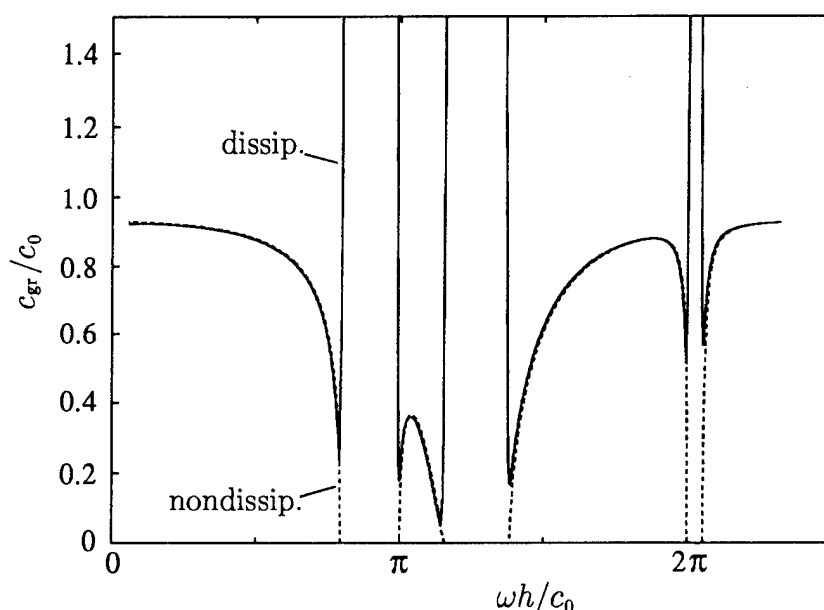
Figure 5.4: The dissipative and nondissipative group velocities for the isotropic periodic side branch waveguide. In the stopbands, the nondissipative group velocity is infinite.

AS-94-743

c_0, and decreases as a band edge is approached. In the stopbands, the group velocity is infinite in the nondissipative case and very large (compared to c_0) but finite in the dissipative case.

An example is illustrative. Consider a pulse with a carrier frequency of 3200 Hz and a duration of 8 carrier cycles that propagates in the isotropic periodic waveguide described in the introduction. The smallest of the characteristic distortion distances is, as shown in Fig. 5.2, about 200 waveguide cycles. The nondistorting pulse solution (Eq. 5.36) is therefore, for this pulse,
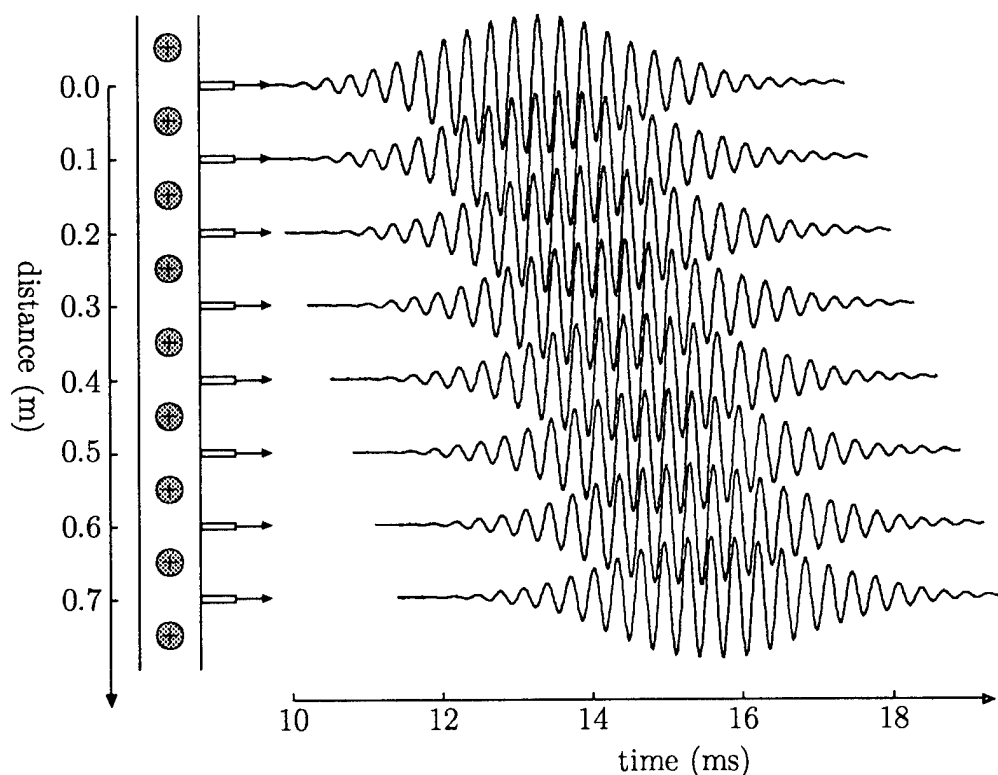
Figure 5.5: The time series measured at a sequence of locations in the isotropic periodic waveguide. The pulse has a carrier frequency of 3200 Hz, a duration of 8 cycles, and a Gaussian envelope. Each time series is placed at a position along the z axis that corresponds to the location of its measurement to result in a sort of characteristics plane view of the propagation of the pulse.

AS-94-744

valid up to distances of $\sim$5 m. In Fig. 5.5 is shown a sequence of measurements (described in Appendix E) of the acoustic pressure at the cell centers[3] for such a pulse. The time series obtained at a particular cell is shown at a position along the z axis that corresponds to that of the cell. The result is a sort of characteristics plane view of the propagating of the pulse. The pulse shows no noticeable distortion over the 0.8 m measurement range, as predicted on the

---

[3]At the cell centers, the Bloch wave pressure field is identical to that of the analogous conventional wave problem.
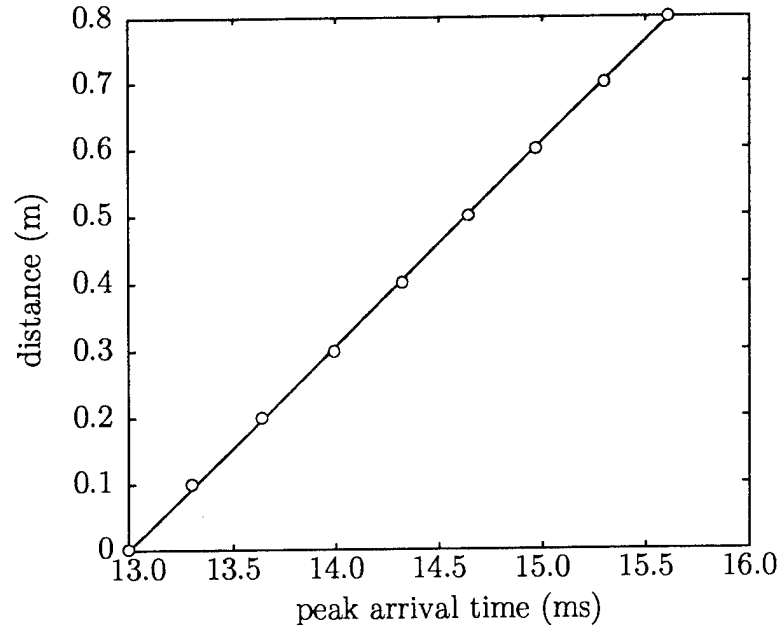
Figure 5.6: The arrival time of the pulse peaks for the data set shown in Fig. 5.5. The pulse has a carrier frequency of 3200 Hz and a duration of 8 cycles. The slope of this distance-time data is the group velocity.

AS-94-745

basis of the theory. In Fig. 5.6 is shown a plot of the time of arrival of the pulse peak as a function of distance. The pulse peak is simply the peak of the magnitude of the pulse envelope, which is determined by AM demodulation of the pulse, as described in Appendix E. The slope of such a curve should be, given the validity of the nondistorting pulse solution, a good measure of the group velocity. A linear regression of the time-distance data yields a slope of 302.0 m/s, and the theoretical value is 302.4 m/s. As is predicted on the basis of the theory, the pulse propagates without distortion at the group velocity.

One particularly intriguing feature of Bloch wave group velocity is that, in the stopbands, the group velocity becomes larger than the free-medium phase speed c_0. Indeed, in the nondissipative case the stopband group velocity is infinite! While such large, so-called "absorption band" group velocities are acknowledged in the literature, it is argued that in the absorption band, where the dispersion relation is complex, the expansion of the wave number, and

hence the solution and the definition of the group velocity, all become invalid (Jackson, 1975). While the real expansions that appear in the literature do indeed become invalid in the stopbands, the expansion used here (Eq. 5.19) is completely general. In our theory, the pulse propagates without distortion up to the smallest characteristic distortion distance regardless of whether or not the dispersion relation is complex.

Consider the case of an 8 cycle pulse of carrier frequency 1560 Hz that propagates in the isotropic waveguide described in the introduction. According to the theory, the pulse should propagate without distortion at a group velocity of 10,004 m/s up to a distance of about 1.4 m. In Fig. 5.7 is shown the characteristics plane view of a series of measurements of the acoustic pressure associated with such a pulse. While the pulse does decay as rapidly as would the unmodulated carrier, the pulse does indeed propagate with little or no distortion for nearly a meter at a very large group velocity. In this case, the linear regression of the peak arrival time against distance yields a group velocity of 3,158 m/s. While the measured group velocity is certainly large, it differs substantially from the theoretical value. This is due to the measurement inaccuracy that is inherent in the measurement approach. When the group velocity is very large, the peak arrival time becomes very small, and inaccuracy in the detection of the peak arrival time causes huge variation in the resultant propagation speed. It is clear, nonetheless, that the large stopband group velocities do indeed correspond to supersonic pulse propagation. While such pulses do propagate very fast, they don't, owing to the large associated attenuation, travel far. It is particularly striking to view all eight time series on the same temporal axis, as is shown in Fig. 5.8. *The pulse arrives at all downstream measurement locations simultaneously!* The phase of the carrier advances by π from cell-to-cell, as is expected of a Bloch wave with a π-stopband carrier frequency.

The Bloch wave group velocity is measured in the following manner. The time of arrival of the pulse peak is detected as a function of propagation distance over a range that is short compared to the smallest characteristic distortion distance for the pulse. Over such a measurement range, the nondistorting pulse solution (Eq. 5.36) is valid and a linear regression of the time-distance data should consequently be a good measure of the Bloch wave group veloc-
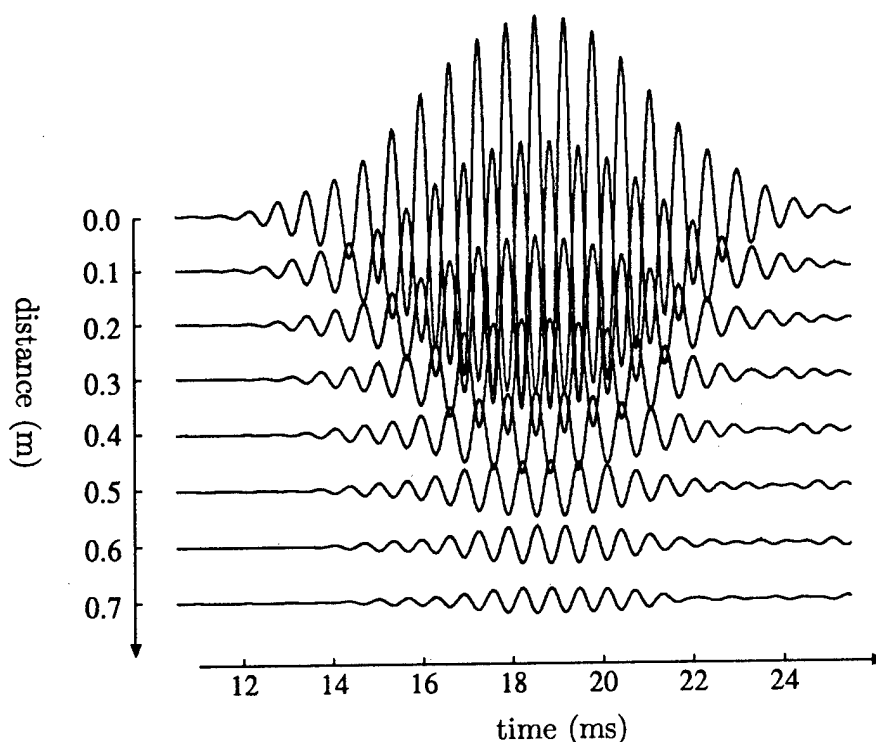
Figure 5.7: The characteristics plane view of measurements of a 1560 Hz (π Bragg stopband) Gaussian pulse with a characteristic duration of 8 cycles. Although it decays rapidly, the pulse arrives at all downstream microphone locations essentially simultaneously, indicating a very large group velocity.

AS–94-746

ity. A difficulty with such a measurement approach arises when the smallest characteristic distortion distance is less than a waveguide cycle length. In such a case the pulse is significantly or even severely distorted before propagating even a single structure period and the Bloch wave group velocity is immeasureable. The peak arrival time technique is therefore invalid over such ranges of frequency. Theoretical and measured values of the Bloch wave group velocity are shown in Fig. 5.9. The darkened bands indicate the frequency bands in which the smallest characteristic distortion distance is less than h. The theoretical and experimental results show fairly good agreement away from the band edges, and poor agreement in the vicinity of the band edges, as expected.

It should be noted that the distortionless pulse solution of the enve-
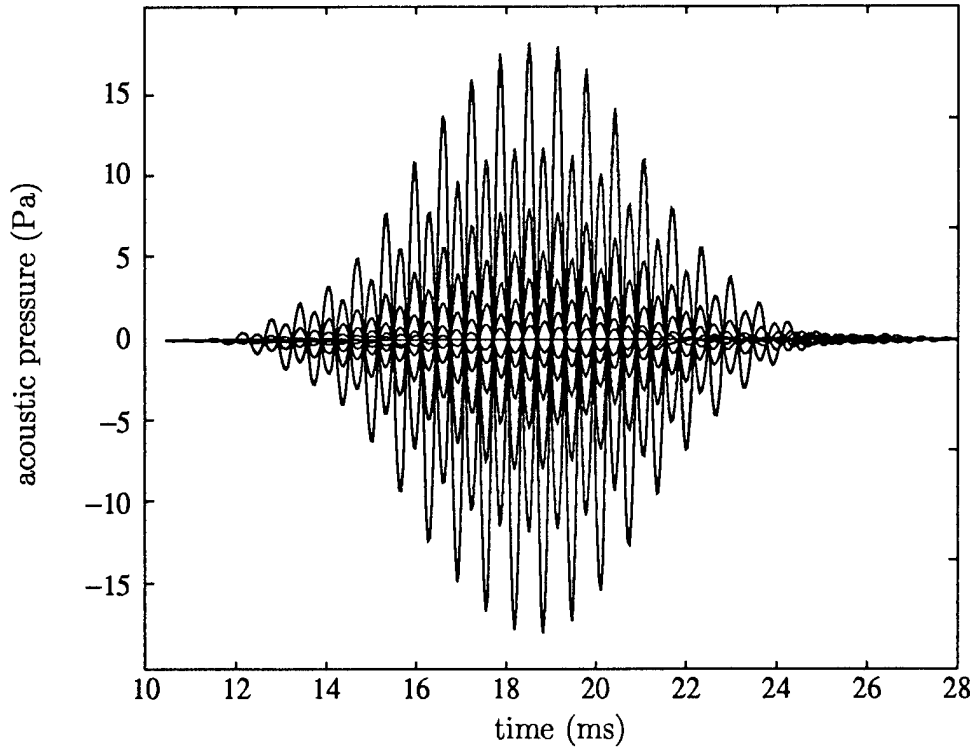
Figure 5.8: The measurements of the 1560 Hz (π Bragg stopband), 8 cycle Gaussian pulse shown in Fig. 5.7 shown on a single time axis. The pulse arrives at all downstream measurement locations essentially simultaneously.

AS–94-747

lope evolution integral is the only solution that may be found for an arbitrary source envelope function. In order to arrive at any further solutions, the source envelope function must be specified. In the remainder of the solutions shown here, for example, the source envelope function is taken to be a Gaussian. While these solutions (and conclusions based thereon) are therefore not as general as that shown above, they do serve to *demonstrate tendencies*, and are in that way of value.

5.3.2 $\kappa^{(2)}$ Distortion

In the case that the smallest characteristic pulse distortion distance is $z_\kappa^{(2)}$ (the dispersive distortion distance of lowest order), we may consider the evolution of a pulse under the influence of the pulse distortion term associ-
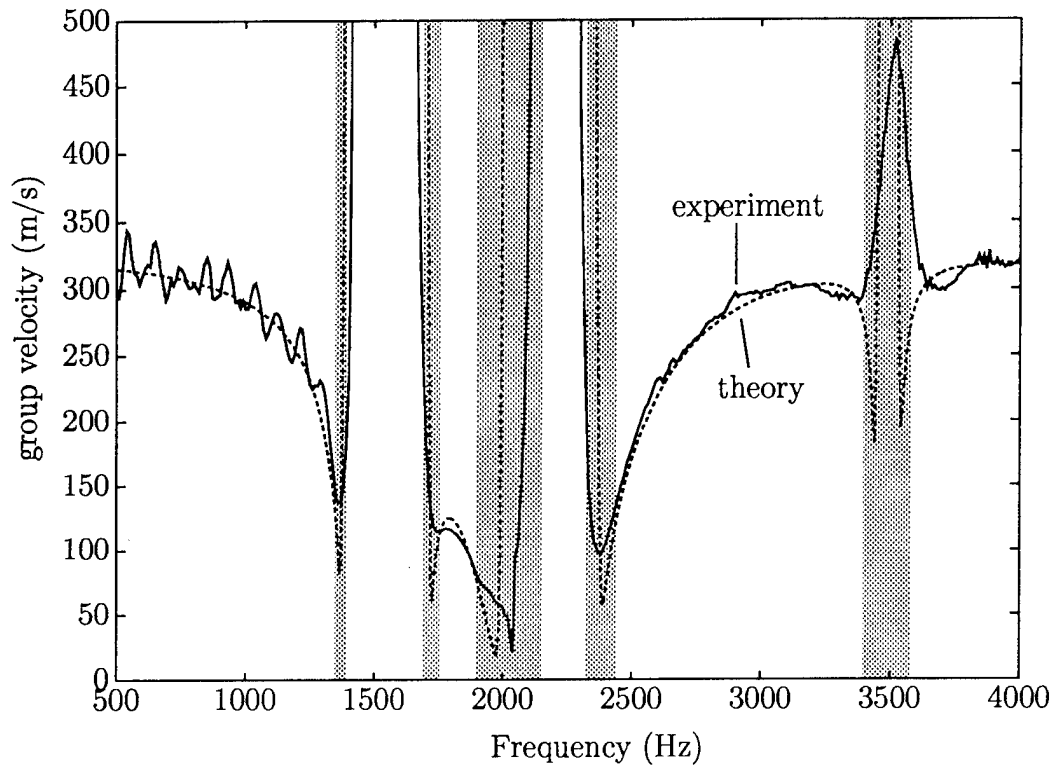
Figure 5.9: Theoretical and experimental values of the Bloch wave group velocity for the isotropic periodic side branch waveguide. The darkened bands indicate the bands of frequency in which the smallest characteristic distortion distance is less than the waveguide period, and the measurement technique consequently invalid.

ated with the distance $z_\kappa^{(2)}$ only. In other words, we restrict the distance of propagation of the pulse to distances such that $z \ll |z_\kappa^{(n)}|$ for all $n \geq 3$ and $z \ll |z_\alpha^{(n)}|$ for all $n \geq 1$. We do, however, allow propagation up to and beyond the distance $z_\kappa^{(2)}$. In such a case we may solve for the evolution of an initially Gaussian envelope to identify the characteristics of $\kappa_0^{(2)}$ distortion.

It should be noted that the $\kappa^{(2)}$ distortion solution shown here is not new. In fact, it is the classic "dispersive spreading" solution that is used to demonstrate the effects of dispersive distortion (Jackson, 1975). As in the case of the distortionless propagation solution (Eq. 5.36), however, it is not pointed out in the literature that the solution has a limited range of validity. In fact, if $z_\kappa^{(2)}$ is not the smallest of the characteristic distortion distances, then the solution is not valid at *any* range. The solution is rederived here simply to cast it in the light of the characteristic distortion distances and determine its range of validity.

Upon discarding all but the $\kappa_0^{(2)}$ distortion term, the envelope wave equation (Eq. 5.27) becomes

$$\frac{\partial a}{\partial z} + \frac{1}{c_{g0}}\frac{\partial a}{\partial t} + \frac{j}{2}\kappa_0^{(2)}\frac{\partial^2 a}{\partial t^2} = 0, \tag{5.37}$$

the associated envelope evolution integral is

$$a(z,t) = \frac{1}{2\pi}\int_{-\infty}^{+\infty} A_0(\Omega)e^{j\kappa_0^{(1)}\Omega z}e^{j\kappa^{(2)}\Omega^2 z}e^{-j\Omega t}d\Omega, \tag{5.38}$$

and the effective dispersion relation is

$$q(\omega) = \kappa_0 + j\alpha_0 + \kappa_0^{(1)}(\omega - \omega_0) + \frac{1}{2}\kappa_0^{(2)}(\omega - \omega_0)^2.$$

Note that the envelope wave equation (Eq. 5.37) is the linearized nonlinear Schrödinger equation for a boundary value problem (i.e., a spatial evolution form of the equation) (Jeffery and Kawahara, 1982). The source envelope function is taken to be the Gaussian function $a_0(t) = C_0 e^{-(t/\tau_0)^2}$, in which case the envelope spectrum is $A_0(\Omega) = C_0\tau_0\pi^{1/2}e^{-(\Omega\tau_0/2)^2}$. For such a source function, Eq. 5.38 is

$$a(z,t) = C_0\tau_0\pi^{1/2}\frac{1}{2\pi}\int_{-\infty}^{+\infty} e^{[-(\tau_0/2)^2+j\kappa_0^{(2)}z/2]\Omega^2}e^{-j[t-z/c_{g0}]\Omega}d\Omega,$$

which may be solved by completion of the quadratic in Ω in the exponential function and integration of the resultant Gauss-Fresnel type integral. The result, which is well known, is

$$a(z,t) = \frac{C_0}{[1 - j2\kappa_0^{(2)}z/\tau_0^2]^{1/2}} \exp\left\{-\frac{(t - z/c_{g0})^2}{\tau_0^2[1 - j2\kappa_0^{(2)}z/\tau_0^2]}\right\}. \tag{5.39}$$

We make use of the fact that $2\kappa_0^{(2)}z/\tau_0^2 = z/z_\kappa^{(2)}$, and rewrite Eq. 5.39

$$a(z,t) = \frac{C_0}{[1 + (z/z_\kappa)^2]^{1/4}} \exp\left\{-\frac{(t - z/c_{g0})^2}{\tau_0^2[1 + (z/z_\kappa)^2]}\right\}$$

$$\cdot \exp\left\{j\frac{1}{2}\tan^{-1}(z/z_\kappa) - j\frac{(t - z/c_{g0})^2}{\tau_0^2}\frac{z/z_\kappa}{1 + (z/z_\kappa)^2}\right\}, \tag{5.40}$$

where the superscript (2) has been left off of $z_\kappa^{(2)}$ for clarity. The scaling of z by the characteristic distortion distance z_κ is evident in its appearance only in the form z/z_κ. If $z \ll z_\kappa$, then Eq. 5.40 reduces to the distortionless solution

$$a(z,t) = C_0 e^{-(t-z/c_{g0})^2/\tau_0^2},$$

as expected (see Eq. 5.35).

The AM distortion effects that arise from the $\kappa_0^{(2)}$ term may be most readily identified by writing the magnitude of the envelope function in the form

$$|a(z,t)| = C(z)e^{-(t-z/c_{g0})^2/\tau(z)^2},$$

where we have introduced the pulse amplitude and duration functions

$$C(z) = \frac{C_0}{[1 + (z/z_\kappa)^2]^{1/4}},$$

$$\tau(z) = \tau_0[1 + (z/z_\kappa)^2]^{1/2}.$$

The envelope remains Gaussian at all values of z and propagates at the group velocity associated with the carrier frequency. The envelope also decays and disperses (i.e., spreads) according to the pulse amplitude and duration functions, which are shown in Fig. 5.10. We see that the pulse propagates essentially without distortion to the distance z_κ, where it begins to decay and
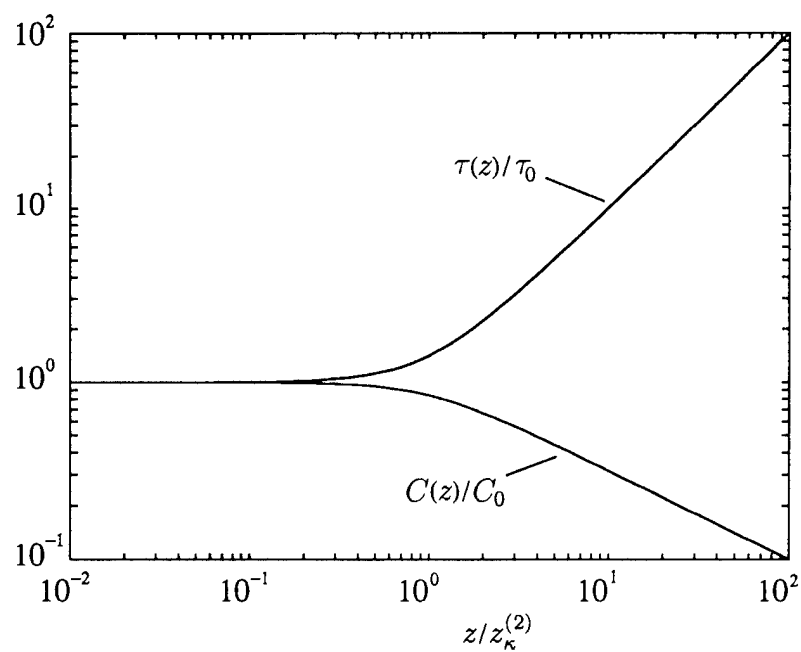
Figure 5.10: The amplitude and duration of a pulse under the influence of $\kappa^{(2)}$ distortion. The pulse propagates essentially without distortion out to the characteristic distortion distance $z_\kappa^{(2)}$, where it begins to decay and spread.

spread. Well beyond the characteristic distance the amplitude and duration functions asymptotically approach $C(z) \sim C_0(z/z_\kappa)^{-1/2}$ and $\tau(z) \sim \tau_0(z/z_\kappa)$, respectively. The pulse width increases without bound and the pulse amplitude decreases without bound.

The FM distortion effects are most readily investigated by consideration of the entire pressure wave function, which may be written

$$p(z,t) = C(z)e^{-(t-z/c_{g0})^2/\tau(z)^2}e^{-\alpha_0 z}e^{j\theta(z,t)}, \tag{5.41}$$

where the phase function

$$\theta(z,t) = \kappa_0 z - \omega_0 t - \left(\frac{t-z/c_{g0}}{\tau_0}\right)^2 \frac{z/z_\kappa}{1+(z/z_\kappa)^2} + \frac{1}{2}\tan^{-1}(z/z_\kappa)$$

has been introduced. The quadratic term in the phase function causes carrier frequency modulation and is most readily interpreted by introducing the local frequency (Whitham)

$$\omega_l(z,t) = -\frac{\partial\theta(z,t)}{\partial t} = \omega_0 + 2\left(\frac{z/z_\kappa}{1+(z/z_\kappa)^2}\right)\frac{t-z/c_{g0}}{\tau_0^2}, \tag{5.42}$$

which shows that the carrier frequency is indeed modulated. The local frequency is ω_0 at the pulse peak (at $t = z/c_{g0}$), and ramps down in time if the dispersion is anomalous (i.e., if $\kappa_0^{(2)} < 0$ and therefore $z_0 < 0$) and ramps up in time if the dispersion is normal (i.e., if $\kappa_0^{(2)} > 0$ and therefore $z_0 > 0$). This makes physical sense, as if the dispersion is anomalous, then the high frequency phase fronts propagate faster than the low frequency phase fronts. The higher (local) frequencies tend to migrate to the head of the group and low frequencies to the tail of the group, and we have downward ramping of the carrier frequency. As such a ramped FM pulse is generally referred to as a "chirp", the chirping that comes about as a consequence of the $\kappa_0^{(2)}$ dispersive distortion is referred to here as "dispersive chirping".

The degree of severity of the dispersive chirping is given by the chirp rate (in Hz/s):

$$m_\omega(z) = \frac{\partial\omega_l(z,t)}{\partial t} = \frac{z/z_\kappa}{1+(z/z_\kappa)^2}\frac{2}{\tau_0^2}.$$
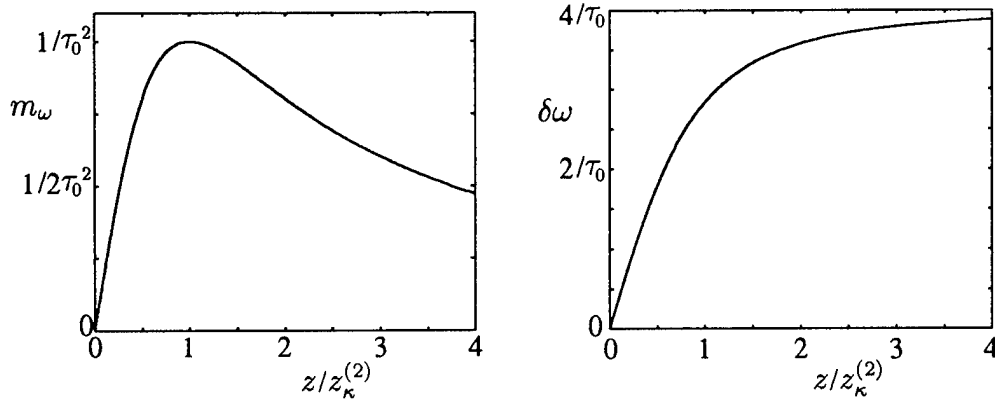
Figure 5.11: The chirp rate m_ω and the chirp magnitude $\delta\omega$ for a pulse under the influence of $\kappa^{(2)}$ distortion. The chirp rate increases until the pulse reaches the characteristic distortion distance, where it begins to decrease. The total chirp magnitude asymptotically approaches the frequency span of the pulse.

AS-94-750

As seen in Fig. 5.11, the chirp slope reaches a maximum value of $2/\tau_0^2$ at $z = z_\kappa$. The overall magnitude of the chirp may be taken to be the difference between the local frequencies at the pulse head (at $t = -\tau(z)$) and at the pulse tail (at $t = \tau(z)$). This frequency difference is

$$\delta\omega = \omega_l\big|_{t=\tau(z)} - \omega_l\big|_{t=-\tau(z)} = \frac{z/z_\kappa}{[1 + (z/z_\kappa)^2]^{1/2}} \frac{4}{\tau_0}.$$

As seen in Fig. 5.11, the chirp magnitude approaches an asymptotic value of $4/\tau_0$; i.e., it is limited by the range of frequencies available in the original pulse, which has a bandwidth of $4/\tau_0$. Indeed, this is the reason the chirp slope has an asymptotic value of zero. The chirp magnitude is limited by the frequency content of the pulse, but the degree of dispersive spreading is unlimited.

It is interesting to note that the $\kappa^{(2)}$ pulse distortion problem and a very well known problem in the theory of the propagation of highly collimated acoustic beams are isomorphic. When transformed into the retarded time frame $\tau = t - z/c_{g0}$, Eq. 5.37 becomes

$$\frac{\partial a}{\partial z} + \frac{j}{2}\kappa_0^{(2)} \frac{\partial^2 a}{\partial \tau^2} = 0.$$

The wave equation that describes the propagation of time harmonic waves from a highly directive axisymmetric source is the so-called paraxial wave equation

$$\frac{\partial p}{\partial z} - \frac{j}{2k}\frac{\partial^2 p}{\partial r_\perp^2} = 0,$$

where the radiation is directed along the axial coordinate z and $r_\perp$ is the transverse or radial cylindrical coordinate. The paraxial approximation is valid provided the beam is highly collimated. In other words, the angular spectrum of the acoustic beam must contain only a narrow band of spatial frequencies, just as the pulse must contain only a narrow band of temporal frequencies. The dispersive distortion of the pulse is analogous to the diffraction distortion of the beam profile. A beam that radiates from a source of characteristic size r_0 propagates as a collimated beam out to the Rayleigh distance $z_R = \frac{1}{2}kr_0^2$, where diffraction first has a significant effect on the beam profile. Up to the Rayleigh distance the beam profile changes little and the amplitude is nealy constant. Beyond the Rayleigh distance, the beam spreads and the amplitude drops. The Rayleigh distance is clearly the characteristic distance associated with diffraction. In a precisely analogous manner, we have shown that the pulse propagates essentially without distortion out to a distance of $z_\kappa^{(2)} = \frac{1}{2}(1/\kappa_0^{(2)})\tau_0^2$, where dispersion first has a significant distorting effect on the pulse. Beyond $z_\kappa^{(2)}$ the pulse spreads and decays, just like the beam.

5.3.3 $\alpha^{(1)}$ Attenuation Distortion

In the case that the smallest characteristic pulse distortion distance is $z_\alpha^{(1)}$ (the attenuation distortion distance of lowest order), we may consider the evolution of a pulse under the influence of the pulse distortion terms associated with the distance $z_\alpha^{(1)}$ only. In other words, we restrict the distance of propagation of the pulse to distances such that $z \ll |z_\kappa^{(n)}|$ for all $n \geq 2$ and $z \ll |z_\alpha^{(n)}|$ for all $n \geq 2$. We do, however, allow propagation up to and beyond the distance $z_\alpha^{(1)}$. Again, we may solve for the evolution of an initially Gaussian envelope to identify the characteristics of $\alpha^{(1)}$ distortion. It is found that, in addition to some other distortion effects, the pulse is subject to a "shifting carrier frequency" effect. At any particular value of z, the carrier frequency is uniform throughout the pulse (i.e., there is no chirping), but shifts as the pulse

propagates. To the author's knowledge, these distortion characteristics have not before been identified.

With the exclusion of all but the first attenuation distortion term, the envelope wave equation becomes

$$\frac{\partial a}{\partial z} + \frac{1}{c_{g0}}\frac{\partial a}{\partial t} + j\alpha_0^{(1)}\frac{\partial a}{\partial t} = 0.$$

The corresponding envelope evolution integral is

$$a(z,t) = \frac{1}{2\pi}\int_{-\infty}^{+\infty} A_0(\Omega)e^{j\kappa_0^{(1)}\Omega z}e^{-\alpha_0^{(1)}\Omega z}e^{-j\Omega t}d\Omega, \tag{5.43}$$

and the effective dispersion relation is

$$q(\omega) = \kappa_0 + j\alpha_0 + \kappa_0^{(1)}(\omega - \omega_0) + j\alpha_0^{(1)}(\omega - \omega_0). \tag{5.44}$$

We again consider the evolution of an initially Gaussian envelope (i.e., $a_0(t) = C_0 e^{-(t/\tau_0)^2}$), in which case Eq. 5.43 becomes

$$a(z,t) = \frac{1}{2\pi}\int_{-\infty}^{+\infty} C_0\tau_0\pi^{1/2}e^{-(\tau_0/2)^2\Omega^2}e^{-\alpha_0^{(1)}\Omega z}e^{-j\Omega(t-z/c_{g0})}d\Omega.$$

As before, completion of the quadratic in Ω results in a Gauss-Fresnel type integral, the solution of which is

$$a(z,t) = C_0 e^{-(t-z/c_{g0}-j\alpha_0^{(1)}z)^2/\tau_0^2}. \tag{5.45}$$

With the introduction of the characteristic distortion distance $z_\alpha^{(1)} = \tau_0/2\alpha_0^{(1)}$, the envelope function may be expressed

$$a(z,t) = C_0 e^{-(t-z/c_{g0})^2/\tau_0^2}e^{(z/2z_\alpha)^2}e^{j(z/z_\alpha)(t-z/c_{g0})/\tau_0}, \tag{5.46}$$

where the superscript (1) has been left off of $z_\alpha^{(1)}$ for clarity. Again we see the appearance of the characteristic form z/z_α, and when $z \ll z_\alpha$ we recover the distortionless solution.

The AM distortion effects are investigated by consideration of the envelope magnitude

$$|a(z,t)| = C_0 e^{(z/2z_\alpha)^2}e^{-(t-z/c_{g0})^2/\tau_0^2}.$$

The pulse propagates at the group velocity and is of constant duration, as in the case of the distortionless solution. The pulse amplitude differs from the distortionless solution by the quadratic exponential term. While the term appears to represent pulse amplification, it is, as is shown later, best explained in terms of FM distortion effects.

The FM distortion effects are investigated by writing the pulse function in the form

$$p(z,t) = C_0 e^{-(t-z/c_{g0})^2/\tau_0^2} e^{-\alpha_0[1-(z/z_\alpha)/4z_\alpha\alpha_0]z} e^{j\theta(z,t)}, \tag{5.47}$$

where the phase function is

$$\theta(z,t) = \kappa_0 \left[1 - \frac{z/z_\alpha}{\kappa_0\tau_0 c_{g0}}\right] z - \omega_0 \left[1 - \frac{z/z_\alpha}{\omega_0\tau_0}\right] t.$$

The local frequency is

$$\omega_l = -\frac{\partial\theta(z,t)}{\partial t} = \omega_0 \left[1 - \frac{z/z_\alpha}{\omega_0\tau_0}\right], \tag{5.48}$$

which is independent of time; i.e., there is no chirping. At a given distance, the local frequency is constant throughout the pulse but *shifts linearly with distance*. The pulse appears as a strictly amplitude modulated carrier with the z-dependent carrier frequency

$$\omega_c(z) = \omega_0 \left[1 - \frac{z/z_\alpha}{\omega_0\tau_0}\right]. \tag{5.49}$$

The pulse solution, it turns out, may be expressed concisely in terms of dispersion parameters evaluated at the shifting carrier frequency $\omega_c(z)$. The value of the Bloch wave number at the carrier frequency is

$$q(\omega_c) = q(\omega_0 - 2\alpha_0^{(1)}z/\tau_0^2) = q(\omega_0) - q_0^{(1)}2\alpha_0^{(1)}z/\tau_0^2$$

$$= \kappa_0[1 - \frac{z/z_\alpha}{c_{g0}\kappa_0\tau_0}] + j\alpha_0[1 - \frac{z/z_\alpha}{2\alpha_0 z_\alpha}],$$

and the full pulse solution may therefore be expressed

$$p(z,t) = C_0 e^{-(z/2z_\alpha)^2} e^{-(t-z/c_{g0})^2/\tau_0^2} e^{j[q(\omega_c)z-\omega_c t]}.$$

Aside from the unusual Gaussian attenuation term, the solution is well represented in terms of the dispersion relation evaluated at the shifted carrier frequency. The attenuation term, however, may be explained in terms of the change in excitation level that occurs as the carrier shifts. Because the carrier frequency shifts linearly with distance and the pulse spectrum is Gaussian, the effective excitation at the carrier frequency decreases in level in a Gaussian manner as the pulse propagates. We have $A_0(\omega) = C_0 \tau_0 \pi^{1/2} e^{-(\omega \tau_0/2)^2}$, so that $A_0(\omega_c - \omega_0) = C_0 \tau_0 \pi^{1/2} e^{-(z/2z_a)^2}$, or $C_0 e^{-(z/2z_a)^2} = \frac{A_0(\omega_c - \omega_0)}{\tau_0 \pi^{1/2}}$. The pulse wave function may therefore be written

$$p(z,t) = \frac{A_0(\omega_c - \omega_0)}{\tau_0 \pi^{1/2}} e^{-(t-z/c_{g0})^2/\tau_0^2} e^{j[q(\omega_c)z - \omega_c t]}.$$

The nondistorting pulse solution found in Sec. 5.3.1 is, for the Gaussian envelope boundary condition $a(0,t) = C_0 e^{(t/\tau_0)^2}$, simply

$$p(z,t) = \frac{A_0(\omega_0 - \omega_0)}{\tau_0 \pi^{1/2}} e^{-(t-z/c_{g0})^2/\tau_0^2} e^{j[q(\omega_0)z - \omega_0 t]}.$$

The solutions are identical except that in the distortionless pulse solution, all frequency dependent parameters are evaluated at the initial carrier frequency ω_0 and in the $\alpha_0^{(1)}$ distortion solution they are all evaluated at the *current* carrier frequency ω_c. It is worth noting that the only frequency dependent parameter that is evaluated at the initial carrier frequency ω_0 instead of at the current carrier frequency $\omega_c(z)$ is the group velocity. This is because we have assumed that $z \ll |z_\kappa^{(2)}|$, which implies that the dispersion relation has effectively zero curvature over the pulse bandwidth (see Eq. 5.44). The group velocity associated with a dispersion relation with zero curvature is frequency independent. The group velocity evaluated at the shifting carrier frequency is equal to that evaluated at the initial carrier frequency. It may be anticipated at this point that if the dispersion had nonzero curvature, the shifting carrier frequency would be accompanied by a shifting group velocity, which would cause pulse *acceleration*. Such a possibility is considered in Sec. 5.3.4.

The mechanism for the variety of pulse distortion effects found in Eq. 5.47 is most clearly demonstrated in the frequency domain. The envelope evolution integral (Eq. 5.43) may be written

$$a(z,t) = \frac{1}{2\pi} \int_{-\infty}^{+\infty} \left[A_0(\Omega) e^{-\alpha_0^{(1)} \Omega z} \right] e^{-j\Omega(t - z/c_{g0})} d\Omega,$$
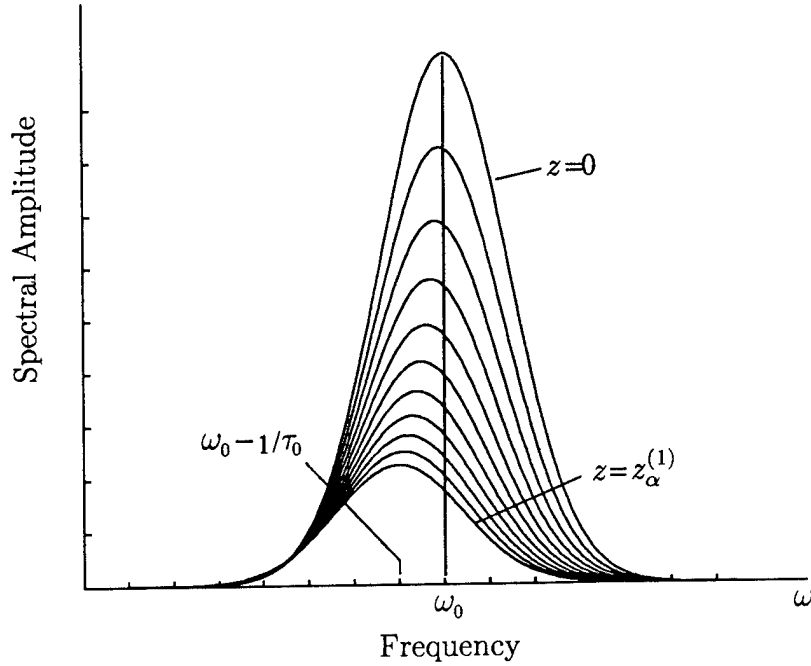
Figure 5.12: The pulse spectrum at a sequence of distances for a pulse under the influence of $\alpha^{(1)}$ distortion. As the pulse propagates, the spectrum is filtered such that the spectral peak, and hence the pulse carrier frequency, are shifted down.

in which form we see that the effective envelope spectrum at some value of z is $A_0(\Omega)e^{-\alpha_0^{(1)}\Omega z}$. The initial envelope spectrum is filtered by an exponential filter function that becomes progressively steeper as the pulse propagates. As the envelope spectrum is Gaussian, the effective spectrum is

$$A_0(\Omega)e^{-\alpha_0^{(1)}\Omega z} \propto e^{-(\tau_0/2)^2\Omega^2}e^{-\alpha_0^{(1)}\Omega z}$$
$$\propto e^{\alpha_0^{(1)2}z^2}e^{-(\tau_0/2)^2[\Omega+2\alpha_0^{(1)}z/\tau_0^2]^2},$$

which, in spite of the progressive filtration, remains Gaussian at all values of z. The center frequency of the Gaussian, however, is shifted by an amount $2\alpha_p^{(1)}/\tau_0^2$ or $z/z_\alpha\tau_0$. We expect the pulse, therefore, to have a carrier frequency that is shifted linearly with distance, which is what we find in Eq. 5.48. When $\alpha_0^{(1)}$ and therefore z_α are positive, the carrier is shifted down in frequency, and when $\alpha_0^{(1)}$ and z_α are negative, the shift in frequency is upward. In other words, *the carrier frequency is shifted away from the more highly attenuated frequencies*. At $z = z_\alpha$, the carrier has been shifted by $1/\tau_0$, or one quarter of
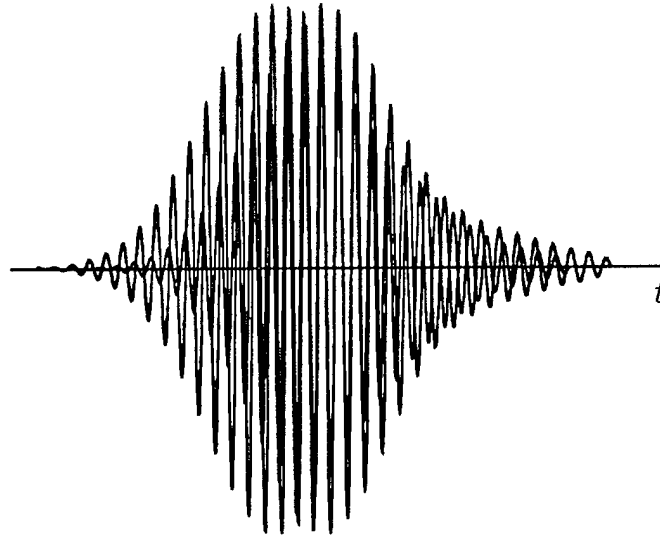
Figure 5.13: Normalized signals measured 0.8 m apart for a 1442 Hz, 12 cycle Gaussian pulse. It may be seen that the two signals go in and out of phase with one another as time advances. This is reflective of the change in carrier frequency after having propagated 0.8 m.

AS-94-752

the pulse bandwidth. An example of this shifting spectrum effect is shown in Fig. 5.12. The pulse spectrum is shown at intervals of $z_\alpha^{(1)}/10$ between $z = 0$ and $z = z_\alpha^{(1)}$.

The shifting carrier frequency effect is seen clearly in measurements. For a 1442 Hz pulse with a duration of 12 carrier cycles, the first several characteristic distortion distances are $z_\alpha^{(1)} = 1.07\text{m}$, $z_\alpha^{(2)} = 3.23\text{m}$, $z_\kappa^{(2)} = 40.4\text{m}$, and $z_\kappa^{(3)} = 668\text{m}$. Such a pulse should, up to a distance of about 1 m, be well described by the $\alpha^{(1)}$ distortion solution. In Fig. 5.13 is shown two of the measurements of the pulse taken 0.8 m apart, normalized and displayed on the same time axis. The difference in the carrier frequency may be seen by noting that the pulse carriers go in and out of phase with one another with time. In Fig. 5.14 is shown the measured local frequency at the pulse peak as a function of distance for such a pulse. The local frequency is found by FM demodulation of the measured pulse time series, as described in Appendix E. Also shown in the plot are theoretical values from Eq. 5.49. The carrier frequency, as predicted by the theory, ramps away from the stopband frequencies, which are associated with strong attenuation. While the data shown in Fig. 5.14 cer-
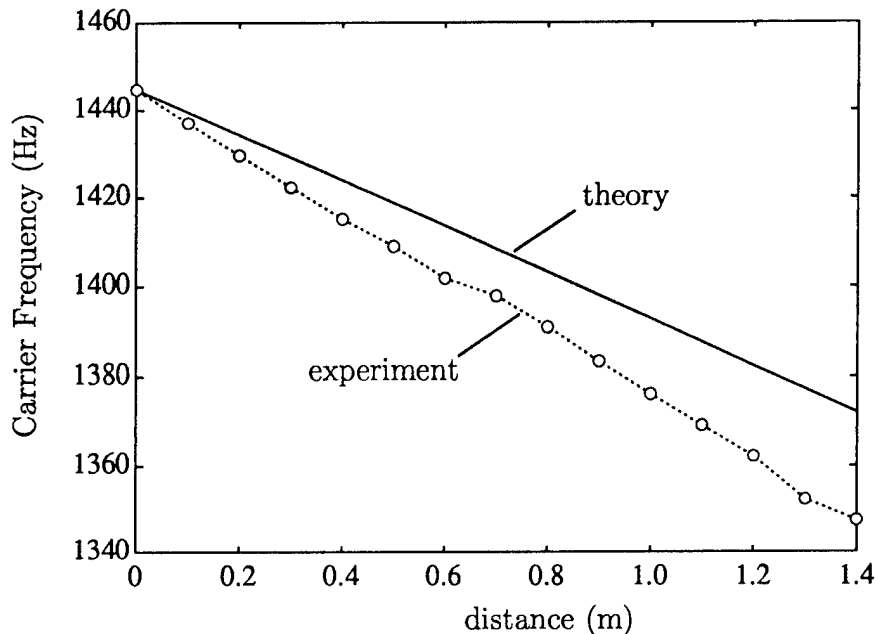
Figure 5.14: Theoretical and experimental values of the carrier frequency of a 1442 Hz, 12 cycle Gaussian pulse at a sequence of distances. The carrier shifts down in frequency as the pulse propagates.

AS-94-753

tainly seem to verify the shifting carrier frequency effect conclusively, the same trend in the data could come about as an artifact of dispersive chirping. The chirping could be such that local frequency *at the pulse peak* shows a monotonic decrease with distance, but the frequency of the pulse as a whole shows no such decrease. In Fig. 5.15 is shown the local frequency as a function of time for the pulse at the sequence of distances. It is seen that the frequency shift does indeed occur across the pulse and is not simply an artifact of chirping. While there is a degree of dispersive chirping (no chirping would be indicated by a time-independent local frequency), it is clear that there is a net decrease in the local frequency as the pulse propagates.
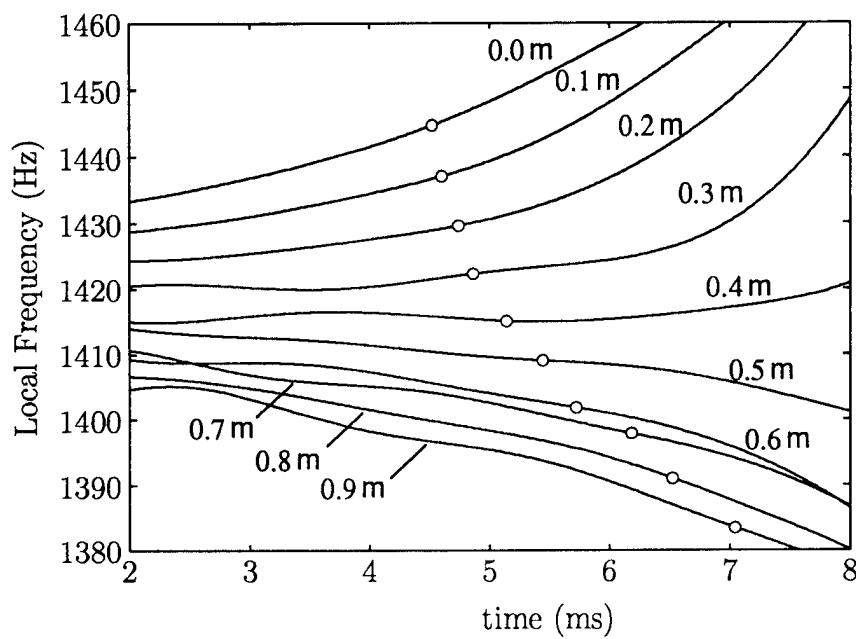
Figure 5.15: The local frequency as a function of time for a Gaussian pulse of carrier frequency 1442 Hz and of 18 cycle duration. While there clearly is evidence of dispersive chirping (the local frequency is not constant), the net frequency of the pulse as a whole does indeed shift down in frequency with distance. The circles indicate the location of the peak of the pulse.

5.3.4 $\alpha^{(1)} \cdot \kappa^{(2)}$ Distortion

In each of the previously considered cases, the envelope distortion due to a single distortion term was considered. The $\kappa^{(2)}$, $\alpha^{(1)}$, and $\alpha^{(2)}$ distortion terms have each been considered independently. Here, the combined effect of the $\alpha^{(1)}$ and the $\kappa^{(2)}$ distortion terms is considered.

With the exclusion of all but the $\alpha^{(1)}$ and the $\kappa^{(2)}$ distortion terms, the envelope wave equation becomes

$$\frac{\partial a}{\partial z} + \frac{1}{c_{g0}}\frac{\partial a}{\partial t} + j\alpha_0^{(1)}\frac{\partial a}{\partial t} + \frac{j}{2}\kappa_0^{(2)}\frac{\partial^2 a}{\partial t^2} = 0.$$

The corresponding envelope evolution integral and dispersion relation are

$$a(z,t) = \frac{1}{2\pi}\int_{-\infty}^{+\infty} A_0(\omega)e^{j\kappa_0^{(1)}\Omega z}e^{j(\kappa_0^{(2)}/2)\Omega^2 z}e^{-\alpha_0^{(1)}\Omega z}e^{-j\Omega t}d\Omega \tag{5.50}$$

and

$$q(\omega) = \kappa_0 + j\alpha_0 + \kappa_0^{(1)}(\omega - \omega_0) + j\alpha_0^{(1)}(\omega - \omega_0) + \tfrac{1}{2}\kappa_0^{(2)}(\omega - \omega_0)^2,$$

respectively. For the case of an initially Gaussian envelope, Eq. 5.50 becomes

$$a(z,t) = C_0\tau_0\pi^{1/2}\frac{1}{2\pi}\int_{-\infty}^{+\infty} e^{[-(\tau_0/2)^2 - j\kappa_0^{(2)}z/2]\Omega^2}e^{-j[t - \kappa_0^{(1)}z - j\alpha_0^{(1)}z]\Omega}d\Omega,$$

which may be integrated to result in

$$a(z,t) = \frac{C_0}{[1 - 2j\kappa_0^{(2)}z/\tau_0^2]^{1/2}}\exp\left\{-\frac{(t - z/c_{g0} - j\alpha_0^{(1)}z)^2}{\tau_0^2(1 - 2j\kappa_0^{(2)}z/\tau_0^2)}\right\}.$$

With the introduction of the distortion distances $z_\kappa^{(2)}$ and $z_\alpha^{(1)}$, which are here abbreviated as z_κ and z_α, respectively, the envelope solution becomes

$$a(z,t) = \frac{C_0}{[1 + (z/z_\kappa)^2]^{1/4}}e^{j\frac{1}{2}\tan^{-1}(z/z_\kappa)}$$

$$\cdot \exp-\left\{\left(\frac{t - z/c_{g0}}{\tau(z)}\right)^2 + \left(\frac{t - z/c_{g0}}{\tau(z)}\right)\frac{(z/z_\alpha)(z/z_\kappa)}{[1 + (z/z_\kappa)^2]^{1/2}} - \frac{(z/z_\alpha)^2}{4[1 + (z/z_\kappa)^2]}\right\}$$

$$\cdot \exp j \left\{ - \left(\frac{t - z/c_{g0}}{\tau(z)} \right)^2 (z/z_\kappa) \right.$$

$$\left. + \left(\frac{t - z/c_{g0}}{\tau(z)} \right) \frac{(z/z_\alpha)}{[1 + (z/z_\kappa)^2]^{1/2}} - \frac{(z/z_\alpha)^2 (z/z_\kappa)}{4[1 + (z/z_\kappa)^2]} \right\},$$

where, again, $\tau(z) = \tau_0 [1 + (z/z_\kappa)^2]^{1/2}$.

The AM distortion effects are found by consideration of the magnitude of the envelope

$$|a(z,t)| = C(z) e^{(z/2z_\alpha)^2} e^{-[t - z(1/c_{g0} - \alpha_0^{(1)} z/z_\kappa)]^2/\tau(z)^2},$$

where $C(z) = C_0 [1 + (z/z_\kappa)^2]^{-1/4}$. The pulse envelope remains Gaussian, has a duration given by $\tau(z)$ (i.e., it spreads after it reaches z_κ), has an amplitude given by $C(z)$ (i.e., it decays after it reaches z_κ), and propagates at a group velocity that differs from $c_{g0} = 1/\kappa^{(1)}(\omega_0)$, the group velocity associated with the initial carrier frequency ω_0. The modified, z-dependent group velocity may be written

$$\hat{c}_{gr}(z) = \frac{c_{g0}}{1 - \alpha_0^{(1)} c_{g0}(z/z_\kappa)}.$$

In other words, the pulse accelerates or decelerates as it propagates!

The FM effects are again investigated by expressing the pulse function in the form

$$p_c(z,t) = |a(z,t)| e^{-\alpha_0 z} e^{j\theta(z,t)},$$

where the phase function is

$$\theta(z,t) = \kappa_0 z - \omega_0 t + \frac{1}{2} \tan^{-1}(z/z_\kappa) - \left(\frac{t - z/c_{g0}}{\tau(z)} \right)^2 (z/z_\kappa)$$

$$+ \left(\frac{t - z/c_{g0}}{\tau(z)} \right) \frac{(z/z_\alpha)}{[1 + (z/z_\kappa)^2]^{1/2}} + \frac{(z/z_\alpha)^2 (z/z_\kappa)}{4[1 + (z/z_\kappa)^2]},$$

and the local frequency is

$$\omega_l(z,t) = \omega_0 - \frac{\tau_0}{\tau(z)^2}(z/z_\alpha) + 2\frac{t - z/c_{g0}}{\tau(z)}(z/z_\kappa).$$

If we define the carrier frequency ω_c to be the local frequency evaluated at the envelope peak, then it is found that

$$\omega_c(z) = \omega_l(z,t)|_{t=z/\hat{c}_{gr}} = \omega_0 - \frac{z/z_\alpha}{\tau_0},$$

which is the same shifting carrier frequency found in the $\alpha^{(1)}$ distortion case. With such a definition of carrier frequency, we also find that the group velocity associated with the carrier frequency is

$$c_{gr}(\omega_c) = 1/\kappa^{(1)}(\omega_c)$$
$$= [\kappa^{(1)}(\omega_0) + \kappa^{(2)}(\omega_0)(\omega_c - \omega_0)]^{-1} = \hat{c}_{gr}.$$

The pulse propagates at the group velocity associated with the carrier frequency. The carrier frequency shifts as the group propagates, and the (frequency dependent) group velocity likewise shifts. The attenuation α and the spectral amplitude $A_0(\omega)$ may similarly be evaluated at the carrier frequency, and the pulse amplitude may be expressed

$$|p_c(z,t)| \propto C(z) A_0(\omega_c - \omega_0) e^{-\alpha(\omega_c)z} e^{-[t-z/c_{gr}(\omega_c)]^2/\tau(z)^2}.$$

In this very concise expression for the pulse magnitude, *all frequency dependent parameters are evaluated at the shifting carrier frequency* $\omega_c(z)$. As the pulse propagates, the carrier frequency, amplitude, attenuation, and group velocity all shift.

Like the shifting carrier frequency, the shifting group velocity is clearly evident in measurement. In Fig. 5.16 is shown the pulse envelope (AM demodulated pulse) for a 1440 Hz Gaussian pulse of 12 carrier cycle duration as measured at a sequence of cell centers. The acoustic pressure waveform measured at each cell center is normalized to unit amplitude and AM demodulated as described in Appendix E. Each resultant envelope function is then placed at the position along the distance axis that corresponds to the measurement location to result in the characteristics plane view of the pulse propagation. In the early part of the pulse propagation, the pulse arrives at successive measurement ports nearly simultaneously, which indicates a very large group velocity (as is expected of a stopband frequency pulse). After about a half meter of propagation, however, a substantial interval of time lapses between the arrival
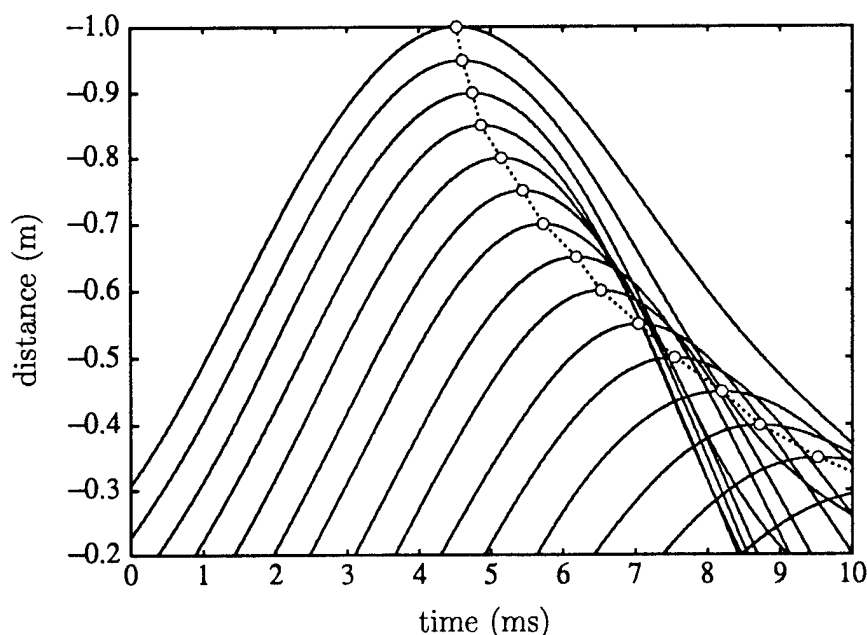
Figure 5.16: The envelope of a Gaussian pulse of carrier frequency 1440 Hz and of 12 cycle duration as measured at a sequence of cell centers. The envelopes are normalized to unit amplitude and arranged according to their measurement locations to result in the characteristics plane view of the propagating pulse. Each envelope peak is encircled to show the trajectory of the pulse peak in the space-time plane, which is that of a decelerating pulse.

AS-94-755

of the pulse at successive measurement ports. This interval of time gradually increases as the pulse propagates, which indicates a gradual deceleration of the pulse.

5.4 The Recovery Operations

In this section we consider the Bloch wave pulse that is recovered from the solution of the analogous conventional wave problem. In other words, we turn the investigation from one of the macrostructures of the Bloch wave pulse to one of its microstructures. We first find more useful forms of the recovery operations found in Sec. 5.1.3. While those recovery operators show that the recovery operator method is indeed a valid approach to the solution

of the Bloch dispersion integral, they are here cast in much more useful forms. It is shown that the operators may be expressed such that (1) they act on the envelope function instead of the full pulse function, and (2) they are in the form of a *differential* operator. The full Bloch wave pulse solution may therefore be expressed simply in terms of the envelope solution and its derivatives.

For each of the three representations of Bloch wave functions, the recovered Bloch wave pulse appears in the form of a series. In addition to the exact expression for the recoverd Bloch wave pulse, then, approximate (i.e., truncated series) expressions are also found. In the quasiperiodic and traveling wave spectral representations the Bloch wave pulse is found to be, to leading order, simply the carrier frequency time harmonic Bloch wave function modulated by the envelope function. In the convolution representation a similar (though not identical) result is found to leading order, and the first higher order correction is found to take the form of a simple modification to the f-wave/g-wave makeup of the pulse.

5.4.1 The Quasiperiodic Recovery Operator

In the quasiperiodic representation, the Bloch wave pulse may be expressed

$$
\begin{aligned}
p(z,t) &= \frac{1}{2\pi} \int_{-\infty}^{+\infty} \Phi_q(z,\omega) P_{\mathrm{c}}(z,\omega) e^{-j\omega t} d\omega \\
&= e^{j(q_0 z - \omega_0 t)} \frac{1}{2\pi} \int_{-\infty}^{+\infty} \Phi_q(z,\omega) A_0(\omega - \omega_0) e^{jQ(\omega - \omega_0)z} e^{-j(\omega - \omega_0)t} d\omega \\
&= e^{j(q_0 z - \omega_0 t)} \frac{1}{2\pi} \int_{-\infty}^{+\infty} \Phi_q(z,\omega_0 + \Omega) A_0(\Omega) e^{jQ(\Omega)z} e^{-j\Omega t} d\Omega \\
&= e^{j(q_0 z - \omega_0 t)} \bar{\phi}_q(z,t) *_t a(z,t),
\end{aligned}
$$

where $\bar{\phi}_q(z,t) = \frac{1}{2\pi} \int \Phi_q(z,\omega_0 + \Omega) e^{-j\Omega t} d\Omega$. The recovery operator that acts on the envelope function is therefore

$$
e^{j(q_0 z - \omega_0 t)} \bar{\phi}_q(z,t) *_t .
$$

The operator is made more useful by expressing it in differential form. The periodic modulation function $\Phi_q(z,\omega_0 + \Omega)$ may be Taylor expanded about

$\Omega = 0$ to yield

$$\Phi_q(z, \omega_0 + \Omega)|_{\Omega \sim 0} = \sum_m \frac{1}{m!} \Phi_q^{(m)}(z, \omega_0)\Omega^m,$$

where $\Phi_q^{(m)}(z, \omega_0) = d^m\Phi_q^{(m)}(z, \omega_0 + \Omega)/d\Omega^m\big|_{\Omega=0}$. The function $\bar{\phi}_q(z, t)$ may be expressed as

$$\bar{\phi}_q(z, t) = \frac{1}{2\pi} \int_{-\infty}^{+\infty} \sum_m \frac{j^m}{m!} \Phi_q^{(m)}(z, \omega_0)(-j\Omega)^m e^{-j\Omega t} d\Omega$$

$$= \sum_m \frac{j^m}{m!} \Phi_q^{(m)}(z, \omega_0)\frac{\partial^m}{\partial t^m}\delta(t),$$

and the recovery operator becomes the differential operator

$$e^{j(q_0 z - \omega_0 t)} \sum_m \frac{j^m}{m!} \Phi_q^{(m)}(z, \omega_0)\frac{\partial^m}{\partial t^m}.$$

When the recovery operator acts on the envelope function, the recovered Bloch wave pulse is

$$p(z, t) = a(z, t)\Phi_q(z, \omega_0)e^{j(q_0 z - \omega_0 t)} + j\dot{a}(z, t)\Phi_q^{(1)}(z, \omega_0)e^{j(q_0 z - \omega_0 t)} + \cdots$$

$$= a(z, t)\Phi_q(z, \omega_0)e^{j(q_0 z - \omega_0 t)}\left[1 + j\frac{\Phi_q^{(1)}(z, \omega_0)}{\Phi_q(z, \omega_0)}\frac{\dot{a}(z, t)}{a(z, t)} + \cdots\right],$$

where $\dot{a}$ represents the partial differentiation, with repect to time, of the enve-lope function. The leading term in the series is

$$p(z, t) = a(z, t)\Phi_q(z, \omega_0)e^{j(q_0 z - \omega_0 t)} = a(z, t)F(z, \omega_0)e^{-j\omega_0 t}, \tag{5.51}$$

which is simply the time harmonic Bloch wave function at the carrier fre-quency, modulated by the envelope function. To this degree of approximation, the recovery operator is simply the multiplicative operator $F(z, \omega_0)e^{-j\omega_0 t}$. For narrowband pulses, the $\dot{a}/a$ term is small on the scale of ω_0. While this would tend to support the validity of the truncated series, we must investigate the magnitude of the $\Phi_q^{(1)}(z, \omega_0)/\Phi_q(z, \omega_0)$ term to be certain. In the interest of conciseness, the effect of the higher order terms in the series is investigated for the convolution representation of the recovery operator only.

5.4.2 The Traveling Wave Spectral Recovery Operator

In the traveling wave spectral representation, the Bloch wave pulse may be expressed

$$
\begin{aligned}
p(z,t) &= \frac{1}{2\pi} \int_{-\infty}^{+\infty} \sum_n C_n(\omega) e^{2\pi j n z/h} \hat{p}_c(z,\omega) e^{-j\omega t} d\omega \\
&= \sum_n e^{j[(q_0+2\pi n/h)z-\omega_0 t]} \frac{1}{2\pi} \int_{-\infty}^{+\infty} C_n(\omega) A_0(\omega-\omega_0) e^{jQ(\omega-\omega_0)z} e^{-j(\omega-\omega_0)t} d\omega \\
&= \sum_n e^{j[(q_0+2\pi n/h)z-\omega_0 t]} \frac{1}{2\pi} \int_{-\infty}^{+\infty} C_n(\omega_0+\Omega) A_0(\Omega) e^{jQ(\Omega)z} e^{-j\Omega t} d\Omega \\
&= \sum_n e^{j[(q_0+2\pi n/h)z-\omega_0 t]} \bar{c}_n(t) *_t a(z,t),
\end{aligned}
$$

where $\bar{c}_n(t) = \int C_n(\omega_0+\Omega) e^{-j\Omega t} d\Omega/2\pi$. The envelope operator form of the recovery operator is therefore

$$
\sum_n e^{j[(q_0+2\pi n/h)z-\omega_0 t]} \bar{c}_n(t) *_t .
$$

In order to find the differential form of the operator, we Taylor expand the traveling wave spectral amplitude function $C_n(\omega_0+\Omega)$ about $\Omega = 0$:

$$
C_n(\omega_0+\Omega)|_{\Omega\sim 0} = \sum_m \frac{1}{m!} C_n^{(m)}(\omega_0) \Omega^m,
$$

where $C_n^{(m)}(\omega_0) = d^m C_n(\omega_0+\Omega)/d\Omega^m|_{\Omega=0}$. The function $\bar{c}_n(t)$ may therefore be expressed

$$
\begin{aligned}
\bar{c}_n(t) &= \frac{1}{2\pi} \int_{-\infty}^{+\infty} \sum_m \frac{j^m}{m!} C_n^{(m)}(\omega_0) (-j\Omega)^m e^{-j\Omega t} d\Omega \\
&= \sum_m \frac{j^m}{m!} C_n^{(m)}(\omega_0) \frac{\partial^m}{\partial t^m} \delta(t),
\end{aligned}
$$

and the recovery operator becomes

$$
\sum_n e^{j[(q_0+2\pi n/h)z-\omega_0 t]} \sum_m \frac{j^m}{m!} C_n^{(m)}(\omega_0) \frac{\partial^m}{\partial t^m}.
$$

When the recovery operator acts on the envelope function, the recovered Bloch wave pulse is

$$
\begin{aligned}
p(z,t) &= \sum_n e^{j[(q_0+2\pi n/h)z-\omega_0 t]} \left[C_n(\omega_0) a(z,t) + j C_n^{(1)}(\omega_0) \dot{a}(z,t) + \cdots \right] \\
&= a(z,t) \sum_n C_n(\omega_0) e^{j[(q_0+2\pi n/h)z-\omega_0 t]} \left[1 + j \frac{C_n^{(1)}(\omega_0)}{C_n(\omega_0)} \frac{\dot{a}(z,t)}{a(z,t)} + \cdots \right].
\end{aligned}
$$

The leading term is

$$p(z,t) = a(z,t) \sum_n C_n(\omega_0) e^{j[(q_0 + 2\pi n/h)z - \omega_0 t]}$$

$$= a(z,t) F(z, \omega_0) e^{-j\omega_0 t},$$

which is, as in the case of the leading term in the quasiperiodic recovery of the Bloch wave pulse, simply the time harmonic Bloch wave function at the carrier frequency, modulated by the envelope function. Each traveling wave spectral component is of the form $a(z,t) e^{j[(q_0 + 2\pi n/h)z - \omega_0 t]}$; i.e., the Bloch wave function is composed of pulsed traveling wave spectral components. It is of interest to note that when z is much smaller than all characteristic distortion distances, half of the components of the traveling wave spectrum are of the form

$$a_0(t - z/c_{g0}) C_{-|n|} e^{j[-|2\pi n/h - q_0|z - \omega_0 t]}.$$

We see explicitly that the "backward wave" behavior of the traveling wave spectral components of Bloch waves occurs in Bloch wave pulses as well as in time harmonic Bloch waves (see Sec. 3.31). The group travels in the $+z$ direction and the phase travels in the $-z$ direction.

5.4.3 The Convolution Recovery Operator

Before we proceed to find an expression for the recovery operator in the convolution representation, it is worthwhile to consider the Bloch wave pulses that are recovered by use of the quasiperiodic and traveling wave spectral recovery operators. In both of those cases it is found that, to leading order, the Bloch wave pulse is given by $p(z,t) = a(z,t) F(z, \omega_0) e^{-j\omega_0 t}$. The pulse is simply the time harmonic Bloch wave of frequency ω_0 modulated by the envelope function $a(z,t)$. This result, expressed in the convolution representation, is, in the nth cell,

$$p(z,t) = a(z,t) \left[\frac{1}{1 + g/f(\omega_0)} e^{j[k_0(z-nh) - \omega_0 t]} \right.$$

$$\left. + \frac{g/f(\omega_0)}{1 + g/f(\omega_0)} e^{j[-k_0(z-nh) - \omega_0 t]} \right] e^{jq_0 n h}. \tag{5.52}$$

The f and g-wave components of this approximate solution are readily identified as

$$f(z,t) = a(z,t)\frac{1}{1+g/f(\omega_0)}e^{jq_0nh}e^{j[k_0(z-nh)-\omega_0t]}$$

$$g(z,t) = a(z,t)\frac{g/f(\omega_0)}{1+g/f(\omega_0)}e^{jq_0nh}e^{j[-k_0(z-nh)-\omega_0t]},$$

where $p(z,t) = f(z,t) + g(z,t)$. In the nth waveguide section, then, this solution predicts the f-wave amplitude to be proportional to $a(z,t)e^{j[k_0(z-nh)-\omega_0t]}$. Such a result is not generally expressible in the form $f(z,t) = \hat{f}[t-(z-nh)/c_0]$, and is therefore not a valid waveguide-type solution. In other words, the approximation made in the truncation of the two preceding representations of the Bloch wave pulse yields an approximate solution that does not represent valid waveguide-type wave propagation. It is shown here that the analogous series truncation in the case of the convolution representation of the Bloch wave pulse results in an apporoximate solution *does* exhibit valid waveguide-type behavior. In other words, the f and g waves may be expressed in the form $f(z,t) = \hat{f}[t-(z-nh)/c_0]$ and $g(z,t) = \hat{g}[t+(z-nh)/c_0]$, respectively.

In the convolution representation, the Bloch wave pulse may be expressed

$$p(z,t) = \frac{1}{2\pi}\int_{-\infty}^{+\infty}\sum_n \hat{p}_c(nh,\omega)\psi(z-nh,\omega)e^{-j\omega t}d\omega$$

$$= \sum_n e^{j(q_0nh-\omega_0t)}\frac{1}{2\pi}\int_{-\infty}^{+\infty}A_0(\Omega)e^{jQ(\Omega)nh}\psi(z-nh,\omega_0+\Omega)e^{-j\Omega t}d\Omega$$

$$= \bar{\psi}(z,t) *_z *_t \sum_n e^{j(q_0nh-\omega_0t)}\delta(z-nh)a(z,t),$$

where $\bar{\psi} = \int\psi(z,\omega_0+\Omega)e^{-j\Omega t}d\Omega/2\pi$, and the multiplication of $a(z,t)$ by the lattice precedes the convolutions. The envelope operator form of the convolution operator is therefore

$$\bar{\psi}(z,t) *_z *_t \sum_n e^{j(q_0nh-\omega_0t)}\delta(z-nh).$$

In order to simplify the derivation of the differential form of the convolution recovery operator, we make an approximation in the expression for $\psi(z,\omega)$.

While the approximation is not necessary, it greatly clarifies the procedure. We have

$$\psi(z,\omega) = \frac{e^{jk(\omega)z} + g/f(\omega)e^{-jk(\omega)z}}{1 + g/f(\omega)}R(z),$$

where $R(z) = H(z + h/2) - H(z - h/2)$ is the rectancular function and $H(z)$ is the Heaviside or unit step function. It is assumed that $k(\omega) \simeq \omega/c_0 + j\text{Im}\{k(\omega_0)\}$. In other words, the f and g waves are assumed to propagate without dispersion and with the dissipation associated with the carrier frequency. This assumption is justified as the amplitudes of the f and g waves are known at the cell centers, and we need only determine the field at points a maximum distance of $h/2$ from the cell center. The error accumulated over such a small distance is, with the exception of cases of extremely large attenuation and pulse bandwidths, extremely small. Using the approximate expression for the wave number, the cell wave function may be expressed

$$\psi(z,\omega_0 + \Omega) = \frac{e^{jk_0 z}e^{j(\Omega/c_0)z} + g/f(\omega_0 + \Omega)e^{-jk_0 z}e^{-j(\Omega/c_0)z}}{1 + g/f(\omega_0 + \Omega)}R(z),$$

and therefore

$$\bar{\psi} = R(z)e^{jk_0 z}\frac{1}{2\pi}\int_{-\infty}^{+\infty} L_f(\Omega)e^{-j\Omega(t-z/c_0)}d\Omega$$

$$+ R(z)e^{-jk_0 z}\frac{1}{2\pi}\int_{-\infty}^{+\infty} L_g(\Omega)e^{-j\Omega(t+z/c_0)}d\Omega, \qquad (5.53)$$

where

$$L_f(\Omega) = \frac{1}{1 + g/f(\omega_0 + \Omega)} \qquad \text{and} \qquad L_g(\Omega)\frac{g/f(\omega_0 + \Omega)}{1 + g/f(\omega_0 + \Omega)}.$$

We may now proceed to find the differential form of the recovery operator. Expansions of $L_f(\Omega)$ and $L_g(\Omega)$ about $\Omega = 0$ are

$$L_f(\Omega)|_{\Omega\sim 0} = \sum_m \frac{1}{m!}L_f^{(m)}(0)\Omega^m \qquad \text{and} \qquad L_g(\Omega)|_{\Omega\sim 0} = \sum_m \frac{1}{m!}L_g^{(m)}(0)\Omega^m,$$

where $L_f^{(m)}(0) = d^m L_f(\Omega)/d\Omega^m|_{\Omega=0}$ and $L_g^{(m)}(0) = d^m L_g(\Omega)/d\Omega^m|_{\Omega=0}$. The substitution of these expansions into Eq. 5.53 yields

$$\bar{\psi}(z,t) = R(z)e^{jk_0 z}\frac{1}{2\pi}\int_{-\infty}^{+\infty}\sum_m \frac{j^m}{m!}L_f^{(m)}(0)(-j\Omega)^m e^{-j\Omega(t-z/c_0)}d\Omega$$

$$+R(z)e^{-jk_0z}\frac{1}{2\pi}\int_{-\infty}^{+\infty}\sum_m\frac{j^m}{m!}L_g^{(m)}(0)(-j\Omega)^m e^{-j\Omega(t+z/c_0)}d\Omega$$

$$=R(z)\sum_m\frac{j^m}{m!}\left\{e^{jk_0z}L_f^{(m)}(0)\frac{\partial^m}{\partial t^m}\delta(z-nh)\right.$$

$$\left.+e^{-jk_0z}L_g^{(m)}(0)\frac{\partial^m}{\partial t^m}\delta(z+nh)\right\}.$$

The recovery operator in differential form may therefore be written

$$R(z)\sum_m\frac{j^m}{m!}\left\{e^{jk_0z}L_f^{(m)}(0)\frac{\partial^m}{\partial t^m}\delta(z-nh)+e^{-jk_0z}L_g^{(m)}(0)\frac{\partial^m}{\partial t^m}\delta(z+nh)\right\}$$

$$*_z*_t\sum_n e^{j(q_0nh-\omega_0)t}\delta(z-nh).$$

When the recovery operator acts on the envelope function, we have

$$p(z,t)=\sum_n\left[e^{j[k_0(z-nh)-\omega_0t]}\sum_m\frac{j^m}{m!}L_f^{(m)}(0)\frac{\partial^m}{\partial t^m}a(nh,t-(z-nh)/c_0)\right.$$

$$\left.+e^{j[-k_0(z-nh)-\omega_0t]}\sum_m\frac{j^m}{m!}L_g^{(m)}(0)\frac{\partial^m}{\partial t^m}a(nh,t+(z-nh)/c_0)\right]R(z-nh).$$

The exponential term before each sum in the square brackets makes it evident that the first sum represents the f wave and the second the g wave. In the nth cell, therefore, the f and g waves are given by the series

$$f(z,t)=e^{j[k_0(z-nh)-\omega_0t]}\sum_m\frac{j^m}{m!}L_f^{(m)}(0)\frac{\partial^m}{\partial t^m}a(nh,t-(z-nh)/c_0)e^{jq_0nh}$$

$$g(z,t)=e^{j[-k_0(z-nh)-\omega_0t]}\sum_m\frac{j^m}{m!}L_g^{(m)}(0)\frac{\partial^m}{\partial t^m}a(nh,t+(z-nh)/c_0)e^{jq_0nh}. \quad (5.54)$$

We now consider the leading order terms in the series representation of the recovered Bloch wave pulse. In the nondissipative case, the leading term in each series represents, in the nth cell, an f wave-g wave field given by

$$f(z,t)=e^{jq_0nh}a(nh,t-(z-nh)/c_0)\frac{1}{1+g/f(\omega_0)}e^{-j\omega_0(t-(z-nh)/c_0)}$$

$$g(z,t)=e^{jq_0nh}a(nh,t+(z-nh)/c_0)\frac{g/f(\omega_0)}{1+g/f(\omega_0)}e^{-j\omega_0(t+(z-nh)/c_0)}.$$

Note that this approximate field is not equal to $a(z,t)F(z,\omega_0)e^{-j\omega_0 t}$ (i.e., that shown in Eq. 5.52). In particular, the wave behavior in the waveguide sections is of the form $f(z,t) = \hat{f}(t - (z - nh)/c_0)$ and $g(z,t) = \hat{g}(t + (z - nh)/c_0)$, which represents valid waveguide-type wave behavior. In other words, the series trunction leads, in this case, to an approximate solution with valid wave behavior in the waveguide sections. The f and g waves are modulated such that at the cell center they are given by

$$f(nh,t) = a(nh,t)\frac{1}{1 + g/f(\omega_0)}e^{j[q_0 nh - \omega_0 t]}$$

$$g(nh,t) = a(nh,t)\frac{g/f(\omega_0)}{1 + g/f(\omega_0)}e^{j[q_0 nh - \omega_0 t]}.$$

The f and g waves are simply counterpropagating conventional wave pulses with the same envelope function as the Bloch wave pulse. The relative amplitude of the f and g wave pulses is, at the cell center, that of the carrier frequency time-harmonic Bloch wave.

To investigate the influence of the higher order terms in the series, we consider the f and g wave envelopes. At the center of the nth cell, these envelope functions are, from Eq. 5.54, given by

$$a_f(nh,t) = e^{jq_0 nh}\sum_m \frac{j^m}{m!}L_f^{(m)}(0)\frac{\partial^m}{\partial t^m}a(nh,t)$$

$$a_g(nh,t) = e^{jq_0 nh}\sum_m \frac{j^m}{m!}L_g^{(m)}(0)\frac{\partial^m}{\partial t^m}a(nh,t).$$

With the inclusion of up to the second terms in the series, the envelope functions may be written[4]

$$a_f(nh,t) = a(nh,t)L_f(0)\exp\left[j\frac{L_f^{(1)}(0)}{L_f(0)}\frac{\dot{a}(nh,t)}{a(nh,t)}\right]e^{jq_0 nh}$$

---

[4]The approximation made in expressing the wave envelopes in this representation is of the same order as that made in the truncation of the series: $\sum_n (j\epsilon)^n = 1 + j\epsilon + \mathcal{O}(\epsilon^2) = e^{j\epsilon} + \mathcal{O}(\epsilon^2)$.

$$a_g(nh, t) = a(nh, t) L_g(0) \exp\left[j \frac{L_g^{(1)}(0)}{L_g(0)} \frac{\dot{a}(nh, t)}{a(nh, t)} \right] e^{jq_0 nh}.$$

If nh is less than the smallest of the characteristic distortion distances, then we have $a(nh, t) = a_0(t - nh/c_{g0})$. If $a_0(t)$ is the Gaussian function $a_0(t) = e^{-(t/\tau_0)^2}$, then the envelope functions are given by

$$a_f(nh, t) = a_0(t - z/c_{g0}) L_f(0) \exp\left[-j \frac{L_f^{(1)}(0)}{L_f(0)} \frac{2(t - nh/c_{g0})}{\tau_0^2} \right]$$

$$a_g(nh, t) = a_0(t - z/c_{g0}) L_g(0) \exp\left[-j \frac{L_g^{(1)}(0)}{L_g(0)} \frac{2(t - nh/c_{g0})}{\tau_0^2} \right].$$

To leading order in the series it was found that the f and g wave envelopes are simply that of the Bloch wave at the cell center. Here we see that the next term in the series introduces a time dependent phase modulation. Such a phase modulation simply causes a frequency shift in the f and g waves:

$$\omega_f = \omega_0 + \frac{L_f^{(1)}(0)}{L_f(0)} \frac{2}{\tau_0^2} = \omega_0 - \frac{g/f_0^{(1)}}{1 + g/f_0} \frac{2}{\tau_0^2}$$

$$\omega_g = \omega_0 - \frac{L_g^{(1)}(0)}{L_g(0)} \frac{2}{\tau_0^2} = \omega_0 + \frac{g/f_0^{(1)}}{g/f_0(1 + g/f_0)} \frac{2}{\tau_0^2}.$$

Shown in Fig. 5.17 is a plot of these frequency shifts as functions of carrier frequency for the case of a pulse with eight carrier cycles over the characteristic pulse duration $2\tau_0$. Away from the stopbands, the shifts are small, which implies the validity of the truncated series. Near the stopbands, the frequency shifts become large and the validity of a truncated version of the series is doubtful.
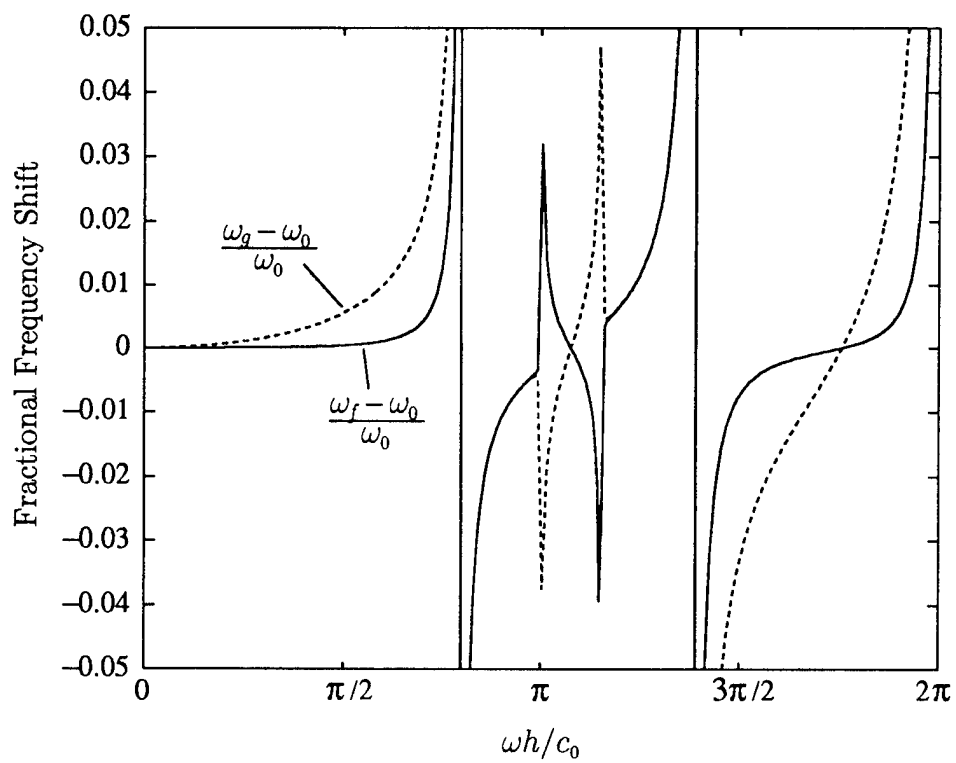
Figure 5.17: The fractional shifts in frequency of the f and g waves as a function of carrier frequency for an 8 cycle Gaussian pulse.

This page intentionally left blank.

Chapter 6

Asymptotic Pulse Propagation

In this chapter we consider the propagation of Bloch wave pulses in the limit as the propagation distance z becomes large. We concentrate on the asymptotic solution of the conventional wave dispersion integral associated with the analogous conventional wave problem in order to find the macrostructure of the Bloch wave pulse in the large z limit. While it is not done here, the full Bloch wave pulse solution may readily be recovered from the solution of the conventional wave dispersion integral with the use of one of the recovery operators found in Chapter 5. We first consider the case in which dissipative mechanisms are absent and later consider the effect of dissipation.

The analysis is composed of two parts. The first is the evaluation of the dispersion integral in the asymptotic sense and the second is the application of the results to the particular system under study. The asymptotic evaluation of the dispersion integral has been performed using a variety of techniques (Whitham, 1974; Lighthill, 1980). Most of the previous work has been directed at the solution of the dispersion integral associated with the *initial* value problem

$$p(z,t) = \frac{1}{2\pi} \int_{-\infty}^{+\infty} \Lambda(k) e^{j[kz-\omega(k)t]} dk$$

for large values of t as opposed to that associated with the *boundary* value problem

$$p(z,t) = \frac{1}{2\pi} \int_{-\infty}^{+\infty} \Lambda(\omega) e^{j[k(\omega)z-\omega t]} d\omega$$

131

for large values of z, which is that solved here. Owing to the similarity of the two integrals, however, the solutions are very simply related.

The asymptotic integration method used is the stationary phase technique. While the method of steepest descent and the asymptotic Fourier integral approach are both valid alternative approaches and are both better suited to the determination of the degree of error in the asymptotic approximation (Whitham, 1974), such errors have been examined extensively (Lighthill, 1980) and the validity of the results firmly established. That work having been done, the method of stationary phase is chosen for its relative simplicity.

The second part of the analysis is the application of the results of the asymptotic integration to a system with Bloch wave dispersion. The approach is based on the fact that the passband portions of the Bloch dispersion curve have a highly characteristic form. A number of characteristics that are common to every passband turn out to be important in the determination of the asymptotic form of the pulse. We are therefore able to determine several substantial characteristics of the pulse at large z for a wide variety of initial pulses. In particular, we are able to determine:

- The functional form and arrival time of the leading edge of the pulse.

- The qualitative form of the "body" of the pulse.

- The functional form of the tail of the pulse, and whether the pulse remains localized or develops a long tail.

The specific integral to be solved for large z is defined as follows. As the problem under consideration is nondissipative (the effect of dissipation is considered in Sec. 6.5) we have $q(\omega) = \kappa(\omega)$ in the passbands and $q(\omega) = n\pi + j\alpha(\omega)$, where n is an integer, in the stopbands. We consider the source spectrum to be the sum of the two disjoint spectra $\Lambda_{pb}(\omega)$ and $\Lambda_{sb}(\omega)$, which are nonzero only in the passband and stopband, respectively. As the waves that arise from stopband frequencies are exponentially localized to the vicinity of the source and do not contribute significantly to the asymptotic field, the contribution to the asymptotic field by $\Lambda_{sb}(\omega)$ is negligible. The dispersion

integral to be solved is therefore

$$p(z,t) = \frac{1}{2\pi} \int_{-\infty}^{+\infty} \Lambda_{\mathrm{pb}}(\omega) e^{j[\kappa(\omega)z - \omega t]} d\omega,$$

where q has been replaced by κ because they differ only in the stopbands, where $\Lambda_{\mathrm{pb}}(\omega) = 0$. With the definition of the phase function $\theta(\omega, z, t) = \kappa(\omega)z - \omega t$, the dispersion integral becomes

$$p(z,t) = \frac{1}{2\pi} \int_{-\infty}^{+\infty} \Lambda(\omega) e^{j\theta(\omega,z,t)} d\omega, \tag{6.1}$$

where the "pb" subscript has been dropped from $\Lambda_{\mathrm{pb}}(\omega)$ with the understanding that, from this point on, we are concerned only with the passband portion of the source spectrum.

It is assumed for the time being that the passband source spectrum $\Lambda(\omega)$ is a real function. The results are generalized to include complex source spectra in Sec. 6.3. The restriction that this assumption imposes upon the source function itself is that the magnitude of the envelope function must be symmetric about $t = 0$ and the phase of the source function (and therefore the phase modulation of the carrier) must be antisymmetric about $t = 0$. Another interpretation of the phase restriction is that the local frequency associated with the source function (and therefore the frequency modulation of the carrier) must be symmetric about $t = 0$. In other words, both amplitude and frequency modulation of the carrier must be symmetric about $t = 0$.

6.1   The Stationary Phase Approach

The stationary phase approach to the solution exploits the fact that, for large values of z, the exponential term in the integral is an extremely rapidly oscillating function of frequency. The oscillation rate is $\partial\theta/\partial\omega = z(\partial\kappa/\partial\omega) - t$, which increases linearly with z and may therefore be made arbitrarily large by imposing the requirement that z be arbitrarily large. If the source spectrum function $\Lambda(\omega)$ changes only negligibly over a range of frequencies in which the argument of the exponential function increases (as a roughly linear function of frequency) by 2π, then the integral over that range of frequecies is itself negligible. It appears, then, that the entire integral becomes trivial. Note,

however, that the oscillation rate becomes *zero* when $\kappa^{(1)}(\omega)z = t$. When z is large the oscillation rate is very large *except in the near vicinity of the frequencies where* $\kappa^{(1)}(\omega)z = t$. The integral is therefore negligible except in the near vicinity of the set of frequencies $\omega = \omega_{sp}(z, t)$, given by the expression

$$\kappa^{(1)}(\omega_{sp})z = t, \tag{6.2}$$

where the phase function is stationary. These are the so-called stationary phase frequencies.[1] The frequency intervals in which the integral is non-trivial are called the stationary phase regions (each stationary phase frequency is encompassed by a stationary phase region). As z increases, each stationary phase region shrinks in size until the integral is negligible everywhere but in the very near vicinity of the stationary phase frequencies. We may therefore simply solve the integral in the vicinity of each stationary phase frequency and sum the results.

While the portions of the integrand that lie in the stationary phase regions certainly make the most significant contribution to the total value of the integral, we must also consider a second set of frequencies. As is shown in Sec. 6.3, for a given distance z there is a critical time t_c before which the phase function $\theta(\omega, z, t)$ increases monotonically with frequency and is not stationary at any frequency. In other words, Eq. 6.2 has no real solutions for $t < t_c$. During this pre-critical time interval, the dominant contributions to the integral arise from the spectral regions in which the phase advance rate is most *gradual* (i.e., most *nearly* stationary). These frequencies, referred to here as the *gradual phase* frequencies, are those at which the phase rate $\kappa^{(1)}(\omega)z - t$ is a minimum:

$$\kappa^{(2)}(\omega_{gp}) = 0. \tag{6.3}$$

An example of the form of the phase function at pre-critical, critical, and post-critical times is shown in Fig. 6.1. During the pre-critical time interval $0 < t < t_c$, there is only the single gradual phase frequency. At the critical time, the gradual phase frequency becomes a stationary phase frequency, which

---

[1] Note that the stationary phase frequency condition may also be written $t = z/c_{gr}(\omega_{sp})$. The stationary phase frequency is that which relates t and z through the group velocity.

then splits into two. During the post-critical time interval the two stationary phase frequencies migrate away from one another. During the pre-critical time interval, we evaluate the dispersion integral only in the vicinity of the gradual phase frequencies given by Eq. 6.3, and during the post-critical interval, only in the vicinity of the stationary phase frequencies given by Eq. 6.2.
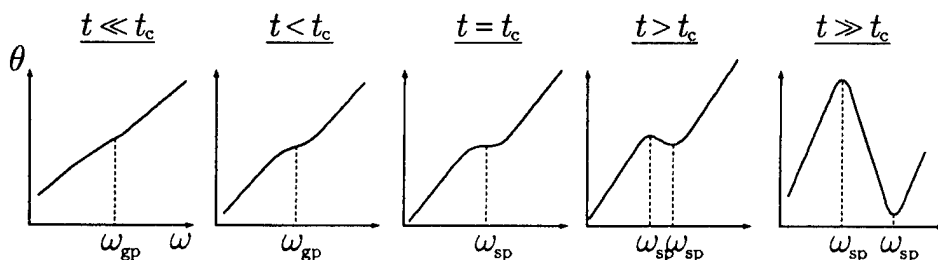
Figure 6.1: The phase function $\theta(\omega, z, t)$ at times less than, equal to, and greater than critical. Prior to the critical time, there is only a single gradual phase frequency. At the critical time a stationary phase frequency first occurs, and at later times there are two.

AS-94-757

The first problem is therefore to determine the solution of the dispersion integral in the vicinity of an arbitrary stationary or gradual phase frequency. The second problem is to determine the dependence of the stationary and gradual phase frequencies on z and t. Owing to the characteristic features of the Bloch dispersion we are able to identify a general qualitative form for the dependence of ω_{gp} and ω_{sp} on z and t. We are then able to find several explicit expressions, each valid in a particular spectral range, for the stationary and gradual phase frequencies. Depending upon how the source spectrum is situated with respect to these spectral ranges, we are able to determine the functional form and arrival time of the leading edge of the pulse, the character of the body of the pulse, and whether the pulse remains localized or develops a long oscillating tail. If such a tail develops, we are able to determine the functional form of the tail.

6.2 The Stationary and Gradual Phase Solutions

The object of this section is to find the solution of the dispersion integral in the vicinity of arbitrary stationary and gradual phase frequencies. As the only significant contribution to the dispersion integral occurs in the very near vicinity of these frequencies, we may safely represent all frequency dependent terms in the dispersion integral as Taylor expansions about the stationary or gradual phase frequency. As the stationary and gradual phase regions over which the dispersion integral is nontrivial shrink as z grows large, the errors incurred in the truncation of the Taylor expansions become arbitrarily small as z becomes large (Lighthill, 1980).

6.2.1 The Stationary Phase Solution

The frequency dependent terms that appear in the dispersion integral are the source spectrum $\Lambda(\omega)$ and the phase function $\theta(\omega, z, t)$. We expand these functions about the stationary phase frequency to result in[2]

$$\Lambda(\omega)|_{\omega \sim \omega_{\text{sp}}} = \Lambda_{\text{sp}} + \Lambda_{\text{sp}}^{(1)}(\omega - \omega_{\text{sp}})$$

$$\theta(\omega, z, t)|_{\omega \sim \omega_{\text{sp}}} = \theta_{\text{sp}} + \tfrac{1}{2}\kappa_{\text{sp}}^{(2)}(\omega - \omega_{\text{sp}})^2 z,$$

where the subscript "sp" denotes the evaluation of the function at $\omega = \omega_{\text{sp}}$ and we have used the identities $\theta_{\text{sp}}^{(1)} = 0$ (the definition of the stationary phase frequency) and $\theta^{(2)} = \kappa^{(2)}z$. When these expansions are substituted into the dispersion integral (Eq. 6.1), it becomes

$$p(z, t) = \Lambda(\omega_{\text{sp}})e^{j\theta_{\text{sp}}} \frac{1}{2\pi} \int_{-\infty}^{+\infty} e^{j\frac{1}{2}\kappa_{\text{sp}}^{(2)}(\omega - \omega_{\text{sp}})^2 z} d\omega$$

$$+ \Lambda^{(1)}(\omega_{\text{sp}})e^{j\theta_{\text{sp}}} \frac{1}{2\pi} \int_{-\infty}^{+\infty} (\omega - \omega_{\text{sp}})e^{j\frac{1}{2}\kappa_{\text{sp}}^{(2)}(\omega - \omega_{\text{sp}})^2 z} d\omega.$$

---

[2] The order to which terms are retained in these expansions determines the degree of error incurred in the technique. It is shown in the literature (Lighthill, 1980) that for the series truncations shown, the errors become arbitrarily small as z becomes large.

The integrand of the second integral is odd, and therefore integrates to zero, and the first is a Gauss-Fresnel type integral which is readily evaluated. The result is

$$p(z,t) = \Lambda(\omega_{\text{sp}})e^{j\theta_{\text{sp}}}\left(\frac{\pi}{\frac{1}{2}j\kappa^{(2)}(\omega_{\text{sp}})z}\right)^{1/2}.$$

We may use $\kappa^{(2)}(\omega_{\text{sp}}) = |\kappa^{(2)}(\omega_{\text{sp}})|\text{sgn}[\kappa^{(2)}(\omega_{\text{sp}})]$, where $\text{sgn}(x)$ is the signum function, to rewrite the result

$$p(z,t) = \frac{\Lambda(\omega_{\text{sp}})}{(2\pi|\kappa^{(2)}(\omega_{\text{sp}})|z)^{1/2}}e^{j[\kappa(\omega_{\text{sp}})z-\omega_{\text{sp}}t]}e^{-j\frac{\pi}{4}\text{sgn}[\kappa^{(2)}(\omega_{\text{sp}})]}. \tag{6.4}$$

This solution is the standard stationary phase solution of the dispersion integral, but in boundary value problem form. In the usual initial value problem form (Whitham, 1974; Lighthill, 1980), the solution is parameterized by the stationary phase *spatial* frequency $k_{\text{sp}}(z,t)$ instead of the stationary phase *temporal* frequency $\omega_{\text{sp}}(z,t)$ seen above, and the dispersion relation and its derivatives reflect the inverted dependence $\omega = \omega(k)$ instead of $\kappa = \kappa(\omega)$, as seen above.

It is interesting to note that the local frequency of the received signal at a particular time is related to the propagation distance z by the group velocity. The phase of Eq. 6.4 is

$$\theta(\omega,z,t) = \kappa[\omega_{\text{sp}}(t)]z - \omega_{\text{sp}}(t)t - j(\pi/4)\text{sgn}\{\kappa^{(2)}[\omega_{\text{sp}}(t)]\},$$

and the local frequency is

$$\omega_l = -\frac{\partial\theta}{\partial t} = \omega_{\text{sp}} + \frac{\partial\omega_{\text{sp}}}{\partial t}[t - z/c_{\text{gr}}(\omega_{\text{sp}})].$$

At the time $t = z/c_{\text{gr}}(\omega_{\text{sp}})$, then, the local frequency is simply

$$\omega_l\big|_{t=z/c_{\text{gr}}(\omega_{\text{sp}})} = \omega_{\text{sp}}. \tag{6.5}$$

6.2.2   The Gradual Phase Solution

The solution of the dispersion integral in the vicinity of a gradual phase frequency is found in much the same way as that in the vicinity of a

stationary phase frequency. The expansions of the source spectrum and the phase function about the gradual phase frequency are[3]

$$\Lambda(\omega)|_{\omega \sim \omega_{gp}} = \Lambda_{gp}$$

$$\theta(\omega, z, t)|_{\omega \sim \omega_{gp}} = \theta_{gp} + \kappa_{gp}^{(1)}(\omega - \omega_{gp})z + \tfrac{1}{6}\kappa_{gp}^{(3)}(\omega - \omega_{gp})^3 z, \qquad (6.6)$$

where we have made use of the fact that, by definition, $\kappa_{gp}^{(2)} = 0$. The substitution of these expansions into the dispersion integral (Eq. 6.1) results in

$$p(z, t) = \Lambda(\omega_{gp})e^{j\theta_{gp}}\frac{1}{2\pi}\int_{-\infty}^{+\infty} e^{j\kappa_{gp}^{(1)}(\omega - \omega_{sp})z}e^{j\frac{1}{6}\kappa_{sp}^{(3)}(\omega - \omega_{sp})^3 z}d\omega. \qquad (6.7)$$

With the introduction of the frequency shift $\hat{\omega} = \omega - \omega_{gp}$ and the subsequent frequency scaling $\hat{\omega} = \nu(\tfrac{1}{2}\kappa_{gp}^{(3)}z)^{-1/3}$, Eq. 6.7 becomes

$$p(z, t) = \frac{\Lambda(\omega_{gp})}{(\tfrac{1}{2}\kappa_{gp}^{(3)}z)^{1/3}}e^{j\theta_{gp}}\frac{1}{2\pi}\int_{-\infty}^{+\infty} e^{j\frac{1}{3}\nu^3}e^{j\kappa_{gp}^{(3)}z(\frac{1}{2}\kappa_{gp}^{(3)}z)^{-1/3}\nu}d\nu. \qquad (6.8)$$

The integral is now the Airy integral (Jeffrey and Kawahara, 1982) and Eq. 6.8 may be written

$$p(z, t) = \frac{\Lambda(\omega_{gp})}{(\tfrac{1}{2}\kappa^{(3)}(\omega_{gp})z)^{1/3}}e^{j[\kappa(\omega_{gp})z - \omega_{gp}t]}\text{Ai}\left[\frac{\kappa^{(1)}(\omega_{gp})z - t}{(\tfrac{1}{2}\kappa^{(3)}(\omega_{gp})z)^{1/3}}\right], \qquad (6.9)$$

where $\text{Ai}(x)$ is the Airy function. Again, Eq. 6.9 is the boundary value problem form of a standard initial value problem result (Lighthill, 1980).

6.3 The Stationary and Gradual Phase Frequency Trajectories

We now have solutions of the dispersion integral in the vicinity of arbitrary stationary and the gradual phase frequencies. Note that these solutions exhibit a parametric dependence upon the stationary and gradual phase frequencies. The next step is to determine the values of these frequencies

---

[3]Again, these series truncations are justified in the literature (Lighthill, 1980).

as functions of z and t. The substitution of the expressions for $\omega_{sp}(z,t)$ and $\omega_{gp}(z,t)$ into Eq. 6.4 and 6.9, respectively, results in explicit expressions for the contributions to the received signal associated with each gradual and stationary phase frequency.

6.3.1 The Stationary Phase Frequencies

In spite of its simple appearance, the stationary phase frequency condition

$$\kappa^{(1)}(\omega_{sp})z = t$$

generally results in stationary phase frequencies that cannot be expressed explicitly in terms of z and t. One method of determination of the stationary phase frequencies that leads to a very substantial if only qualitative understanding of their behavior is a graphical approach. To make use of the graphical approach, we consider the dependence of the problem on z to be parametric. That is, we consider the solution $p(z,t)$ to be the *signal* $p(t)$ that arrives at some fixed point z. We similarly consider the stationary phase frequency $\omega_{sp}(z,t)$ to have the time dependence $\omega_{sp}(t)$ for some fixed value of the parameter z. In this spirit, we write the stationary phase condition $\kappa^{(1)}[\omega_{sp}(t)]z = t$. The stationary phase frequency is simply a time dependent frequency that serves to map frequency to time. Equation 6.4 shows that the signal at time t is proportional to $\Lambda[\omega_{sp}(t)]e^{-j\omega_{sp}(t)t}$. *Each frequency in the source spectrum is mapped to a particular time in the received signal.* We may think of the stationary phase frequencies as migrating along the frequency axis "reading" the source spectrum.

It is worth noting that the treatment of z as a parameter is consistent with the general nature of the boundary value problem. We are usually interested in the signals that occur at various, fixed values of z. The signal is generated at one fixed value of z (in this case, at $z = 0$), evolves as it propagates, and is received at another fixed value of z.

The graphical approach to its solution makes use of the fact that the stationary phase condition may be rewritten

$$\left.\frac{\partial}{\partial\omega}\kappa(\omega)z\right|_{\omega=\omega_{sp}} = \left.\frac{\partial}{\partial\omega}\omega t\right|_{\omega=\omega_{sp}}.$$

The stationary phase frequencies are those at which the slope of $\kappa(\omega)z$ is equal to the slope of ωt. Consider the functions $\kappa(\omega)z$ and ωt. As z increases, $\kappa(\omega)z$ simply becomes an increasingly stretched version of the dispersion function. We then fix z at some value and allow t to sweep from $t = 0$ forward. The function ωt is simply a linear function that pivots at the origin. As time increases, the initially horizontal linear function tips up. If at some particular time the slopes of the two curves are equal at some frequency, then that frequency is a stationary phase frequency. As time evolves, the ωt curve tips farther up and the stationary phase frequency magrates up or down in frequency.

Consider now the structure of the Bloch dispersion curve. Each passband is bounded by a pair of stopbands and has a single inflection frequency roughly midway between the two stopbands (see Fig. 3.1). The inflection frequency divides each stopband into a low frequency, negative curvature region and a high frequency, positive curvature region. As this dispersion structure is universal for any passband, we may determine the general trajectories of the stationary phase frequencies associated with Bloch wave dispersion.

In Fig. 6.2 is shown $\kappa(\omega)z$ and ωt for a fixed value of z and successive instants of time near the critical time (note that the difference between these functions results in the type of phase fucnctions shown in Fig. 6.1). At $t = 0$, the slopes of $\kappa(\omega)z$ and ωt are equal across all stopband frequencies. While this implies that the dispersion integral is nonzero at some large z at $t = 0$ and is supportive of the infinite stopband group velocities found earlier (Sec. 5.3.1), we have already argued that these contributions are strongly attenuated and thus negligible for large z. As time advances and the function ωt tips up, we see that the slopes of $\kappa(\omega)$ and ωt first match at the inflection frequency, which is that associated with the largest group velocity in the passband. The earliest stationary phase frequency is therefore $\omega_{sp} = \omega_i$, which occurs at the critical time $t_c = z/c_{gi}$, where $c_{gi} = 1/\kappa^{(1)}(\omega_i)$ is the group velocity associated with the inflection frequency. As time advances further, the single stationary phase frequency splits and becomes a pair of stationary phase frequencies on opposite sides of the inflection frequency. One of the resultant pair migrates up in frequency towards the high frequency band edge and the other migrates down in frequency towards the low frequency band edge. The migration is most rapid near the inflection point and slows as the frequencies split further.
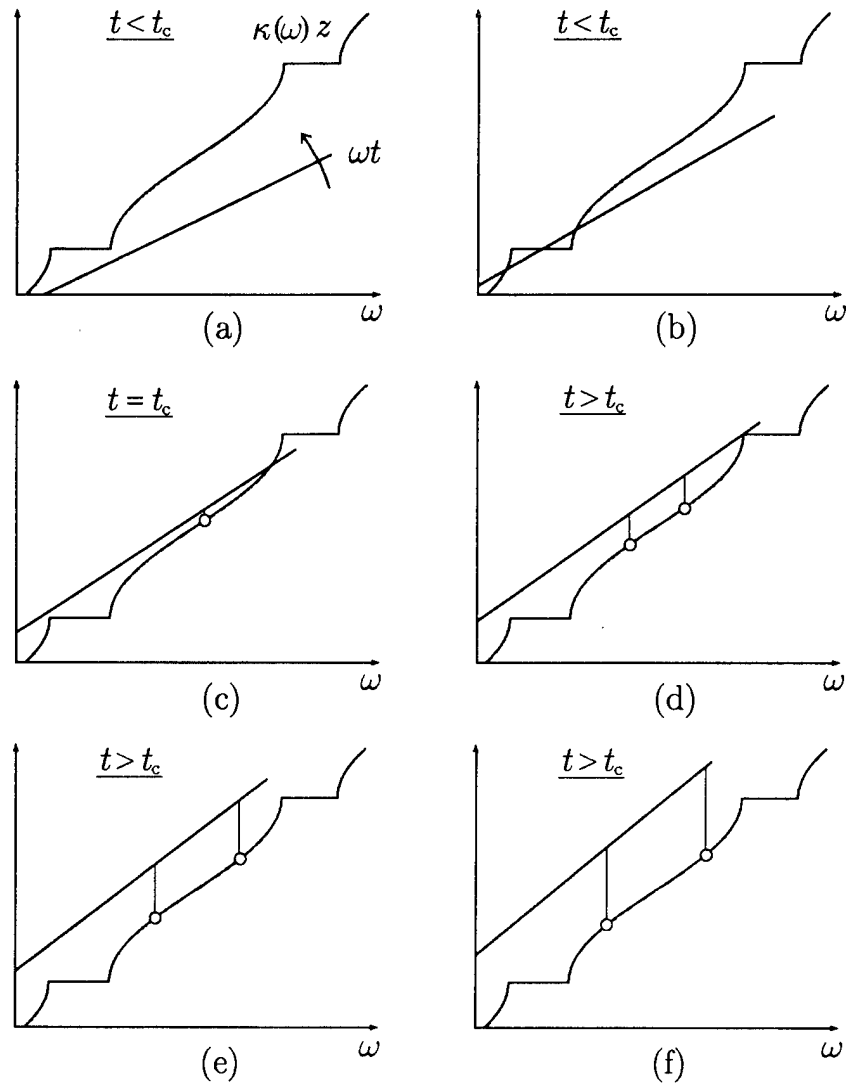
Figure 6.2: The functions $\kappa(\omega)z$ and ωt at times less than (a,b), equal to (c), and greater than (d,e,f) critical. The points where the slopes of the two functions are equal (the encircled points) are the stationary phase frequencies.

As the slope of $\kappa(\omega)z$ is infinite at the band edges, the pair of stationary phase frequencies only reaches the band edges as $t \to \infty$. The migration paths of the stationary phase frequencies that occur in several passbands is shown in Fig. 6.3
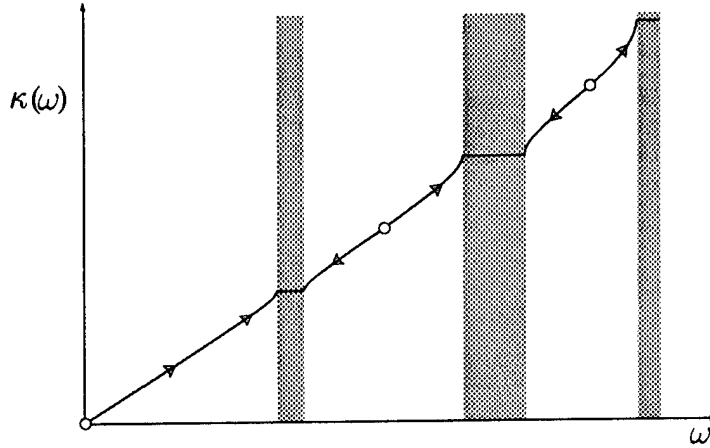
Figure 6.3: The direction of migration of the stationary phase frequencies. The circled points are inflection points, where the stationary phase frequencies originate. The arrows indicate the migration paths towards the band edges.

AS-94-759

6.3.2 The Gradual Phase Frequencies

As was pointed out earlier, prior to the critical time no stationary phase frequencies exist and the dominant contributions to the dispersion integral arise from the vicinity of the gradual phase frequencies. From Eq. 6.3 we see that the gradual phase frequencies are those for which $\kappa(\omega)$ has zero curvature. In other words, the gradual phase frequencies are simply the inflection frequencies

$$\omega_{gp} = \omega_i.$$

In contrast to the stationary phase frequencies, the gradual phase frequencies are independent of z and t.

The gradual and stationary phase frequencies for the isotropic periodic waveguide described in the introduction (with $S/S_0 = 1$ and $d/h = .14$)

are shown in Fig. 6.4. For each band there is a gradual phase frequency at the inflection frequency. At the critical time associated with a particular band, the gradual phase frequency bifurcates and becomes a pair of stationary phase frequencies that each migrate towards a band edge. If the source spectrum $\Lambda(\omega)$ does not include the inflection frequency, then we may simply consider the stationary phase frequency or frequencies that pass through the nonzero spectral region. If the source spectrum does include an inflection frequency, then the solution is composed of two parts: a pre-critical part that arises from the gradual phase frequency and a post-critical part that arises from the ensuing pair of stationary phase frequencies.
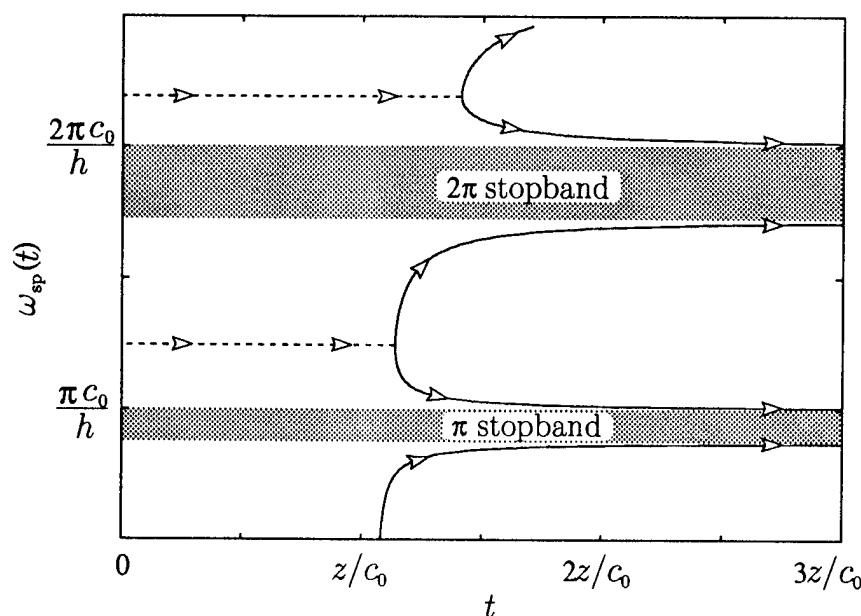
Figure 6.4: The gradual and stationary phase frequency trajectories. At the critical time associated with each passband, each gradual phase frequency (shown as dashed lines) becomes a stationary phase frequency (shown as solid lines) and subsequently undergoes a bifurcation. Each of the resultant pairs of stationary phase frequencies then asymptotically approaches a band edge.

6.3.3 Complex Source Spectra

The results thus far have hinged upon the assumption that the source spectrum is real; i.e., that the amplitude and frequency modulation of the carrier at the source is symmetric about $t = 0$. We now consider the case in which the source function is arbitrary, and the associated source spectrum consequently complex.

For the complex source spectrum $\hat{\Lambda}(\omega)$, the dispersion integral to be solved is

$$p(z,t) = \frac{1}{2\pi} \int_{-\infty}^{+\infty} \hat{\Lambda}(\omega) e^{j[\kappa(\omega)z - \omega t]} d\omega.$$

With the definition

$$\hat{\Lambda}(\omega) = |\hat{\Lambda}(\omega)| e^{j\phi(\omega)} = \Lambda(\omega) e^{j\phi(\omega)},$$

where $\Lambda(\omega)$ is now the magnitude of $\hat{\Lambda}(\omega)$ and $\phi(\omega)$ is the phase, the dispersion integral becomes

$$p(z,t) = \frac{1}{2\pi} \int_{-\infty}^{+\infty} \Lambda(\omega) e^{j[\phi(\omega) + \kappa(\omega)z - \omega t]} d\omega.$$

We may now redefine the phase function $\theta(\omega, z, t) = \phi(\omega) + \kappa(\omega)z - \omega t$, and the dispersion integral is identical to that shown in Eq. 6.1. The stationary and gradual phase solutions are, with the new definition of the phase function, still valid. The difference occurs in the trajectories of the stationary and gradual phase frequencies. The frequencies at which the total phase of the integrand is stationary and most gradual are dependent upon $\phi(\omega)$. The stationary phase condition $\partial\theta/\partial\omega|_{\omega=\omega_{\text{sp}}} = 0$ is now

$$\phi^{(1)}(\omega_{\text{sp}}) + \kappa^{(1)}(\omega_{\text{sp}})z - t = 0,$$

and the gradual phase condition $\partial^2\theta/\partial\omega^2|_{\omega=\omega_{\text{gp}}} = 0$ is

$$\phi^{(2)}(\omega_{\text{gp}}) + \kappa^{(2)}(\omega_{\text{gp}})z = 0.$$

The stationary and gradual phase frequencies are modified by variations in the phase of the source spectrum. It is worth noting that in previous investigations of this sort, the contribution to the stationary phase condition by the source spectrum phase is neglected, but it is not stated that the source spectrum is assumed to have zero or constant phase. From this point on, only real source spectra are considered.

6.4 The Solutions

We now find explicit expressions for the stationary and gradual phase frequencies so that the solutions, which depend parametrically on these quantities, may themselves be expressed explicitly in terms of z and t. While we cannot find *globally valid* explicit expressions for the frequencies, we are able to find expressions that are valid in a limited spectral range. The resultant solutions are then valid only over a limited range of time.

6.4.1 The Fourier Transform Pulse Solution

An interesting narrowband pulse solution is found when the pulse spectrum occupies a frequency range in which the dispersion curve has roughly constant (and nonzero) curvature. We see in Fig. 3.1 that a large fraction of the Bloch dispersion curve is such that this requirement is easily met. As the spectrum occupies a range of frequencies with nonzero curvature it does not include an inflection frequency and we need not consider the gradual phase frequency. In fact, we need consider only a single stationary phase frequency trajectory, and one that is simple enough that the dependence of ω_{sp} on z and t may be expressed explicitly. This expression for ω_{sp} may be substituted directly into the stationary phase solution to obtain a fully explicit solution.

To arrive at an expression for the stationary phase frequency, we expand the dispersion relation about $\omega = \omega_0$, the source carrier frequency. As the curvature of $\kappa(\omega)$ is very nearly constant over the pulse bandwidth, we need keep terms to quadratic order only:

$$\kappa(\omega)|_{\omega \sim \omega_0} = \kappa_0 + \kappa_0^{(1)}(\omega - \omega_0) + \frac{1}{2}\kappa_0^{(2)}(\omega - \omega_0)^2. \qquad (6.10)$$

The consequence of the presence of higher order terms is addressed in the following section. Differentiation of the expansion leads to

$$\kappa^{(1)}(\omega)\Big|_{\omega \sim \omega_0} = \kappa_0^{(1)} + \kappa_0^{(2)}(\omega - \omega_0). \qquad (6.11)$$

Using this expression, the stationary phase condition becomes

$$[\kappa_0^{(1)} + \kappa_0^{(2)}(\omega_{sp} - \omega_0)]z - t = 0,$$

which may be rewritten as

$$\omega_{\text{sp}} = \omega_0 + \frac{t - z/c_{\text{gr}}}{\kappa_0^{(2)} z}. \tag{6.12}$$

In the interval over which the dispersion curve has constant curvature, the stationary phase frequency sweeps *linearly with time*. The sweep rate is determined by the magnitude of the curvature of the dispersion function (i.e., by $|\kappa_0^{(2)}|$) and decreases with z. As we expect from the qualitative analysis of Sec. 6.3, the sweep direction is determined by the sign of the curvature. A negative curvature indicates a downward sweep in frequency and a positive curvature indicates an upward sweep, as is found on the low and high frequency sides of the inflection frequency, respectively.

In order to express the stationary phase solution (Eq. 6.4) explicitly in terms of z and t, we need, in addition to the expression for the stationary phase frequency, explicit expressions for $\kappa(\omega_{\text{sp}})$ and $\kappa^{(2)}(\omega_{\text{sp}})$. Differentiation of Eq. 6.11 and evaluation of the result at the stationary phase frequency results in

$$\kappa^{(2)}(\omega_{\text{sp}}) = \kappa_0^{(2)}. \tag{6.13}$$

The evaluation of Eq. 6.10 at the stationary phase frequency and the subsequent substitution of Eq. 6.12 into the right hand side results in

$$\kappa(\omega_{\text{sp}}) = \kappa_0 + \frac{(t/z)^2 - (1/c_{\text{gr}})^2}{2\kappa_0^{(2)}}. \tag{6.14}$$

We may now write down the solution. Using the notation of the previous chapter, the source envelope spectrum is $A_0(\omega)$ and the source spectrum is $\Lambda(\omega) = A_0(\omega - \omega_0)$. The substitution of Eqs. 6.12, 6.13, and 6.14 into Eq. 6.4 results in the solution

$$p(z,t) = \frac{1}{(2\pi|\kappa_0^{(2)}|z)^{1/2}} A_0 \left(\frac{t - z/c_{\text{gr}}}{\kappa_0^{(2)} z} \right) e^{j[\kappa_0 z - \omega_0 t + (t - z/c_{\text{gr}})^2/2\kappa_0^{(2)} z]} e^{-j\frac{\pi}{4}\text{sgn}(\kappa_0^{(2)})}.$$

The pulse envelope, which propagates at the group velocity associated with the carrier frequency, is the source envelope spectrum. In other words, *the pulse envelope distorts into its Fourier transform!* The pulse decays as $1/\sqrt{z}$ and, owing to the denominator in the argument of the envelope spectrum, spreads

out linearly with z. As was found in the analysis of Eq. 5.41, the quadratic term in the exponential function causes dispersive chirping of the carrier. The carrier frequency ramps linearly with time at a rate of $2\pi/\kappa_0^{(2)} z$ Hz/s.

It is interesting to consider this Fourier transform pulse solution in light of the isomorphism that was pointed out in Sec. 5.3.2. It was noted that the dispersive distortion of a pulse envelope and the diffraction distortion of the profile of a highly collimated beam are essentially the same problem.[4] The pulse envelope loses amplitude and spreads in precisely the same manner that the beam profile loses amplitude and spreads. It is well known (Goodman, 1968) that the asymptotic solution of the beam diffraction problem is that the beam profile distorts into the Fourier transform of the initial beam profile (i.e., the aperture function). While the pulse distortion solution is a strictly *short range* solution, the isomorphism appears to hold for long distances as well.

6.4.2   The Half-Band Pulse Solution

In this section the findings of the previous section are generalized to include the case of pulses that do not meet the bandwidth requirement of that section. In other words, we consider the consequences of the relaxation of the bandwidth limitation. The Fourier transform pulse solution is valid when the source spectrum is confined to a spectral region over which the dispersion curve has very nearly constant curvature. Here we consider a source spectrum that occupies any part of the spectral region between the band edge and the inflection frequency; i.e., the source spectrum is confined to one half of a passband.

The key to the approach is the nature of the stationary phase frequency trajectory in a half-band. In Sec. 6.3 it was found that in any half band there is but one stationary phase frequency, and that it sweeps monotonically upward or downward in frequency through the half-band. If the half-band lies on the high frequency side of the inflection frequency, then the frequency sweep

---

[4]The problems are isomorphic under the assumption that we are interested only in the propagation of the pulse over a distance that is much smaller than all but the $\kappa^{(2)}$ characteristic envelope distortion distance.

is upward, and is otherwise downward. In the constant curvature case the frequency sweep was found to be linear in time (Eq. 6.12). When the expression for this linearly sweeping stationary phase frequency was substituted into the stationary phase solution, the argument of the source spectrum function Λ was found to become a linear function of time. The signal envelope simply became the source envelope spectrum. In the half-band case, the stationary phase frequency sweep is not linear, but is still monotonic. The argument of the source spectrum function is therefore a nonlinear, but monotonic function of time. *The signal envelope is therefore simply a distorted version of the source envelope spectrum.* The early parts of the pulse envelope are a compressed version of the source envelope spectrum and the later parts are dilated. A second distortion mechanism is due to the frequency dependence of the $|\kappa^{(2)}(\omega_{sp})|^{-1/2}$ term. As the stationary phase frequency migrates from the inflection frequency towards the band edge, the curvature of $\kappa(\omega)$ increases monotonically. The magnitude of the pulse envelope, therefore, is attenuated by an amount that increases with time.

As an example, consider a sequence of pulses that begins with a very narrow band pulse and ends with a wide band pulse. All intervening pulses are of gradually increasing bandwidth, and all pulse spectra are confined to a half-band portion of the spectrum. The first pulse, being of very narrow bandwidth, distorts such that its envelope becomes its initial envelope spectrum. Later pulses, owing to their larger bandwidths, show distortion due to the nonlinear dependence of the stationary phase frequency on time. The pulse envelopes still resemble their initial envelope spectrum, but the early portions of the envelope are compressed and the later portions are dilated and attenuated. Each pulse in the sequence resembles a more severely distorted version of its initial envelope spectrum than that preceding it. An example of such a sequence of pulses is shown in Fig. 6.5, where the half-band is that above the first scatterer resonance stopband for the isotropic periodic side branch waveguide.

The significance of the group velocity in long range pulse propagation is made clear in this example. The information contained in a feature of the source spectrum (such as the spectral peak) is reflected in the received signal at the time $t = z/c_{gr}$, where c_{gr} is the group velocity evaluated at the frequency of the feature. The peak of the triangular spectrum shown in Fig. 6.5, for example,
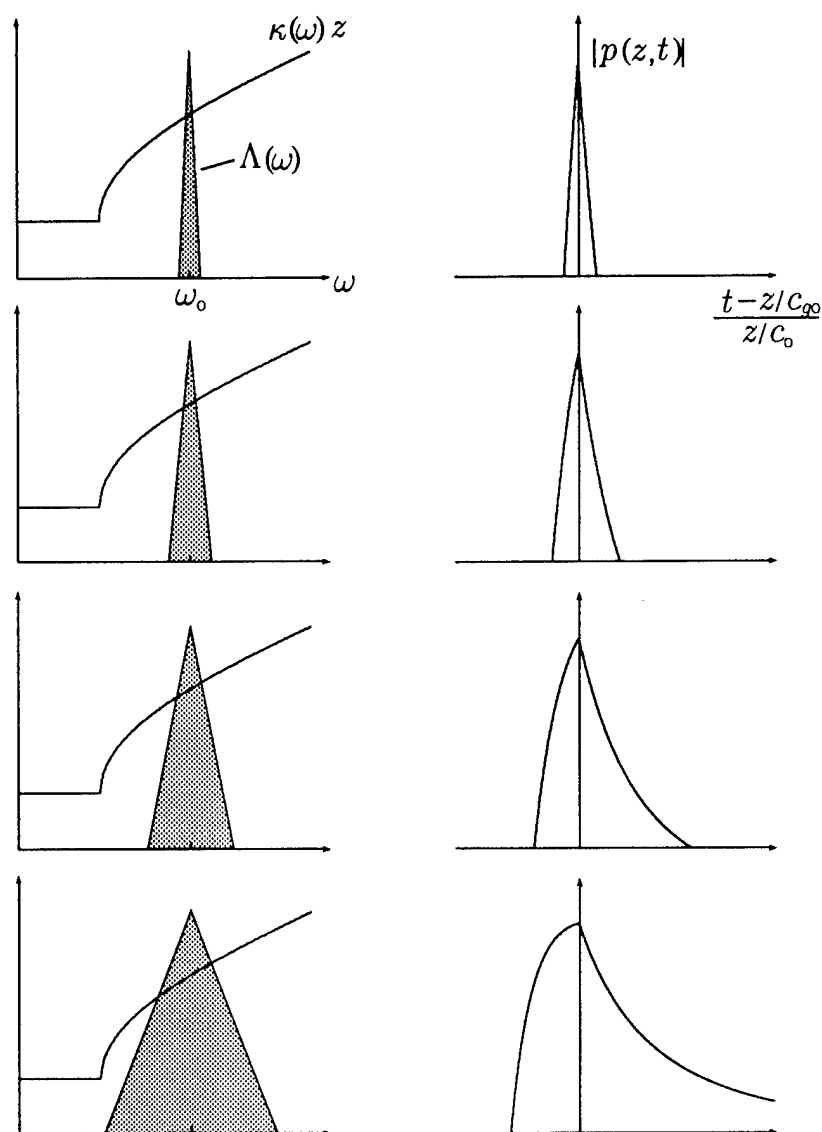
Figure 6.5: The spectra of four pulses and the associated asymptotic pulse envelopes. The pulse with the narrowest bandwidth distorts such that its envelope is the pulse spectrum. As the pulse bandwidth increases, the pulse envelope becomes an increasingly distorted version of the pulse spectrum.

which occurs at the frequency ω_0, results in a peak in the pulse envelope at the time $t = z/c_{\text{gr}}(\omega_0)$.

There may be, if the source spectrum has a particularly flat, broad peak, a slight modification to the peak arrival time that is due to this distortion effect. The received pulse envelope is $a_c(t) = \Lambda(\omega_{\text{sp}}(t))|2\pi z\kappa^{(2)}(\omega_{\text{sp}}(t))|^{-1/2}$. The time of arrival of the envelope peak is given by $d|a_c(t)|/dt|_{t=t_{\text{pk}}} = 0$. The equivalent expression in terms of the stationary phase frequency associated with the arrival time, $\omega_{\text{pk}} = \omega_{\text{sp}}(t_{\text{pk}})$, is

$$\frac{d}{d\omega}\frac{\Lambda(\omega)}{[2\pi z\kappa^{(2)}(\omega)]^{1/2}}\bigg|_{\omega=\omega_{\text{pk}}} = 0,$$

or

$$\frac{\Lambda(\omega_{\text{pk}})}{\Lambda^{(1)}(\omega_{\text{pk}})} = \frac{1}{2}\frac{\kappa^{(3)}(\omega_{\text{pk}})}{\kappa^{(2)}(\omega_{\text{pk}})}.$$

The ratios may be expressed as logarithmic derivatives, and the peak frequency is given by

$$\frac{d}{d\omega}\ln\Lambda(\omega)\bigg|_{\omega=\omega_{\text{pk}}} = \frac{d}{d\omega}\ln|\kappa^{(2)}(\omega)|^{1/2}\bigg|_{\omega=\omega_{\text{pk}}}. \tag{6.15}$$

As the right hand side of Eq. 6.15 is positive for $\omega > \omega_{\text{i}}$ and is negative for $\omega < \omega_{\text{i}}$, we have $\omega_{\text{pk}} < \omega_0$ for $\omega_0 > \omega_{\text{i}}$ and $\omega_{\text{pk}} > \omega_0$ for $\omega_0 < \omega_{\text{i}}$. Owing to the fact that the frequencies nearest ω_{i} are associated with the earliest arrivals, the received envelope peak is found to arrive slightly earlier than the time associated with the spectral peak. Except when the peak of the pulse spectrum has very small curvature, however, this effect is negligible.

6.4.3   The Airy Leading Edge Solution

We now consider the form of the leading edge of a pulse that arises from a source spectrum that includes an inflection frequency. As it was found in the last two sections that the earliest arrivals are associated with the frequencies nearest the inflection frequency, we concentrate on that spectral region. If the source spectrum does not include the inflection frequency, then, by the analysis of Sec. 6.4.2, the leading edge of the pulse envelope resembles the edge of the source envelope spectrum nearest the inflection frequency. When the

source spectrum *does* include the inflection frequency, then the analysis differs significantly from that of the previous two sections. We must take two stationary phase frequencies into account and must also consider the contribution to the solution by the gradual phase frequency. We must therefore consider the leading edge solution in two parts: the pre-critical part that arises from the gradual phase frequency and the post-critical part that arises from the two stationary phase frequencies.

The solution for times up to the critical time is given by Eq. 6.9, where the gradual phase frequency is given by Eq. 6.3. The gradual phase frequency is simply $\omega_{gp} = \omega_i$, from which we find $\kappa^{(1)}(\omega_{gp}) = 1/c_{gi}$, in which case we may write $t - \kappa^{(1)}(\omega_i)z = t - z/c_{gi} = t - t_c(z)$. Equation 6.9 therefore becomes

$$p(z,t) = \frac{\Lambda(\omega_i)}{(\frac{1}{2}\kappa_i^{(3)}z)^{1/3}} e^{j[\kappa_i z - \omega_i t]} \mathrm{Ai}\left[-\frac{t - t_c}{(\frac{1}{2}\kappa_i^{(3)}z)^{1/3}}\right], \qquad (6.16)$$

which is the explicit solution for the pre-critical time interval.

While the phase function does, at the critical time, develop a pair of stationary phase frequencies, the stationary phase *regions* associated with these frequencies overlap until some time after the critical time. The stationary phase solution may not be used for the two stationary phase frequencies independently until their stationary phase regions become disjoint. It appears, then, that we have no valid solutions for the early part of the post-critical time interval. The pre-critical solution (Eq. 6.16), however, remains valid for some time after the critical time. The expansion of the phase function used in the gradual phase solution (Eq. 6.6), and therefore the gradual phase solution itself (Eq. 6.9), remain valid in the early portion of the post-critical interval. It may be seen quite clearly in Fig. 6.1 that Eq. 6.6 remains a valid representation of $\theta(\omega, z, t)$ for some time after the critical time. Equation 6.16 is therefore the solution up *through* the critical time and the ensuing pair of stationary phase solutions do not gain validity until some time after the critical time.

Once the stationary phase regions become disjoint, the solution is given by Eq. 6.4 with the stationary phase frequencies given by Eq. 6.2. In order to find an explicit expression for the stationary phase frequencies, we begin with the expansion of the dispersion relation about the inflection frequency

$$\kappa(\omega)\big|_{\omega \sim \omega_i} = \kappa(\omega_i) + \kappa^{(1)}(\omega_i)(\omega - \omega_i) + \frac{1}{6}\kappa^{(3)}(\omega_i)(\omega - \omega_i)^3, \qquad (6.17)$$

where we have made use of the definition of the inflection frequency ($\kappa^{(2)}(\omega_i) = 0$). The derivative of the above expansion, evaluated at the stationary phase frequency, may be substituted into the stationary phase frequency condition to result in

$$\kappa_i^{(1)} + \frac{1}{2}\kappa_i^{(3)}(\omega_{\mathrm{sp}} - \omega_i)^2 = t/z,$$

where the notation $\kappa^{(n)}(\omega_i) = \kappa_i^{(n)}$ has been introduced. The two stationary phase frequencies are therefore given by

$$\omega_{\mathrm{sp}}(t) = \omega_{\pm}(t) = \omega_i \pm \left[\frac{t - t_c}{\frac{1}{2}\kappa_i^{(3)}z}\right]^{1/2}, \qquad (6.18)$$

where the $+$ case represents one stationary phase frequency and the $-$ case represents the other. Note that Eq. 6.18 is the classic expression for the stable part of a pitchfork-type supercritical bifurcation (Drazin, 1992).

In order to evaluate the stationary phase solution (Eq. 6.4) at the stationary phase frequencies, we must obtain expressions for $\kappa(\omega_{\pm})$ and $\kappa^{(2)}(\omega_{\pm})$. Derivatives of the expansion of $\kappa(\omega)$ about ω_i (Eq. 6.17) may be evaluated at the stationary phase frequency (Eq. 6.18) to result in

$$\kappa(\omega_{\pm}) = \kappa_i \pm \left[\frac{t - t_c}{\frac{1}{2}\kappa_i^{(3)}z}\right]^{1/2} \frac{1}{3z}(t + 2z/c_{\mathrm{gi}})$$

$$\kappa^{(2)}(\omega_{\pm}) = \pm \left[\frac{2\kappa_i^{(3)}}{z}(t - t_c)\right]^{1/2}.$$

We may now evaulate the stationary phase solution at the two stationary phase frequencies and add the results to obtain

$$
\begin{aligned}
p(z,t) &= \frac{\Lambda(\omega_+)}{[2\pi|2\kappa_i^{(3)}z(t - t_c)|^{1/2}]^{1/2}}e^{j[\kappa_i z - \omega_i t]}e^{-j\frac{2}{3}(t - t_c)^{3/2}(\frac{1}{2}\kappa_i^{(3)}z)^{-1/2}}e^{j\pi/4} \\
&\quad + \frac{\Lambda(\omega_-)}{[2\pi|2\kappa_i^{(3)}z(t - t_c)|^{1/2}]^{1/2}}e^{j[\kappa_i z - \omega_i t]}e^{j\frac{2}{3}(t - t_c)^{3/2}(\frac{1}{2}\kappa_i^{(3)}z)^{-1/2}}e^{-j\pi/4}.
\end{aligned}
$$

It was shown earlier (Eq. 6.5) that the local frequency of a solution that arises from a particular stationary phase frequency is simply the stationary phase frequency. The signal that arises from the ω_+ stationary phase frequency therefore

ramps up in frequency with time and that from ω_- ramps down in frequency with time. The sum of the two signals that arise from these stationary phase frequencies is therefore expected to undergo envelope oscillations that increase in frequency with time.

We may now proceed to find explicit expressions for the post-critical part of the leading edge of the pulse. As we are interested in only the leading edge, the structure of which involves only frequencies in the neighborhood of the inflection frequency, we expand the pulse spectrum about the inflection frequency:

$$
\begin{aligned}
\Lambda(\omega_\pm) &= \Lambda(\omega_i) + \Lambda^{(1)}(\omega_i)(\omega_\pm - \omega_i) \\
&= \Lambda(\omega_i) \pm \Lambda^{(1)}(\omega_i) \left[\frac{t - z/c_{gi}}{\frac{1}{2}\kappa_i^{(3)} z} \right]^{1/2} .
\end{aligned}
$$

If the spectrum has zero slope at the inflection frequency, then the post-critical part of the solution is

$$
p(z,t) = (2/\pi)^{1/2} \frac{\Lambda(\omega_i)}{|2\kappa_i^{(3)} z(t - t_c)|^{1/4}} e^{j[\kappa_i z - \omega_i t]} \cos \left[\frac{2}{3} \frac{(t - t_c)^{3/2}}{(\frac{1}{2}\kappa_i^{(3)} z)^{1/2}} - \pi/4 \right] . \quad (6.19)
$$

If the spectrum has nonzero slope at the inflection frequency, then the leading edge is given by

$$
\begin{aligned}
p(z,t) &= \frac{\Lambda(\omega_i)}{(2\pi)^{1/2}|2\kappa_i^{(3)} z(t - t_c)|^{1/4}} e^{j[\kappa_i z - \omega_i t]} \\
&\cdot \left\{ \left[1 + \frac{\Lambda_i^{(1)}}{\Lambda_i} \left(\frac{t - t_c}{\frac{1}{2}\kappa_i^{(3)} z} \right)^{1/2} \right] e^{-j[(2/3)(t-z/c_{gi})^{3/2}(\frac{1}{2}\kappa_i^{(3)} z)^{-1/2} - pi/4]} \right. \\
&\left. + \left[1 - \frac{\Lambda_i^{(1)}}{\Lambda_i} \left(\frac{t - t_c}{\frac{1}{2}\kappa_i^{(3)} z} \right)^{1/2} \right] e^{j[(2/3)(t-t_c)^{3/2}(\frac{1}{2}\kappa_i^{(3)} z)^{-1/2} - pi/4]} \right\} . \quad (6.20)
\end{aligned}
$$

In Fig. 6.6 is shown the envelopes of the pre-critical part of the solution (Eq. 6.16) and the $\Lambda_i^{(1)} = 0$ post-critical solution (Eq. 6.19). Except for the singularity in the post-critical part of the solution at the critical time, the pre and post-critical parts of the solution are very nearly identical. As we have argued, in the early part of the post-critical interval, it is the gradual phase

$|p(z,t)|$

post-critical
solution

pre-critical
solution

$$\frac{t-t_{\mathrm{c}}}{(\frac{1}{2}\kappa_{\mathrm{i}}^{(3)}z)^{1/3}}$$

−4   −2   0   2   4   6   8 $\cdot 10^{-3}$
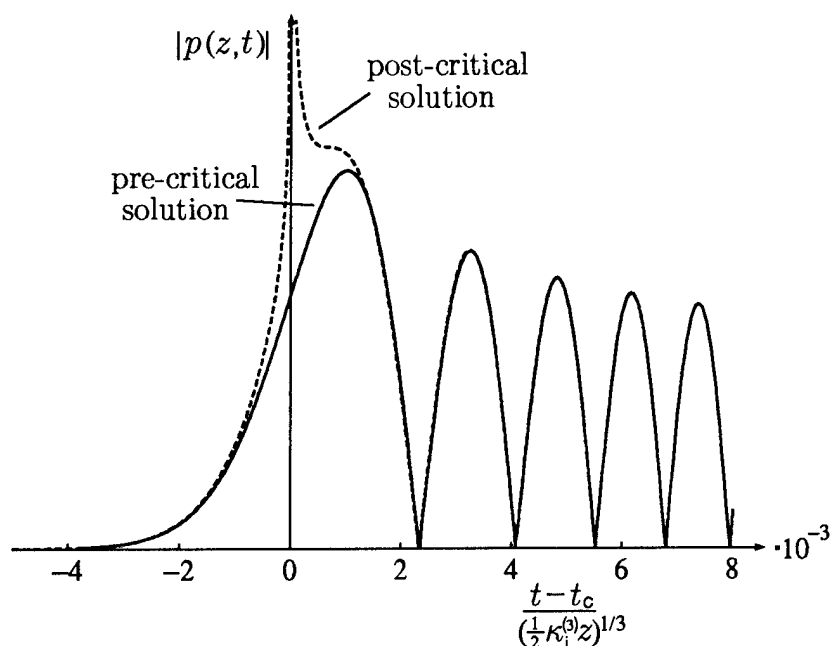
Figure 6.6: The leading edge of the pulse envelope when the pulse spectrum has a slope of zero at the inflection frequency. The solid line is the pre-critical solution, which is valid up through the critical time and the dashed line is the post-critical solution, which becomes valid after the critical time.

AS-94-762

solution and not the stationary phase solution that is valid. We may therefore take the pre-critical solution (Eq. 6.16) alone as a good representation of both pre and post-critical parts of the leading edge of the pulse. Note that the solution is consistent with what we expect to result from a bifurcation in the stationary phase frequency trajectory. During the pre-critical time inteval, there is only the single gradual phase frequency, and the solution is composed of a signal with a well-defined frequency and very small amplitude. As the phase rate becomes increasingly gradual (as $t \to t_{\mathrm{c}}$), the signal grows in strength. At $t = t_{\mathrm{c}}$, the bifurcation occurs, and the solution is thereafter composed of two signals of differing frequency that beat with one another. As the frequencies of these signals diverge, the beat rate increases (as is clearly evident as envelope oscillations in Fig. 6.6) as $t^{3/2}$.

In Fig. 6.7 is shown the envelopes of the pre-critical part of the solu-
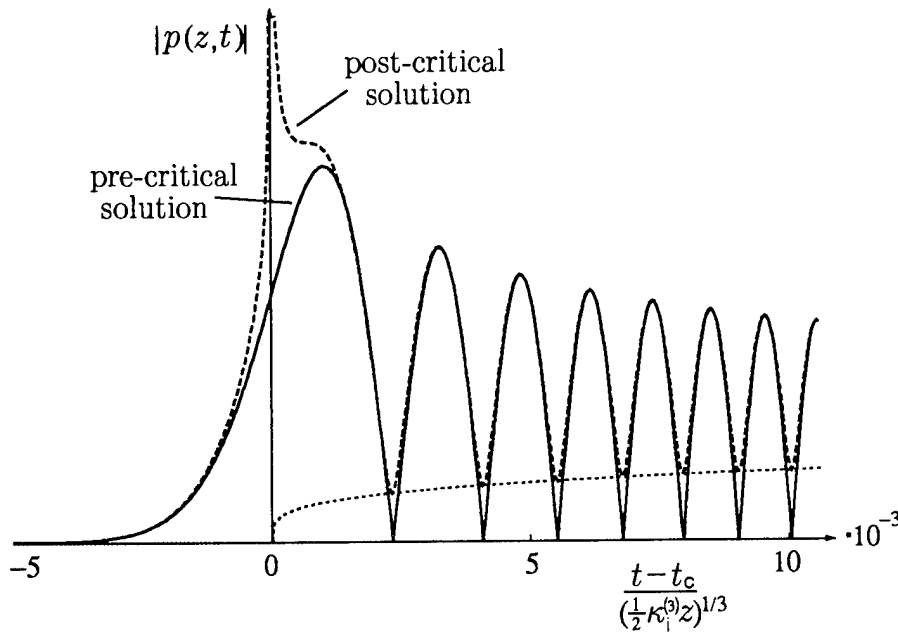
Figure 6.7: The leading edge of the pulse envelope when the pulse spectrum has a nonzero slope at the inflection frequency. The solid line is the pre-critical solution, which is valid up through the critical time, and the dashed line is the post-critical solution, which becomes valid after the critical time. Also indicated with a dotted line are the envelope minima.

AS-94-763

tion (Eq. 6.16) and the $\Lambda_i^{(1)} \neq 0$ post-critical solution (Eq. 6.20). The result is very similar to that of the $\Lambda_i^{(1)} = 0$ case, but the signal nulls are now signal minima. This is because in the $\Lambda_i^{(1)} \neq 0$ case the pulse spectrum is non-constant in the vicinity of the inflection frequency, and therefore the strengths of the signals associated with the two stationary phase frequencies are not equal. In order to obtain perfect destructive interference (i.e., perfect nulls in the total signal), the interfering signals must be of equal amplitude. As the signal strengths are not equal, the nulls are not complete. The resultant signal minima occur at the same times that the nulls occur in the $\Lambda_i^{(1)} = 0$ case, but the signal level at the minima are proportional to

$$\frac{\Lambda_i^{(1)}}{\Lambda_i} \frac{(t - t_c)^{1/4}}{(\frac{1}{2}\kappa_i^{(3)} z)^{5/12}}.$$

6.4.4   The -3/2 Law Tail Solution

We now consider the form of the trailing edge of the pulse. As it was found in the Fourier transform and half-band pulse sections that the last arrivals are associated with the frequencies nearest the band edges, we concentrate on that spectral region. Recall that the stationary phase frequencies all asymptotically approach the band edges. If the pulse spectrum does not include a band edge frequency, the stationary phase frequencies eventually migrate out of the spectral region occupied by the source spectrum. The signal amplitude therefore becomes zero a finite time after the arrival of the leading edge. In other words, *the pulse remains localized.* By the results of the Fourier transform pulse and half-band solution sections, the tail end of the pulse envelope resembles the edge of the source envelope spectrum nearest the band edge. If, on the other hand, the pulse spectrum *does* include the band edge frequency, then the stationary phase frequency does not, in finite time, leave the spectral region occupied by the source spectrum. The signal amplitude never reaches zero, and the pulse is no longer localized. It is instead trailed by a long, asymptotically decaying tail. This is the case considered here.

Again, an explicit expression for the stationary phase frequency is found by expansion of the dispersion relation in the vicinity of the frequency of interest: the band edge frequency. We first introduce some notation. The band edge frequency is ω_{be}. Each band edge is associated with a Bragg index n, which is the integer such that

$$\lim_{\omega \to \omega_{be}} \mathrm{Re}\{q(\omega)h\} = n\pi.$$

While the band edges on either side of a Bragg stopband have the same index, those on either side of a scatterer resonance stopband have indices that differ (one must be even and the other odd). Recall (see Eq. 3.6) that the nondissipative dispersion relation is given by

$$\cos(qh) = \mathrm{Re}\{T_{11}^C(\omega)\} = \gamma(\omega), \tag{6.21}$$

and that the band edges occur where $q(\omega)h = n\pi$ and $|\gamma(\omega)| = 1$. The expansion of $\cos(qh)$ about $qh = n\pi$ is

$$\cos(qh)|_{qh \sim n\pi} = (-1)^n \left[1 - \frac{(qh - n\pi)^2}{2} \right].$$

We solve for qh to find

$$qh = n\pi \pm 2^{1/2} \left[1 - (-1)^n \cos(qh)\right]^{1/2}, \tag{6.22}$$

where the upper of the stacked signs (here a $+$) refers to the high frequency edge of the stopband and the lower (here a $-$) refers to the low frequency edge. The expansion of $\gamma(\omega)$ about ω_{be} is

$$\gamma(\omega)\big|_{\omega \sim \omega_{\mathrm{be}}} = (-1)^n + \gamma_{\mathrm{be}}^{(1)}(\omega - \omega_{\mathrm{be}}), \tag{6.23}$$

where the identity $\gamma(\omega_{\mathrm{be}}) = (-1)^n$ has been used (see discussion following Eq. 3.7) and $\gamma_{\mathrm{be}}^{(1)}$ stands for $d\gamma/d\omega|_{\omega = \omega_{\mathrm{be}}}$. Equations 6.21, 6.22 and 6.23 may be combined to yield the expansion of the dispersion relation about the band edge frequency:

$$q(\omega)\big|_{\omega \sim \omega_{\mathrm{be}}} = \frac{n\pi}{h} \pm \frac{(2\gamma_{\mathrm{be}}^{(1)})^{1/2}}{h} \left[(-1)^{n+1}(\omega - \omega_{\mathrm{be}})\right]^{1/2}. \tag{6.24}$$

As we are concerned only with passband frequencies, for which $q(\omega) = \kappa(\omega)$, Eq. 6.24 may be taken to be an expansion of $\kappa(\omega)$ as well.

It is worth noting that this expansion does a surprisingly good job at modeling the behavior of the dispersion curve in the vicinity of the band edge. As the band edge is approached from the passband side, the imaginary part of q is zero and the slope of the real part becomes infinite, as it should. At the band edge frequency both the real and imaginary part of q are cusped, and as the band edge frequency is approached from the stopband side the real part of q is constant and the slope of the imaginary part of q becomes infinite. The highly unusual behavior of the dispersion curve at the band edge is beautifully modeled with a simple square root function!

We may now find an explicit expression for the stationary phase frequency. The derivative of Eq. 6.24 is

$$\kappa^{(1)}(\omega)\big|_{\omega \sim \omega_{\mathrm{be}}} = \pm \left(\frac{\gamma_{\mathrm{be}}^{(1)}}{2h^2}\right)^{1/2} (-1)^{n+1} \left[(-1)^{n+1}(\omega - \omega_{\mathrm{be}})\right]^{-1/2}, \tag{6.25}$$

which may be substituted into the stationary phase condition and the resultant expression solved for the stationary phase frequency. With the use of the

relation $\gamma_{be}^{(1)} = \pm(-1)^{n+1}|\gamma_{be}^{(1)}|$, the stationary phase frequency is

$$\omega_{sp} = \omega_{be} \pm \frac{|\gamma_{be}^{(1)}|}{2h^2}(z/t)^2, \tag{6.26}$$

which approaches the band edge frequency as $\sim 1/t^2$.

Again, in order to evaluate the quadratic dispersion solution, we must find expressions for $\kappa(\omega_{sp})$ and $\kappa^{(2)}(\omega_{sp})$. The substitution of Eq. 6.26 into Eq. 6.24 results in

$$\kappa(\omega_{sp}) = \frac{n\pi}{h} \pm \frac{|\gamma_{be}^{(1)}|}{h^2}(z/t). \tag{6.27}$$

The derivative of Eq. 6.25, when evaluated at the stationary phase frequency, becomes

$$\kappa^{(2)}(\omega_{sp}) = \mp \frac{h^2}{|\gamma_{be}^{(1)}|}(t/z)^3. \tag{6.28}$$

The substitution of Eqs. 6.26, 6.27, and 6.28 into the stationary phase solution (Eq. 6.4) results in

$$p(z,t) = \Lambda(\omega_{sp}) \left(\frac{|\gamma_{be}^{(1)}|}{2\pi h^2} \right)^{1/2} zt^{-3/2} e^{j[(n\pi/h)z - \omega_{sp}(t)t]} e^{j\pm\pi/4}.$$

We see that indeed the pulse is trailed by a long oscillatory tail that only approaches zero amplitude as $t \to \infty$. In such a limit, the solution becomes

$$p(z,t) = \Lambda(\omega_{be}) \left(\frac{|\gamma_{be}^{(1)}|}{2\pi h^2} \right)^{1/2} zt^{-3/2} e^{j[(n\pi/h)z - \omega_{be}t]} e^{j\pm\pi/4}.$$

The frequency of the tail portion of the signal approaches the band edge frequency and the signal envelope decays as $t^{-3/2}$.

6.5   The Effect of Dissipation

The approach used to evaluate the dispersion integral in the nondissipative case may easily be extended to include the effects of dissipation. In the presence of dissipation the conventional wave dispersion integral becomes

$$p(z,t) = \frac{1}{2\pi} \int_{-\infty}^{+\infty} [\Lambda(\omega)e^{-\alpha(\omega)z}]e^{j\theta(\omega,z,t)}d\omega.$$

Again, we treat z as a parameter and the dispersion integral may be written

$$p(t) = \frac{1}{2\pi} \int_{-\infty}^{+\infty} \bar{\Lambda}(\omega) e^{j\theta(\omega,z,t)} d\omega, \tag{6.29}$$

where $\bar{\Lambda}(\omega) = \Lambda(\omega) e^{-\alpha(\omega)z}$ is the effective source spectrum at the distance z. Equation 6.29 is now identical to Eq. 6.1, the nondissipative dispersion integral that we have been working to solve. Equations 6.4 and 6.9, the stationary and gradual phase solutions of the nondissipative dispersion integral, are therefore valid solutions for the dissipative case as well. The stationary and gradual phase frequency trajectories, however, are in some frequency ranges substantially influenced by dissipation. The explicit solutions derived in Sec. 6.4 are therefore not necessarily solutions in the dissipative case. We must consider the dissipative gradual and stationary phase frequency trajectories, which necessitates a consideration of the effect of dissipation on the real part of the Bloch wave number.

It was found in Sec. 3.2 that, while the real part of the Bloch wave number is, for the most part, not greatly affected by dissipation, there are, particularly in the vicinity of the band edges, some substantial dissipative effects. The primary effect was found to be that the sharply cusped transitions that occur at the band edges are smoothed out (see Fig. 3.1). Away from the band edges, however, the qualitative features of $\kappa(\omega)$ are unaffected by dissipation. As in the nondissipative case, $\kappa(\omega)$ has zero curvature (i.e., a point of inflection) near the middle of the band, and increasing curvature as the band edges are approached. These are the qualitative features of $\kappa(\omega)$ that were found to give rise to (1) a constant gradual phase frequency, (2) an earliest stationary phase frequency and a stationary phase frequency bifurcation at the frequency of the inflection, and (3) a decelerating migration of the resultant stationary phase frequency pair towards opposite band edges. Dissipation does, to a small degree, change the fine details of the trajectories, but they remain, away from the band edges, *qualitatively* unchanged. For this reason, the Fourier transform, half-band, and Airy leading edge solutions all remain valid in the dissipative case as well as in the nondissipative case. The source spectrum $\Lambda(\omega)$ must simply be replaced by the effective source spectrum $\Lambda(\omega) e^{-\alpha(\omega)z}$.

The parts of the frequency trajectories that depend upon the structure of the dispersion relation near the band edges are, in contrast, substantially

affected by the presence of dissipation. In the nondissipative case, the slope of $\kappa(\omega)$ becomes infinite at the band edges, and the stationary phase frequencies consequently approach, but never in finite time reach, the band edges. In the dissipative case, however, the cusp that demarcates each band edge is replaced by a point of inflection. Another inflection point appears near the center of each stopband. As inflections in the dispersion function have been found to be very significant in the determination of the trajectories of the stationary and gradual phase frequencies, these trajectories must be reconsidered.

The structure of the gradual and stationary phase frequency trajectories may again be found by the graphical approach. Prior to the critical time associated with any of the inflection frequencies, only gradual phase frequencies exist. There is one associated with the inflection frequency that lies near the center of each stopband and each passband. Note that this set of inflection frequencies is such that $\kappa_i^{(3)} > 0$. At the critical time $t_c = z/c_{gi}$ associated with each of these inflection frequencies, the gradual phase frequency becomes a stationary phase frequency and undergoes bifurcation. In each passband and each stopband, therefore, a pair of stationary phase frequencies is generated at the critical time and the pair migrate towards the band edges. At each band edge, then, there are two converging stationary phase frequencies. At the critical time associated with the inflection frequency that now defines the band edge, these two stationary phase frequencies merge and become a single gradual phase frequency. This second set of inflection frequencies, where the stationary phase frequencies undergo confluence instead of bifurcation, are such that $\kappa_i^{(3)} < 0$. These modified stationary and gradual phase frequency trajectories are shown in Fig. 6.8.

Just as the earliest possible signal arrival occurs at the critical time associated with the bifurcation inflections, the latest possible signal arrival occurs at the critical time associated with the confluence inflections. In fact, the analysis of Sec. 6.4.3 that led to the Airy function solution for the leading edge of the pulse may be applied here to arrive at an Airy function solution for the trailing edge of the pulse. The only difference is in the sign of the argument of the envelope function; i.e., the trailing edge of the envelope function is a reversed Airy function. The long ringing tail found in the nondissipative case does not exist in the dissipative case. The signal shuts off at a signal shut-off
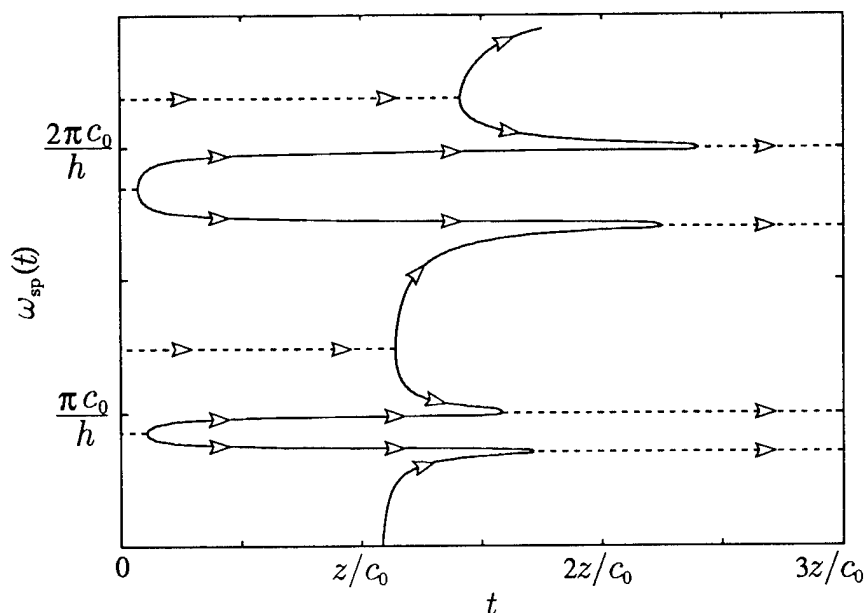
Figure 6.8: The gradual and stationary phase frequency trajectories in the dissipative case. Each pair of stationary phase frequencies (shown as solid lines) originates from a single gradual phase frequency (shown as dashed lines). Pairs of stationary phase frequencies then merge and again become a single gradual phase frequency.

AS-94-764

time

$$t_{so} = z/c_{gi},$$

where c_{gi} is the group velocity at the band edge inflection frequency. Realistically, the form of the tail of the signal is more probably determined by the large attenuation encountered near the band edges. It was found in Sec. 3.2 that thermoviscous losses are greatly enhanced near the band edges. The signal shut-off time is therefore, more practically, a conservative estimate of the latest time a signal may be received.

This page intentionally left blank.

Chapter 7

Bloch Wave Energy Transport

Here we consider the transport of energy by Bloch waves. First, expressions for the intensity, power, and energy density of time-harmonic Bloch waves are derived. These expressions are then used to calculate the energy transport velocity for both time-harmonic Bloch waves and narrowband Bloch wave pulses. It is shown that there are two energy transport velocities that are of relevance, each of which has a well defined physical interpretation. One of the two is shown to be both the velocity of energy transport by a time-harmonic Bloch wave and the velocity of energy transport in the waveguide sections for a narrowband Bloch wave pulse. The other is shown to be the net velocity of energy transport by a narrowband Bloch wave pulse as a whole.

It is assumed that the system is nondissipative. While dissipative effects may be included without a great amount of complication, the essential properties of energy transport by Bloch waves are more clearly shown in the context of nondissipative waves.

7.1 The Bloch Wave Intensity, Power, and Energy Density

Here we find the energy density, the intensity, and the power associated with the Bloch wave field. The Bloch wave field for which we derive

these quantities is, in this section, not the full, three-dimensional Bloch wave field, but the one-dimensional global field alone. Recall (see Sec. 2.2) that the global field is composed of only the one-dimensional compound traveling wave field that occurs in the waveguide sections (i.e., the f-wave/g-wave field). As is true of the results of the preceding chapters, the results found for the global field alone leads, with some care, to results that are valid for the full three-dimensional Bloch wave field as well. As the global field is a good representation of the full three-dimensional field in the waveguide sections away from the scatterers, the findings apply with equal validity to the full three-dimensional Bloch wave field in that region. The energy density, intensity, and power derived from the global field are therefore those of the full three-dimensional field away from the scatterers. In the waveguide sections near the scatterers, the full field has evanescent higher order modal components that are not accounted for in the global field representation. There is, however, no intensity or power associated with an evanescent wave field. Both the intensity and power derived from the global field are therefore exactly those of the full field in the waveguide sections. There is, however, energy density associated with an evanescent wave field, and the energy density calculations shown here are consequently not exact near the scatterers. The issue of the contribution of evanescent modes to the energy field is addressed in Sec. 7.3.3.

7.1.1 The Bloch Wave Intensity

The definition of the acoustic intensity field is

$$\mathbf{I}(\mathbf{r}, t) = \text{Re}\{p(\mathbf{r}, t)\}\text{Re}\{\mathbf{u}(\mathbf{r}, t)\},$$

or, equivalently,

$$\mathbf{I} = \frac{1}{4}\left[p\mathbf{u} + p^*\mathbf{u}^* + p\mathbf{u}^* + p^*\mathbf{u}\right].$$

The time average intensity $\langle \mathbf{I} \rangle$ is defined, for periodic signals, to be

$$\langle \mathbf{I} \rangle = \frac{\omega}{2\pi} \int_{t_0}^{t_0 + 2\pi/\omega} \mathbf{I} \, dt,$$

where ω is the fundamental frequency. The time average intensity is therefore

$$\langle \mathbf{I} \rangle = \frac{1}{4}\left[\langle p\mathbf{u} \rangle + \langle p^*\mathbf{u}^* \rangle + \langle p\mathbf{u}^* \rangle + \langle p^*\mathbf{u} \rangle\right]. \tag{7.1}$$

Under the assumption that the field is time-harmonic, the complex acoustic pressure and particle velocity fields may be expressed

$$p(\mathbf{r}, t) = p_\omega(\mathbf{r}) e^{-j\omega t}$$

$$\mathbf{u}(\mathbf{r}, t) = \mathbf{u}_\omega(\mathbf{r}) e^{-j\omega t}, \tag{7.2}$$

where $p_\omega(\mathbf{r})$ and $\mathbf{u}_\omega(\mathbf{r})$ are the complex, time-harmonic field variables seen in Chaps. 2 and 3. The subscript ω denotes the parametric dependence of the time-harmonic field on the frequency. An expression for the time-averaged intensity of a time-harmonic field is found by substitution of Eqs. 7.2 into Eq. 7.1. The resultant terms $\langle p_\omega \mathbf{u}_\omega e^{-2j\omega t} \rangle$ and $\langle p_\omega^* \mathbf{u}_\omega^* e^{2j\omega t} \rangle$ are both zero, and the time-averaged, time-harmonic intensity vector is

$$\langle \mathbf{I}_\omega \rangle = \frac{1}{4} \left[p_\omega \mathbf{u}_\omega^* + p_\omega^* \mathbf{u}_\omega \right]. \tag{7.3}$$

A property of the time-averaged intensity field that is made use of later is found by consideration of the divergence of Eq. 7.3:

$$\nabla \cdot \langle \mathbf{I}_\omega \rangle = \frac{1}{4} \left[p_\omega \nabla \cdot \mathbf{u}_\omega^* + \mathbf{u}_\omega^* \cdot \nabla p_\omega + p_\omega^* \nabla \cdot \mathbf{u}_\omega + \mathbf{u}_\omega \cdot \nabla p_\omega^* \right]. \tag{7.4}$$

The substitution of Eqs. 7.20, 7.21, and their complex conjugates into the right-hand side of Eq. 7.4 results in

$$\nabla \cdot \langle \mathbf{I}_\omega \rangle = 0. \tag{7.5}$$

The time-averaged intensity field is solenoidal.

The intensity associated with a forward traveling Bloch wave of amplitude A is found by substitution of the expressions for the pressure and velocity fields associated with a time-harmonic Bloch wave into Eq. 7.3. These fields are, in the nth cell,

$$p_\omega(z) = A \frac{e^{jk(z-nh)} + g/f e^{-jk(z-nh)}}{1 + g/f} e^{jqnh}$$

$$\mathbf{u}_\omega(z) = \frac{A}{\rho_0 c_0} \frac{e^{jk(z-nh)} - g/f e^{-jk(z-nh)}}{1 + g/f} e^{jqnh} \hat{\mathbf{e}}_z, \tag{7.6}$$

and the resultant Bloch wave intensity is

$$\langle \mathbf{I}_\omega \rangle = \frac{1}{2}\frac{|A|^2}{\rho_0 c_0}\frac{1 - |g/f|^2}{|1 + g/f|^2}e^{-2\alpha n h}\hat{\mathbf{e}}_z,$$

where n is the cell number. As the Bloch wave is nondissipative, α is nonzero only in the stopbands. In the stopbands, however, $|g/f| = 1$ (see Appendix B) and the Bloch wave intensity is therefore zero. The Bloch wave intensity is therefore given more simply by

$$\langle \mathbf{I}_\omega \rangle = \frac{1}{2}\frac{|A|^2}{\rho_0 c_0}\frac{1 - |g/f|^2}{|1 + g/f|^2}\hat{\mathbf{e}}_z. \tag{7.7}$$

In the uniform waveguide limit (that in which the periodic waveguide becomes uniform), the compound conventional wave field in each cell becomes progressive and the Bloch wave as a whole becomes a progressive conventional wave. In such a limit $g/f \to 0$ and the Bloch intensity becomes

$$\langle \mathbf{I}_\omega \rangle = \frac{1}{2}\frac{|A|^2}{\rho_0 c_0}\hat{\mathbf{e}}_z,$$

the time averaged intensity of a time-harmonic conventional wave of amplitude A. The ratio of the Bloch wave and the conventional wave intensities is therefore

$$\frac{\langle \mathbf{I}_\omega \rangle(\text{Bloch})}{\langle \mathbf{I}_\omega \rangle(\text{conv})} = \frac{1 - |g/f|^2}{|1 + g/f|^2}. \tag{7.8}$$

This intensity ratio is shown plotted in Fig. 7.1. Note that the intensity of a Bloch wave of amplitude A carries, over a sizeable fraction of the spectrum, more energy than a conventional wave of amplitude A. While such an occurrence seems impossible, it is simply an artifact of the normalization of the Bloch wave functions. In alternating passbands, the g-wave adds destructively to the f-wave at the cell center. The normalization forces the cell center pressure to have unit amplitude, and as a result the f and g-wave amplitudes may become much larger than unity.

7.1.2 The Bloch Wave Power Delivery

The time-averaged power delivered by a time-harmonic Bloch wave of amplitude A may be found by integration of the intensity over a plane normal
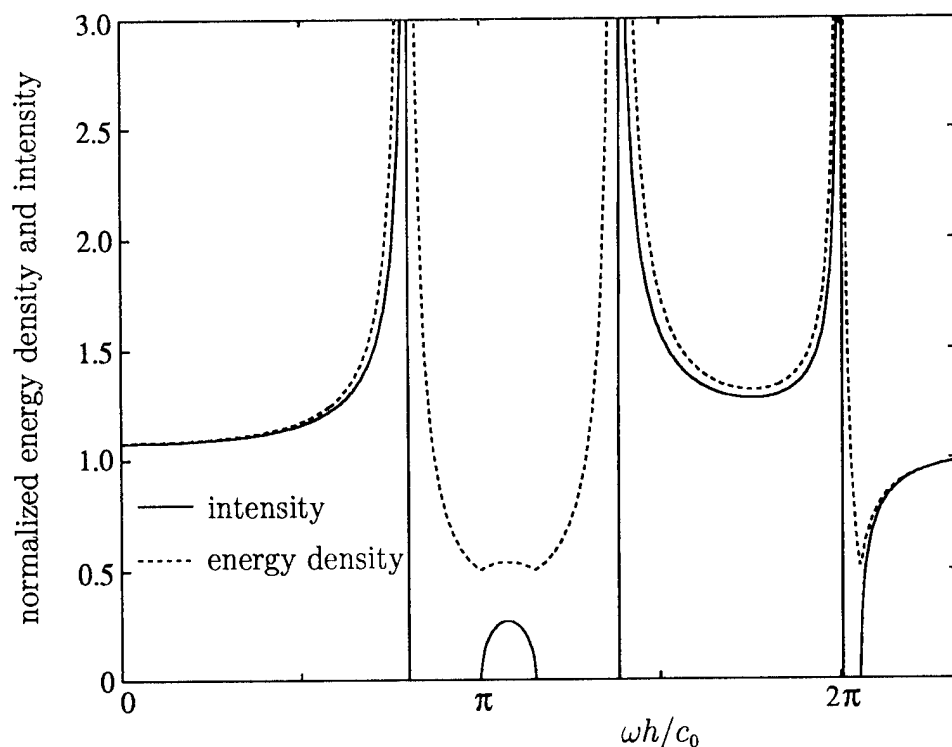
Figure 7.1: The Bloch wave energy density and intensity. The values shown are normalized by the energy density and intensity of a conventional wave of the same amplitude as the Bloch wave.   AS-94-765

to the z axis. As the intensity is independent of z, the placement of the plane of integration along the z axis is arbitrary. The intensity is also independent of the transverse coordinates, and integration of the intensity is trivial:

$$\langle P_\omega \rangle = \int \langle \mathbf{I}_\omega \rangle \cdot d\mathbf{S} = A_{\text{wg}} \langle \mathbf{I}_\omega \rangle,$$

or

$$\langle P_\omega \rangle = \frac{1}{2} \frac{|A|^2}{\rho_0 c_0 / A_{\text{wg}}} \frac{1 - |g/f|^2}{|1 + g/f|^2}. \tag{7.9}$$

The ratio between Bloch and conventional wave power is the same as that of the Bloch and conventional wave intensities (see Eq. 7.8).

It was argued at the beginning of this section that the results of the intensity and power analyses are valid for the full, three-dimensional Bloch

wave field in the waveguide sections only. In the case of the power we may extend that range of validity to include the scattering region. Consider the integral of the exact time-averaged intensity field over a closed surface S. The surface is composed of three sections. Two of the sections are planar end-caps, labeled S_1 and S_2, that are normal to the z-axis, and the third, labeled S_{ww}, connects S_1 and S_2 along the waveguide wall. The end cap surfaces S_1 and S_2 are located in a waveguide section and a scatterer, respectively. Using the divergence theorem and Eq. 7.5 we have

$$\int_V \nabla \cdot \langle \mathbf{I}_\omega \rangle dV = \oint_S \langle \mathbf{I}_\omega \rangle \cdot d\mathbf{S} = 0$$
$$= \int_{S_{ww}} \langle \mathbf{I}_\omega \rangle \cdot d\mathbf{S} + \int_{S_2} \langle \mathbf{I}_\omega \rangle \cdot \hat{\mathbf{e}}_z dS - \int_{S_1} \langle \mathbf{I}_\omega \rangle \cdot \hat{\mathbf{e}}_z dS.$$

Because the normal component of the particle velocity is zero at the waveguide wall, the time-averaged intensity is likewise zero (see Eq. 7.3) and the integral over the waveguide wall surface S_{ww} is zero. The integrals over S_1 and S_2, which are simply the power delivered to those surfaces, are therefore equal and we have

$$\langle P_\omega \rangle|_{S_1} = \langle P_\omega \rangle|_{S_2}.$$

As must be the case, the same power is delivered to any surface that completely blocks the cross section of the waveguide, regardless of the location of the surface in the waveguide.

7.1.3 The Bloch Wave Energy Density

We now consider the energy density associated with a Bloch wave field. The kinetic energy density of an acoustic field is given by

$$e_K(\mathbf{r}, t) = \frac{1}{2}\rho_0 \text{Re}\{\mathbf{u}(\mathbf{r}, t)\} \cdot \text{Re}\{\mathbf{u}(\mathbf{r}, t)\} = \frac{1}{8}\rho_0 [\mathbf{u} \cdot \mathbf{u} + 2\mathbf{u} \cdot \mathbf{u}^* + \mathbf{u}^* \cdot \mathbf{u}^*],$$
(7.10)

and the potential energy density is given by

$$e_P(\mathbf{r}, t) = \frac{1}{2}\frac{1}{\rho_0 c_0^2}\text{Re}\{p(\mathbf{r}, t)\}^2 = \frac{1}{8}\frac{1}{\rho_0 c_0^2}\left[p^2 + 2pp^* + p^{*2}\right].$$
(7.11)

When the time-harmonic field expressions (Eq. 7.2) are substituted into Eqs. 7.10 and 7.11 and the resultant equations time-averaged, we find the kinetic and potential energy densities associated with a time-harmonic field:

$$\langle e_{K\omega} \rangle = \frac{1}{4}\rho_0 \mathbf{u}_\omega \cdot \mathbf{u}_\omega^* \tag{7.12}$$

$$\langle e_{P\omega} \rangle = \frac{1}{4}\frac{1}{\rho_0 c_0^2} p_\omega p_\omega^*. \tag{7.13}$$

The total energy density associated with a time-harmonic field is therefore

$$\langle e_\omega \rangle = \langle e_{K\omega} \rangle + \langle e_{P\omega} \rangle = \frac{1}{4}\rho_0 \mathbf{u}_\omega \cdot \mathbf{u}_\omega^* + \frac{1}{4}\frac{1}{\rho_0 c_0^2} p_\omega p_\omega^*.$$

The kinetic and potential energy densities associated with a time-harmonic Bloch wave field may be found by the substitution of the Bloch wave field expressions (Eqs. 7.6) into Eqs. 7.12 and 7.13:

$$\langle e_{K\omega} \rangle = \frac{1}{4}\frac{|A|^2}{\rho_0 c_0^2}\frac{1 - g/f^* e^{2jk(z-nh)} - g/f e^{-2jk(z-nh)} + |g/f|^2}{|1 + g/f|^2}e^{-2\alpha nh}$$

$$\langle e_{P\omega} \rangle = \frac{1}{4}\frac{|A|^2}{\rho_0 c_0^2}\frac{1 + g/f^* e^{2jk(z-nh)} + g/f e^{-2jk(z-nh)} + |g/f|^2}{|1 + g/f|^2}e^{-2\alpha nh}.$$

The total Bloch wave energy density is therefore

$$\langle e_\omega \rangle = \langle e_{K\omega} \rangle + \langle e_{P\omega} \rangle = \frac{1}{2}\frac{|A|^2}{\rho_0 c_0^2}\frac{1 + |g/f|^2}{|1 + g/f|^2}e^{-2\alpha nh}. \tag{7.14}$$

At passband frequencies $\alpha = 0$ and we have

$$\langle e_\omega \rangle = \frac{1}{2}\frac{|A|^2}{\rho_0 c_0^2}\frac{1 + |g/f|^2}{|1 + g/f|^2},$$

and at stopband frequencies $|g/f| = 1$ and we have

$$\langle e_\omega \rangle = \frac{1}{2}\frac{|A|^2}{\rho_0 c_0^2}\frac{2}{|1 + g/f|^2}e^{-2\alpha nh}.$$

In the uniform waveguide limit (that in which the periodic waveguide degenerates to a uniform waveguide), the Bloch wave field becomes a progressive

conventional wave field ($g/f \to 0$ and $\alpha \to 0$). In such a case the Bloch wave energy density in the zeroth cell reduces to

$$\langle e_\omega \rangle = \frac{1}{2} \frac{|A|^2}{\rho_0 c_0^2},$$

the energy density associated with a progressive conventional wave of amplitude A. The ratio of the Bloch and conventional wave energy densities is

$$\frac{\langle e_\omega \rangle (\text{Bloch})}{\langle e_\omega \rangle (\text{conv})} = \frac{1 + |g/f|^2}{|1 + g/f|^2}.$$

This energy ratio is shown plotted in Fig. 7.1. As in the case of the Bloch wave intensity, the unusually large energy density near some of the band edges is due to the Bloch wave normalization.

While the energy densities considered thus far are all volumetric energy densities (i.e., they are measured in Joules per unit volume), we may alternatively consider *linear* energy densities. The volumetric energy density may be made linear by an integration with respect to the transverse coordinates:

$$\langle e_\omega \rangle_l = \int \int \langle e_\omega \rangle dx dy.$$

As the volumetric energy density in the waveguide sections depends only upon the axial coordinate z, it may be made linear simply by multiplication by the waveguide cross sectional area.

7.2 The Microscopic Energy Transport Velocity

We may now consider the velocity of energy transport by time-harmonic Bloch waves. We have thus far found expressions for the density of energy and the rate of delivery of energy. Implicit in the definitions of these quantities is the definition of a velocity, the energy transport velocity. Consider an infinitesimal surface dS that has arbitrary orientation. By the definition of the intensity, the rate at which energy is delivered to this surface (i.e., the energy flux at the surface) is given by the differential power $d\langle P_\omega \rangle = \langle \mathbf{I}_\omega \rangle \cdot d\mathbf{S}$. Consider

now the energy field in the vicinity of the surface. In order to deliver energy to the surface, the energy field must be in motion. The power delivered to the surface by the energy field in motion at the velocity $\mathbf{v}_E$ is $d\langle P_\omega \rangle = \langle e_\omega \rangle \mathbf{v}_E \cdot d\mathbf{S}$. In order for the two expressions for the power at the surface to be consistent, it must be the case that $\langle e_\omega \rangle \mathbf{v}_E = \langle \mathbf{I}_\omega \rangle$, or, equivalently, that the energy transport velocity is given by

$$\mathbf{v}_E = \frac{\langle \mathbf{I}_\omega \rangle}{\langle e_\omega \rangle}. \tag{7.15}$$

Equation 7.15 is the definition of the velocity of energy transport that is implicit in the definitions of energy density and intensity. The same argument, when cast in terms of the power and linear energy density, leads to the scalar energy transport velocity

$$v_E = \frac{\langle P_\omega \rangle}{\langle e_\omega \rangle_l}, \tag{7.16}$$

where the velocity is directed along the axis associated with the linear energy density.

The flow of acoustic energy bears a strong resemblance to the flow of mass in a hydrodynamic system. The density and flux of energy in the acoustic system is analogous to the density and flux of mass in the hydrodynamic system. Consider the flow of liquid through a channel such as those which compose the waveguide sections of the periodic waveguide. If the mass density and flux rate at a plane that is normal to the channel axis are given by ρ_F and $\dot{M}$, respectively, then the flow velocity is given by $v_\text{F} = \dot{M}/\rho_\text{F}$. Note the similarity between this expression for fluid velocity and the expression for energy transport velocity (Eq. 7.16). Just as the flow of the liquid delivers mass, the flow of acoustic energy delivers power. This analogy is expanded upon in Sec. 7.4, where it proves to be quite useful.

Upon substitution of the expessions for the Bloch wave energy density and power (Eqs. 7.14 and 7.9) into the definition of the energy transport velocity (Eq. 7.16), we find

$$v_E = c_0 \frac{1 - |g/f|^2}{1 + |g/f|^2}. \tag{7.17}$$

This is the expression for the velocity of energy transport by time-harmonic Bloch waves. The energy transport velocity is less than c_0, the free-medium

sound speed, at all frequencies, and in the stopbands, where $|g/f| = 1$, we have $v_E = 0$. In Fig. 7.2 is shown a plot of the energy transport velocity. Included in the plot is the Bloch wave group velocity c_{gr}, to show that the energy transport velocity and the group velocity differ, particularly in the stopbands, where the
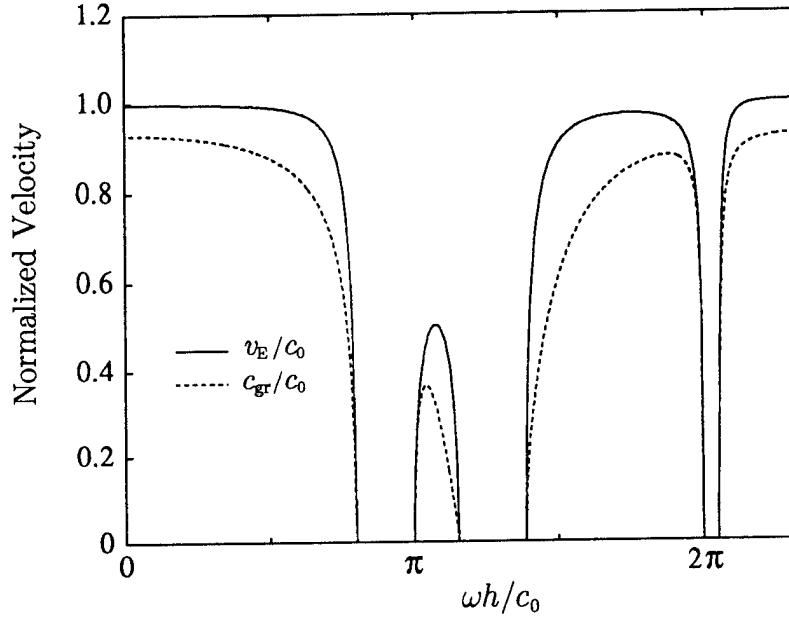
Figure 7.2: The microscopic energy transport velocity and group velocity for the isotropic periodic waveguide described in the introduction.

AS-94-766

energy transport velocity is zero and the group velocity is infinite.

As the Bloch wave field used in the derivation of the Bloch wave energy transport velocity is the global field, the validity of the result as it applies to the full three-dimensional field is worthy of some discussion. It is pointed out in the beginning of Sec. 7.1 that the calculation of energy density, power, and intensity based on the global field are valid for the full three-dimensional field in various regions of the waveguide. The Bloch wave intensity field (Eq. 7.7) is valid anywhere in the waveguide sections. The expression for the Bloch wave power (Eq. 7.9) is valid everywhere in the waveguide, and the expression for the Bloch wave energy density (Eq. 7.14) is valid in the waveguide sections away from the scatterers. The validity of the expression for the Bloch wave energy

transport velocity (Eq. 7.17) is therefore limited by that of the energy density. Equation 7.17, the energy transport velocity associated with the global field, is therefore that of the full three-dimensional field in the waveguide sections away from the scatterers.

The energy transport velocity in the waveguide sections is a (indirectly) measureable quantity. Recall that the measurement of the field at two points in the waveguide section yields sufficient information to determine the structure of the f-wave/g-wave field (see Appendix E). Such a measurement is likewise, via Eqs. 7.7 and 7.14, sufficient to determine the time average energy density and intensity in the waveguide section. As the energy transport velocity is simply the ratio of these two quantities, the two point measurement is therefore a determination of the energy transport velocity as well. We may therefore simply use the measured value of g/f (as described in Appendix E) in Eq. 7.17 to result in a measured value of the energy transport velocity. In Fig. 7.3 is shown a plot of the experimental values of v_E along with plots of theoretical values derived from both the dissipative and the nondissipative theories.[1] The agreement between theory and experiment serves to verify that energy is transported through the waveguide sections at the velocity v_E.

While several of the characteristics of the energy transport velocity (such as those pointed out in the discussion following Eq. 7.17) are certainly consistent with what we would expect, we must ask how the energy transport velocity can *not* be equal to the group velocity. For propagation distances that are small compared to the smallest characteristic distortion distance, a Bloch wave pulse propagates without distortion at the group velocity. Certainly in that case the energy *must* be transported at the group velocity, as in the case of dispersive conventional waves (see Eq. 5.36). On the other hand, the energy transport velocity shown in Eq. 7.17 is that which is measured by an energy transport probe placed in a waveguide section. We may recongnize the source of

---

[1]The expressions for energy density and intensity derived here for the nondissipative case may easily be generalized to include the approximate effect of dissipation. As mainstream thermoviscous losses have been taken to be insignificant as compared to the thermoviscous acoustic boundary layer losses, the impedance of the plane wave mode is the same as that in the absence of dissipation (see, for example, the book by Pierce, 1981). Equation 7.17 may therefore be made dissipative simply by using the dissipative value of g/f.
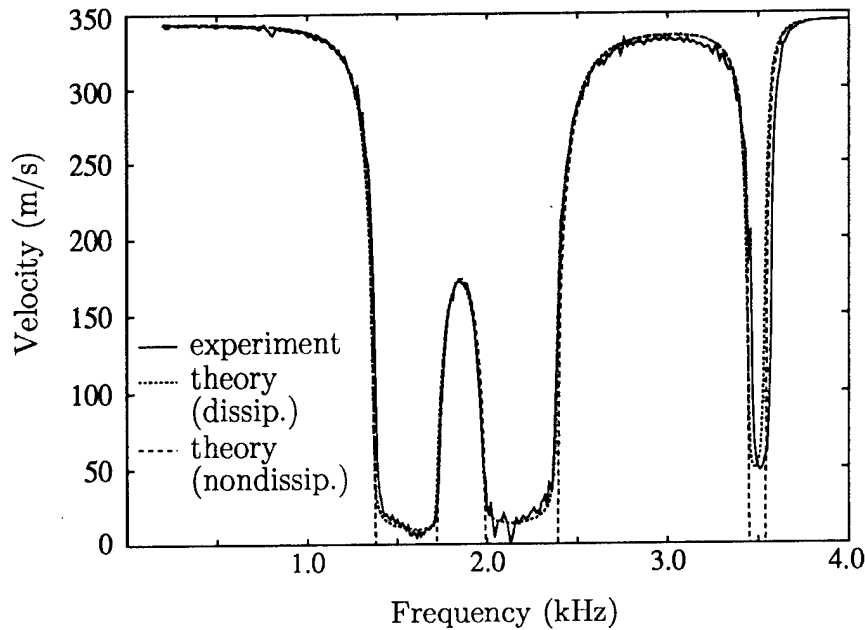
Figure 7.3: Theoretical and experimental values of the microscopic energy transport velocity.

this apparent contradiction by consideration of another definition of the linear energy density and hence another energy transport velocity. While this second definition of the linear energy density is rather contrived, it is one that both yields an interesting result and sheds light on the reason the energy transport velocity differs from the group velocity. As the energy transport velocity of Eq. 7.17 applies to the transport of energy within a cell, it is referred to as the microscopic energy transport velocity and is labeled $v_E^{(mi)}$.

7.3 The Macroscopic Energy Transport Velocity

In this section we find a second expression for the energy transport velocity that is based on a different definition of linear energy density. While the microscopic energy transport velocity derived in Sec. 7.2 is based on the energy density in the waveguide sections, that derived here, called the macroscopic en-

ergy transport velocity, is based on the linear energy density averaged over a waveguide cycle. As this cycle-averaged or *macroscopic* value of the linear energy density necessarily involves the field in the scattering sections, we must here use the full three-dimensional field in its calculation. We first derive an integral expression for the total time-averaged energy in a given volume. The time-averaged energy contained in a waveguide cycle is then calculated and divided by the length of the cycle to result in an expression for the cycle-averaged linear energy density. We are then able to find the associated expression for the macroscopic energy transport velocity and consider the findings.

7.3.1 The Time-Averaged Energy Integral

The total time-averaged acoustic energy contained within a closed surface may be calculated using an interesting surface integral approach that is similar to one used for electromagnetic fields (e.g., Collin, 1960). It is shown that the net time-averaged energy in a volume is given by an integral over the surface that encloses that volume.

The linear, nondissipative governing equations may be written

$$\rho_0 \frac{\partial \mathbf{u}}{\partial t} + \nabla p = 0 \tag{7.18}$$

$$\frac{\partial p}{\partial t} + \rho_0 c_0^2 \nabla \cdot \mathbf{u} = 0, \tag{7.19}$$

where Eq. 7.18 is the momentum equation and Eq. 7.19 is the combined mass continuity and state equation. For time-harmonic fields, Eqs. 7.18 and 7.19 may be written

$$\nabla p_\omega = j\omega \rho_0 \mathbf{u}_\omega \tag{7.20}$$

$$\nabla \cdot \mathbf{u}_\omega = j\omega \left(\frac{1}{\rho_0 c_0^2} \right) p_\omega. \tag{7.21}$$

The partial differentiation of Eqs. 7.20 and 7.21 with respect to frequency yields

$$\nabla \frac{\partial p_\omega}{\partial \omega} = j\rho_0 \mathbf{u}_\omega + j\omega \rho_0 \frac{\partial \mathbf{u}_\omega}{\partial \omega} \tag{7.22}$$

and

$$\nabla \cdot \frac{\partial \mathbf{u}_\omega}{\partial \omega} = j \left(\frac{1}{\rho_0 c_0^2} \right) p_\omega + j\omega \left(\frac{1}{\rho_0 c_0^2} \right) \frac{\partial p_\omega}{\partial \omega}, \tag{7.23}$$

respectively. With the use of Eqs. 7.20-7.23 and their complex conjugates, the following identities are readily derived

$$\nabla \cdot \left(\frac{\partial p_\omega^*}{\partial \omega} \mathbf{u}_\omega \right) = j\omega \left(\frac{1}{\rho_0 c_0^2} \right) p_\omega \frac{\partial p_\omega^*}{\partial \omega} - j\rho_0 \mathbf{u}_\omega \cdot \mathbf{u}_\omega^* - j\omega\rho_0 \mathbf{u}_\omega \cdot \frac{\partial \mathbf{u}_\omega^*}{\partial \omega} \quad (7.24)$$

$$\nabla \cdot \left(p_\omega \frac{\partial \mathbf{u}_\omega^*}{\partial \omega} \right) = -j \left(\frac{1}{\rho_0 c_0^2} \right) p_\omega p_\omega^* - j\omega \left(\frac{1}{\rho_0 c_0^2} \right) p_\omega \frac{\partial p_\omega^*}{\partial \omega} + j\omega\rho_0 \mathbf{u}_\omega \cdot \frac{\partial \mathbf{u}_\omega^*}{\partial \omega}. \quad (7.25)$$

When these two identities are added, several terms cancel and we are left with

$$\nabla \cdot \left[p_\omega \frac{\partial \mathbf{u}_\omega^*}{\partial \omega} + \frac{\partial p_\omega^*}{\partial \omega} \mathbf{u}_\omega \right] = -4j \left[\frac{1}{4} \left(\frac{1}{\rho_0 c_0^2} \right) p_\omega p_\omega^* + \frac{1}{4} \rho_0 \mathbf{u}_\omega \cdot \mathbf{u}_\omega^* \right]. \quad (7.26)$$

We recongnize the two terms on the right hand side of Eq. 7.26 to be the potential and kinetic energy densities, respectively (see Eqs. 7.12 and 7.13). Equation 7.26 may therefore be written

$$\langle e_\omega \rangle = \frac{j}{4} \nabla \cdot \left[p_\omega \frac{\partial \mathbf{u}_\omega^*}{\partial \omega} + \frac{\partial p_\omega^*}{\partial \omega} \mathbf{u}_\omega \right]. \quad (7.27)$$

We next integrate Eq. 7.27 over a volume enclosed by the surface S. The resultant volume integral over the divergence may be converted, by way of the divergence theorem, into a surface integral, and we have

$$\langle E_\omega \rangle = \int_V \langle e_\omega \rangle dV = \frac{j}{4} \oint_S \left[p_\omega \frac{\partial \mathbf{u}_\omega^*}{\partial \omega} + \frac{\partial p_\omega^*}{\partial \omega} \mathbf{u}_\omega \right] \cdot d\mathbf{S}, \quad (7.28)$$

where $\langle E_\omega \rangle$ is the total time-averaged energy enclosed by the surface S.

7.3.2 The Macroscopic Energy Density

We may now use Eq. 7.28 to calculate the total time-averaged energy in a single cycle of the periodic waveguide, and therefore the macroscopic energy density. The particular cycle over which we average is arbitrary, and is taken (completely generally) to be that between the planes defined by $z = z_0$ and $z = z_0 + h$. The surface of integration S therefore has planar end-caps normal to $\hat{\mathbf{e}}_z$ at $z = z_0$ and $z = z_0 + h$, and covers the inner surface of the waveguide in between (see Fig. 7.4). If the waveguide contains inclusions, then the surface

must also include detached sub-surfaces that enclose all inclusions at their surfaces. Because the waveguide wall and the inclusions, if present, are rigid, the normal component of the particle velocity at these surfaces is zero. The integrand of Eq. 7.28 is consequently also zero at these surfaces, and the only nonzero contributions to the surface integral arise from two end-cap surfaces at $z = z_0$ and $z = z_0 + h$. The integral expression for the energy enclosed in the waveguide cycle therefore reduces to

$$\langle E_\omega \rangle = -\frac{j}{4} \int_S \left[p_\omega \frac{\partial \mathbf{u}_\omega^*}{\partial \omega} + \frac{\partial p_\omega^*}{\partial \omega} \mathbf{u}_\omega \right]_{z=z_0} \cdot \hat{\mathbf{e}}_z dS + \frac{j}{4} \int_S \left[p_\omega \frac{\partial \mathbf{u}_\omega^*}{\partial \omega} + \frac{\partial p_\omega^*}{\partial \omega} \mathbf{u}_\omega \right]_{z=z_0+h} \cdot \hat{\mathbf{e}}_z dS.$$
(7.29)

It was shown in Sec. 3.5 that the acoustic pressure field, and consequently the particle velocity field, associated with a forward traveling Bloch wave are such that

$$p_\omega(\mathbf{r} + h\hat{\mathbf{e}}_z) = p_\omega(\mathbf{r})e^{jqh}$$

$$\mathbf{u}_\omega(\mathbf{r} + h\hat{\mathbf{e}}_z) = \mathbf{u}_\omega(\mathbf{r})e^{jqh}.$$

These expressions may be used to relate the integral over the surface at $z_0 + h$
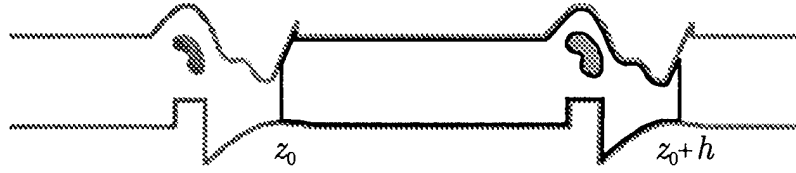
Figure 7.4: An example of an integration surface that may be used in the calculation of the total time-averaged energy contained in a cycle of a periodic waveguide.

to that at z_0, and Eq. 7.29 may be written

$$\langle E_\omega \rangle = \frac{j}{4} \int_S \left[\frac{\partial p_\omega^*}{\partial \omega} \mathbf{u}_\omega - p_\omega \frac{\partial \mathbf{u}_\omega^*}{\partial \omega} \right.$$

$$\left. + p_\omega e^{jqh} \frac{\partial}{\partial \omega} \left(\mathbf{u}_\omega e^{jqh} \right)^* - \mathbf{u}_\omega e^{jqh} \frac{\partial}{\partial \omega} \left(p_\omega e^{jqh} \right)^* \right]_{z=z_0} \cdot \hat{\mathbf{e}}_z dS. \quad (7.30)$$

The integral is now over the single end cap surface at $z = z_0$, which is an arbitrary cross-section of the periodic waveguide. The integrand therefore need

not be evaluated at $z = z_0$; we simply perform the integral for an arbitrary value of z. Upon differentiation of the indicated complex conjugates with respect to ω, Eq. 7.30 may be expressed

$$\langle E_\omega \rangle = \frac{dq^*}{d\omega} h e^{-2\alpha h} \int_S \frac{1}{4}(p_\omega \mathbf{u}_\omega^* + p_\omega^* \mathbf{u}_\omega) \cdot \hat{\mathbf{e}}_z dS$$

$$\frac{j}{4}(1 - e^{-2\alpha h}) \int_S \left[\frac{\partial p_\omega^*}{\partial \omega} \mathbf{u}_\omega - p_\omega \frac{\partial \mathbf{u}_\omega^*}{\partial \omega} \right] \cdot \hat{\mathbf{e}}_z dS. \tag{7.31}$$

As the integrand of the first integral on the right-hand side is the time-averaged intensity (see Eq. 7.3), the integral itself is the time-averaged power, and Eq. 7.31 may be written

$$\langle E_\omega \rangle = \frac{dq^*}{d\omega} h e^{-2\alpha h} \langle P_\omega \rangle + \frac{j}{4}(1 - e^{-2\alpha h}) \int_S \left[\frac{\partial p_\omega^*}{\partial \omega} \mathbf{u}_\omega - p_\omega \frac{\partial \mathbf{u}_\omega^*}{\partial \omega} \right] \cdot \hat{\mathbf{e}}_z dS.$$

In the passbands, $\alpha = 0$, $q = \kappa$, and the total energy in a waveguide cycle is given by

$$\langle E_\omega \rangle = \frac{d\kappa}{d\omega} h \langle P_\omega \rangle. \tag{7.32}$$

In the stopbands $\langle P_\omega \rangle = 0$ (see Eq. 7.9), and the total energy in a waveguide cycle is given by

$$\langle E_\omega \rangle = \frac{j}{4}(1 - e^{-2\alpha h}) \int_S \left[\frac{\partial p_\omega^*}{\partial \omega} \mathbf{u}_\omega - p_\omega \frac{\partial \mathbf{u}_\omega^*}{\partial \omega} \right] \cdot \hat{\mathbf{e}}_z dS.$$

We may now calculate a linear energy density for a forward traveling Bloch wave in which the energy variations over a waveguide cycle are taken into account. As we have integrated the energy contained in a cycle of the waveguide, we may simply divide that value by h, the length of the cycle, to obtain the macroscopic linear energy density:

$$\langle e_\omega \rangle_1 = \frac{\langle E_\omega \rangle}{h}. \tag{7.33}$$

From Eqs. 7.32 and 7.33, therefore, the macroscopic linear energy density for passband Bloch waves is given by

$$\langle e_\omega \rangle_1 = \frac{d\kappa}{d\omega} \langle P_\omega \rangle. \tag{7.34}$$

7.3.3 The Macroscopic Energy Transport Velocity

We may now find the energy transport velocity associated with the macroscopic definition of the linear energy density. At stopband frequencies, the energy density in the cell is nonzero, the power delivered is zero (see Eq. 7.7) and, by Eq. 7.16, the energy transport velocity is zero. At passband frequencies the macroscopic energy transport velocity is found, by the substitution of Eq. 7.34 into Eq. 7.16, to result in

$$v_E = \frac{\langle P_\omega \rangle}{d\kappa/d\omega \langle P_\omega \rangle} = c_{gr} \quad \text{(passband)}$$

$$v_E = 0 \qquad\qquad \text{(stopband)}.$$

The energy transport velocity based on the macroscopic definition of the energy density yields the "expected" result that the energy travels at the group velocity. This energy transport velocity, however, is not that which would be measured by an energy transport velocity probe.[2]

7.4 The Stagnant and Mobile Energy

In order to make sense of the difference between the two energy transport velocities, we must consider the differences between the macroscopic definition of the linear energy density, which leads to an energy transport velocity that is equal to the group velocity, and the microscopic definition of the linear energy density, which leads to a slightly larger energy transport velocity. While the microscopic definition only accounts for the energy field in the waveguide sections, the macroscopic definition accounts for all energy present in a waveguide cycle. In the case of the isotropic periodic waveguide described in the introduction, it is found that the linear energy density associated with the field in the waveguide sections (i.e., the linear microscopic energy density) is less than the linear energy density associated with the entire cell (i.e., the

---

[2]By probe we mean a *point* probe. An energy transport velocity probe that integrates over either exactly one cycle or a very large number of cycles would indeed measure the macroscopic energy transport velocity.

linear macroscopic energy density). This may be deduced from Eq. 7.16 and the finding that $v_E^{(mi)} > c_{gr}$ (see Fig. 7.2). The field in the vicinity of the scatterer must therefore have a "store" of energy that does not leave the scattering region. Indeed, this is the energy associated with a nondissipative scattering reactance. This stored energy is, for obvious reasons, termed *stagnant* energy and is the reason for the disparity between $v_E^{(mi)}$ and $v_E^{(ma)} = c_{gr}$.

A clear example of the stagnant energy stored by the scatterer is found in the case of the isotropic periodic waveguide described in the introduction. For this waveguide, the scattering is caused by a rigidly terminated side branch. The field in the side branch is a standing wave field composed of counter-propagating waves of equal amplitude. This field consequently has nonzero energy yet *zero intensity*, and consequently makes no contribution to the transport of energy. Indeed, as the intensity associated with the stagnant energy field is zero, the energy transport velocity associated with the field is likewise zero (see Eq. 7.15). The energy field is truly stagnant. Another component of the field that is capable of energy storage is that made up of evanescent waveguide modes. Recall that in the waveguide sections on either side of the scatterer is a field that is composed of evanescent waveguide modes and is confined to the near-vicinity of the scatterer. The field composed of these evanescent modes has nonzero energy yet zero intensity, and is therefore also a stagnant energy field.
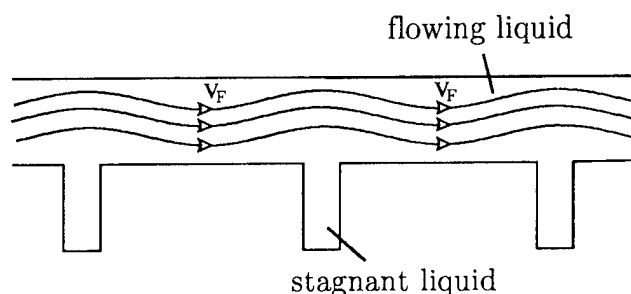
Figure 7.5: The steady-state flow of liquid through the isotropic periodic waveguide described in the introduction. The fluid in the side branches is stagnant while that in the waveguide sections and the region above the side branches flows.   AS-94-769

The concepts of stagnant and mobile energy are nicely reflected in

the hydrodynamic flow analogy introduced in Sec. 7.2. Consider the steady-state flow of the liquid through the isotropic periodic waveguide described in the introduction, as shown schematically in Fig. 7.5. In the case of steady state flow, which is analogous to the case of time-harmonic Bloch waves, a fraction of the liquid is trapped in the side branches and doesn't ever flow through the waveguide sections. This is precisely the situation of the stagnant acoustic energy. The liquid was deposited in the side branches at $t = -\infty$ and is forever stagnant. Clearly, if we are to determine the fluid flow velocity on the basis of the linear mass density and flux, the linear mass density that must be used is that in the waveguide sections. If we decided to use a cell-averaged value of the linear mass density (i.e., if the stagnant liquid in the side branches were included in the calculation) then the value of the linear mass density would become larger than the waveguide value. Consequently, the resultant flow velocity would be smaller than that obtained from the waveguide density value. This smaller flow velocity, which is analogous to the macroscopic energy transport velocity, *has no physical significance.* It is simply a velocity that results from an arbitrary definition that does not correspond to any physical, measurable flow velocity.

Just as the inclusion of the stagnant liquid in the calculation of fluid mass density results in a nonphysical fluid flow velocity, the inclusion of stagnant energy in the calculation of the linear energy density results in a nonphysical energy flow velocity. As the stagnant energy is indeed stagnant and makes no contribution to the transport of energy, it should not be included in the calculation of the energy density. Its inclusion is simply a contrivance that produces the "attractive" result that the energy is transported at the group velocity, as it is for dispersive conventional waves. The energy that makes up the stagnant energy field was deposited at $t = -\infty$ and has remained stationary since. The remaining energy, the *mobile energy,* travels down the waveguide at a fixed rate; that given by $v_E^{(mi)}$. For this reason, $v_E^{(mi)}$ *is the true velocity at which energy is transported by time-harmonic Bloch waves.*

7.5 Energy Transport by Bloch Wave Pulses

While it is clear that the stagnant energy should not be included in the calculation of the energy transport velocity for time-harmonic Bloch waves, what of the case of Bloch waves that are not time-harmonic? Consider the case of a narrowband Bloch wave pulse. Over distances that are small compared to the smallest of the characteristic distortion distances, the pulse propagates without distortion at the group velocity. As the energy associated with the pulse is confined to the location of the pulse, the energy of the pulse as a whole *must* travel at the group velocity. On the other hand, it was found in Sec. 5.4 that a narrowband Bloch wave pulse has the functional form of a carrier frequency time-harmonic Bloch wave that is modulated by an envelope function (see Eq. 5.51). The energy transport velocity in the waveguide sections is therefore that of a carrier frequency time-harmonic Bloch wave: $v_E^{(mi)}(\omega_0)$. In other words, energy is transported through the waveguide sections at the velocity $v_E^{(mi)}(\omega_0)$ yet the energy associated with the pulse as a whole moves at the carrier frequency group velocity c_{g0}. This apparent inconsistency is the subject of this section.

The key to the difference between the time-harmonic and the pulsed cases lies in the stagnant energy at the scatterers. In the time-harmonic case, the energy is not just stagnant, but is *forever* stagnant. It was deposited at $t = -\infty$, and is never transported. In the case of the Bloch wave pulse, on the other hand, there is no *permanently* stagnant energy. As the pulse must eventually pass, the stagnant energy must eventually become mobile. *The stagnant energy must be deposited at the leading edge of the pulse and reclaimed at the trailing edge.* While energy is transmitted through the waveguide sections at the velocity $v_E^{(mi)}$, *this energy transport channel is charged with the additional task of the transportation of the stagnant energy as well as the mobile energy.* This "bucket brigade" transport of energy is the reason the pulse travels at a velocity that is less than the energy transport velocity.

Again, the hydrodynamic analogy is useful to illustrate the point. Consider a "packet" of liquid (like a highly compliant liquid filled balloon) that flows through the isotropic periodic waveguide described in the introduction. The liquid packet is driven by a force (perhaps by compressed gas or gravity) such that the fluid flow velocity in the waveguide sections is v_F. This flow

velocity is analogous to $v_E^{(mi)}(\omega_0)$, the microscopic energy transport velocity associated with the carrier frequency of a narrowband pulse. Such a situation is illustrated in Fig. 7.6. In Fig. 7.6(a) the liquid packet is shown in a situation in which the fluid in the side branches is all stagnant, and the fluid transport channel (i.e., the waveguide section) transports only the fluid that occupies the waveguide section (i.e., the mobile fluid). During such a flow condition, which is very similar to the steady-state flow condition, the fluid flows as though the side branches were not present and the packet as a whole moves at a velocity of v_F. As the packet moves farther along, the tail of the packet eventually reaches a side branch, and the liquid in the side branch, which was stagnant, begins to flow, as shown in Fig. 7.6(b). The fluid transport channel (i.e., the waveguide section), which has a specified flow velocity of v_F, is temporarily dedicated to the transport of the stagnant liquid from the side branch. At the same time, liquid is deposited into a side branch at the leading edge of the packet. During this time interval, *the packet as a whole has come to a halt.* Once the side branch at the tail is empty and that at the head full, the fluid transport channel is again dedicated to the transport of mobile fluid, and the cycle repeats. In such a "bucket brigade" cycle of fluid transport, *the net velocity of the packet is less than* v_F.

The transport of the acoustic energy in a narrowband Bloch wave pulse is less than the microscopic energy transport velocity for precisely the same reason the velocity of transport of liquid mass in the liquid packet is less than the flow rate in the waveguide sections. In the time-harmonic case there is truly stagnant acoustic energy associated with the scatterer; i.e., energy that *never* moves. In the case of the narrowband pulse, however, there is no truly stagnant acoustic energy. The energy transport channels (the waveguide sections) must eventually transport the stagnant energy, and the pulse consequently propagates at a velocity that is less than $v_E^{(mi)}(\omega_0)$. If we are concerned with the gross velocity of energy transport by the pulse as a whole, then we must consider that *all* energy is mobile at one time or another and all energy must therefore be included in the calculation of the energy density. The cycle-averaged or macroscopic linear energy density is therefore the appropriate density for use in the calculation of the gross energy transport velocity.

It should be noted that the issue of the difference between the mi-
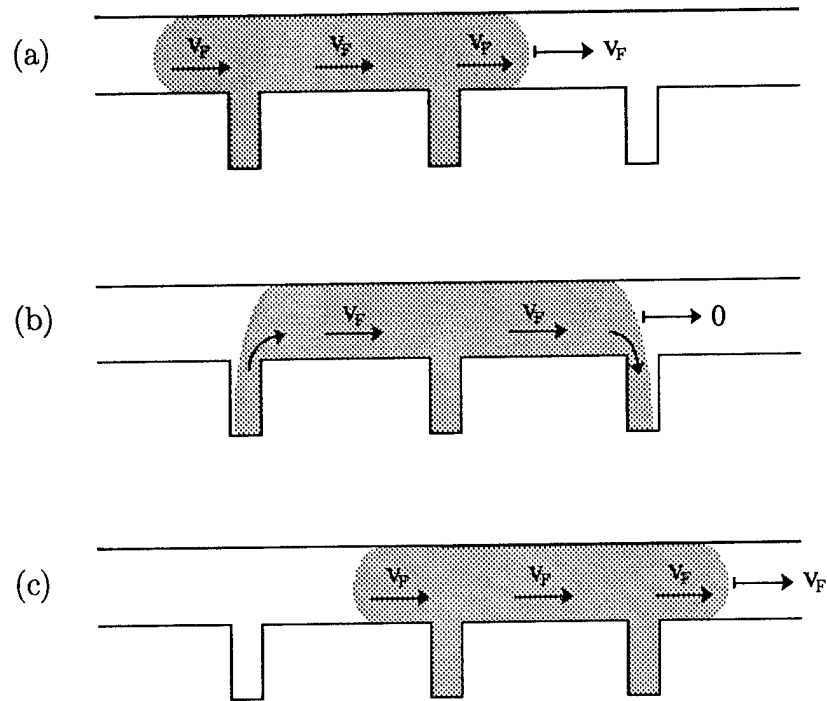
Figure 7.6: The flow of a "packet" of liquid through the isotropic periodic waveguide described in the introduction. In (a) the liquid in the side branches is stagnant and the packet moves at the velocity v_F, that of the liquid in the waveguide sections. In (b), the liquid in the side branches at the head and tail of the packet becomes mobile and the packet as a whole stops. The flow through the waveguide sections is dedicated to the transport of the side branch fluid. In (c), the side branch fluid has been transported and the packet again moves at the velocity v_F, as in (a).

croscopic and the macroscopic energy transport velocities for Bloch waves is remarkably similar to that for electromagnetic wave propagation in dispersive dielectrics (Hines, 1952). In that case, the stagnant energy is stored in the oscillations of electrons relative to their parent ions. The microscopic energy transport velocity, found by excluding the energy of oscillation of the electrons from the calculation of the energy density, is the velocity of the time-harmonic electromagnetic field energy between the scattering molecules. The macroscopic energy transport velocity, on the other hand, is found by inclusion of the electronic energy in the energy density calculation and is equal to the group velocity. A substantial difference between the Bloch wave and the dispersive dielectric wave cases is the difference in scale. In the case of the dispersive dielectric, the microscopic energy transport velocity cannot, owing to the scale, be measured. Any measurement of energy density would include the stagnant electronic energy, and the resultant velocity would be the macroscopic energy transport velocity.

To conclude, there are *two* energy transport velocities that are relevant in the description of energy transport by Bloch waves. The first of the two is the microscopic energy transport velocity $v_E^{(mi)}$, as defined in Eq. 7.17. This velocity is (1) the velocity of energy transport by time-harmonic Bloch waves, and (2) the velocity of energy transport in the waveguide sections for narrowband Bloch wave pulses. The second of the two is the macroscopic energy transport velocity $v_E^{(ma)} = c_{gr}$, which is the net velocity of energy transport by a narrowband Bloch wave pulse as a whole.

This page intentionally left blank.

Chapter 8

Nonlinear Bloch Wave Propagation

In this chapter we consider the effects of nonlinearity in the propagation of Bloch waves. More specifically, the nonlinearly generated second harmonic distortion component is considered. It was found in Chapter 2 that for a linear, progressive, time-harmonic Bloch wave, the field within a cell is, up to a constant factor, identical to that in any other cell of the waveguide. This peculiarity in the structure of the Bloch wave is exploited in the derivation of a discrete Green's function solution for the second harmonic field. In this framework it is straightforward to show that a forward traveling fundamental Bloch wave excites both forward and backward traveling second harmonic Bloch waves. The amplitudes of these second harmonic waves oscillate periodically as the waves propagate, much like the spatial beating of the second harmonic wave that comes about in the case of conventional nonlinear wave propagation in dispersive media. The effective nonlinearity, however, is different from that of conventional waves. Nonetheless, the spatial beats indicate that the Bloch wave dispersion, like conventional wave dispersion, disrupts the synchronous propagation of the fundamental and second harmonic that is responsible for the cumulative growth of the harmonic distortion components. The imposition of some sort of periodic structure in a uniform waveguide is therefore a possible means of disrupting the distorting effect of nonlinearity in guided wave propagation.

The particular system under study consists of a 48 cycle length of periodic waveguide (the isotropic periodic waveguide described in Sec. 1.3.2)

that lies between a source at $z = 0$ and a semi-infinite uniform waveguide at $z = (N - 1)h$. The source boundary condition is given generally by

$$p|_{z=0} = p_0(t), \qquad (8.1)$$

where $p_0(t)$ is periodic. The uniform waveguide, which serves as a termination, is simply an extension of the periodic waveguide that contains no scatterers. It is assumed that the fundamental and second harmonic Bloch waves that are incident upon the termination waveguide obey the linear Bloch wave reflection laws. From Sec. 4.2, the ratio of the reflected to the incident fundamental Bloch wave amplitude at $z = (N - 1)h$ is given by $R_B(\omega_1) = -(g/f)_1$, and that for the second harmonic is given by $R_B(\omega_2) = -(g/f)_2$. These conditions serve as the termination boundary conditions. While the system under study is a finite periodic waveguide system, much of the solution approach is developed in the context of a semi-infinite periodic waveguide system. It is then argued that the results are applicable to the finite system. This approach simply allows for a more straightforward presentation of the solution method.

We begin with a presentation of the system of nonlinear equations to be solved. The approximate approach to the solution of the system is outlined and the resultant nonlinear wave equation presented. The discrete Green's function is then derived and the particular solution for the second harmonic field is found. The characteristics of the particular solution are investigated and the similarities and differences between this solution and that of a nonlinear dispersive conventional wave problem are discussed. Finally, the full second harmonic solution is found and compared with measurements.

8.1 The Nonlinear System of Equations and the Solution Approach

In this section, the nonlinear, dissipative system of equations is presented and the approach to the determination of the second harmonic field is outlined. We begin with a discussion of the approximate solution approach in which the effects of nonlinearity and dissipation are accounted for to leading order. A straightforward perturbation technique is used to derive a linear, inhomogeneous wave equation that governs the second harmonic field. A

Green's function approach to the solution of this equation is used and, with the introduction of complex field variables, a *discrete* Green's function solution technique is developed. As is pointed out in the introduction to this chapter, while the system of interest is a finite periodic waveguide system, the discrete Green's function solution technique is developed for the case of a semi-infinite periodic waveguide system. In this way the presentation is greatly simplified and the resultant discrete Green's function may be used in the anaylysis of the finite periodic waveguide system.

The system of equations that governs the dynamics of a viscous, heat conducting fluid is composed of three conservation laws and two state relations. The equations of conservation of mass, momentum, and entropy are

$$\frac{\partial \hat{\rho}}{\partial t} + \nabla \cdot (\hat{\rho}\mathbf{u}) = 0, \tag{8.2}$$

$$\hat{\rho}\left(\frac{\partial \mathbf{u}}{\partial t} + \mathbf{u} \cdot \nabla \mathbf{u}\right) = -\nabla \hat{P} + \mu \nabla^2 \mathbf{u} + (\mu/3 + \mu_B)\nabla\nabla \cdot \mathbf{u}, \tag{8.3}$$

and

$$\hat{\rho}\hat{T}\left(\frac{\partial \hat{s}}{\partial t} + \mathbf{u} \cdot \nabla \hat{s}\right) = \nabla \cdot (\kappa \nabla \hat{T}) + \frac{\mu}{2}\left(\frac{\partial u_i}{\partial x_k} + \frac{\partial u_k}{\partial x_i} - \frac{2}{3}\delta_{ik}\frac{\partial u_l}{\partial x_l}\right)^2 + \mu_B(\nabla \cdot \mathbf{u})^2,$$

respectively (e.g., Landau and Lifshitz, 1987). The equilibrium thermodynamic relations

$$\hat{\rho} = \hat{\rho}(\hat{P}, \hat{s})$$

and

$$\hat{T} = \hat{T}(\hat{P}, \hat{s}) \tag{8.4}$$

serve as state relations. The field variables and fluid parameters are defined in Sec. 2.1.

The boundary conditions that the system of nonlinear equations must meet are (1) the waveguide wall or 'transverse' boundary conditions, and (2) the source and termination boundary conditions or 'z' boundary conditions. As the waveguide boundary is rigid and isothermal, the transverse boundary conditions are

$$\mathbf{u}|_S = 0 \qquad\qquad T|_S = 0,$$

the same as those shown for the linear system. The source boundary condition is given by

$$p|_{z=0} = A_1 \cos(\omega_1 t - \phi_1), \tag{8.5}$$

where ω_1 is the fundamental frequency and A_1 is real. As the waveguide is semi-infinite, the termination boundary condition is the radiation condition.

8.1.1 The Approximate Combination of Nonlinear and Dissipative Effects

Clearly, the system of nonlinear dissipative equations with periodic waveguide boundary conditions may not be solved exactly. The combined effect of nonlinearity and dissipation is simply too complicated. Even the *linearized* system with *uniform waveguide* boundary conditions proves to be too complicated to solve exactly; only approximate expressions for the thermoviscous acoustic boundary layer exist. The standard approach to the solution of nonlinear, dissipative guided wave problems is to account for nonlinearity and dissipation separately and later combine their effects in an *ad hoc* manner. We first solve the linear dissipative system to determine the effect of dissipation on the linear field. We then solve, by a perturbation method, the nonlinear, nondissipative system. The linear dissipative effects are then imposed upon the field that is obtained from the nonlinear, nondissipative system. The result is an approximate solution of the full nonlinear, dissipative system. This approach has been formally justified for the case of weakly nonlinear, dissipative propagation in a uniform waveguide (Anderson and Vaidya, 1991), and has produced theoretical results that show excellent agreement with measurements (Hamilton and TenCate, 1987).

A qualitative justification for the method follows. It is found in the solution of the linear system of equations that, over a broad range of frequencies, the free-field, or so-called ω^2 losses are dominated by those associated with the thermoviscous acoustic boundary layer, the $\omega^{1/2}$ losses. The free-field dissipation may therefore be neglected. Over a broad range of frequency in which this approximation is justified, most of the waveguide cross-section is occupied by the effectively nondissipative, so-called acoustic mode alone. Only a very small fraction of the waveguide cross-section is occupied by the entropy and vorticity

modes that make up the very thin thermoviscous acoustic boundary layer. As the nonlinear generation of distortion components occurs throughout the entire volume of the waveguide, and most of the field is effectively nondissipative, the nonlinear generation of distortion components is very nearly identical to that which occurs in a nondissipative system. It is therefore reasonable to assume that nonlinear effects may be effectively accounted for in a nondissipative setting.

As we have already considered the solution of the linear dissipative system, we turn now to the nonlinear nondissipative system. That is, we consider the nonlinear system of equations (Eqs. 8.2-8.4) when $\mu = \mu_B = \kappa = 0$. Even this system proves to be too difficult to solve exactly. To proceed, we limit the analysis to consider only cases in which the magnitude of the acoustic disturbance is very small; i.e., we consider the propagation of weakly nonlinear Bloch waves. As the magnitude of the acoustic disturbance is characterized by the acoustic Mach number $\epsilon = u_0/c_0$, where u_0 is a characteristic acoustic particle velocity, we consider the case in which $\epsilon \ll 1$. Such a restriction is not particularly limiting as it has been found that profoundly nonlinear acoustic phenomena such as shock formation, harmonic and intermodulation distortion, and acoustic streaming may occur even when the Mach number is less than 1% (Beyer, 1974). As all acoustic field variables are of $\mathcal{O}(\epsilon)$, we neglect cubic and higher order terms in the system of equations. That is, we consider the effect of nonlinearity to leading (i.e., quadratic) order only. In such a case, the nonlinear system of equations may be expressed in the form of a single equation, the modified Westervelt equation

$$\nabla^2 p - \frac{1}{c_0^2} \frac{\partial^2 p}{\partial t^2} = \frac{-\beta}{\rho_0 c_0^4} \frac{\partial^2 p^2}{\partial t^2} - \left(\nabla^2 + \frac{1}{c_0^2} \frac{\partial^2}{\partial t^2} \right) \mathcal{L}, \qquad (8.6)$$

where

$$\mathcal{L} = \frac{1}{2} \rho_0 \mathbf{u} \cdot \mathbf{u} - \frac{1}{2} \frac{1}{\rho_0 c_0^2} p^2$$

is the Lagrangian density and β is the coefficient of nonlinearity (Naze Tjotta and Tjotta, 1987). This is a nonlinear, nondissipative wave equation valid to quadratic order in the acoustic Mach number.

A further simplification may be made by the identification of terms associated with local and cumulative nonlinear distortion effects. The second

harmonic distortion components that arise from the Lagrangian density term have been found to be non-propagating or so-called *local* distortion components that are generally not significant when compared to the propagating, so-called *cumulative* components (Naze Tjotta and Tjotta, 1987). While the local second harmonic field that arises from the Lagrangian density term is eventually incorporated into the solution (see Sec. 8.3.4), it is for the time being assumed to be insignificant and the Lagrangian density term is therefore discarded. The nonlinear, nondissipative equation of interest here is therefore

$$\nabla^2 p - \frac{1}{c_0^2}\frac{\partial^2 p}{\partial t^2} = \frac{-\beta}{\rho_0 c_0^4}\frac{\partial^2 p^2}{\partial t^2},\tag{8.7}$$

which is the Westervelt equation (Westervelt, 1963).

We may now proceed to derive, by a straightforward perturbation approach, the equation that governs the generation of the second harmonic distortion component of the acoustic field. As the acoustic pressure is of $\mathcal{O}(\epsilon)$ and we have assumed that $\epsilon \ll 1$, the acoustic Mach number is, as usual, chosen to be the small parameter in the perturbation expansion. The acoustic pressure may be expressed $p = p_1 + p_2 + \mathcal{O}(\epsilon^3)$, where $p_1 = \mathcal{O}(\epsilon)$ and $p_2 = \mathcal{O}(\epsilon^2)$. When this expanded representation of the acoustic pressure is substituted into Eq. 8.7, we find, at the leading two orders in ϵ:

$$\mathcal{O}(\epsilon): \qquad \nabla^2 p_1 - \frac{1}{c_0^2}\frac{\partial^2 p_1}{\partial t^2} = 0 \tag{8.8}$$

$$\mathcal{O}(\epsilon^2): \qquad \nabla^2 p_2 - \frac{1}{c_0^2}\frac{\partial^2 p_2}{\partial t^2} = \frac{-\beta}{\rho_0 c_0^4}\frac{\partial^2 p_1^2}{\partial t^2} \tag{8.9}$$

In the absence of dissipation the transverse boundary condition is $\mathbf{u} \cdot \hat{\mathbf{n}}|_S = 0$, where $\hat{\mathbf{n}}$ is the unit vector normal to the surface S. With the use of the momentum equation (Eq. 8.3) in nondissipative form, the boundary condition may be expressed,[1] at $\mathcal{O}(\epsilon)$ and $\mathcal{O}(\epsilon^2)$,

$$\nabla p_1 \cdot \hat{\mathbf{n}}|_S = 0 \qquad \text{and} \qquad \nabla p_2 \cdot \hat{\mathbf{n}}|_S = 0,$$

---

[1]The $\mathcal{O}(\epsilon^2)$ boundary condition is, strictly speaking, valid only for planar waveguide geometries (Hamilton and TenCate, 1987). For more general geometries, this boundary condition is approximate.

respectively. By definition $A_1 = \mathcal{O}(\epsilon)$, and the substitution of the expanded representation of the acoustic pressure into the source boundary condition (Eq. 8.5) yields, at $\mathcal{O}(\epsilon)$ and $\mathcal{O}(\epsilon^2)$,

$$p_1|_{z=0} = A_1 \cos(\omega_1 t - \phi_1) \quad \text{and} \quad p_2|_{z=0} = 0. \tag{8.10}$$

The equation that governs the second harmonic field, Eq. 8.9, is a linear inhomogeneous partial differential equation, which we solve by means of Green's function.

8.1.2 The Use of Complex Field Variables

We now consider the variables with which the acoustic pressure field is to be represented. In the context of linear waves we are able to exploit the superposability of solutions and use complex field variables. In the context of nonlinear waves, however, solutions do not linearly superpose and we must use only real variables. The development of the particular Green's function approach used here, the discrete Green's function approach, is far simpler if we are able to justify the use of complex field variables. It is shown in this section that, for the case of a time-harmonic fundamental field, complex field variables may indeed be used at second order.

The first order system may be extended to result in complex field solutions in the usual manner. Instead of being concerned with the solution of the wave equation in the real pressure p_1 (Eq. 8.8) subject to the real source boundary condition (Eq. 8.10), we are concerned with the solution of the wave equation in the complex pressure $\hat{p}_1$

$$\nabla^2 \hat{p}_1 - \frac{1}{c_0^2} \frac{\partial^2 \hat{p}_1}{\partial t^2} = 0$$

subject to the augmented source boundary condition[2]

$$\hat{p}_1|_{z=0} = \hat{A}_1 e^{-j\omega_1 t},$$

---

[2]While we are free to augment the real boundary condition with any imaginary part we like, the choice of an imaginary part that is in phase quadrature with the real part is a particularly judicious choice that greatly simplifies the resultant solution.

where $\hat{A}_1 = A_1 e^{j\phi_1}$. The terminiation boundary condition remains the radiation condition. This system, which is the subject of Chaps. 2-4 of this dissertation, has the solution

$$\hat{p}_1 = \hat{A}_1 F^{(+)}(\mathbf{r}, \omega_1) e^{-j\omega_1 t}. \tag{8.11}$$

The real, physical acoustic pressure field is recovered from the complex field simply by taking the real part: $p_1 = \text{Re}\{\hat{p}_1\}$.

The real second order system may likewise, with care, be converted into a complex system. We begin with the substitution of the complex field representation of the real fundamental pressure field

$$p_1 = \frac{1}{2}[\hat{p}_1 + \hat{p}_1^*]$$

into the right-hand side of the real second order equation (Eq. 8.9):

$$\nabla^2 p_2 - \frac{1}{c_0^2}\frac{\partial^2 p_2}{\partial t^2} = \frac{-\beta}{4\rho_0 c_0^4}\frac{\partial^2}{\partial t^2}(\hat{p}_1 + \hat{p}_1^*)^2$$

$$= \frac{\beta}{\rho_0 c_0^4}\omega_1^2[\hat{p}_1^2 + \hat{p}_1^{*2}]$$

$$= \left[\frac{\beta}{\rho_0 c_0^4}\omega_1^2\hat{p}_1^2\right] + \left[\frac{\beta}{\rho_0 c_0^4}\omega_1^2\hat{p}_1^2\right]^*$$

$$= \text{Re}\left\{2\frac{\beta}{\rho_0 c_0^4}\omega_1^2\hat{p}_1^2\right\}.$$

We define the real part of the complex second order pressure to be equal to the physical second order pressure; i.e., $\text{Re}\{\hat{p}_2\} = p_2$. In other words, the real part of $\hat{p}_2$ is defined

$$\text{Re}\left\{\nabla^2\hat{p}_2 - \frac{1}{c_0^2}\frac{\partial^2\hat{p}_2}{\partial t^2}\right\} = \text{Re}\left\{2\frac{\beta}{\rho_0 c_0^4}\omega_1^2\hat{p}_1^2\right\}.$$

If we arbitrarily define the imaginary part of $\hat{p}_2$ such that

$$\text{Im}\left\{\nabla^2\hat{p}_2 - \frac{1}{c_0^2}\frac{\partial^2\hat{p}_2}{\partial t^2}\right\} = \text{Im}\left\{2\frac{\beta}{\rho_0 c_0^4}\omega_1^2\hat{p}_1^2\right\},$$

then the complex second order field pressure is given by

$$\nabla^2 \hat{p}_2 - \frac{1}{c_0^2} \frac{\partial^2 \hat{p}_2}{\partial t^2} = 2 \frac{\beta}{\rho_0 c_0^4} \omega_1^2 \hat{p}_1^2, \tag{8.12}$$

where the field must satisfy the source boundary condition

$$\hat{p}_2 \big|_{z=0} = 0.$$

What we have done is develop an alternative approach to the solution of Eq. 8.9. In the usual approach, the expression for the real fundamental pressure field p_1 is substituted in the right-hand side and the resultant real inhomogeneous equation solved. We have shown here that we may alternatively substitute the expression for the complex fundamental pressure field $\hat{p}_1$ into the right-hand side of Eq. 8.12 and solve that equation. The real part of the resultant complex solution is the same as the real solution of Eq. 8.9.

8.1.3 The Infinite Periodic Waveguide Green's Function

We must now solve an inhomogeneous partial differential equation in a boundary value problem setting. There are two fundamental Green's function solution approaches that may be used. In the first, the boundary conditions are incorporated in the Green's function. That is, the Green's function itself satisfies the boundary conditions. The Green's function is then convolved with the source distribution function (the inhomogeneous term) and the resultant field is the solution of the problem. The field satisfies both the differential equation and the boundary conditions, and no homogeneous solutions need be added. In a sense, the necessary homogeneous solutions have already been incorporated in the Green's function. In the second approach, the free-space Green's function, which does not generally satisfy the boundary conditions, is used. When this Green's function is convolved with the source distribution, the resultant field, while being a solution to the partial differential equation, does not meet the boundary conditions. In this case, homogeneous solutions of the equation must be added to the field in order to meet the boundary conditions.

The approach used here is a combination of these two approaches. The Green's function meets the transverse or periodic waveguide boundary

conditions, but does *not* meet the z or source/termination boundary conditions. In other words, the Green's function is an infinite periodic waveguide Green's function. When convolved with the source distribution, the resultant field meets the transverse boundary conditions, but does not meet the z boundary conditions. In order to satisfy these, we must add solutions of the homogeneous equation that meet the transverse boundary conditions. The homogeneous equation is the classical wave equation, and it has been shown that the solutions of the classical wave equation that meet the transverse boundary conditions are the nondissipative Bloch wave solutions. In other words, we must simply add homogeneous Bloch wave solutions to the field in order to meet the source and termination boundary conditions.

8.1.4   The Discrete Green's Function

We now consider the infinite periodic waveguide Green's function solution for the second harmonic field. It is shown that the particular solution may be expressed in a form that is much simpler than the usual Green's function solution owing to the functional form of the fundamental field, which is a progressive Bloch wave field. As the fundamental field is, up to a constant factor, identical in every cell of the periodic waveguide, the inhomogeneous term in the second order equation, and consequently the resultant generation of a second harmonic field is, up to a constant factor, identical in every cell of the waveguide. In other words, the cell-to-cell similarity in structure of the fundamental field results in a cell-to-cell similarity in the generation of second harmonic waves. This pattern in the generation of the second harmonic field may be exploited to result in a simpler Green's function type of representation of the second harmonic field. This representation, which is referred to here as the *discrete* Green's function representation of the solution, is derived in this section.

The equation for the second order pressure (Eq. 8.12) is a linear inhomogeneous partial differential equation. The first order pressure field appears in the inhomogeneous term, which acts as a source distribution that drives the second order pressure field. We may think of the inhomogeneous term in Eq. 8.12 as being representative of a volume distribution of acoustic sources.

In this spirit, we rewrite Eq. 8.12 as

$$\nabla^2 \hat{p}_2 - \frac{1}{c_0^2}\frac{\partial^2 \hat{p}_2}{\partial t^2} = \Delta(\mathbf{r}, t),$$

where

$$\Delta(\mathbf{r}, t) = 2\frac{\beta}{\rho_0 c_0^4}\omega_1^2 \hat{p}_1^2 \tag{8.13}$$

is the (complex) distribution of virtual sources. We next substitute the complex first order solution (Eq. 8.11) into the expression for the virtual source distribution (Eq. 8.13), and find

$$\Delta(\mathbf{r}, t) = 2\frac{\beta}{\rho_0 c_0^4}\omega_1^2 A_1^2 \sum_{n=0}^{\infty} e^{2jnq_1 h}\psi_1^2(\mathbf{r} - nh\hat{\mathbf{e}}_z)e^{-2j\omega_1 t}.$$

Note that the virtual source distribution is expressed as a sum over functions that are proportional to $\psi_1^2(\mathbf{r} - nh\hat{\mathbf{e}}_z)$, the squared fundamental cell wave function, which is nonzero only in the nth cell. The virtual source distribution may therefore be expressed

$$\Delta(\mathbf{r}, t) = \sum_{n=0}^{\infty} \Delta_n(\mathbf{r})e^{-2j\omega_1 t},$$

where

$$\Delta_n(\mathbf{r}) = 2\frac{\beta}{\rho_0 c_0^4}\omega_1^2 A_1^2 \psi_1^2(\mathbf{r} - nh\hat{\mathbf{e}}_z)e^{2jnq_1 h} \tag{8.14}$$

is the portion of the complex virtual source distribution that occupies the nth cell of the waveguide. This partial virtual source distribution is referred to as the nth cell source. With these definitions, the inhomogeneous partial differential equation to be solved (Eq. 8.12) may be written

$$\nabla^2 \hat{p}_2 - \frac{1}{c_0^2}\frac{\partial^2 \hat{p}_2}{\partial t^2} = \sum_{n=0}^{\infty} \Delta_n(\mathbf{r})e^{-2j\omega_1 t}. \tag{8.15}$$

In this form it is seen that the complex second order pressure $\hat{p}_2$ is driven by a string of disjoint virtual source distributions, each of which occupies a single cell. As the fundamental Bloch wave function in a cell bears a strong resemblance to that in any other cell, the virtual source distribution in one cell must likewise bear a strong similarity to that in any other cell. It stands to reason

that the second order pressure field that arises from the virtual source distribution in a particular cell likewise resembles that which arises from another cell. Such an argument is best expressed in terms of a Green's function solution.

The Green's function solution to Eq. 8.15 is, owing to the time-harmonicity of the inhomogeneous term, given by

$$\hat{p}_2 = \int \sum_{n=0}^{\infty} \Delta_n(\mathbf{r}') G(\mathbf{r}|\mathbf{r}') d^3 r' e^{-2j\omega_1 t}$$

$$= \sum_{n=0}^{\infty} \int \Delta_n(\mathbf{r}') G(\mathbf{r}|\mathbf{r}') d^3 r' e^{-2j\omega_1 t}, \tag{8.16}$$

where $G(\mathbf{r}|\mathbf{r}')$ is the Green's function associated with the Helmholtz equation for the infinite periodic waveguide. Note that, as this is the *infinite* periodic waveguide Green's function solution, it is the particular solution only. We must add homogeneous second harmonic Bloch wave solutions to this particular solution in order to satisfy the source and termination boundary conditions. The substitution of Eq. 8.14 into Eq. 8.16 yields

$$\hat{p}_2 = 2\frac{\beta}{\rho_0 c_0^4} \omega_1^2 A_1^2 e^{-2j\omega_1 t} \sum_{n=0}^{\infty} e^{2jnq_1 h} \int \psi_1^2(\mathbf{r}' - nh\hat{\mathbf{e}}_z) G(\mathbf{r}|\mathbf{r}') d^3 r', \tag{8.17}$$

the Green's function solution for the complex second order pressure field. Under the shifting transformation $\mathbf{r}'' = \mathbf{r}' - nh\hat{\mathbf{e}}_z$, Eq. 8.17 becomes

$$\hat{p}_2 = 2\frac{\beta}{\rho_0 c_0^4} \omega_1^2 A_1^2 e^{-2j\omega_1 t} \sum_{n=0}^{\infty} e^{2jnq_1 h} \int \psi_1^2(\mathbf{r}'') G(\mathbf{r}|\mathbf{r}'' + nh\hat{\mathbf{e}}_z) d^3 r''. \tag{8.18}$$

Because the Green's function is the infinite periodic waveguide Green's function and the periodic waveguide is, by definition, invariant under axial translations by nh, the following translation property exists:

$$G(\mathbf{r}|\mathbf{r}' + nh\hat{\mathbf{e}}_z) = G(\mathbf{r} - nh\hat{\mathbf{e}}_z|\mathbf{r}').$$

The field at $\mathbf{r}$ due to a source at $\mathbf{r}' + nh\hat{\mathbf{e}}_z$ must be the same as the field at $\mathbf{r} - nh\hat{\mathbf{e}}_z$ due to an identical source at $\mathbf{r}'$. Equation 8.18 may therefore be expressed

$$\hat{p}_2 = 2\frac{\beta}{\rho_0 c_0^4} \omega_1^2 A_1^2 e^{-2j\omega_1 t} \sum_{n=0}^{\infty} e^{2jnq_1 h} \int \psi_1^2(\mathbf{r}'') G(\mathbf{r} - nh\hat{\mathbf{e}}_z|\mathbf{r}'') d^3 r''. \tag{8.19}$$

We see that the total second harmonic pressure field is composed of a sum over a series of contributing pressure fields, each of which arises from the virtual source distribution in a particular cell. The second harmonic field that arises from the virtual source distribution in the nth cell (i.e., the nth cell source) may be written

$$\hat{p}_2^{(n)} = \left[A_1^2 e^{2jnq_1 h} e^{-2j\omega_1 t} \right] \cdot 2 \frac{\beta}{\rho_0 c_0^4} \omega_1^2 \int \psi_1^2(\mathbf{r}'') G(\mathbf{r} - nh\hat{\mathbf{e}}_z | \mathbf{r}'') d^3 r''.$$

The term in square brackets is recognized to be the square of the complex first order pressure field at the center of the cell; i.e., $[\hat{p}_1(nh, t)]^2 = A_1^2 e^{2jnq_1 h} e^{-j2\omega_1 t}$. The second order pressure field that arises from the nth cell source may therefore be expressed

$$\hat{p}_2^{(n)} = [\hat{p}_1(nh, t)]^2 2 \frac{\beta}{\rho_0 c_0^4} \omega_1^2 \int \psi_1^2(\mathbf{r}'') G(\mathbf{r} - nh\hat{\mathbf{e}}_z | \mathbf{r}'') d^3 r''. \qquad (8.20)$$

The $[\hat{p}_1(nh, t)]^2$ term is a measure of the amplitude and phase of the excitation of the nth cell source. The remainder of the expression represents the second harmonic field due to a cell source of unit excitation. Note that the second harmonic field of Eq. 8.20 is, aside from its magnitude, phase, and placement, *identical for each cell source.* This makes sense. The nth cell source is excited at a level that is proportional to the squared value of the fundamental pressure at the cell center. As the fundamental Bloch wave field is, apart from factors of $e^{jq_1 h}$, identical in each cell of the waveguide, each cell source is, up to factors of $e^{2jq_1 h}$, identical in each cell of the waveguide. The second harmonic field that arises from each cell source is therefore, apart from factors of $e^{2jq_1 h}$ and placement, identical.

It is Eq. 8.20 that suggests the concept of a discrete Green's function type of approach. In the standard Green's function approach, the Green's function is the field that arises from a simple source of unit amplitude and arbitrary placement. The field that arises from a more complicated source configuration may be expressed as a sum over the fields that arise from each of a distribution of simple sources. In our case, the simplest source unit may be taken to be the zeroth cell source. All other cell sources are identical, up to a constant factor, to the zeroth cell source. The second order pressure field that arises from the zeroth cell source is therefore something like a Green's function

associated with this simplest unit source. The total second order pressure field may be expressed as a discrete sum over appropriately shaded, phased, and placed copies of this simplest unit field. The discrete Green's function is therefore defined as

$$G_D(\mathbf{r}) = 2\frac{\beta}{\rho_0 c_0^4}\omega_1^2 \int \psi_1^2(\mathbf{r}')G(\mathbf{r}|\mathbf{r}')d^3r'. \tag{8.21}$$

From Eqs. 8.20 and 8.21, the partial pressure field due to the nth cell source may therefore be written

$$\hat{p}_2^{(n)} = [\hat{p}_1(nh,t)]^2 G_D(\mathbf{r} - nh\hat{\mathbf{e}}_z)$$

$$= \hat{A}_1^2 G_D(\mathbf{r} - nh\hat{\mathbf{e}}_z)e^{j2q_1nh}e^{-j2\omega_1 t}.$$

Aside from amplitude and phase, each cell source radiates the same second harmonic field. The fundamental and second harmonic components of the Bloch wave field are therefore given by

$$\hat{p}_1 = A_1\psi_1(r) * \sum_{n=0}^{\infty} \delta(\mathbf{r} - nh\hat{\mathbf{e}}_z)e^{jnq_1h}e^{-j\omega_1 t}$$

$$\hat{p}_2 = A_1^2 G_D(\mathbf{r}) * \sum_{n=0}^{\infty} \delta(\mathbf{r} - nh\hat{\mathbf{e}}_z)e^{jn2q_1h}e^{-j2\omega_1 t}, \tag{8.22}$$

where again, the second harmonic solution is the particular solution only.

The problem has been reduced to that of finding an expression for $G_D(\mathbf{r})$. The second harmonic field that arises from the portion of the virtual source distribution that occupies the zeroth cell is given by

$$\nabla^2\hat{p}_2^{(0)} - \frac{1}{c_0^2}\frac{\partial^2\hat{p}_2^{(0)}}{\partial t^2} = \Delta_0(\mathbf{r})e^{-2j\omega_1 t}$$

$$= 2\frac{\beta}{\rho_0 c_0^4}\omega_1^2 A_1^2\psi_1^2(\mathbf{r})e^{-2j\omega_1 t}. \tag{8.23}$$

As $\hat{p}_2^{(0)}(\mathbf{r},t)$ and $G_D(\mathbf{r})$ are simply related by

$$\hat{p}_2^{(0)}(\mathbf{r},t) = A_1^2 G_D(\mathbf{r})e^{-j\omega_2 t}, \tag{8.24}$$

the discrete Green's function is given by

$$\nabla^2 G_D(\mathbf{r}) + \frac{\omega_2^2}{c_0^2}G_D(\mathbf{r}) = 2\frac{\beta}{\rho_0 c_0^4}\omega_1^2\psi_1^2(\mathbf{r}). \tag{8.25}$$

8.2 The Evaluation of the Discrete Green's Function

Here we derive an expression for the discrete Green's function. The discrete Green's function is defined by Eq. 8.25, which is an inhomogeneous Helmholtz equation, with infinite periodic waveguide boundary conditions. An alternative method of solution of Eq. 8.25 is to solve Eq. 8.23 for the second harmonic field $\hat{p}_2^{(0)}$ that arises from the zeroth cell source, and relate the result to the discrete Green's function by way of Eq. 8.24. As the two methods are equivalent, we choose the latter method as we are then faced with the solution of an actual physical problem. The intermediate results are more readily interpreted, and the derivation therefore more easily followed.

The zeroth cell source problem is itself treated in two parts. The virtual source distribution in the zeroth cell is considered to be the sum of two spatially disjoint sub-distributions:

$$\Delta_0(\mathbf{r}) = \Delta_0^{(\text{wg})}(\mathbf{r}) + \Delta_0^{(\text{s})}(\mathbf{r}).$$

One sub-distribution is the portion of the zeroth cell source that occupies the the waveguide section, and is given by

$$\Delta_0^{(\text{wg})}(\mathbf{r}) = \begin{cases} \Delta_0(\mathbf{r}) & |z| < l_\text{w}/2 \\ 0 & \text{elsewhere} \end{cases},$$

and the other is that which occupies the scatterers at the ends of the zeroth cell, and is given by

$$\Delta_0^{(\text{s})}(\mathbf{r}) = \begin{cases} \Delta_0(\mathbf{r}) & -h/2 < z < -l_\text{w}/2 \text{ and } l_\text{w} < z < h/2 \\ 0 & \text{elsewhere.} \end{cases}$$

As the problem to be solved is linear, the second harmonic fields that arise from each of these sub-distributions may be found separately and the results added.

8.2.1 Second Harmonic Generation in the Waveguide Sections

Here we find an expression for the second harmonic field that is generated by the portion of the virtual source distribution that occupies the wave-

guide section of the zeroth cell of the waveguide. In other words, we wish to find the second harmonic field that arises from the nonlinear propagation of the first order f and g-waves in the zeroth waveguide section. This field is given by the equation

$$\nabla^2 \hat{p}_2 - \frac{1}{c_0^2}\frac{\partial^2 \hat{p}_2}{\partial t^2} = \Delta_0^{(wg)}(\mathbf{r})e^{-2j\omega_1 t}, \tag{8.26}$$

where

$$\Delta_0^{(wg)}(\mathbf{r}) = \begin{cases} 2(\beta/\rho_0 c_0^4)\omega_1^2 A_1^2 \psi_1^2(\mathbf{r}) & |z| < l_w/2 \\ 0 & \text{elsewhere.} \end{cases}$$

The approach is to treat the zeroth waveguide section as a uniform waveguide of length l_w that is bounded on both ends by semi-infinite periodic waveguides. The second harmonic waves that are generated in this finite section of uniform waveguide are incident upon, and partially reflected from, the bounding periodic waveguides. The incident waves are also partially transmitted *into* the periodic waveguides as freely propagating second harmonic Bloch waves.

Recall that the fundamental cell wave function $\psi_1(\mathbf{r})$ is, in the waveguide section, composed of the propagating f-wave/g-wave field and a series of evanescent, higher order modal fields that are confined to the near-vicinity of the scatterers. It is assumed that the evanescent, higher order modal field makes a negligible contribution to the generation of the second harmonic field, and is therefore neglected. The portion of the fundamental cell wave function that resides in the waveguide section may therefore be expressed

$$\psi_1(\mathbf{r}) = \frac{1}{1+g/f_1}e^{jk_1 z} + \frac{g/f_1}{1+g/f_1}e^{-jk_1 z} \quad |z| < l_w/2 \quad . \tag{8.27}$$

The right-hand side of Eq. 8.26 is therefore given by

$$\Delta_0^{(wg)}(\mathbf{r})e^{-2j\omega_1 t} = 2\frac{\beta}{\rho_0 c_0^4}\omega_1^2 A_1^2 \left\{ \left(\frac{1}{1+g/f_1}\right)^2 e^{j(2k_1 z - 2\omega_1 t)} \right.$$

$$\left. + \left(\frac{g/f_1}{1+g/f_1}\right)^2 e^{j(-2k_1 z - 2\omega_1 t)} + 2\frac{g/f_1}{(1+g/f_1)^2}e^{-2j\omega_1 t} \right\} \tag{8.28}$$

for $|z| < l_w/2$ and is zero for $|z| > l_w/2$. It therefore follows that in the waveguide section the second harmonic field is given by the sum of a particular and a homogeneous solution, and in the region outside of the waveguide section

the solution is given by homogeneous solutions only. The particular solution of this equation is given, for $|z| < l_{\rm w}/2$, by the expression

$$\hat{p}_2 = -j\frac{\beta}{2\rho_0 c_0^3}\omega_1 A_1^2\left(\frac{1}{1+g/f_1}\right)^2 ze^{j(2k_1 z - 2\omega_1 t)} \tag{8.29}$$

$$+j\frac{\beta}{2\rho_0 c_0^3}\omega_1 A_1^2\left(\frac{g/f_1}{1+g/f_1}\right)^2 ze^{j(-2k_1 z - 2\omega_1 t)} + \frac{\beta}{\rho_0 c_0^2}A_1^2\frac{g/f_1}{(1+g/f_1)^2}e^{-2j\omega_1 t}.$$

The first two terms in the particular solution are the linearly growing forward and backward traveling second harmonic waves, respectively, and the third is a local (i.e., nonpropagating), spatially uniform second harmonic component, which is, for the time being, neglected. It is worth noting, as a simple check, that the real part of this particular solution is the particular solution of Eq. 8.9 with the right-hand side given by the real part of Eq. 8.28, as it should.

The forward and backward traveling second harmonic waves that are generated in the zeroth waveguide section are incident upon the two semi-infinite periodic waveguides that bound it. The boundary conditions that must be met by the field at the entrances to these periodic waveguides are taken to be the usual interface conditions: the acoustic pressure and volume velocity associated with the second harmonic field must be continuous across the interface. These requirements are usually expressed in the form of a reflection coefficient. In Sec. 4.2 the reflection coefficient for a conventional wave incident upon a semi-infinite periodic waveguide is shown to be $R = g/f$, where R is defined to be the ratio of the reflected to the incident wave amplitude at $z = 0$. The reflection coefficient at the points $z = \pm l_{\rm w}/2$ is, for the second harmonic field, therefore $R = g/f_2 e^{-jkl_{\rm w}}$.

With the inclusion of homogeneous wave terms, the second harmonic pressure field in the zeroth waveguide section is given by

$$\hat{p}_2^{({\rm FT})} = -j\frac{\beta}{2\rho_0 c_0^3}\omega_1 A_1^2\left(\frac{1}{1+g/f_1}\right)^2 ze^{j(2k_1 z - 2\omega_1 t)} + h^{(+)}e^{j(k_2 z - \omega_2 t)}$$

$$\hat{p}_2^{({\rm BT})} = j\frac{\beta}{2\rho_0 c_0^3}\omega_1 A_1^2\left(\frac{g/f_1}{1+g/f_1}\right)^2 ze^{j(-2k_1 z - 2\omega_1 t)} + h^{(-)}e^{j(-k_2 z - \omega_2 t)},$$

where the superscripts (FT) and (BT) denote the forward and backward traveling components, respectively. The boundary conditions for this field, which may be written

$$\left.\frac{\hat{p}_2^{(BT)}}{\hat{p}_2^{(FT)}}\right|_{z=l_w/2} = g/f_2 e^{-jk_2 l_w}$$

$$\left.\frac{\hat{p}_2^{(FT)}}{\hat{p}_2^{(BT)}}\right|_{z=-l_w/2} = g/f_2 e^{-jk_2 l_w},$$

serve to define the homogeneous wave amplitudes, which are found to be

$$h^{(+)} = -\frac{j}{2}\frac{\beta}{\rho_0 c_0^3}\omega_1 A_1^2 \frac{l_w}{2}\frac{1+(g/f_2)^2+2g/f_2(g/f_1)^2}{[1+g/f_1]^2[1-(g/f_2)^2]}$$

$$h^{(-)} = -\frac{j}{2}\frac{\beta}{\rho_0 c_0^3}\omega_1 A_1^2 \frac{l_w}{2}\frac{2g/f_2+(g/f_1)^2+(g/f_1)^2(g/f_2)^2}{[1+g/f_1]^2[1-(g/f_2)^2]}.$$

The total second harmonic field in the zeroth waveguide section is therefore given by

$$\hat{p}_2 = A_1^2 Q^{(WC)}(z,\omega_2)e^{-j\omega_2 t} \qquad |z| < l_w/2,$$

where

$$Q^{(WC)}(z,\omega_2) = -\frac{j}{2}\frac{\beta}{\rho_0 c_0^3}\omega_1$$

$$\left(\frac{l_w}{2}\frac{[1+(g/f_2)^2+2g/f_2(g/f_1)^2]e^{jk_2 z}+[2g/f_2+(g/f_1)^2+(g/f_1 g/f_2)^2]e^{-jk_2 z}}{[1+g/f_1]^2[1-(g/f_2)^2]}\right.$$

$$\left.+\frac{ze^{j2k_1 z}-(g/f_1)^2 ze^{-j2k_1 z}}{[1+g/f_1]^2}\right).$$

The function $Q^{(WC)}(z,\omega_2)$ is that which represents the second harmonic field in the waveguide section due to the portion of the cell source that occupies the waveguide section.

The amplitudes of the second harmonic Bloch waves that are transmitted into the semi-infinite waveguides on either side of the zeroth waveguide section may be found using the Bloch wave transmission coefficient found in Sec. 4.2: $T_B = 1 + g/f$. Again correcting for the phase, the amplitudes of the Bloch waves launched into the periodic waveguides that occupy $z > l_w/2$ and $z < -l_w/2$ are simply $T_B \hat{p}_2^{(FT)}(l_w/2)e^{-jk_2 l_w/2}$ and $T_B \hat{p}_2^{(BT)}(-l_w/2)e^{-jk_2 l_w/2}$,

respectively. The second harmonic pressure solution outside of the zeroth wave-guide section is therefore given by

$$\hat{p}_2 = A_1^2 Q^{(W+)} F^{(+)}(z, \omega_2) e^{-j\omega_2 t} \qquad z > l_w/2$$

$$= A_1^2 Q^{(W-)} F^{(-)}(z, \omega_2) e^{-j\omega_2 t} \qquad z < -l_w/2,$$

where $Q^{(W+)}$ and $Q^{(W-)}$, defined by

$$Q^{(W+)} = -\frac{j}{2}\frac{\beta}{\rho_0 c_0^3}\omega_1 l_w \left(\frac{[1 + g/f_2][1 + g/f_2(g/f_1)^2]}{[1 + g/f_1]^2[1 - (g/f_2)^2]} \right)$$

$$Q^{(W-)} = -\frac{j}{2}\frac{\beta}{\rho_0 c_0^3}\omega_1 l_w \left(\frac{[1 + g/f_2][g/f_2 + (g/f_1)^2]}{[1 + g/f_1]^2[1 - (g/f_2)^2]} \right),$$

are the coefficients that represent the amplitudes of the forward and backward traveling second harmonic Bloch waves that are generated in the waveguide section.

8.2.2 Nonlinear Scattering

We now consider the second harmonic field that is generated by the portion of the zeroth cell source that resides in the scatterers on either side of the zeroth cell waveguide section. This field is given by the equation

$$\nabla^2 \hat{p}_2 - \frac{1}{c_0^2}\frac{\partial^2 \hat{p}_2}{\partial t^2} = \Delta_0^{(s)}(\mathbf{r}) e^{-2j\omega_1 t}, \qquad (8.30)$$

where

$$\Delta_0^{(s)}(\mathbf{r}) = \begin{cases} 2(\beta/\rho_0 c_0^4)\omega_1^2 A_1^2 \psi_1^2(\mathbf{r}) & -h/2 < z < -l_w/2 \text{ and } l_w < z < h/2 \\ 0 & \text{elsewhere.} \end{cases}$$

In other words, we consider the contribution to the second harmonic field that is due to nonlinear scattering. As the periodic waveguide being treated is general (i.e., the specific form of the scatterers is unspecified), we give here only a very general result in which it is assumed that the nonlinear scattering problem has been solved. As an example of the solution of such a problem, the nonlinear scattering that occurs in a waveguide loaded with a periodic array of rigidly

terminated side branches (such as the isotropic periodic waveguide described in the introduction) is calculated in Sec. 8.2.3.

It was shown in Sec. 8.1.4 that we may solve the full waveguide problem simply by finding the second harmonic generation by the virtual source distribution in the zeroth cell of the periodic waveguide. The zeroth cell is defined to be the volume given by $-h/2 < z < h/2$. This volume includes the zeroth waveguide section, which was the topic of the last section, and half of a scatterer on either side of the waveguide section. Our task in this section is therefore to find an expression for the second harmonic field generated by the portion of the virtual source distribution that resides in these half scatterers. Consider the scatterer on the $z > 0$ side of the zeroth waveguide section. According to the theory, the left half of this scatterer is associated with the zeroth cell, and the right half is associated with the first cell. While such a division leads to a very tidy theoretical form, the determination of the second harmonic generated by the virtual source distribution in half of a scatterer is prohibitively difficult. Instead, we simply divide the magnitude of the virtual source distribution in the entire scatterer by two to result in two *half-strength* virtual source distributions. One of the half-strength distributions is associated with the zeroth cell and the other with the first cell. Similarly, the virtual source distribution in the scatterer on the $z < 0$ side of the zeroth waveguide section is taken to be composed of two half-strength distributions, one of which is associated with the zeroth cell and the other with the minus first cell. The problem to be solved is therefore the inhomogeneous wave equation (Eq. 8.30) with a virtual source distribution given by

$$\Delta_0^{(s)}(\mathbf{r}) = \begin{cases} (\beta/\rho_0 c_0^4)\omega_1^2 A_1^2 \psi_1^2(\mathbf{r}) & -h + l_w/2 < z < -l_w/2, \ l_w < z < h - l_w/2 \\ 0 & \text{elsewhere.} \end{cases}$$

Like the original scheme, this division of the virtual source distribution accounts consistently for the total distribution.

As the fundamental field is a forward traveling Bloch wave of amplitude A_1, the excitation of the virtual source distributions in the scatterers at $z = \pm h/2$ is proportional to A_1^2. The resultant second harmonic field must likewise be proportional to A_1^2. While the second harmonic field in the scatterer is dependent upon the geometry of the scatterer and cannot be determined

generally, the field in the periodic waveguide on either side of the scatterer must take the form of forward and backward traveling second haromonic Bloch waves. The second harmonic field generated in the scatterer on the right (that at $z = h/2$) couples to a forward traveling second harmonic Bloch wave for $z > h - l_w/2$ and to a backward traveling second harmonic Bloch wave for $z < l_w/2$. The amplitudes of these Bloch waves are taken to be $Q^{(R+)}A_1^2$ and $Q^{(R-)}A_1^2$, respectively. Likewise, the scatter on the left (at $z = -h/2$) couples to a forward traveling second harmonic Bloch wave for $z > -l_w/2$ and to a backward traveling second harmonic Bloch wave for $z < -(h - l_w/2)$. The amplitudes of these Bloch waves are taken to be $Q^{(L+)}A_1^2$ and $Q^{(L-)}A_1^2$, respectively. Recall that it is only half of these fields that is associated with the zeroth cell. The second harmonic field associated with the zeroth cell may therefore be expressed as follows. The field in the zeroth cell waveguide section $(-l_w/2 < z < l_w/2)$ is given by

$$\hat{p}_2 = \frac{1}{2}Q^{(L+)}A_1^2F^{(+)}(z,\omega_2)e^{-j\omega_2 t} + \frac{1}{2}Q^{(R-)}A_1^2F^{(-)}(z,\omega_2)e^{-j\omega_2 t},$$

and that outside the zeroth cell is given by

$$\hat{p}_2 = \frac{1}{2}\left(Q^{(L+)} + Q^{(R+)}\right)A_1^2F^{(+)}(z,\omega_2)e^{-j\omega_2 t} \qquad z > h - l_w/2 \qquad (8.31)$$

$$\hat{p}_2 = \frac{1}{2}\left(Q^{(L-)} + Q^{(R-)}\right)A_1^2F^{(-)}(z,\omega_2)e^{-j\omega_2 t} \qquad z < l_w/2 - h. \qquad (8.32)$$

Note that the second harmonic field in the left and right scatterers is not specified as it is not determined.

8.2.3 Nonlinear Scattering by Side Branches

As an example of the determination of the second harmonic generation by nonlinear scattering we consider the case of the isotropic periodic waveguide described in the introduction. The nonlinear scattering may readily be calculated for such a case as nonlinearity in the scatterer is simply due to the nonlinear propagation of the waves in the side branch. For a forward traveling Bloch wave of amplitude A_1, the fundamental waves incident upon the side branch on the right are the f-wave in the zeroth cell and the g-wave of the first cell. Likewise, the waves incident upon the side branch on the left

are the g-wave of the zeroth cell and the f-wave of the minus first cell. As the side branch is of depth d and is rigidly terminated, the fundamental pressure field in the side branch is of the form

$$\hat{p}_1 = a_1(e^{jk_1y'} + e^{2jk_1d}e^{-jk_1y'})e^{-j\omega_1t}, \tag{8.33}$$

where $y' = -y$ is the coordinate along the side branch axis and a_1 is the amplitude of the fundamental traveling waves in the side branch. The requirements that the pressure field be continuous and that mass be conserved at at the side branch entrance results in expressions for the two side branch fields. The fundamental field in the left side branch is such that

$$a_1 = A_1 S_{\text{sb}} \left[\frac{e^{-jq_1h} + g/f_1}{1 + g/f_1} e^{jk_1h/2} \right], \tag{8.34}$$

and that in the right side branch is such that

$$a_1 = A_1 S_{\text{sb}} \left[\frac{1 + g/f_1 e^{jq_1h}}{1 + g/f_1} e^{jk_1h/2} \right], \tag{8.35}$$

where

$$S_{\text{sb}} = \frac{1}{(1 + A_{\text{sb}}/2A_{\text{wg}}) + (1 - A_{\text{sb}}/2A_{\text{wg}})e^{2jk_1d}}$$

is the coefficient of scattering into the side branch.

Before we proceed to find the second harmonic field generated in the two side branches, we must consider the boundary condition that the second harmonic side branch field must meet at the side branch entrance. It is again assumed that the second harmonic field obeys the same reflection and transmission laws that a linear field of the same frequency would obey. Consider a wave of amplitude a_2 and frequency ω_2 that propagates in the right side branch and is incident upon the periodic waveguide. The field in the side branch is given by

$$\hat{p}_2 = a_2(e^{-jk_2y'} + R_{\text{sb}}e^{jk_2y'}), \tag{8.36}$$

where R_{sb} is the coefficient of reflection of the wave back into the side branch, and the field in the periodic waveguide is given by

$$\hat{p}_2 = \begin{cases} a_2 T_{\text{sb}} F^{(+)}(z - h, \omega_2)e^{-j\omega_2t} & z > h/2 \\ a_2 T_{\text{sb}} F^{(-)}(z, \omega_2)e^{-j\omega_2t} & z < h/2, \end{cases} \tag{8.37}$$

where T_{sb} is the coefficient of transmission of the wave into the periodic wave-guide, where it excites outgoing Bloch waves of amplitude $T_{\text{sb}}a_2$. We again impose the requirements of pressure continuity and mass conversation at the side branch entrance and find

$$T_{\text{sb}} = \frac{2(1 + g/f_2)}{(1 + 2A_{\text{wg}}/A_{\text{sb}})e^{-jk_2h/2} + g/f_2(1 - 2A_{\text{wg}}/A_{\text{sb}})e^{jk_2h/2}} \tag{8.38}$$

$$R_{\text{sb}} = \frac{(1 - 2A_{\text{wg}}/A_{\text{sb}})e^{-jk_2h/2} + g/f_2(1 + 2A_{\text{wg}}/A_{\text{sb}})e^{jk_2h/2}}{(1 + 2A_{\text{wg}}/A_{\text{sb}})e^{-jk_2h/2} + g/f_2(1 - 2A_{\text{wg}}/A_{\text{sb}})e^{jk_2h/2}}.$$

We may now find the second harmonic field that is generated by the portions of the virtual source distribution that occupy the left and right side branches. The particular solution of Eq. 8.12 for the generic side branch field of Eq. 8.33 is given by

$$\hat{p}_2 = -\frac{j}{2}\frac{\beta}{\rho_0 c_0^3}\omega_1 a_1^2 \left[y'e^{j2k_1y'} - y'e^{-j2k_1(y'-2d)} \right] e^{-j\omega_2 t} + \frac{\beta}{\rho_0 c_0^2}a_1^2 e^{-j\omega_2 t}.$$

With the inclusion of the homogeneous solutions and the exclusion of the local term, the general second harmonic solution is given by

$$\hat{p}_2^{(\text{DT})} = \left[h^{(+)}e^{jk_2y'} - \frac{j}{2}\frac{\beta}{\rho_0 c_0^3}\omega_1 a_1^2 y'e^{j2k_1y'} \right] e^{-j\omega_2 t}$$

$$\hat{p}_2^{(\text{UT})} = \left[h^{(-)}e^{-jk_2y'} + \frac{j}{2}\frac{\beta}{\rho_0 c_0^3}\omega_1 a_1^2 y'e^{-j2k_1(y'-2d)} \right] e^{-j\omega_2 t},$$

where the superscripts UT and DT denote the upward and downward traveling components of the solution. The boundary conditions that this field must meet are given by

$$\left. \frac{\hat{p}_2^{(\text{UT})}}{\hat{p}_2^{(\text{DT})}} \right|_{y'=d} = 1$$

and

$$\left. \frac{\hat{p}_2^{(\text{DT})}}{\hat{p}_2^{(\text{UT})}} \right|_{y'=0} = R_{\text{sb}},$$

and the resultant solution is given by

$$\hat{p}_2^{(\text{DT})} = -\frac{j}{2}\frac{\beta}{\rho_0 c_0^3}\omega_1 a_1^2 \left[y'e^{2jk_1y'} + R_{\text{sb}}\frac{2de^{2jk_1d}}{e^{-jk_2d} - R_{\text{sb}}e^{jk_2d}}e^{jk_2y'} \right] e^{-j\omega_2 t}$$

$$\hat{p}_2^{(UT)} = -\frac{j}{2}\frac{\beta}{\rho_0 c_0^3}\omega_1 a_1^2 \left[-y' e^{-2jk_1(y'-2d)} + \frac{2de^{2jk_1d}}{e^{-jk_2d} - R_{\rm sb}e^{jk_2d}}e^{-jk_2y'} \right] e^{-j\omega_2 t}.$$

The amplitude of the second harmonic field that is incident upon the periodic waveguide from the side branch is therefore given by

$$\hat{p}_2^{(UT)}\Big|_{y'=0} = -j\frac{\beta}{\rho_0 c_0^3}\omega_1 a_1^2 d\frac{e^{2jk_1d}}{e^{-jk_2d} - R_{\rm sb}e^{jk_2d}}e^{-j\omega_2 t}. \tag{8.39}$$

The value of a_1, the amplitude of the fundamental frequency traveling waves in a side branch, is given by Eqs. 8.34 and 8.35 for the left and right side branches, respectively. From Eq. 8.39, therefore, the amplitudes of the resultant second harmonic waves that are incident on the periodic waveguide from the left and right side branches are also known. As the coefficient of conversion of these second harmonic conventional waves into Bloch waves is given by Eq. 8.38, the second harmonic field everywhere in the periodic waveguide is known. The quasilinear Bloch wave generation coefficients (see Eqs. 8.31 and 8.32) for scattering by side branches are therefore given by

$$Q^{(L+)} = -j\frac{\beta}{\rho_0 c_0^3}\omega_1 d\frac{e^{jk_1(h+2d)}}{e^{-jk_2d} - R_{\rm sb}e^{+jk_2d}}\left[S_{\rm sb}\frac{e^{-jq_1h} + g/f_1}{1 + g/f_1} \right]^2 T_{\rm sb}$$

$$Q^{(L-)} = Q^{(L+)}e^{-jq_2h}$$

$$Q^{(R-)} = -j\frac{\beta}{\rho_0 c_0^3}\omega_1 d\frac{e^{jk_1(h+2d)}}{e^{-jk_2d} - R_{\rm sb}e^{+jk_2d}}\left[S_{\rm sb}\frac{1 + g/f_1 e^{jq_1h}}{1 + g/f_1} \right]^2 T_{\rm sb}$$

$$Q^{(R+)} = Q^{(R-)}e^{-jq_2h}.$$

8.2.4 The Discrete Green's Function

Recall that the discrete Green's function is simply proportional to the second harmonic field that is generated by the portion of the virtual source distribution that occupies the zeroth cell:

$$\hat{p}_2^{(0)} = A_1^2 G_{\rm D}(\mathbf{r})e^{-j\omega_2 t}.$$

As this second harmonic field has been determined, an expression for the discrete Green's function may now be written down. The second harmonic field

in the zeroth cell waveguide section is composed of three fields: (1) that generated by the fundamental f-wave/g-wave field, (2) the forward traveling second harmonic Bloch wave field generated in the left scatterer (that at $z = -h/2$), and (3) the backward traveling second harmonic Bloch wave field generated in the right scatterer (that at $z = h/2$). The second harmonic field on the $z > 0$ side of the zeroth cell is simply a forward traveling second harmonic Bloch wave that is contributed to by all three cell source regions (the waveguide section and the left and right scatterers). The second harmonic field on the $z < 0$ side of the zeroth cell is a backward traveling second harmonic Bloch wave that is likewise contributed to by all three source regions. The discrete Green's function may therefore be expressed

$$
G_{\mathrm{D}}(\mathbf{r}) = \left\{ \begin{array}{ll} G_{\mathrm{D}}^{(-)} F^{(-)}(\mathbf{r}, \omega_2) & z < l_{\mathrm{w}}/2 - h \\ G_{\mathrm{D}}^{(0)}(\mathbf{r}, \omega_2) & |z| < l_{\mathrm{w}}/2 \\ G_{\mathrm{D}}^{(+)} F^{(+)}(\mathbf{r}, \omega_2) & z > h - l_{\mathrm{w}}/2 \end{array} \right. \tag{8.40}
$$

where

$$
G_{\mathrm{D}}^{(-)} = Q^{(\mathrm{W}-)} + \frac{1}{2}\left(Q^{(\mathrm{L}-)} + Q^{(\mathrm{R}-)}\right)
$$

and

$$
G_{\mathrm{D}}^{(+)} = Q^{(\mathrm{W}+)} + \frac{1}{2}\left(Q^{(\mathrm{L}+)} + Q^{(\mathrm{R}+)}\right)
$$

are (frequency dependent) constants and

$$
G_{\mathrm{D}}^{(0)}(\mathbf{r}, \omega_2) = \frac{1}{2}Q^{(\mathrm{L}+)} F^{(+)}(\mathbf{r}, \omega_2) + \frac{1}{2}Q^{(\mathrm{R}-)} F^{(-)}(\mathbf{r}, \omega_2) + Q^{(\mathrm{WC})}(\mathbf{r}, \omega_2)
$$

has a spatial dependence. It is seen in Eq. 8.40 that the virtual source distribution in the zeroth cell excites not only forward traveling second harmonic Bloch wave, but a backward traveling one as well. In Fig. 8.1 is shown a plot of the magnitudes of $G_{\mathrm{D}}^{(+)}$ and $G_{\mathrm{D}}^{(-)}$, which are proportional to the amplitudes of these forward and backward traveling Bloch waves. When the fundamental frequency is such that either the fundamental or the second harmonic lies in a stopband, then $|G_{\mathrm{D}}^{(+)}| = |G_{\mathrm{D}}^{(-)}|$. The forward and backward traveling Bloch waves generated in the zeroth cell are of equal amplitude.

To conclude, we have considered the problem of second harmonic generation in a semi-infinite periodic waveguide in order to (1) show that the particular solution may be cast in terms of a discrete Green's function, and
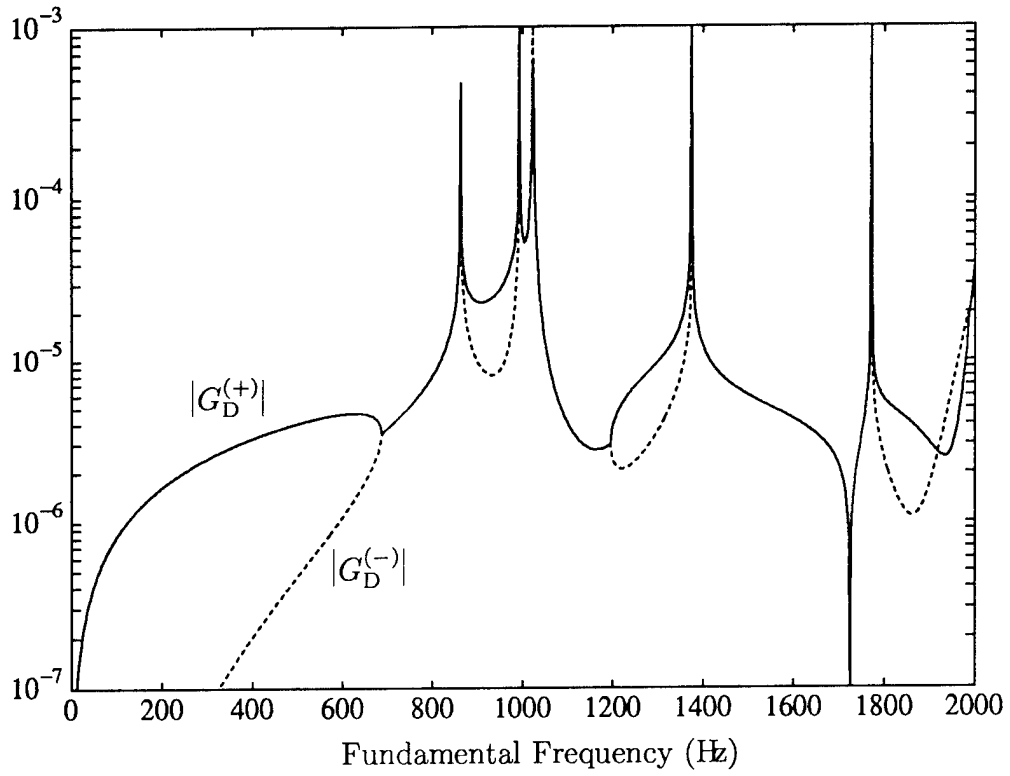
Figure 8.1: The discrete Green's function coefficients $G_D^{(+)}$ and $G_D^{(-)}$ that determine the amplitude of the forward and backward traveling Bloch waves generated by a cell source.

(2) solve for the discrete Green's function. Recall that the discrete Green's function is an infinite periodic waveguide Green's function (see Sec. 8.1.3). That is, the sum of appropriately shaded, phased, and placed copies of the discrete Green's function (as seen in Eq. 8.22), results in an expression for the second harmonic *particular* solution. Homogeneous second harmonic solutions must be added to the particular solution in order to satisfy the source and terminiation boundary conditions. As the z boundary conditions are not incorporated in the discrete Green's function, it is the appropriate discrete Green's function for a finite periodic waveguide as well as for the semi-infinite periodic waveguide. The only restriction is that the fundamental field must either be progressive or, as far as second harmonic generation is concerned, effectively progressive (i.e., the backward traveling fundamental Bloch wave amplitude must be small). In other words, we have derived the infinite periodic waveguide discrete Green's function associated with any progressive or effectively progressive fundamental Bloch wave field.

8.3   The Particular Solution

In this section the particular solution for the finite periodic waveguide problem is found. While this field does not meet the z boundary conditions, its general form tells us a great deal about the generation of a second harmonic field by a forward traveling fundamental Bloch wave. It is found that the forward traveling fundamental Bloch wave generates both forward and backward traveling second harmonic Bloch waves. It also generates a second harmonic field that is identified as a local field. As in the case of nonlinear dispersive conventional wave propagation, the Bloch wave dispersion serves to disrupt the synchrony of the nonlinear interaction between fundamental and second harmonic. The propagating second harmonic waves oscillate in amplitude and the wave as a whole never undergoes any large net distortion. In addition, it is found that the effective nonlinearity of the Bloch waves differs from that of conventional waves.

As is pointed out at the end of Sec. 8.2, the infinite periodic waveguide discrete Green's function may be used for the finite periodic waveguide problem provided the backward traveling fundamental Bloch wave is of sufficiently small

amplitude. The source boundary condition is assumed to be given by[3]

$$\left.\hat{p}_1\right|_{z=0} = \bar{A}_1 e^{-j\omega_1 t}$$

$$\left.\hat{p}_2\right|_{z=0} = \bar{A}_2 e^{-j\omega_2 t}. \tag{8.41}$$

The solution of the problem at first order is therefore given by

$$\hat{p}_1(\mathbf{r}, t) = \frac{\bar{A}_1}{1 + R_{\mathrm{B}} e^{2jq_1(N-1)h}} \left[F^{(+)}(\mathbf{r}, \omega_1) + R_{\mathrm{B}} e^{2jq_1(N-1)h} F^{(-)}(\mathbf{r}, \omega_1) \right] e^{-j\omega_1 t}$$

$$= \hat{A}_1 \left[F^{(+)}(\mathbf{r}, \omega_1) + R_{\mathrm{B}} e^{2jq_1(N-1)h} F^{(-)}(\mathbf{r}, \omega_1) \right] e^{-j\omega_1 t},$$

where $\hat{A}_1 = \bar{A}_1 / (1 + R_{\mathrm{B}} e^{2jq_1(N-1)h})$ is the forward traveling fundamental Bloch wave amplitude. The argument that the backward traveling fundamental Bloch wave is negligible hinges on a combination of the effect of dissipation and the frequency dependence of the reflection coefficient $R_{\mathrm{B}}(\omega_1)$. Near stopband frequencies the effect of dissipation is enhanced and the reflected fundamental Bloch wave has relatively small amplitude (i.e., $e^{-\alpha_1 N h}$ is small compared to one). Away from stopband frequencies, where the effect of dissipation is not as strong, the reflection coefficient $R_{\mathrm{B}} = -g/f_1$ is small (see Fig. 3.8). As the forward traveling fundamental Bloch wave has been assumed to be only weakly nonlinear, it is expected that the backward traveling fundamental Bloch wave propagates linearly.

8.3.1 The N Cell Particular Solution

In order to derive a useful form of the particular solution, we consider the second harmonic field at some point $\mathbf{r}$ in the mth cell of the periodic waveguide (i.e., $|\hat{\mathbf{e}}_z \cdot \mathbf{r} - mh| < h/2$). From Eq. 8.22, the second harmonic field is given by

$$\hat{p}_2 = \hat{A}_1^2 \sum_{n=0}^{N-1} G_{\mathrm{D}}(\mathbf{r} - nh\hat{\mathbf{e}}_z) e^{2jq_1 nh} e^{-j\omega_2 t}.$$

---

[3]This is a practical consideration. While in theory we could have a source boundary condition that held the second harmonic field at zero amplitude, in practice we have no such source. Instead we simply account for the second harmonic field that propagates back to the source in the boundary condition.

The nth term in the sum represents the contribution to the field at $\mathbf{r}$ due to the virtual source distribution in the nth cell. We now break up the sum over the $N - 1$ cells into three parts:

$$\hat{p}_2 = \hat{A}_1^2 \left\{ \sum_{n=0}^{m-1} G_{\text{D}}(\mathbf{r} - nh\hat{\mathbf{e}}_z)e^{2jq_1 nh} + G_{\text{D}}(\mathbf{r} - mh\hat{\mathbf{e}}_z)e^{2jq_1 mh} \right.$$

$$\left. + \sum_{n=m+1}^{N-1} G_{\text{D}}(\mathbf{r} - nh\hat{\mathbf{e}}_z)e^{2jq_1 nh} \right\} e^{-j\omega_2 t}. \qquad (8.42)$$

The first term represents the field in the mth cell due to the cell sources in the zero through $m - 1$ cells (i.e., all cells upstream of the mth cell). The second term represents the field in the mth cell due to the cell source in that cell, and the third term represents that due to the cell sources in the $m + 1$ through $N - 1$ cells (i.e., all downstream cells). With consideration of the z component of the arguments of the discrete Green's functions that appear in Eq. 8.42, that equation may, using the definition of the discrete Green's function (Eq. 8.40), be rewritten

$$\hat{p}_2 = \hat{A}_1^2 \left\{ \sum_{n=0}^{m-1} G_{\text{D}}^{(+)} F^{(+)}(\mathbf{r} - nh\hat{\mathbf{e}}_z, \omega_2)e^{2jq_1 nh} + G_{\text{D}}^{(0)}(\mathbf{r} - mh\hat{\mathbf{e}}_z, \omega_2)e^{2jq_1 mh} \right.$$

$$\left. + \sum_{n=m+1}^{N-1} G_{\text{D}}^{(-)} F^{(-)}(\mathbf{r} - nh\hat{\mathbf{e}}_z, \omega_2)e^{2jq_1 nh} \right\} e^{-j\omega_2 t}. \qquad (8.43)$$

The series that appear in Eq. 8.43 may be simplified by consideration of the translation properties of the Bloch wave functions:

$$F^{(+)}(\mathbf{r} - nh\hat{\mathbf{e}}_z, \omega_2) = F^{(+)}(\mathbf{r}, \omega_2)e^{-jnq_2 h}$$

$$F^{(-)}(\mathbf{r} - nh\hat{\mathbf{e}}_z, \omega_2) = F^{(-)}(\mathbf{r}, \omega_2)e^{jnq_2 h}.$$

Equation 8.43 may therefore be expressed

$$\hat{p}_2 = \hat{A}_1^2 \left\{ G_{\text{D}}^{(+)} \left(\sum_{n=0}^{m-1} e^{j(2q_1 - q_2)nh} \right) F^{(+)}(\mathbf{r}, \omega_2) + G_{\text{D}}^{(0)}(\mathbf{r} - mh\hat{\mathbf{e}}_z, \omega_2)e^{2jq_1 mh} \right.$$

$$\left. + G_{\text{D}}^{(-)} \left(\sum_{n=m+1}^{N-1} e^{j(2q_1 + q_2)nh} \right) F^{(-)}(\mathbf{r}, \omega_2) \right\} e^{-j\omega_2 t}. \qquad (8.44)$$

We see that these three terms represent (1) a forward traveling Bloch wave that arises from the upstream cell sources, (2) a term due only to the cell source in the mth cell, and (3) a backward traveling Bloch wave that arises from downstream cell sources. Both of the series in Eq. 8.44 may be summed, and the resultant components of the particular solution may be written

$$\hat{p}_2^{(\text{FT})}(\mathbf{r}, t) = \hat{A}_1^2 G_{\text{D}}^{(+)} e^{j(q_1 - q_2/2)(m-1)h} \frac{\sin[(q_1 - q_2/2)mh]}{\sin[(q_1 - q_2/2)h]} F^{(+)}(\mathbf{r}, \omega_2) e^{-j\omega_2 t} \quad (8.45)$$

$$\hat{p}_2^{(\text{BT})}(\mathbf{r}, t) = \hat{A}_1^2 G_{\text{D}}^{(-)} e^{j(q_1 + q_2/2)(m+N)h} \frac{\sin[(q_1 + q_2/2)(N-1-m)h]}{\sin[(q_1 + q_2/2)h]}$$
$$\cdot F^{(-)}(\mathbf{r}, \omega_2) e^{-j\omega_2 t} \quad (8.46)$$

$$\hat{p}_2^{(\text{L})}(\mathbf{r}, t) = \hat{A}_1^2 e^{j(2q_1 mh - \omega_2 t)} G_{\text{D}}^{(0)}(\mathbf{r} - mh\hat{\mathbf{e}}_z, \omega_2),$$
$$= [\hat{p}_1(mh\hat{\mathbf{e}}_z, t)]^2 G_{\text{D}}^{(0)}(\mathbf{r} - mh\hat{\mathbf{e}}_z, \omega_2), \quad (8.47)$$

where $\hat{p}_2 = \hat{p}_2^{(\text{FT})} + \hat{p}_2^{(\text{BT})} + \hat{p}_2^{(\text{L})}$. The first two components of the particular solution have been labeled (FT) and (BT) as they represent the forward and backward traveling Bloch wave components of the solution. The third component differs from the first two in that its magnitude in a particular cell is dependent only upon the magnitude of the fundamental field in that cell. In other words, the third term represents a locally generated second harmonic field and is, in the spirit of nonlinear conventional wave theory, labelled with an (L). Note that in any particular cell, the value of the local term is spatially dependent, but the overall amplitude of the local term depends only upon the value of the fundamental field at the cell center.

8.3.2 The Forward Traveling Second Harmonic Bloch Wave

As was found to be true in the case of linear Bloch wave pulse propagation (Chapters 4 and 5), the form of the Bloch wave field is most easily interpreted when we consider the analogous conventional wave field. To generate this field we simply evaluate the Bloch wave field at the cell centers (at $\mathbf{r} = mh\hat{\mathbf{e}}_z$) and replace the resultant mh terms by z. Recall that the analogous conventional wave field and the Bloch wave field are equal at the cell centers and generally differ elsewhere.
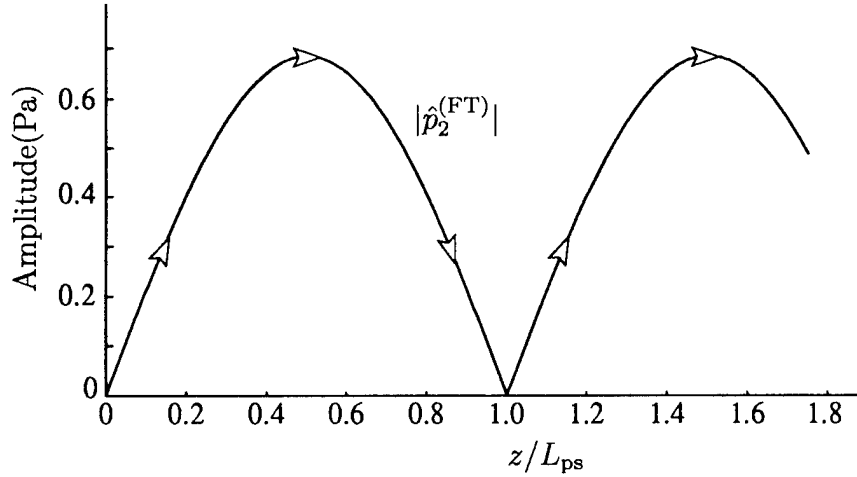
Figure 8.2: The amplitude of the forward traveling Bloch wave component of the second harmonic field. The particular trajectory shown is for the case of a 675 Hz, 144 Pa ($\epsilon = .001$) fundamental Bloch wave in the absence of dissipation.

AS-94-772

The analogous conventional wave field associated with the forward traveling second harmonic component of the particular solution (Eq. 8.45) is

$$\hat{p}_2^{(FT)}(z,t) = \hat{A}_1^2 G_D^{(+)} e^{-j(q_1 - q_2/2)h} \frac{\sin[(q_1 - q_2/2)z]}{\sin[(q_1 - q_2/2)h]} e^{j[(q_1 + q_2/2)z - \omega_2 t]}. \tag{8.48}$$

Owing to the $\sin[(q_1 - q_2/2)z]$ term, the forward traveling Bloch wave oscillates in amplitude as it propagates. The wave amplitude begins at zero at $z = 0$, grows with increasing z, peaks, and then returns to zero (in the nondissipative case) at $z = \pi/|\kappa_1 - \kappa_2/2|$, where $\kappa = \text{Re}\{q\}$ (see Fig. 8.2). The oscillations are due to the fact that the fundamental and the second harmonic do not, owing to the effect of dispersion, remain in phase as they propagate. This is a well known effect in the context of nonlinear dispersive conventional waves. In the absence of dispersion, the second harmonic that is generated at some point in the field always adds constructively to that generated at another point. The interaction between the fundamental and second harmonic fields is *resonant* and the second harmonic wave (to $\mathcal{O}(\epsilon^2)$) grows linearly with distance as it propagates. The second harmonic field constantly accumulates energy and eventually obtains a large amplitude. In the presence of dispersion, the fundamental and the second
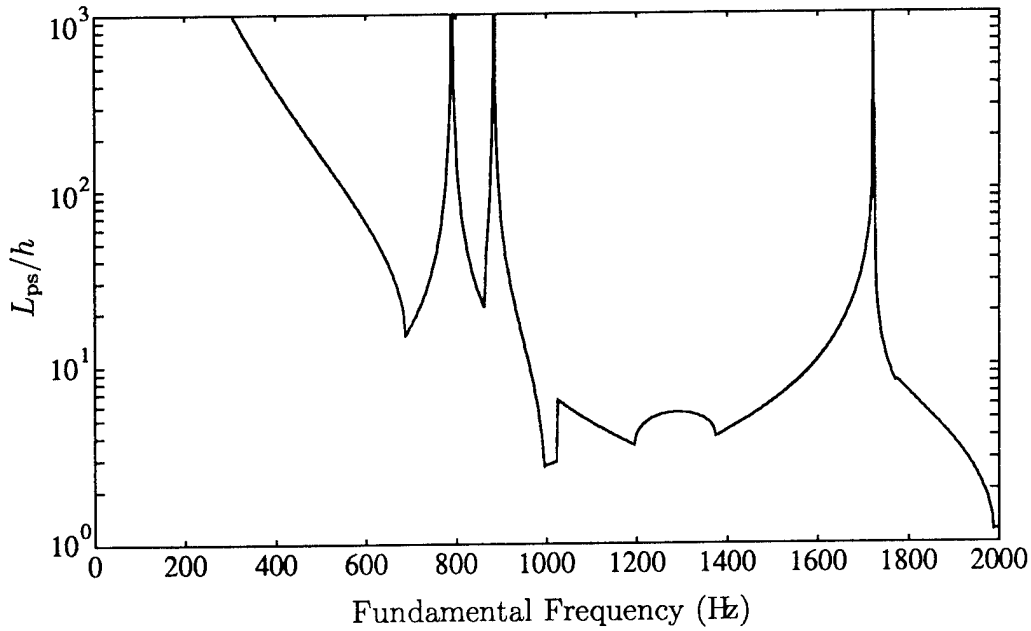
Figure 8.3: The characteristic phase synchrony distance L_{ps} in the nondissipative case.

AS-94-773

harmonic waves go in and out of phase with one another as they propagate. The resonance is disrupted and the second harmonic field consequently oscillates in amplitude. The characteristic distance over which the fundamental and second harmonic remain in phase with one another is termed the "phase synchrony" distance and is given by

$$L_{ps} = \frac{\pi}{|\kappa_1 - \kappa_2/2|}.$$

Note that the phase synchrony distance is also the spatial period of the oscillations in the second harmonic wave amplitude. This characteristic phase synchrony length, which is shown plotted in Fig. 8.3, is a measure of the strength of the dispersion with respect to its role in the disruption of second harmonic growth. Where the characteristic length is very small, the dispersion is very strong, and the resultant generation of a second harmonic field is strongly disrupted. As such, the characteristic phase synchrony length is a measure of the degree to which nonlinear effects may be nullified by the introduction of dispersion into a wave medium.

As the oscillations in the amplitude of the forward traveling second

harmonic Bloch wave bears such a marked similarity to those found for the case of nonlinear dispersive conventional waves, we investigate the similarity further. Consider, for example, the frequency domain Korpel wave equation

$$\frac{\partial \tilde{p}}{\partial z} - jq(\omega)\tilde{p} = -j\omega \frac{\beta}{2\rho_0 c_0^3} \frac{1}{2\pi} \tilde{p} * \tilde{p},$$

where

$$\tilde{p}(z,\omega) = \int_{-\infty}^{\infty} \hat{p}(z,t) e^{j\omega t} dt$$

is the frequency domain acoustic pressure. The Korpel equation is one that is used to model the propagation of conventional waves with dispersion given by $q(\omega)$ and quadratic nonlinearity (Korpel, 1980). Given the real source boundary condition $p(z,t)|_{z=0} = A_1 \cos(\omega_1 t)$, the (complex) solution is given, to second order, by

$$\hat{p}_1 = A_1 e^{j(q_1 z - \omega_1 t)}$$

$$\hat{p}_2 = -j\frac{\beta}{2\rho_0 c_0^3}\omega_1 A_1^2 \frac{\sin[(q_1 - q_2/2)z]}{q_1 - q_2/2} e^{j[(q_1 + q_2/2)z - \omega_2 t]}. \tag{8.49}$$

In the absence of dispersion (and dissipation) $q_1 - q_2/2 = 0$, and the second harmonic solution reduces to

$$\hat{p}_2 = -j\frac{\beta}{2\rho_0 c_0^3}\omega_1 A_1^2 z e^{j[(q_1 + q_2/2)z - \omega_2 t]}. \tag{8.50}$$

An example of the dispersive and nondispersive second harmonic solutions are shown in Fig. 8.4. When $z \ll L_{\mathrm{ps}}$ the second harmonic amplitude in both cases increases linearly with distance. Where the nondispersive solution continues to grow linearly with distance, the dispersive solution returns, at $z = L_{\mathrm{ps}}$ to zero amplitude. This is an example of the disruption of nonlinear distortion by dispersion.

A comparison of Eqs. 8.48 and 8.49 shows that the functional forms of the conventional wave field and the forward traveling component of the Bloch wave field are very similar. The forward traveling Bloch wave component of the solution (Eq. 8.48) may be written

$$\hat{p}_2^{(\mathrm{FT})}(z,t) = -j\frac{\beta}{2\rho_0 c_0^3}\omega_1 \hat{A}_1^2 \Gamma(\omega_1)\frac{\sin[(q_1 - q_2/2)z]}{q_1 - q_2/2} e^{j[(q_1 + q_2/2)z - \omega_2 t]}, \tag{8.51}$$
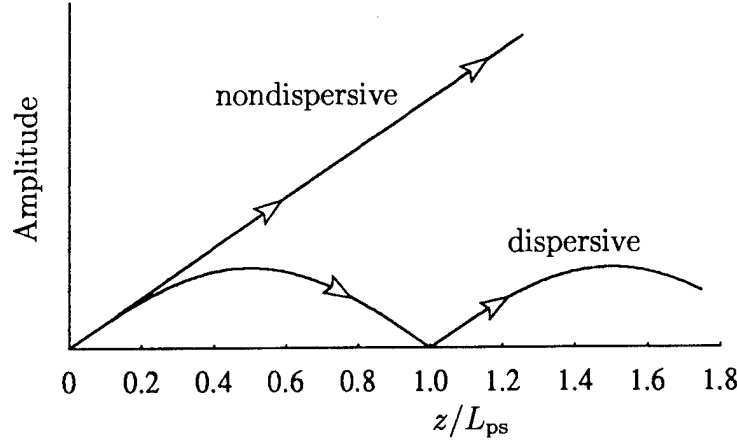
Figure 8.4: Characteristic dispersive and nondispersive second harmonic amplitude trajectories for nonlinear conventional wave propagation.

where

$$\Gamma(\omega_1) = \left\{ \frac{[1 + g/f_2][1 + g/f_2(g/f_1)^2]}{[1 + g/f_1]^2[1 - (g/f_2)^2]} + \frac{2d}{h} \frac{e^{jk_1(h+2d)}}{e^{-jk_2d} - R_{sb}e^{jk_2d}} \frac{S_{sb}^2 T_{sb}}{[1 + g/f_1]^2} \right.$$

$$\left. \cdot \left([1 + g/f_1 e^{jq_1h}]^2 + [e^{-jq_1h} + g/f_1]^2 \right) \right\} \frac{(q_1 - q_2/2)h}{\sin[(q_1 - q_2/2)h]} e^{-j(q_1 - q_2/2)h}.$$

Aside from the frequency dependent factor Γ, the conventional and Bloch wave solutions (Eqs. 8.49 and 8.51) are *identical*. Only the magnitude and not the form of the second harmonic fields differ. The forward traveling second harmonic Bloch wave is generated as if the coefficient of nonlinearity were $\Gamma\beta$ instead of β. We therefore identify the effective coefficient of nonlinearity for second harmonic generation by Bloch waves as

$$\beta_B = \Gamma(\omega_1) \cdot \beta.$$

When a uniform waveguide is made periodic, the system not only becomes dispersive, but becomes effectively either more or less nonlinear as well. The ratio of the Bloch wave to the conventional wave coefficient of nonlinearity is shown in Fig. 8.5. In some ranges of frequency near the stopband edges, nonlinearity
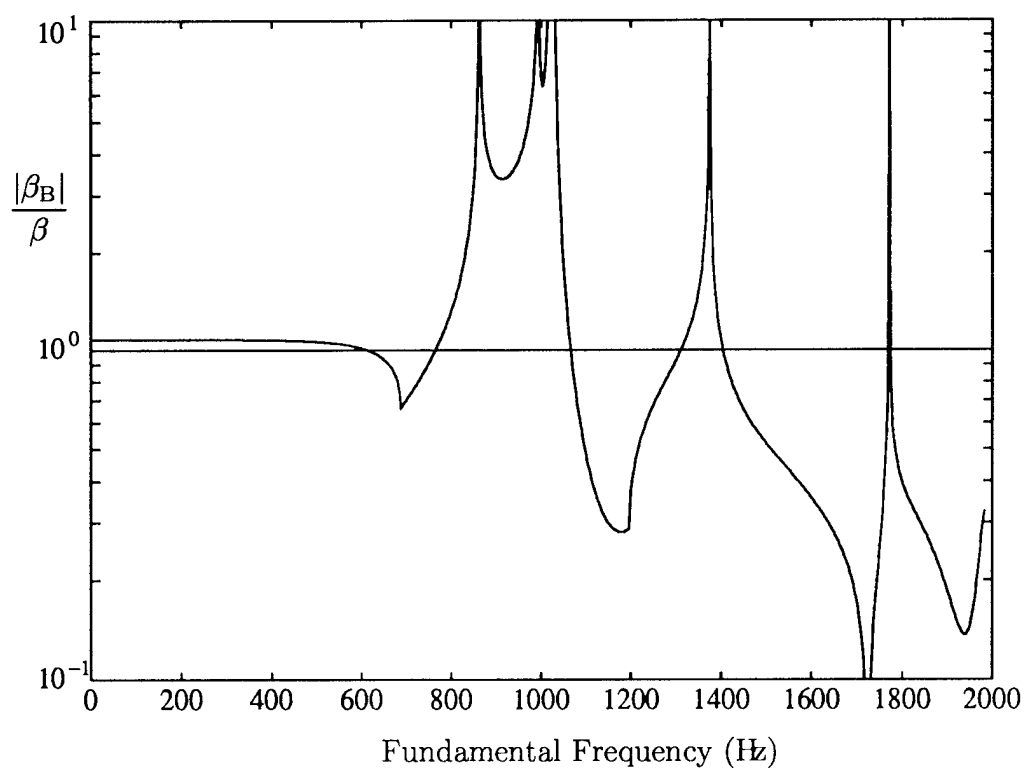
Figure 8.5: The effective coefficient of nonlinearity for Bloch waves.

affects the Bloch wave over ten times more than it affects a conventional wave of equal amplitude. In other frequency ranges, the opposite is true.

The effective increase in nonlinearity is due to several effects. In a nondispersive conventional wave field the second harmonic wave grows linearly with distance as the fundamental propagates (see Eq. 8.50). In having propagated a distance h, the fundamental generates a second harmonic wave field of some given amplitude. In the case of a Bloch wave, the fundamental f-wave generates a second harmonic wave in much the same manner. There is, however, an additional second harmonic wave field generated by the g-wave and by the fields in the scatterers. When these second harmonic fields add constructively, the fundamental Bloch wave generates more second harmonic energy per unit length than does the conventional wave. *The overall effective propagation distance is larger for the Bloch wave than for a conventional wave.* In addition, particularly near second harmonic stopbands, the second harmonic level may be increased by resonant amplification. It should also be noted that there is also a somewhat artificial increase (or decrease) in the effective nonlinearity that comes about as an artifact of the normalization of the Bloch wave functions (see Sec. 3.5). In passbands in which the phase of g/f_1 is $n_o\pi$, where n_o is an odd integer, the f-wave amplitude is larger than that of the Bloch wave itself, and the second harmonic field generation appears to be abnormally large. Note also that in some frequency ranges the effective nonlinearity is *decreased.* This occurs in frequency ranges in which the second harmonic field generated in a waveguide section and that generated in the two neighboring side branches add *destructively,* and the fundamental Bloch wave consequently generates *less* second harmonic energy per unit length than a conventional wave. The Bloch wave function normalization also causes, in some frequency ranges, a decrease in the effective nonlinearity.

Just as the phase synchrony distance is a measure of the strength of the dispersion, there is a characteristic distance that is a measure of the strength of the nonlinearity. The characteristic length scale associated with nonlinear effects in conventional waves is the shock formation distance, defined as

$$L_{\text{sf}} = \frac{1}{\beta \epsilon k_1} = \frac{\rho_0 c_0^3}{\beta \omega_1 |\hat{A}_1|}. \tag{8.52}$$

The shock formation distance is the distance at which shocks first appear (in that absence of dissipation) in an initially sinusoidal wave field. If we consider only the solution at second order, as we have here, the shock formation distance is that at which the amplitude of the linearly growing second harmonic wave (see Eq. 8.50) becomes half the amplitude of the fundamental.[4] Even when dissipation and/or dispersion mechanisms are present in the system, the shock formation distance is valuable as a measure of the strength of the nonlinear effects that act on the wave. The characteristic length scale associated with nonlinearity in a Bloch wave is simply that shown in Eq. 8.52 with β replaced by $|\beta_{\mathrm{B}}|$:

$$L_{\mathrm{sf}} = \frac{1}{|\beta_{\mathrm{B}}|\epsilon k_1}.$$

The conventional and Bloch wave shock formation distances are shown for acoustic Mach numbers of $\epsilon = .001$ and $\epsilon = .01$ in Fig. 8.6.

Evidently, the introduction of periodicity into a waveguide affects the nonlinear generation of the forward traveling second harmonic field in two distinct ways: (1) through the modification of the effective nonlinearity of the medium, and (2) through the introduction of dispersion. The modification of the nonlinearity of the medium affects the *rate* at which nonlinear distortion effects occur. The Bloch wave distorts at a rate that generally differs from a conventional wave of identical amplitude. The effect of the dispersion that is introduced when the waveguide becomes periodic is to limit the *net degree* of nonlinear distortion that occurs. The synchrony of the fundamental and second harmonic is disrupted and the resultant peak amplitude of the second harmonic field becomes limited, as is seen clearly in Fig. 8.4.

The net amount of (forward traveling) second harmonic distortion that the Bloch wave undergoes is dependent upon the effective nonlinearity of the system and the degree to which the dispersion is able to oppose this nonlinearity. As the shock formation distance and phase synchrony distance quantify the nonlinearity and dispersion independently, we now find the combination of these quantities that reflects the net degree of wave distortion. The

---

[4]Note that the second order solution becomes invalid long before the shock formation distance.
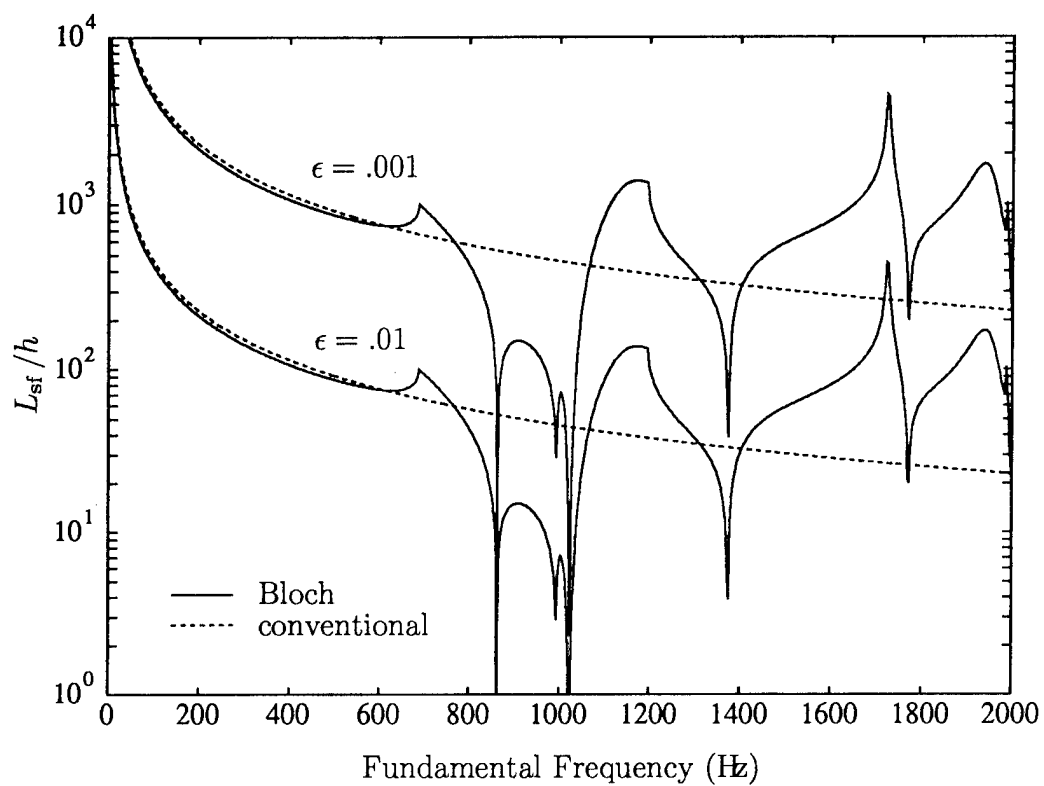
Figure 8.6: The shock formation distance for Bloch and conventional waves of acoustic Mach number $\epsilon = .001$ and $\epsilon = .01$.

net amount of nonlinear distortion that a Bloch wave undergoes may be quantified by the ratio of the peak second harmonic amplitude to the fundamental amplitude. From Eq. 8.51, the peak second harmonic amplitude, which occurs at $z = L_{ps}/2$, is in the nondissipative case given by

$$\left|\hat{p}_2^{(FT)}\right|_{z=L_{ps}/2} = \frac{\beta_B}{2\rho_0 c_0^3}\omega_1\frac{|\hat{A}_1|^2}{|\kappa_1 - \kappa_2/2|}. \tag{8.53}$$

Note that it has been assumed that both the fundamental and second harmonic frequencies lie in passbands. If either lies in a stopband (or if dissipation is present) then the amplitude is less than that predicted by Eq. 8.53. From Eq. 8.53 we see that the peak second harmonic level is increased for large effective nonlinearity (large β_B) and is decreased for strong dispersion (large $|\kappa_1 - \kappa_2/2|$). The ratio of the peak second harmonic level to the fundamental field level may be written simply

$$\frac{\left|\hat{p}_2^{(FT)}\right|_{z=L_{ps}/2}}{|\hat{A}_1|} = \frac{1}{2\pi}\frac{L_{ps}}{L_{sf}}. \tag{8.54}$$

The ratio of the phase synchrony distance to the shock formation distance is a measure of the net effect of nonlinearity as opposed by dispersion. A small shock formation distance indicates a strongly nonlinear wave and the resultant second harmonic peak is large. Strong dispersion is associated with a small phase synchrony distance and the resultant second harmonic level is small. In Fig. 8.7 is shown a plot of the ratio of these two distances for an acoustic Mach number of $\epsilon = .001$. Over nearly the entire range of frequencies the effect of nonlinearity is very effectively suppressed by the dispersion. While the curve shown is, strictly speaking, only valid in the nondissipative case in which both the fundamental and second harmonic frequencies lie in passbands, attenuation only serves to further suppress the second harmonic level.

What we have done is characterize and quantify the nonlinear distortion of Bloch waves by way of analysis of only the *forward traveling* component of the second harmonic distortion field. What of the backward traveling and local components? It is shown in the next two sections that, while these latter two components of the field are not negligible, they are smaller in amplitude than the forward traveling component. The forward traveling component alone then, for the most part, determines the net amount of distortion that is undergone by the Bloch wave.
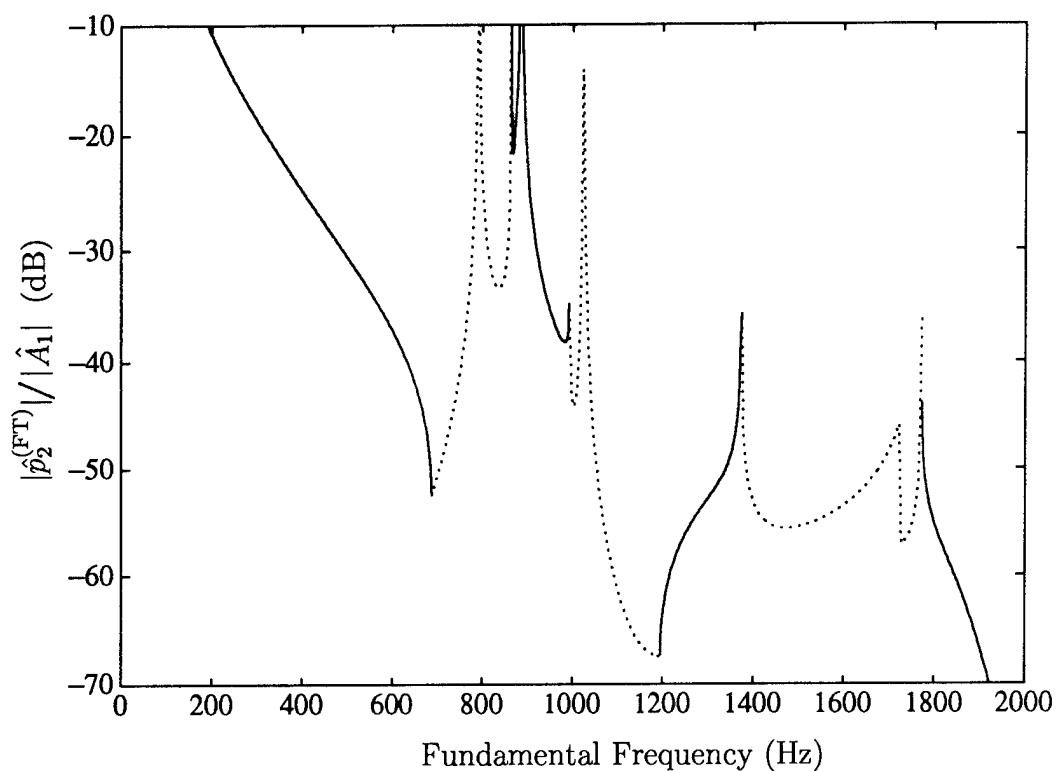
Figure 8.7: The ratio of the phase synchrony to the shock formation distance (divided by 2π) for an acoustic Mach number of $\epsilon = .001$. In the passbands (where the curve is a solid line) this ratio is equal to the peak forward traveling second harmonic Bloch wave level relative to the fundamental level. In the frequency ranges where attenuation is significant (where the curve is dotted) the actual peak level is smaller than that indicated.

8.3.3 The Backward Traveling Second Harmonic Bloch Wave

The backward traveling Bloch wave component of the particular solution is, like the forward traveling component, most readily analyzed when cast in the form of an analogous conventional wave field. We evaluate Eq. 8.46 at $\mathbf{r} = mh\hat{\mathbf{e}}_z$ and replace mh by z to result in

$$\hat{p}_2^{(BT)}(z,t) = \hat{A}_1^2 G_D^{(-)} e^{j(q_1+q_2/2)Nh} \frac{\sin[(q_1+q_2/2)(Nh-h-z)]}{\sin[(q_1+q_2/2)h]} e^{j[(q_1-q_2/2)z-\omega_2 t]}.$$

(8.55)

The backward traveling Bloch wave component, like the forward traveling component, oscillates in amplitude with distance, though at a very different spatial frequency. Where the spatial frequency of oscillation is $\kappa_1 - \kappa_2/2$ for the forward traveling Bloch wave (see Eq. 8.48), it is $\kappa_1 + \kappa_2/2$ for the backward traveling Bloch wave. The wave begins with an amplitude of zero at $z = (N-1)h$ (at the waveguide termination) and grows in the negative z direction, the direction of propagation of the wave. The amplitude then peaks and decreases back to zero (in the absence of dissipation) at $z = \pi/(\kappa_1 + \kappa_2/2)$ and the cycle repeats. While the oscillation period *appears* to be given by $\pi/(\kappa_1 + \kappa_2/2)$, recall that Eq. 8.55 only has physical meaning at the cell centers (i.e., at $z = mh$). The analogous conventional wave field only carries information as to the overall amplitude of the f-wave/g-wave field at the cell center. From the cell center out, the field has the form of the cell wave function $\psi_2(\mathbf{r}, \omega_2)$. The actual oscillation period is therefore the low spatial frequency alias of the apparent period $\pi/(\kappa_1 + \kappa_2/2)$. The backward traveling Bloch wave amplitude is shown in Fig. 8.8 as a function of distance for the case of a 675 Hz, $\epsilon = .001$ (144 Pa) fundamental Bloch wave. The solid lines are the analogous conventional wave amplitudes from Eq. 8.55 and the circles represent the points at which the analogous conventional wave field corresponds to the actual Bloch wave solution. Owing to this spatial aliasing effect, the actual spatial period of the backward traveling Bloch wave is always greater than or equal to the apparent period $\pi/(\kappa_1 + \kappa_2/2)$.

In Fig. 8.9(a) is shown the amplitudes of the forward and backward traveling Bloch wave components of the second harmonic field for the case of a 675 Hz, $\epsilon = .001$ (144 Pa) fundamental Bloch wave. As is demonstrated in
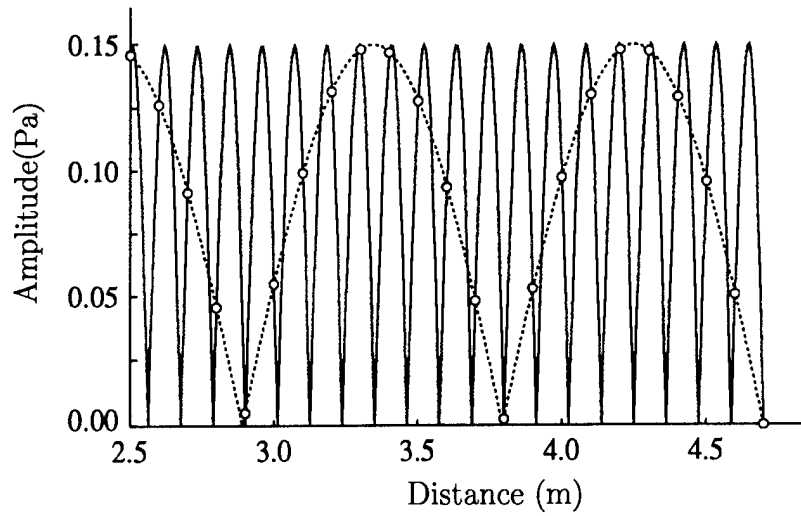
Figure 8.8: The spatial aliasing effect in the backward traveling Bloch wave component of the second harmonic field. The amplitude of the analogous conventional wave field is shown for the particular case of a 675 Hz, $\epsilon = .001$ (144 Pa) fundamental Bloch wave in the absence of dissipation. The circles denote the amplitude at the cell centers, where the analogous conventional wave and the Bloch wave amplitudes coincide.

AS-94-778

this example, the forward traveling second harmonic Bloch wave typically has a substantially larger spatial period and amplitude than the backward traveling wave. Both effects are consequences of the lack of synchrony between the fundamental and the second harmonic. The forward traveling second harmonic Bloch wave typically maintains a greater degree of phase synchrony with the fundamental than the backward traveling second harmonic wave does. The exception occurs when $(\kappa_1 + \kappa_2/2)h \simeq 2\pi n$, where n is an integer (note that this is also a spatial aliasing condition). In that case the backward traveling second harmonic wave and the fundamental wave become synchronous. The spatial beat frequency of the backward traveling Bloch wave becomes very low and the amplitude becomes very large. This resonant feeding of energy into the backward traveling Bloch wave is, however, difficult to observe as the backward phase synchrony condition $(\kappa_1 + \kappa_2/2)h \simeq 2\pi n$ is only met near stopband edges, where the attenuation of the backward traveling wave is very large. Where the forward traveling wave is proportional to $e^{j(q_1 - q_2/2)z}$, the backward traveling wave is proportional to $e^{j(q_1 + q_2/2)z}$, and is therefore very strongly attenuated near the stopband edge. In practice, therefore, the forward traveling Bloch
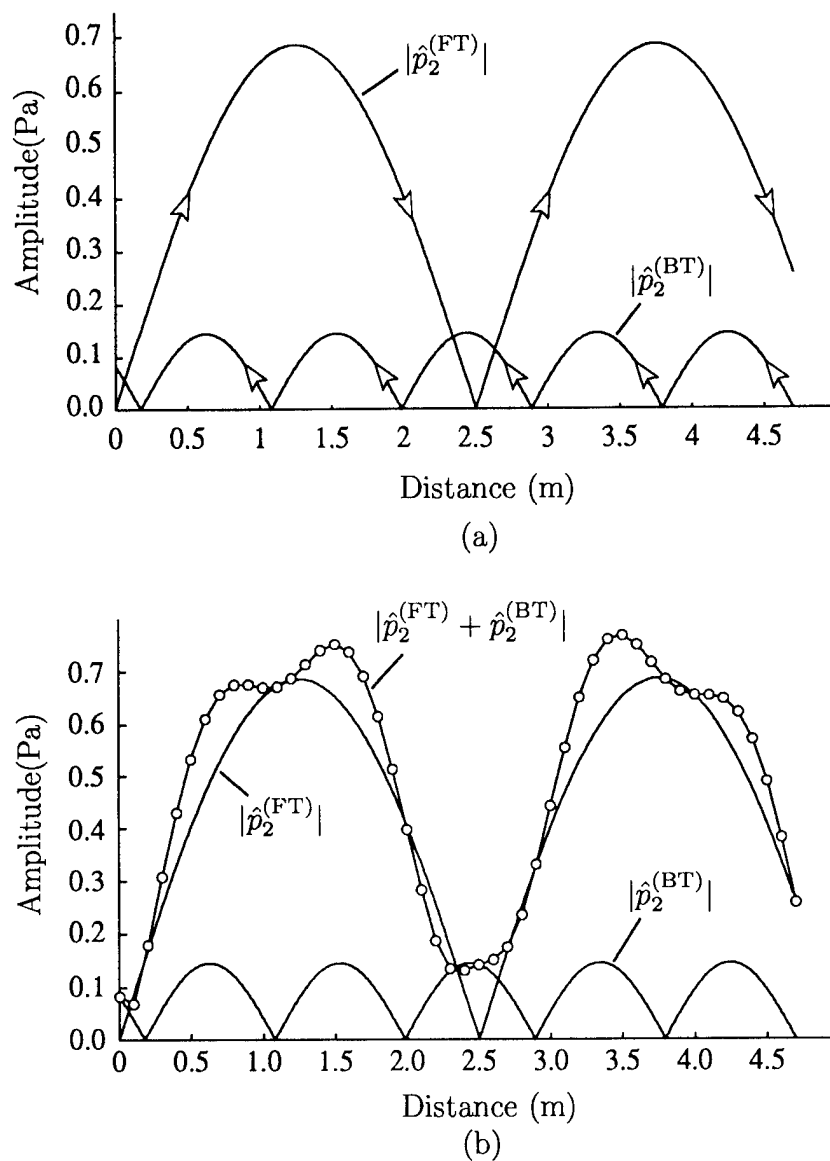
Figure 8.9: The forward and backward traveling Bloch wave amplitudes for the case of a 675 Hz, $\epsilon = .001$ (144 Pa) fundamental Bloch wave. In (a) is shown the two amplitude trajectories, and in (b) is shown the trajectory of the resultant compound field amplitude.

wave has a larger amplitude and lower spatial beat frequency than the forward traveling Bloch wave. The case shown in Fig. 8.9(b) is therefore, away from stopbands, typical. The sum of the forward and backward traveling second harmonic Bloch waves has an amplitude trajectory that is very similar to the forward traveling Bloch wave but has ripples that are due to the presence of the backward traveling wave.

In Fig. 8.10 is shown the maximum amplitudes of the forward and backward traveling second harmonic Bloch waves for the case of a fundamental Bloch wave with an acoustic Mach number of $\epsilon = .001$. For simplicity, it is assumed that there is no attenuation. The maximum amplitude of the backward traveling wave is smaller than that of the forward traveling wave except at frequencies for which either the fundamental or second harmonic lies in a stopband, where the amplitudes are equal. In and near the stopbands, however, the attenuation that the backward traveling Bloch wave undergoes is very large, and the indicated maximum will not be realized. Note that in the vicinity of 1950 Hz the backward traveling Bloch wave amplitude exceeds that of the forward traveling wave. This is an example of the backward wave phase synchrony condition.

8.3.4 The Local Second Harmonic Field

We now consider the local Bloch wave term (Eq. 8.47). Up to this point, the locally generated second harmonic components of the field have been taken to be insignificant and have therefore been discarded. In Sec. 8.1.1 it is argued that the Lagrangian density term gives rise to only a local second harmonic field and is therefore discarded from the nonlinear wave equation. Similarly, in Sec. 8.2 a local second harmonic field term is identified and is likewise discarded (see Eq. 8.29). While the neglect of these terms is a standard procedure, the justification is based on the behavior of nonlinear *nondispersive* conventional waves. In the absence of dispersion, the nonlinearly generated propagating second harmonic field remains in phase with the virtual source distribution (i.e., $\kappa_1 = \kappa_2/2$), and the resultant second harmonic field accumulates energy monotonically (see Fig. 8.4). The second harmonic field that is brought about by this resonant generation pathway easily dominates the locally generated second harmonic field and we are justified in discarding the
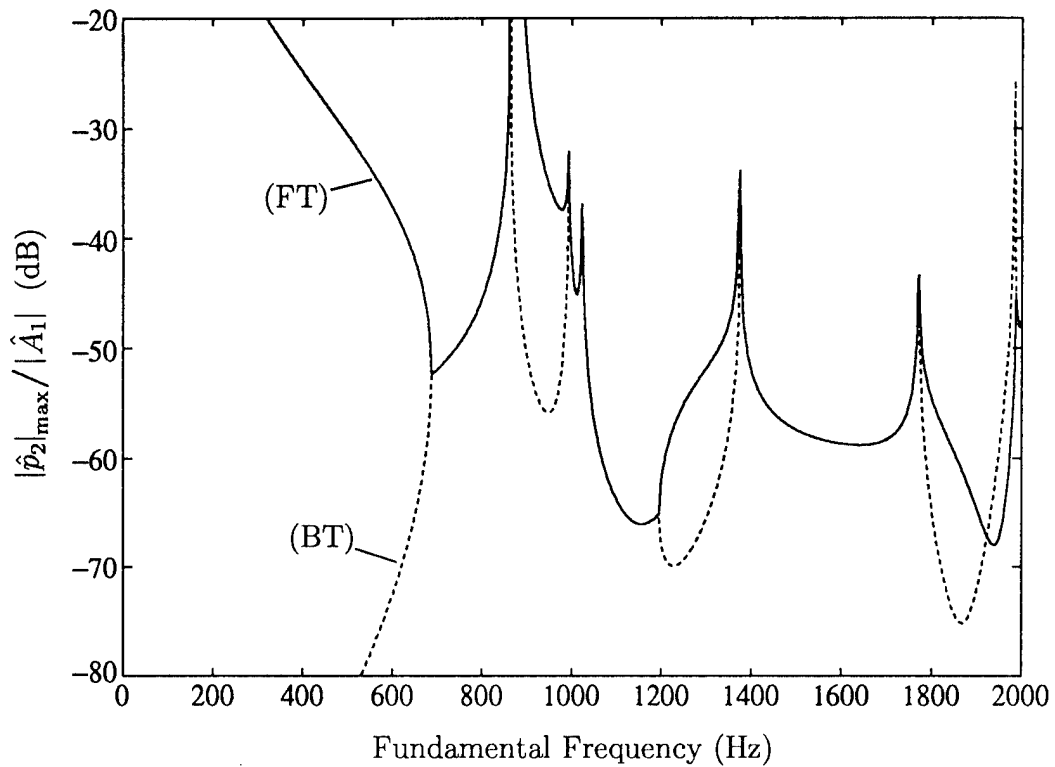
Figure 8.10: The peak forward traveling (FT) and backward traveling (BT) second harmonic Bloch wave amplitudes relative to the fundamental amplitude. The acoustic Mach number is $\epsilon = .001$ (144 Pa), and it is assumed that there is no attenuation. In the stopbands (where the curves are confluent), the attenuation is significant and the actual levels are smaller than indicated.

local terms. In the presence of dispersion, however, the resonant feeding of energy into the second harmonic field is disrupted and, as we have seen, the field does not grow monotonically but oscillates in amplitude. When the dispersion is strong (i.e., when L_{ps} is very small), the peak amplitude of the propagating second harmonic field is very effectively suppressed by the dispersion and the discarding of the local terms is no longer justified (see Figs. 8.7 and 8.10). In a sense, the propagating second harmonic field has itself become locally generated. It is effectively only contributed to by the virtual source distribution within a characteristic phase synchrony distance of the observation point.

While we have discarded terms associated with the locally generated second harmonic field, it is a straightforward matter to back track and account for the previously discarded terms. These terms may easily be incorporated in the Bloch wave local effect term shown in Eq. 8.47. Local field components arise from the term on the right-hand side of Eq. 8.7 (see, for example, the third term on the right-hand side of Eq. 8.29) and from the Lagrangian density term in Eq. 8.6. With the inclusion of these terms, the local second harmonic field in the waveguide sections becomes

$$\hat{p}_2^{(L)}(\mathbf{r}, t) = \hat{p}_1(mh\hat{\mathbf{e}}_z, t)^2 \left[G_D^{(0)}(\mathbf{r} - mh\hat{\mathbf{e}}_z, \omega_2) + \frac{\beta - 1}{\rho_0 c_0^2} \frac{g/f_1}{(1 + g/f_1)^2} \right]. \quad (8.56)$$

The analogous conventional wave representation of the local field may be written

$$\hat{p}_2^{(L)}(z, t) = A_1^2 G_D^{(L)} e^{j(2q_1 z - \omega_2 t)},$$

where

$$G_D^{(L)} = \left\{ \frac{1}{2}(Q^{(L+)} + Q^{(R-)}) - \frac{j}{2} \frac{\beta}{\rho_0 c_0^2} (\omega_1 h / c_0) \frac{(1 - g/f_1)(1 + g/f_2)}{(1 + g/f_1)(1 - g/f_2)} \right.$$

$$\left. + \frac{\beta - 1}{\rho_0 c_0^2} \frac{g/f_1}{(1 + g/f_1)^2} \right\}.$$

Recall that the analogous conventional wave field coincides with the physical second harmonic pressure field only at the cell centers ($z = mh$). Just as $G_D^{(+)}$ and $G_D^{(-)}$ represent the amplitudes of the forward and backward traveling Bloch waves generated by the zeroth cell source, the coefficient $G_D^{(L)}$ represents the amplitude of the locally generated second harmonic in the zeroth cell. In
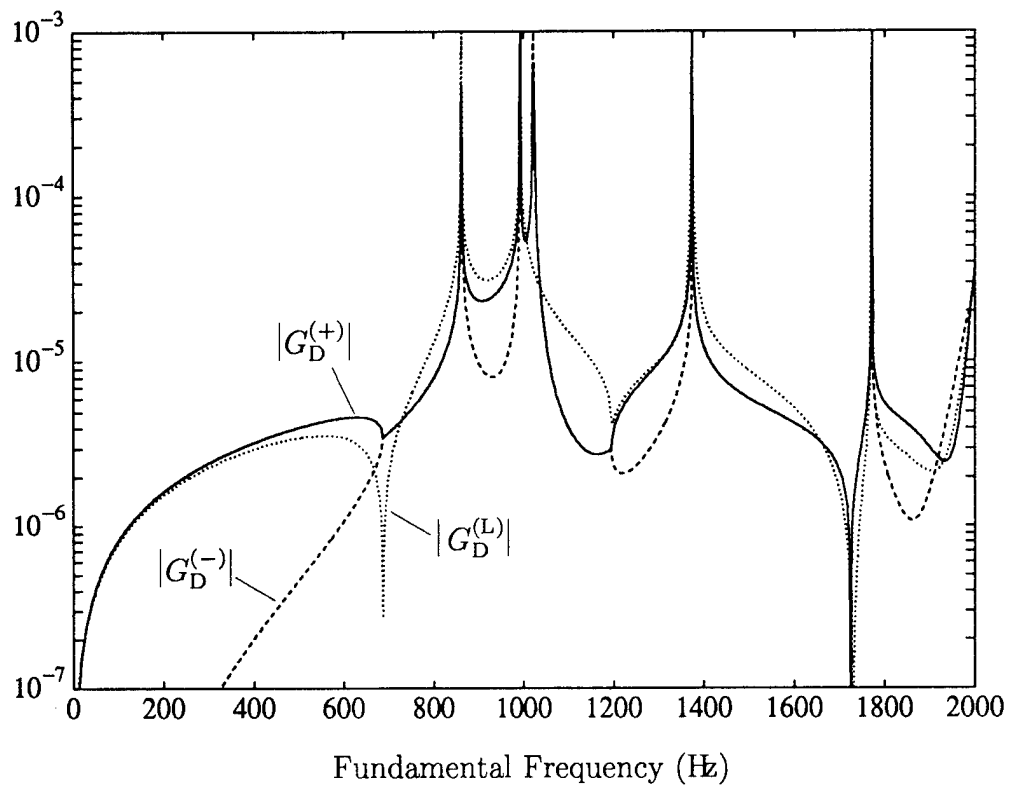
Figure 8.11: The discrete Green's function coefficient $G_D^{(L)}$ that determines the amplitude of the local second harmonic field in a cell. Included in the plot are the coefficients $G_D^{(+)}$ and $G_D^{(-)}$, which determine amplitudes of the forward and backward traveling second harmonic Bloch wave generated in a cell.
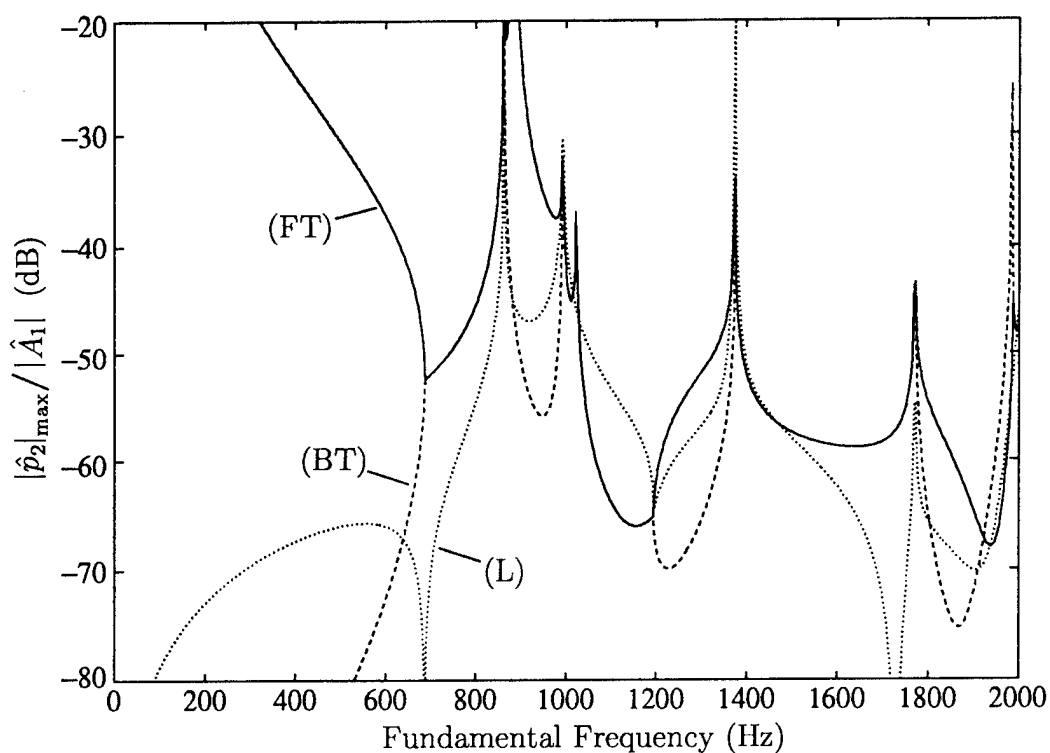
Figure 8.12: The peak levels of the forward traveling (FT), the backward traveling (BT), and the local (L) components of the second harmonic field relative to the fundamental level for an acoustic Mach number of $\epsilon = .001$. It is assumed that there is no attenuation. At stopband frequencies, where attenuation is significant, the propagating field amplitudes are smaller than those indicated.

Fig. 8.11 is shown a plot of $|G_D^{(L)}|$ as compared to $|G_D^{(+)}|$ and $|G_D^{(-)}|$. The local second harmonic field generated in a cell is indeed generally comparable in amplitude to the propagating second harmonic field generated in a cell. The propagating field, however, accumulates over a characteristic phase synchrony distance, and the magnitudes of the coefficients are therefore not a direct reflection of the resultant propagating second harmonic field amplitudes. The peak amplitudes of the forward traveling, backward traveling, and local second harmonic fields are shown in Fig. 8.12 for the case of an acoustic Mach number of $\epsilon = .001$. While in some ranges of frequency the local field is not significant as compared to the forward traveling Bloch wave field, it is clear that this is not true for all frequencies. Particularly where the dispersion is strong and very effectively suppresses the accumulation of large propagating second harmonic field levels, the local field is significant.

8.4 The Full Second Harmonic Solution

We may now add homogeneous second harmonic Bloch wave solutions to the particular solution to satisfy the source and termination boundary conditions. The total second harmonic field may be written

$$\hat{p}_2 = \hat{p}_2^{(FT)} + \hat{p}_2^{(BT)} + \hat{p}_2^{(L)} + H^{(+)}F^{(+)}e^{-j\omega_2 t} + H^{(-)}F^{(-)}e^{-j\omega_2 t},$$

where the first three terms represent the particular solution and the other two represent the homogeneous solution. The source and termination boundary conditions determine the homogeneous wave amplitudes, which are given by

$$H^{(+)} = \frac{-g/f_2 \bar{p}_2^{(FT)}((N-1)h\hat{e}_z) + [\bar{p}_2^{(BT)}(0) + \bar{p}_2^{(L)}(0) - \hat{A}_2]e^{-jq_2(N-1)h}}{g/f_2 e^{jq_2(N-1)h} - e^{-jq_2(N-1)h}}$$

$$H^{(-)} = \frac{g/f_2 \bar{p}_2^{(FT)}((N-1)h\hat{e}_z) - [\bar{p}_2^{(BT)}(0) + \bar{p}_2^{(L)}(0) - \hat{A}_2]g/f_2 e^{jq_2(N-1)h}}{g/f_2 e^{jq_2(N-1)h} - e^{-jq_2(N-1)h}},$$

where $\bar{p}_2(\mathbf{r})$ is defined such that $\hat{p}_2(\mathbf{r},t) = \bar{p}_2(\mathbf{r})e^{-j\omega_2 t}$ and we have used $\hat{p}_2^{(FT)}(0,t) = \hat{p}_2^{(BT)}((N-1)h\hat{e}_z,t) = 0$.

The measurement of the second harmonic field is the most straightforward of the measurements. The microphone is used in the flush mount

configuration (see Fig. E.2) and the signal routed to the spectrum analyzer. The spectrum analyzer is programmed to report the magnitude and phase of the fundamental and second harmonic components of the signal. While the magnitude of the second harmonic component is the quantity in which we are interested, the magnitude of the fundamental and the phase of the second harmonic relative to the fundamental must be measured at the entrance to the periodic waveguide in order to compare the measured second harmonic amplitude trajectory with theory.

In Fig. 8.13(a) is shown the amplitudes of the various components of the second harmonic field for a 650 Hz, 135.7 dB ($\epsilon = .0012$) fundamental Bloch wave. In Fig. 8.13(b) is shown the resultant total second harmonic field amplitude along with measurements. The spatial beats associated with the forward traveling second harmonic is clearly evident in the measurement. It is also clear that there are smaller scale beats superposed upon the large scale beats. These smaller scale beats are of the spatial frequency expected for the backward traveling second harmonic field (see the beats in the backward traveling component of the particular solution shown in Fig. 8.13(a)). These beats are to some degree due to the oscillating amplitude of the backward traveling wave, but are to a more significant degree due simply to the interaction of the forward and backward traveling components of the total field. The forward traveling component of the field is composed of one Bloch wave that arises from the particular solution (the so-called forced wave) that oscillates in amplitude and one that arises from the homogeneous solution (the so-called free wave) that does not. The backward traveling component of the field is similarly composed of a forced wave that oscillates in amplitude and a free wave that does not. Because the field is compound, there are spatial oscillations in the net field due simply to constructive and destructive interference between the forward and backward traveling wave components. These are simply the classical standing wave beats. The spatial period of these oscillations is given by π/q_2 (or the low frequency alias thereof). This spatial period is very nearly identical to that of the oscillations in the backward traveling forced wave, which is given by $\pi/(q_1 + q_2/2)$. For this reason it is very difficult to determine to what degree the small scale beats are due to the oscillations in the backward traveling forced wave. Nonetheless, the measurement clearly shows the oscillations in

Figure 8.13: The second harmonic field for a 650 Hz, 135.7 dB fundamental Bloch wave. In (a) is shown the forward traveling, backward traveling, and local field components from the particular solution and the forward and backward traveling field components from the homogeneous solution. In (b) is shown both theoretical and experimental values of the resultant total field amplitude.

the amplitude of the forward traveling forced wave, and shows fairly good agreement with the theory.

In Fig. 8.14(a) is shown the amplitudes of the various components of the second harmonic field for a 880 Hz, 134.9 dB ($\epsilon = .0011$) fundamental Bloch wave. In Fig. 8.14(b) is shown the resultant total second harmonic field amplitude along with measurements. The forward traveling forced wave exhibits oscillations that peak near the waveguide termination. The amplitude of the forward traveling forced wave is near maximum at the terminiation and the backward traveling free wave is consequently of large amplitude. The resultant small scale oscillations are of large amplitude but are again primarily due to the compound field effect and not the backward traveling forced wave oscillations. The point of interest here is the *magnitude* of the generated second harmonic. The rate of increase in the forward traveling second harmonic forced wave amplitude with distance is much larger than that of a conventional wave. In other words, 880 Hz is a frequency for which the Bloch wave has a large effective nonlinearity (see Fig. 8.5). The effective value of beta for this wave is $|\beta_B| = 4.87$. In Fig. 8.15 is shown the data from Fig. 8.14(b) in the vicinity of the source along with the theoretical trajectory for the forward traveling forced wave. Included in the plot is the theoretical trajectory for the forward traveling forced wave for that case in which the effective nonlinearity is that of a conventional wave (i.e., $\beta_B = \beta = 1.20$). If we ignore the presence of the small scale oscillations due to the counter propagating waves, it is clear that the forward traveling forced wave indeed increases in amplitude at a rate that corresponds to a value of β that is closer to 4.87 than to 1.20, as the theory predicts.

In Fig. 8.16(a) is shown the amplitudes of the various components of the second harmonic field for a 940 Hz, 134.3 dB ($\epsilon = .0010$) fundamental Bloch wave. In Fig. 8.16(b) is shown the resultant total second harmonic field amplitude along with measurements. The large scale oscillations of the forward traveling forced wave are again clearly evident, and the rapid rate of increase of the second harmonic near the source is again a verification of a large effective nonlinearity (here, $|\beta_B| = 4.31$. The point of interest in this measurement, however, is to verify the presence of the local field. As may be seen in Fig. 8.12, the local field component is expected to be fairly significant
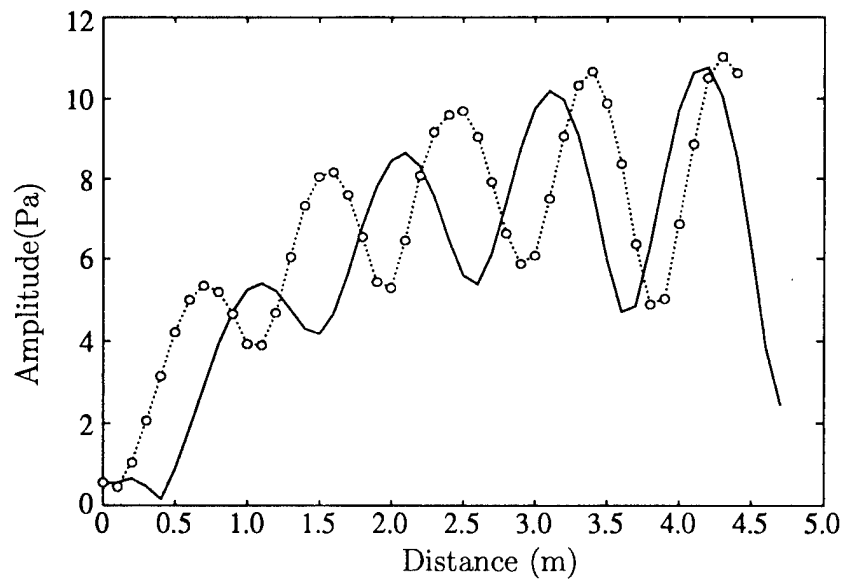
Figure 8.14: The second harmonic field for a 880 Hz, 134.9 dB fundamental Bloch wave. In (a) is shown the forward traveling, backward traveling, and local field components from the particular solution and the forward and backward traveling field components from the homogeneous solution. In (b) is shown both theoretical and experimental values of the resultant total field amplitude.
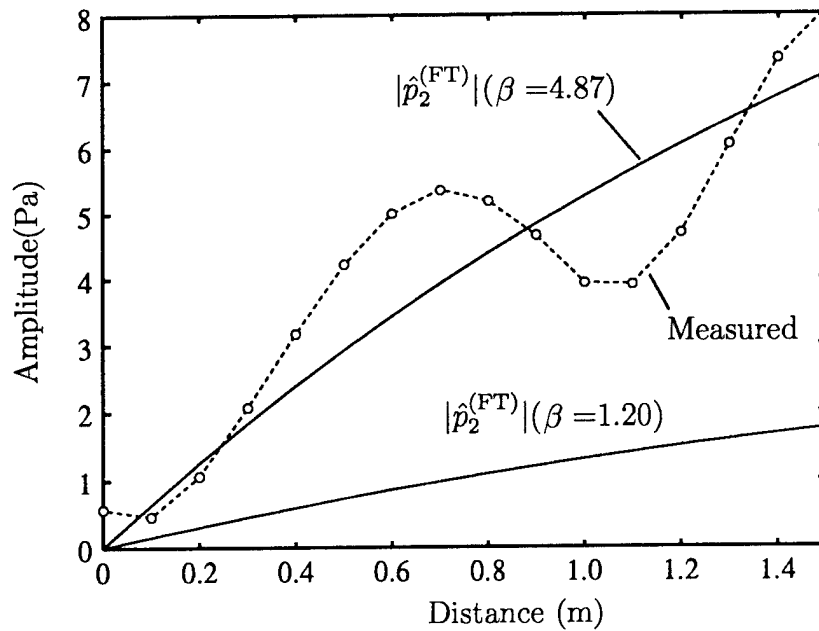
Figure 8.15: The second harmonic field near the source for a 880 Hz, 134.9 dB fundamental Bloch wave.

in the range of frequency near 940 Hz. In Fig. 8.16(a) it may be seen that the local field component is larger than all but the forward traveling forced wave component. While the theoretical and experimental trajectories do differ in some respects, the presence of a strong local field component is clearly evident in the large offset of the amplitude trajectory.
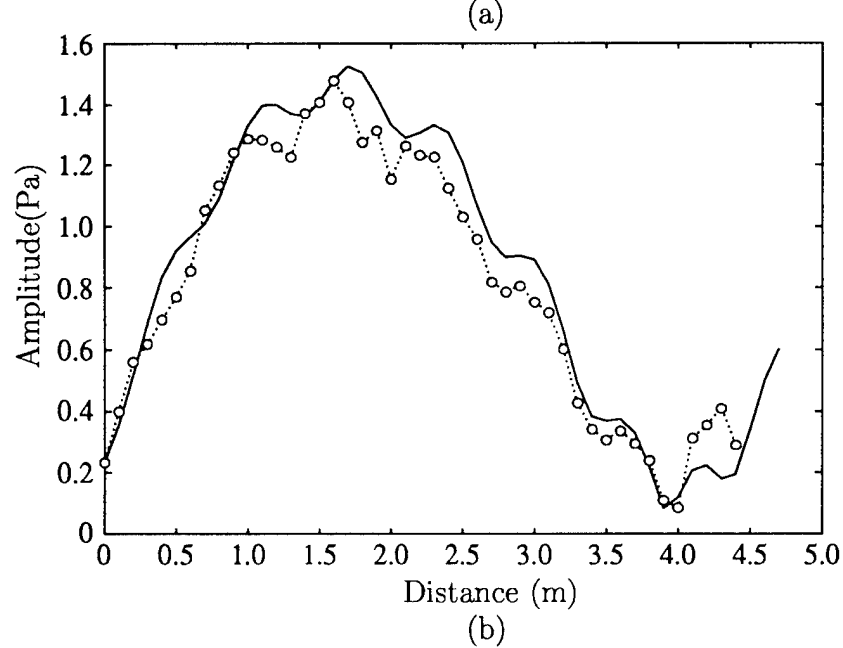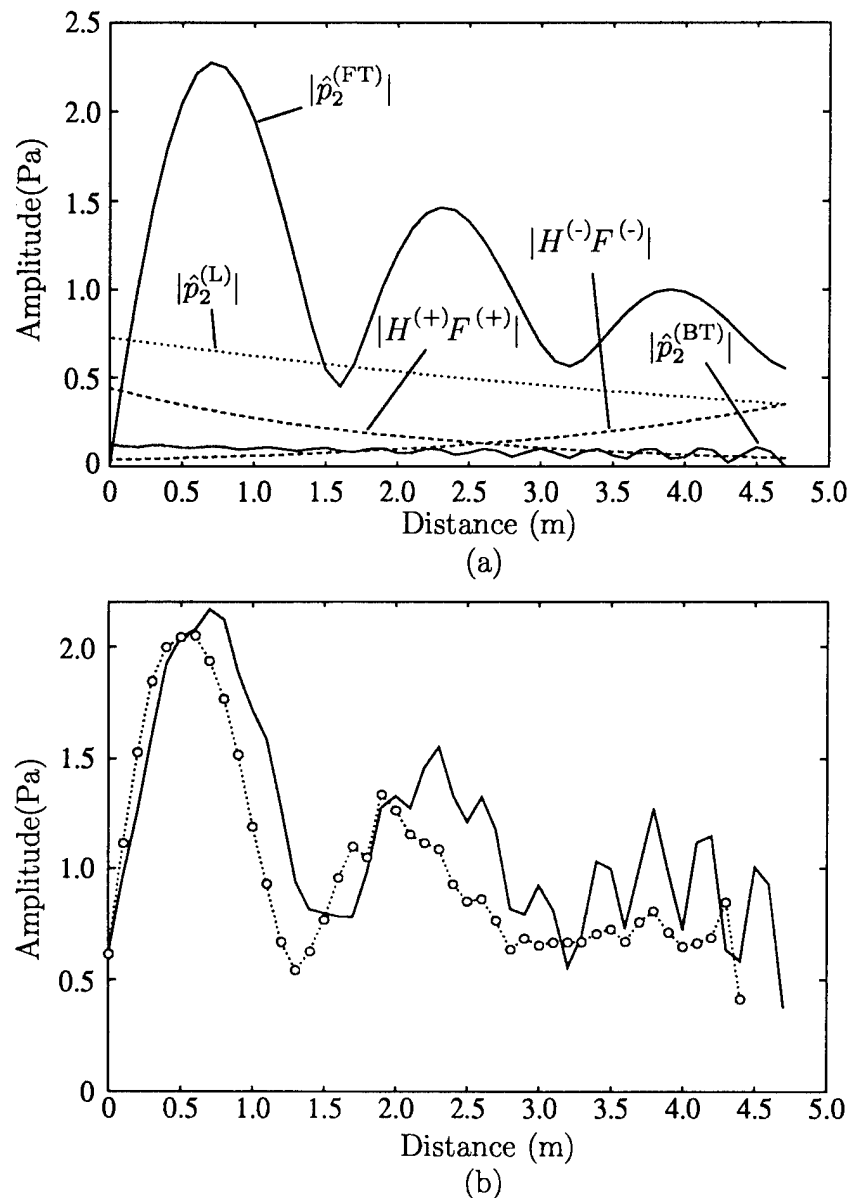
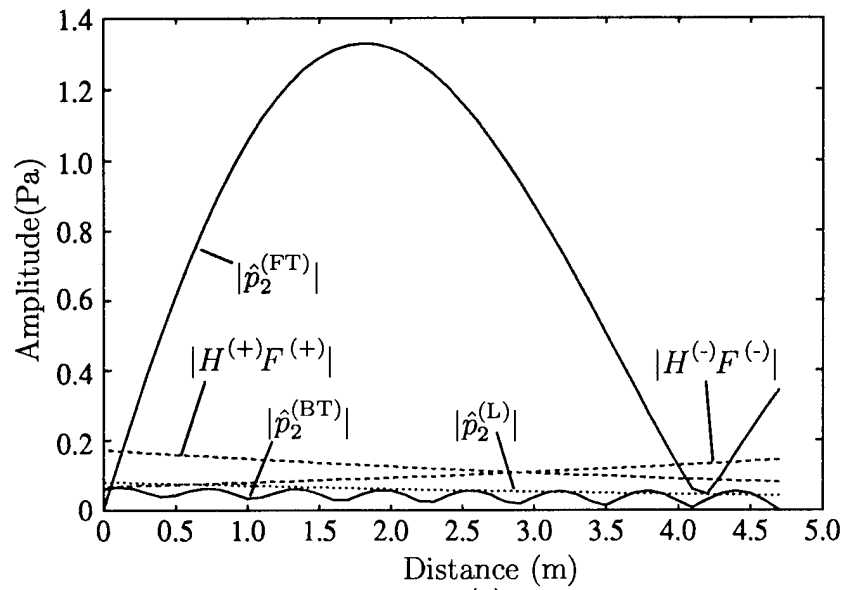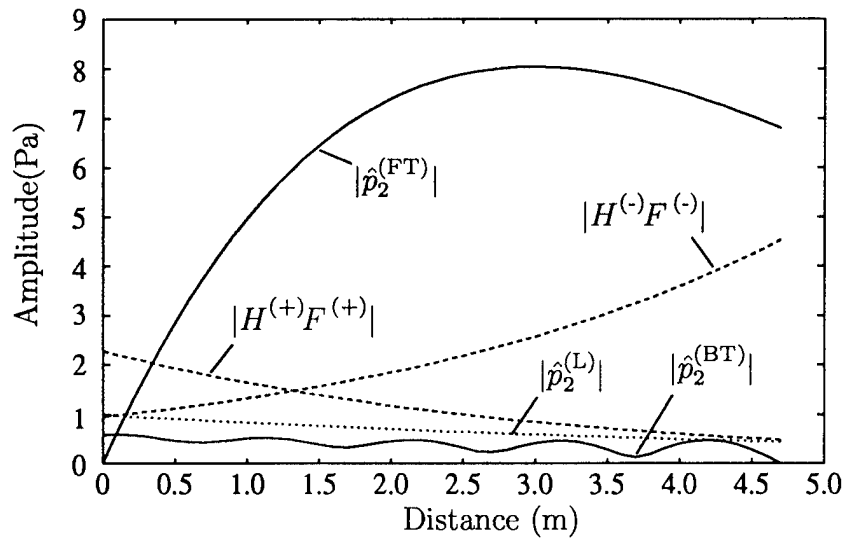**Figure 8.16**: The second harmonic field for a 940 Hz, 134.3 dB fundamental Bloch wave. In (a) is shown the forward traveling, backward traveling, and local field components from the particular solution and the forward and backward traveling field components from the homogeneous solution. In (b) is shown both theoretical and experimental values of the resultant total field amplitude.

This page intentionally left blank.

Chapter 9

Summary and Proposals for Future Work

9.1 Summary

This dissertation is composed of four parts. In the first part the problem of linear, time-harmonic wave propagation in a large class of periodic waveguides is addressed. It is shown that the Floquet theorem may be applied to the system in order to determine that the solutions may be expressed in terms of Bloch wave functions. The approach avoids the use of approximate model equations that have been used in the past and accounts for mechanisms of dissipation. Expressions for the parameters that characterize the Bloch waves (the dispersion function $q(\omega)$ and the relative component wave amplitude $g/f(\omega)$) are derived and their band structures investigated. It is found that reciprocity places significant constraints on the allowed Bloch wave solutions. These findings are verified experimentally for both isotropic and anisotropic periodic waveguides.

In the second part, the problem of Bloch wave pulse propagation is addressed. The dispersion integral that governs the propagation of Bloch wave pulses is derived and a straightforward method of solution is found. Several novel pulse propagation solutions that exhibit very unusual behavior are identified and verified experimentally. For example, it is found that in some cases the carrier frequency of the pulse shifts as it propagates, the pulse accelerates,

or the pulse propagates at near-infinite group velocity. The Bloch wave pulse problem is also considered for the case of asymptotically large propagation distances. Dependent upon how the pulse spectrum is situated with respect to the band structure of the dispersion function, several solutions are found. According to the various solutions, the pulse envelope may or may not remain localized, may distort into its own Fourier transform, or may be trailed by a long oscillating tail. Unfortunately, an experiment to verify these results is not practical.

In the third part, the problem of energy transport by acoustic Bloch waves is addressed. It is found that there are two different but physically relevant energy transport velocities associated with periodic waveguides. One of the energy transport velocities is verified experimentally and the other, which is simply the group velocity, is verified experimentally in Chapter 5.

In the fourth part, the effect of nonlinearity in the propagation of Bloch waves is considered. The approach to the solution of the problem is to first develop and then use a discrete Green's function method. This method does not require the approximate representations of the fundamental and second harmonic fields that have been used in earlier work. It is found that a forward traveling fundamental Bloch wave generates both forward and backward traveling second harmonic Bloch waves, each of which oscillates in amplitude as it propagates. As in the case of conventional nonlinear waves, dispersion disrupts the resonant generation of a second harmonic field and the second harmonic field level consequently remains small. In other words, the fundamental Bloch wave propagates with very little net distortion. This and other effects predicted by the theory are verified experimentally. The imposition of some sort of periodic structure into an otherwise uniform waveguide is therefore a means of suppressing the waveform distortion caused by nonlinearity.

9.2   The Contributions of the Work

In this work a number of contributions are made to the base of knowledge of acoustic Bloch waves in periodic waveguides. In addition, several contributions are made to the field of dispersive wave propagation in general. These contributions, which are both theoretical and experimental, are outlined here.

The contributions in the area of linear, time-harmonic Bloch waves are as follows. As is pointed out in Sec. 1.1, it had previously been shown that the solutions to periodic waveguide problems are Bloch waves only when (1) the system may be modeled by a (necessarily restrictive) ordinary differential equation, and (2) the system is nondissipative. It is found here that the solutions are Bloch wave functions for a very broad class of periodic waveguides that generally cannot be modeled with an ordinary differential equation, and are dissipative as well. To the author's knowledge, it had not before been shown that the Bloch wave formalism is valid in the presence of dissipation for *any* type of Bloch wave. While the features of the band structure of the Bloch wave dispersion are well known, these features had not been derived for a general system as they are here. The occurence of a stopband at the resonance frequencies of the scatterer is, to the author's knowledge, a previously unknown phenomenon. While detailed measurements of Bloch wave dispersion have been made in microwave systems, they have not been made before in acoustic systems. The measurements of g/f are certainly the first made for an acoustic Bloch wave system and are believed to be the first made for a Bloch wave system of any kind. The restrictions that reciprocity imposes on the allowed solutions of anisotropic periodic waveguide problems was not previously known.

The contributions of the work on Bloch wave pulse propagation are mainly in the area of narrowband pulse propagation in general. As far as the author is aware, the concept of the characteristic pulse distortion distance was not before known. It was not previously recognized that the key to the determination of the validity of solutions to the dispersion integral is a distance. As a result, the validity of the concept of group velocity was not recognized before as simply being distance dependent. As the large, absorption band group velocities were thought to not be valid, they had not been measured before. Similarly, the new pulse distortion solutions (the shifting carrier solution and the accelerating pulse solution) were neither known of nor verified in measurement. As far as the general theory of Bloch waves is concerned, the Bloch dispersion integral and the recovery operator solutions are also new.

While no previous work had been done on energy transport by acoustic Bloch waves, such work has been done in the context of microwaves. In that

discipline, however, the microscopic energy transport velocity had not been recognized. The measurement of the microscopic energy transport velocity here is therefore the first. While in the field of electromagnetic wave propagation in dispersive dielectrics it had been recognized that two different energy transport velocities exist, it was not before known that the same is true of Bloch wave systems.

While a substantial amount of work has been done in the area of nonlinear Bloch waves, the previous work was all done using a weak Bloch wave dispersion approximation. The present work represents an entirely different approach to the problem that is valid for arbitrarily strong Bloch wave dispersion. The measurement of the nonlinear effects is the first in an acoustic system.

Two interesting integral relations that did not previously exist were derived for this work. One is the exact dissipative reciprocity relation derived in Appendix A. Dissipative reciprocity relations derived in the past have made use of the lossy Helmholtz equation, which is valid only for irrotational flow and therefore valid only far from boundaries. The reciprocity relation derived here is exact and therefore valid even in the thermoviscous acoustic boundary layer. The other integral relation is the time-averaged energy integral derived in Chapter 7. The integral gives the time-averaged acoustic energy contained in a volume given the field at the boundary.

9.3 Proposals for Future Work

One interesting phenomenon that deserves more attention is the infinite stopband group velocity. It appears that it is allowable (in the causal sense) that the group velocity exceed the phase velocity *as long as the attenuation is large enough*. It seems that there must be a local causal constraint that relates the group velocity and the attenuation at any particular frequency. It may be that for a given group velocity, there is some minimum prescribed amount of attenuation.

While linear time-harmonic, nonlinear time-harmonic, and linear pulsed Bloch waves have been considered, nonlinear pulsed Bloch waves have not. As

it was found in the time harmonic case that a forward traveling fundamental Bloch wave generates both forward and backward traveling second harmonic Bloch waves, it seems that a forward traveling Bloch wave pulse must emit a steady stream of backward traveling second harmonic energy from its tail. Similarly, if the fundamental and second harmonic group velocities differ, the forward traveling second harmonic field that is generated in the body of the pulse could "leak out" of the region occupied by the fundamental pulse. While the importance of phase synchrony is clear in the nonlinear time harmonic problem, it appears that for the pulse problem *group* synchrony may be important as well.

While the problem of the nonlinear self interaction for a progressive Bloch wave field has been considered here, there are many other interesting nonlinear interaction scenarios that may yield interesting results. The nonlinear interaction of copropagating Bloch waves of different frequency, for example, is the simplest generalization of the present work that appears interesting. Further development could address the nonlinear interaction of counterpropagating Bloch waves. Once these issues are addressed, the nonlinear behavior of Bloch waves is well characterized. At that point, nonlinear dispersive model equations could be developed that model this behavior. These equations would undoubtedly be quite unusual as they must model the bidirectional generation of a second harmonic field by a progressive fundamental field. These equations could then be investigated for interesting solutions such as stationary (i.e., soliton) solutions.

This page intentionally left blank.

Appendix A

A Dissipative Reciprocity Theorem

A principle of reciprocity for a viscous, heat conducting fluid may be derived from the linearized set of governing equations (Eqs. 2.1-2.5) by way of the divergence theorem. With the inclusion of a mass source term, the equation of mass continuity becomes (e.g., Morse and Ingard, 1986)

$$\frac{\partial \rho}{\partial t} + \rho_0 \nabla \cdot \mathbf{u} = \dot{m}, \tag{A.1}$$

where $\dot{m}(\mathbf{r}, t)$ (in $kg/s/m^3$) is the mass injection rate density. We next use the entropy equation (Eq. 2.3) and the first of the thermodynamic expansions (Eq. 2.4) to replace the mass density term in Eq. A.1, which may then be written

$$\frac{\partial p}{\partial t} + \rho_0 c_0^2 \nabla \cdot \mathbf{u} = \frac{\beta c_0^2}{C_p} \kappa \nabla^2 T + \dot{m} c_0^2. \tag{A.2}$$

Under the time harmonic assumption, the momentum equation (Eq. 2.2) and Eq. A.2 become

$$\nabla p = j \omega \rho_0 \mathbf{u} + \mu \nabla^2 \mathbf{u} + (\mu_{\mathrm{B}} + \mu/3) \nabla \nabla \cdot \mathbf{u} \tag{A.3}$$

$$\nabla \cdot \mathbf{u} = \frac{j\omega}{\rho_0 c_0^2} p + \frac{\beta \kappa}{\rho_0 C_p} \nabla^2 T + \frac{1}{\rho_0} \dot{m}, \tag{A.4}$$

respectively.

A Lorentz-type reciprocity integral results from the following statement of the divergence theorem

$$\oint_S (p_1 \mathbf{u}_2 - p_2 \mathbf{u}_1) \cdot d\mathbf{S} = \int_V [p_1 \nabla \cdot \mathbf{u}_2 + \mathbf{u}_2 \cdot \nabla p_1 - p_2 \nabla \cdot \mathbf{u}_1 - \mathbf{u}_1 \cdot \nabla p_2] dV. \quad (A.5)$$

where p_1 and $\mathbf{u}_1$ represent the acoustic pressure and velocity fields due to the source distribution $\dot{m}_1$ and p_2 and $\mathbf{u}_2$ represent those due to the source distribution $\dot{m}_2$. The substitution of Eqs. A.3 and A.4 into the volume integral causes several terms to drop out and we are left with

$$\oint_S (p_1 \mathbf{u}_2 - p_2 \mathbf{u}_1) \cdot d\mathbf{S} = \frac{1}{\rho_0} \int_V [p_2 \dot{m}_1 - p_1 \dot{m}_2] dV + \frac{\beta \kappa}{\rho_0 C_p} \int_V [p_1 \nabla^2 T_2 - p_2 \nabla^2 T_1] dV$$

$$+ (\mu_B + \mu/3) \int_V [\mathbf{u}_2 \cdot \nabla(\nabla \cdot \mathbf{u}_1) - \mathbf{u}_1 \cdot \nabla(\nabla \cdot \mathbf{u}_2)] dV$$

$$+ \mu \int_V [\mathbf{u}_2 \cdot \nabla^2 \mathbf{u}_1 - \mathbf{u}_1 \cdot \nabla^2 \mathbf{u}_2] dV. \quad (A.6)$$

The combination of the entropy equation (Eq. 2.3) with the second of the thermodynamic expansions (Eq. 2.5) results in the pressure-temperature relation

$$p = \frac{\rho_0 C_p}{T_0 \beta} T + \frac{\kappa}{j\omega \beta T_0} \nabla^2 T. \quad (A.7)$$

We next use Eq. A.7 to eliminate the pressure in the second volume integral of Eq.A.6, which becomes

$$\frac{\beta \kappa}{\rho_0 C_p} \int_V [p_1 \nabla^2 T_2 - p_2 \nabla^2 T_1] dV = \frac{\kappa}{T_0} \int_V [T_1 \nabla^2 T_2 - T_2 \nabla^2 T_1] dV. \quad (A.8)$$

We next use the following relations to convert the integrands in the second through the fourth volume integrals of Eq. A.6 into divergences:

$$\nabla \cdot [T_1 \nabla T_2 - T_2 \nabla T_1] = T_1 \nabla^2 T_2 - T_2 \nabla^2 T_1$$

$$\frac{\partial}{\partial x_i} \left[u_{2j} \frac{\partial u_{1j}}{\partial x_i} - u_{1j} \frac{\partial u_{2j}}{\partial x_i} \right] = \mathbf{u}_2 \cdot \nabla^2 \mathbf{u}_1 - \mathbf{u}_1 \cdot \nabla^2 \mathbf{u}_2$$

$$\frac{\partial}{\partial x_j} \left[u_{2i} \frac{\partial u_{1j}}{\partial x_i} - u_{1i} \frac{\partial u_{2j}}{\partial x_i} \right] = \mathbf{u}_2 \cdot \nabla(\nabla \cdot \mathbf{u}_1) - \mathbf{u}_1 \cdot \nabla(\nabla \cdot \mathbf{u}_2).$$

The substitution of the above relations into Eq. A.6 (also making use of Eq. A.8) and the conversion of the resultant volume integrals over divergences into surface integrals results in

$$\oint_S (p_1 \mathbf{u}_2 - p_2 \mathbf{u}_1) \cdot d\mathbf{S} - \frac{1}{\rho_0} \int_V [p_2 \dot{m}_1 - p_1 \dot{m}_2] dV =$$

$$\frac{\kappa}{T_0} \oint_S [T_1 \nabla T_2 - T_2 \nabla T_1] \cdot d\mathbf{S} + \mu \oint_S [u_{2j} \frac{\partial u_{1j}}{\partial x_i} - u_{1j} \frac{\partial u_{2j}}{\partial x_i}] dS_i$$

$$+ (\mu_B + \mu/3) \oint_S [u_{2i} \frac{\partial u_{1j}}{\partial x_i} - u_{1i} \frac{\partial u_{2j}}{\partial x_i}] dS_j. \quad (A.9)$$

Equation A.9 is a Lorentz-type reciprocity relation that is exact in the dissipation parameters. Note that in the absence of dissipative mechanisms the right-hand side of Eq. A.9 is zero and we have

$$\oint_S (p_1 \mathbf{u}_2 - p_2 \mathbf{u}_1) \cdot d\mathbf{S} = \frac{1}{\rho_0} \int_V [p_2 \dot{m}_1 - p_1 \dot{m}_2] dV,$$

the standard Lorentz-type reciprocity relation for acoustic fields. Note also that the dissipative terms all appear in the surface integrals, and that the surface integrals vanish on rigid, isothermal surfaces such as the waveguide wall.

In order to investigate the implications of reciprocity on the behavior of the scatterers, we apply the reciprocity principle to a system that consists of a single scatterer in an otherwise uniform waveguide. More specifically, we consider a volume that includes the scatterer and lengths of uniform waveguide on either side of the scatterer. The surface S that encloses this volume is composed of four parts: the waveguide wall surface S_{WW}, the surface of any inclusions S_I, and the end cap surfaces S_1 and S_2, which are normal to the z-axis. The source distributions $\dot{m}_1$ and $\dot{m}_2$ are assumed to be confined to regions of the waveguide far enough from the volume under consideration that any evanescent modal fields generated at the sources are negligible at S_1 and S_2. The surfaces S_1 and S_2 are also assumed to be far enough from the scatterer that evanescent modal fields generated at the scatterer are likewise negligible. The reciprocity integral (Eq.A.9) simplifies greatly in the case of this system because (1), the volume is source-free, and (2), owing to the boundary conditions (Eq. 2.6), the integrands of the surface integrals are zero on S_{WW} and S_I. The only nonzero contributions come from the end cap surface integrals.

In order to evaluate the end cap integrals, we develop a convenient notation for the dissipative zeroth order mode (i.e., quasi-planar mode) wave functions associated with the uniform waveguide. We define $P^{(\pm)}(\mathbf{r}_\perp)$, $\mathbf{U}^{(\pm)}(\mathbf{r}_\perp)$, and $T^{(\pm)}(\mathbf{r}_\perp)$ to be the transverse mode functions for the pressure, velocity, and temperature fields associated with a forward (+) or backward (-) traveling wave. The transverse coordinate $\mathbf{r}_\perp$ is defined such that $\mathbf{r} = \mathbf{r}_\perp + z\hat{\mathbf{e}}_z$, and the functions are normalized such that $\max|P^{(\pm)}| = \max|\mathbf{U}^{(\pm)}| = \max|T^{(\pm)}| = 1$. In this notation, the field variables associated with a forward traveling wave are

$$p(\mathbf{r}) = AP^{(+)}(\mathbf{r}_\perp)e^{jkz}$$

$$\mathbf{u}(\mathbf{r}) = \frac{A}{Z_u}\mathbf{U}^{(+)}(\mathbf{r}_\perp)e^{jkz} \tag{A.10}$$

$$T(\mathbf{r}) = \frac{A}{Z_T}T^{(+)}(\mathbf{r}_\perp)e^{jkz}, \tag{A.11}$$

where

$$Z_u = \frac{\max|p(\mathbf{r})|}{\max|\mathbf{u}(\mathbf{r})|} \quad \text{(fixed } z\text{)} \tag{A.12}$$

is a sort of dissipative mode impedance and

$$Z_T = \frac{\max|p(\mathbf{r})|}{\max|T(\mathbf{r})|} \quad \text{(fixed } z\text{)} \tag{A.13}$$

is a "thermal impedance". With the use of simple symmetry arguments, it is found that the transverse mode functions associated with the backward traveling field may be related to those associated with the forward traveling field by

$$P^{(-)} = P^{(+)} \qquad T^{(-)} = T^{(+)} \qquad \mathbf{U}^{(-)} = \mathbf{U}_\perp^{(+)} - U_z^{(+)}\hat{\mathbf{e}}_z,$$

where $\mathbf{U}_\perp^{(\pm)}$, the transverse component of the velocity field, is defined by $\mathbf{U}^{(\pm)} = \mathbf{U}_\perp^{(\pm)} + U_z^{(\pm)}\hat{\mathbf{e}}_z$.

The acoustic pressure field at the end caps that arise from each of the source distributions may be expressed completely generally as follows. The waves incident upon the scatterer from the left and right due to the source distribution $\dot{m}_1$ are of amplitudes C^+ and C^-, respectively[1]. Likewise, the

---

[1] All wave amplitudes are referenced to their values at the scatterer.

waves incident upon the scatterer from the left and right due to the source distribution $\dot{m}_2$ are of amplitudes D^+ and D^-, respectively. The field at the each end cap surface is composed of these incident waves and the resultant scattered waves. The field in the waveguide in the vicinity of the end cap surface S_1 (that to the left of the scatterer) may be written

$$p_1(\mathbf{r}) = C^+ P^{(+)}(\mathbf{r}_\perp)e^{jkz} + (S_{11}C^+ + S_{12}C^-)P^{(-)}(\mathbf{r}_\perp)e^{-jkz}$$

$$p_2(\mathbf{r}) = D^+ P^{(+)}(\mathbf{r}_\perp)e^{jkz} + (S_{11}D^+ + S_{12}D^-)P^{(-)}(\mathbf{r}_\perp)e^{-jkz},$$

and that in the vicinity of the end cap surface S_2 (that to the right of the scatterer) may be written

$$p_1(\mathbf{r}) = C^- P^{(-)}(\mathbf{r}_\perp)e^{-jkz} + (S_{21}C^+ + S_{22}C^-)P^{(+)}(\mathbf{r}_\perp)e^{jkz}$$

$$p_2(\mathbf{r}) = D^- P^{(-)}(\mathbf{r}_\perp)e^{-jkz} + (S_{21}D^+ + S_{22}D^-)P^{(+)}(\mathbf{r}_\perp)e^{jkz}.$$

The associated velocity and temperature fields may be found from the pressure fields by way of Eqs. A.10-A.13. The substitution of these fields into the reciprocity relation (Eq. A.9) results in

$$[S_{21} - S_{12}](C^+D^- - C^-D^+)\left\{ \frac{2}{Z_u}\int P^{(+)}U_z^{(+)}dS + \frac{\kappa}{T_0}\frac{2jk}{Z_T^2}\int T^{(+)2}dS \right.$$

$$+\mu\frac{2jk}{Z_u^2}\int[\mathbf{U}_\perp^{(+)}\cdot\mathbf{U}_\perp^{(+)} - U_z^{(+)2}]dS$$

$$\left. + (\mu_B + \mu/3)\frac{2jk}{Z_u^2}\int[\frac{1}{jk}\mathbf{U}_\perp^{(+)}\cdot\nabla_\perp U_z^{(+)} - U_z^{(+)2}]dS \right\} = 0.$$

$$\text{(A.14)}$$

The implications of this result are most readily found by consideration first of the nondissipative case. In the absence of dissipation we have $\kappa = \mu = \mu_B \to 0$, $P^{(+)} = U_z^{(+)} \to 1$ (plug flow), $Z_u \to Z_0 = \rho_0 c_0$, and Eq. A.14 becomes

$$[S_{21} - S_{12}](C^+D^- - C^-D^+)(2/Z_{0a}) = 0.$$

Because C^-, C^+, D^-, and D^+ are *incident* wave amplitudes and are therefore independently adjustable, it is generally the case that $C^+D^- - C^-D^+ \neq 0$. It therefore must be the case that $S_{12} = S_{21}$. This is the constraint reciprocity

places on the scattering matrix elements. In the dissipative case, the term in Eq. A.14 enclosed in curly braces $\{\cdot\}$, like the term $(C^+D^- - C^-D^+)$, is not generally equal to zero. Because the fluid dissipation parameters κ, μ, and μ_B may take on any positive, real value, the integrals do not generally balance to exactly zero, and again we must have $S_{12} = S_{21}$. A simple approximation is illustrative. As the dissipation becomes small, we have $P^{(+)}, U_z^{(+)}, T^{(+)} \simeq 1$, $U_\perp^{(+)} \simeq 0$ (nearly plug flow), $Z_u \simeq \rho_0 c_0$, and $Z_T \simeq \rho_0 C_p/T_0\beta$. Equation A.14 becomes

$$[S_{21} - S_{12}](C^+D^- - C^-D^+)\frac{2}{Z_{0a}}\left\{1 + \frac{jk}{\rho_0 c_0}\left[\frac{\beta^2 T_0 c_0^2 \kappa}{C_p^2} - \mu_B - 4\mu/3\right]\right\} = 0.$$

The real and imaginary terms in the curly braces cannot combine to zero, and again we must have $S_{12} = S_{21}$.

Appendix B

The Scattering and Transmission Matrices

The S-matrix and T-matrix approaches are equivalent methods of relating the amplitudes of the traveling waves that occur in the vicinity of a scatterer. The S-matrix or scattering matrix relates the amplitudes of the outgoing or scattered waves to those of the incoming or incident waves. The T-matrix or transmission matrix relates the amplitudes of the forward and backward traveling waves on one side of a scatterer to those on the other side. In order to define these matrices, we first define the amplitudes of the forward and backward traveling waves on one side of a scatterer to be $a^{(+)}$ and $a^{(-)}$, respectively, and those on the other side to be $b^{(+)}$ and $b^{(-)}$, as shown schematically in Fig. B.1.

The elements of the S matrix are simply reflection and transmission coefficients. The reflection coefficients for waves incident from the left and right are labeled S_{11} and S_{22}, respectively, and the transmission coefficients for waves incident from the left and right are S_{21} and S_{12}, respectively. These waves are shown schematically in Fig. 2.1. The amplitudes of the outgoing waves ($a^{(-)}$ and $b^{(+)}$) may be expressed in terms of the amplitudes of the incoming waves ($a^{(+)}$ and $b^{(-)}$) as follows:

$$a^{(-)} = S_{11}a^{(+)} + S_{12}b^{(-)}$$

$$b^{(+)} = S_{21}a^{(+)} + S_{22}b^{(-)}.$$

255

This is the S-matrix form of the relationship among the incident and scattered waves. The T-matrix is found by solving for the amplitudes of the waves on the right of the scatterer in terms of those on the left of the scatterer. The result is a similar pair of equations. In matrix form, these equations may be expressed

$$\begin{bmatrix} a^{(-)} \\ b^{(+)} \end{bmatrix} = \mathbf{S} \begin{bmatrix} a^{(+)} \\ b^{(-)} \end{bmatrix} \qquad \begin{bmatrix} b^{(+)} \\ b^{(-)} \end{bmatrix} = \mathbf{T} \begin{bmatrix} a^{(+)} \\ a^{(-)} \end{bmatrix}, \qquad (B.1)$$

where

$$\mathbf{S} = \begin{bmatrix} S_{11} & S_{12} \\ S_{21} & S_{22} \end{bmatrix} \qquad \mathbf{T} = \frac{1}{S_{12}} \begin{bmatrix} -|S| & S_{22} \\ -S_{11} & 1 \end{bmatrix}. \qquad (B.2)$$
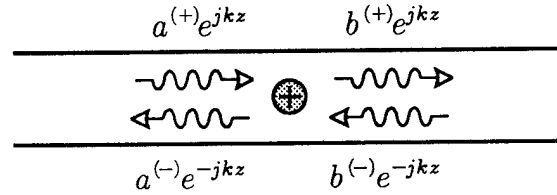
Figure B.1: The traveling waves near a scatterer.

The *cell* T-matrix $\mathbf{T}^C$ is defined to be the T-matrix that relates the field at a point a distance $h/2$ to one side of the scatterer and that at a point a distance $h/2$ to the other side. In other words, the cell T-matrix relates the fields at the centers of neighboring cells. With the definition of the propagation T-matrix or propagator $\mathbf{T}^P(z)$, which is that associated with propagation over a distance z,

$$\mathbf{T}^P(z) = \begin{bmatrix} e^{jkz} & 0 \\ 0 & e^{-jkz} \end{bmatrix}, \qquad (B.3)$$

the cell T-matrix may be expressed $\mathbf{T}^C = \mathbf{T}^P(h/2)\mathbf{T}\mathbf{T}^P(h/2)$, or

$$\mathbf{T}^C = \begin{bmatrix} T_{11}e^{jkh} & T_{12} \\ T_{21} & T_{22}e^{-jkh} \end{bmatrix}.$$

As the S and T-matrices are equivalent characterizations of a scatterer, the elements of the T-matrix may be expressed in terms of those of the S-matrix

and vice-versa. From Eqs. B.1 we find

$$\mathbf{T}^C = \frac{1}{S_{12}} \begin{bmatrix} -|S|e^{jkh} & S_{22} \\ -S_{11} & e^{-jkh} \end{bmatrix} \qquad \mathbf{S} = \frac{e^{-jkh}}{T_{22}^C} \begin{bmatrix} -T_{21}^C & 1 \\ |T^C| & T_{12}^C \end{bmatrix}, \qquad (B.4)$$

where $|T^C|$ denotes the determinant of the cell T-matrix. Note that the relationship between the T-matrix and the S-matrix is simply that shown in Eq. B.4 in the limit as $h \to 0$.

We may now investigate the restrictions that are placed on the values of the elements of these matrices by such conditions as reciprocity, energy conservation, and symmetry in the scatterer. In Appendix A it is shown that the principle of reciprocity, regardless of whether or not energy is conserved, requires that $S_{12} = S_{21}$. With the use of expressions for S_{12} and S_{21} from Eq. B.4, we find that the principle of reciprocity requires

$$S_{12} = S_{21} \quad \text{or} \quad |T^C| = 1. \qquad (B.5)$$

If the system is nondissipative, then the power incident upon a scatterer must equal the power scattered from the scatterer. If there is no wave incident from the $-z$ side (i.e., if $b^{(-)} = 0$), then the statement of power conservation is $|a^{(+)}|^2 = |a^{(-)}|^2 + |b^{(+)}|^2$ or, from Eq. B.1,

$$|S_{11}|^2 + |S_{21}|^2 = 1. \qquad (B.6)$$

If instead there is no wave incident from the $+z$ side, then

$$|S_{12}|^2 + |S_{22}|^2 = 1. \qquad (B.7)$$

If both incident waves are present, then we find, using Eqs. B.6 and B.7,

$$S_{11}S_{12}^* + S_{21}S_{22}^* = 0. \qquad (B.8)$$

In terms of the cell T-matrix, the above power conservation relations may be written

$$1 + |T_{21}^C|^2 = |T_{22}^C|^2 \qquad 1 + |T_{12}^C|^2 = |T_{22}^C|^2 \qquad -T_{21}^C + |T^C|T_{12}^{C*} = 0. \qquad (B.9)$$

With the use of the reciprocity requirement $|T^C| = 1$, Eqs. B.9 may be combined and the energy conservation requirement becomes

$$T_{21}^C = T_{12}^{C*} \qquad T_{11}^C = T_{22}^{C*}. \qquad (B.10)$$

If the scatterer is symmetric under axial reversal (as they are in an isotropic periodic waveguide), then the reflection and transmission properties of the scatter must be the same for waves incident from either side. It therefore must be the case that

$$S_{12} = S_{21} \qquad S_{11} = S_{22},$$
(B.11)

or, equivalently,

$$T_{21}^{\mathrm{C}} = -T_{12}^{\mathrm{C}}.$$

Appendix C

The Solutions of the Microstructure Equation

In this appendix we consider the constraints on the solutions to the microstructure equation (Eq. 3.11) that are imposed by the principles of reciprocity and conservation of energy. In Appendix B it is shown that the principle of conservation of energy imposes three conditions on the T-matrix elements (see Eq. B.9) and the principle of reciprocity imposes one (see Eq. B.5). These constraints may be combined to yield the alternative set of constraints

$$T_{21}^C = T_{12}^{C*} \qquad T_{11}^C = T_{22}^{C*} \qquad 1 + |T_{12}^C|^2 = |T_{22}|^2. \qquad (C.1)$$

From these relations it follows that $\mathrm{Re}\{T_{11}^C\}^2 - 1 = |T_{12}^C|^2 - \mathrm{Im}\{T_{11}^C\}^2$. Because $|\mathrm{Re}\{T_{11}^C\}| > 1$ is the condition for a stopband (see the discussion following Eq. 3.7), it follows that the condition

$$|T_{12}^C|^2 - \mathrm{Im}\{T_{11}^C\}^2 > 0 \qquad (C.2)$$

is also a stopband condition.

We now consider the magnitudes of $\sigma_{02}/\sigma_{01}^{(\pm)}$ and $g/f^{(\pm)}$. In the absence of dissipation, the microstructure equation (Eq. 3.11) becomes

$$T_{12}^C(\sigma_{02}/\sigma_{01})^2 + 2j\mathrm{Im}\{T_{11}^C\}(\sigma_{02}/\sigma_{01}) - T_{12}^{C*} = 0,$$

and the solutions may be written

$$\sigma_{02}/\sigma_{01}^{(\pm)} = \frac{-j\mathrm{Im}\{T_{11}^C\} \mp \left[|T_{12}^C|^2 - \mathrm{Im}\{T_{11}^C\}^2\right]^{1/2}}{T_{12}^C}. \qquad (C.3)$$

In the stopbands, the argument of the square root is, by the stopband condition (Eq. C.2), positive and real, and we have

$$|\sigma_{02}/\sigma_{01}^{(\pm)}| = 1. \qquad (C.4)$$

In the passbands, the argument of the square root is negative and real, and we have

$$|\sigma_{02}/\sigma_{01}^{(\pm)}| = \frac{|\mathrm{Im}\{T_{11}^C\}|}{|T_{12}^C|} \left[1 \mp \left(1 - \frac{|T_{12}^C|^2}{\mathrm{Im}\{T_{11}^C\}^2}\right)^{1/2}\right]. \qquad (C.5)$$

From Eq. C.2 it must be the case that in the passbands

$$0 \leq \left(1 - |T_{12}^C|^2/\mathrm{Im}\{T_{11}^C\}^2\right)^{1/2} \leq 1.$$

From this passband condition and Eq. C.5 it follows that, in the passbands,

$$|\sigma_{02}/\sigma_{01}^{(-)}| > 1 \quad \text{and} \quad |\sigma_{02}/\sigma_{01}^{(+)}| < 1. \qquad (C.6)$$

These findings may be cast in terms of the parameter g/f, and we have (from Eq. C.4) the stopband condition

$$|g/f^{(\pm)}| = 1,$$

and (from Eq. C.6) the passband condition

$$|g/f^{(\pm)}| < 1.$$

The relationship between $\sigma_{02}/\sigma_{01}^{(+)}$ and $\sigma_{02}/\sigma_{01}^{(-)}$ is found by consideration of Eq. C.3. In the passbands, we have

$$\sigma_{02}/\sigma_{01}^{(\pm)} = \frac{-j\mathrm{Im}\{T_{11}^C\} \mp j \left[\mathrm{Im}\{T_{11}^C\}^2 - |T_{12}^C|^2\right]^{1/2}}{T_{12}^C}, \qquad (C.7)$$

where the argument of the square root is real and positive. Using the relations $\sigma_{02}/\sigma_{01}^{(-)} = [-(T_{12}^C/T_{21}^C)\sigma_{02}/\sigma_{01}^{(+)}]^{-1}$ (from the discussion following Eq. 3.11) and $T_{21}^C = T_{12}^{C*}$ (from Eq. C.1), we find

$$\sigma_{02}/\sigma_{01}^{(-)} = \frac{T_{12}^{C*}}{j\mathrm{Im}\{T_{11}^C\} + j\,[\mathrm{Im}\{T_{11}^C\}^2 - |T_{12}^C|^2]^{1/2}}. \qquad (C.8)$$

Equations C.7 and C.8 may be used to verify the relation

$$[\sigma_{02}/\sigma_{01}^{(-)}][\sigma_{02}/\sigma_{01}^{(+)*}] = 1,$$

which in turn implies

$$g/f^{(-)} = g/f^{(+)*}.$$

If the scatterers are symmetric (under axial reversal) as well as nondissipative, then we must have $S_{21} = S_{12}$ and $S_{11} = S_{22}$ or, equivalently, $T_{21}^C = -T_{12}^C$. As reciprocity and energy conservation require $T_{21}^C = T_{12}^{C*}$, it must be that for a nondissipative scatterer, T_{12}^C and T_{21}^C are imaginary. From Eq. C.3, therefore, it must be that σ_{02}/σ_{01}, and therefore g/f as well, are real in the passbands.

This page intentionally left blank.

Appendix D

The Side Branch Scattering Parameters

Here we derive the cell T-matrix elements associated with the isotropic and anisotropic periodic waveguides described in the introduction. The approach is to derive the S-matrix elements associated with a single side branch and then use Eqs. B.3 and B.4 to determine the associated cell T-matrices.

The S-matrix elements associated with a single side branch are derived by imposition of the requirement that the acoustic pressure and velocity fields must be continuous at the side branch opening. For the case of a wave of amplitude A incident on the side branch from the left, the acoustic pressure field in the waveguide may be expressed

$$p = \begin{cases} Ae^{jk\xi} + S_{11}Ae^{-jk\xi} & \xi < 0 \\ S_{21}Ae^{jk\xi} & \xi > 0 \end{cases},$$

where ξ is a shifted axial coordinate centered on the side branch. The field in the side branch may be written

$$p = S_{\mathrm{sb}}A(e^{-jk_{\mathrm{sb}}y} + e^{jk_{\mathrm{sb}}(y+2d)}),$$

where S_{sb} is the coefficient of scattering into the side branch. The requirement that the acoustic pressure field be continuous yields

$$1 + S_{11} = S_{21} = S_{\mathrm{sb}}(1 + e^{2jk_{\mathrm{sb}}d}),$$

263

and the requirement that the velocity field be continuous yields

$$A_{\text{wg}}(1 - S_{11}) - A_{\text{wg}}S_{21} - A_{\text{sb}}S_{\text{wg}}(1 - e^{2jk_{\text{sb}}d}) = 0.$$

The solution of these equations for the scattering parameters yields

$$S_{\text{sb}} = \frac{1}{[1 + \frac{1}{2}(A_{\text{sb}}/A_{\text{wg}})] + [1 - \frac{1}{2}(A_{\text{sb}}/A_{\text{wg}})]e^{2jk_{\text{sb}}d}}$$

$$S_{11} = \frac{-1}{1 + 2j(A_{\text{wg}}/A_{\text{sb}})\cot(k_{\text{sb}}d)}$$

$$S_{21} = \frac{1}{1 - \frac{1}{2}j(A_{\text{sb}}/A_{\text{wg}})\tan(k_{\text{sb}}d)}.$$

Because the scatterer is symmetric, from Eq. B.11 we also have $S_{22} = S_{11}$ and $S_{12} = S_{21}$. We may now use Eq. B.4 to find the T-matrix elements:

$$\mathbf{T}(d) = \begin{bmatrix} 1 + \frac{1}{2}j(A_{\text{sb}}/A_{\text{wg}})\tan(k_{\text{sb}}d) & \frac{1}{2}j(A_{\text{sb}}/A_{\text{wg}})\tan(k_{\text{sb}}d) \\ -\frac{1}{2}j(A_{\text{sb}}/A_{\text{wg}})\tan(k_{\text{sb}}d) & 1 - \frac{1}{2}j(A_{\text{sb}}/A_{\text{wg}})\tan(k_{\text{sb}}d) \end{bmatrix}. \qquad (\text{D.1})$$

The cell T-matrix for the isotropic periodic waveguide is simply given by

$$\mathbf{T}^{\text{C}} = \mathbf{T}^{\text{P}}(h/2)\mathbf{T}(d)\mathbf{T}^{\text{P}}(h/2)$$

$$= \begin{bmatrix} [1 + \frac{1}{2}j(A_{\text{sb}}/A_{\text{wg}})\tan(k_{\text{sb}}d)]e^{jkh} & \frac{1}{2}j(A_{\text{sb}}/A_{\text{wg}})\tan(k_{\text{sb}}d) \\ -\frac{1}{2}j(A_{\text{sb}}/A_{\text{wg}})\tan(k_{\text{sb}}d) & [1 - \frac{1}{2}j(A_{\text{sb}}/A_{\text{wg}})\tan(k_{\text{sb}}d)]e^{-jkh} \end{bmatrix}, \qquad (\text{D.2})$$

where $\mathbf{T}^{\text{P}}(z)$ is the propagator defined in Appendix B. The cell T-matrix for the anisotropic periodic waveguide is given by

$$\mathbf{T}^{\text{C}} = \mathbf{T}_{\text{p}}(h/3)\mathbf{T}(d_1)\mathbf{T}_{\text{p}}(h/3)\mathbf{T}(d_2)\mathbf{T}_{\text{p}}(h/3), \qquad (\text{D.3})$$

the explicit form of which is very lengthy and not worth showing.

The S and T-matrix elements may be adjusted to improve their accuracy by use of the end-corrected side branch length $\hat{d} = d + \Delta d$ in place of the physical length d. The additional length Δd corrects for the inertial load on the side branch field due to the mass of the fluid at its opening. The usual end correction is for a circular opening of radius a and is given by $\Delta d = 8a/3\pi$ (e.g., Morse, 1976). Using the side branch width l in place of the diameter of the circular opening we get $\hat{d} = d + 4l/3\pi$, which is the corrected side branch depth used here.

Appendix E

Measurement and Data Analysis Techniques

In this appendix the details of the experiment are presented. The design and construction of the periodic waveguide and the various microphone configurations are described. The setup of the instrumentation is presented and the data acquisition algorithms are outlined. In the cases of the dispersion, g/f, and pulse measurements, for which the post-measurement analysis of the data is substantial, the subsequent processing of the data is described.

The periodic waveguide systems in which the measurements are made are described in Sec. 1.3.1. On one end of the section of periodic waveguide is mounted a compression driver and on the other is a termination of acoustic impedance $\rho_0 c_0 / A_{\rm wg}$. Because the throat of the driver is a nearly uniform waveguide, we have a system in which conventional waves are incident upon (and partially reflected from) the periodic waveguide, in which a Bloch wave is excited. The resultant Bloch wave is in turn incident upon, and partially reflected from, the terminating waveguide, in which the resultant conventional wave field is progressive. *The Bloch wave field, however, is compound.*

It should be noted that the extraction of information from the data set would be much simpler if the measurements were performed in a progressive Bloch wave field. As a practical matter, however, we are limited to making measurements in a compound Bloch wave field. The realization of a progressive Bloch wave field requires the termination of the periodic waveguide into the

265

Bloch acoustic impedance, which is a wildly varying function of frequency that would be prohibitively difficult to synthesize for anything but a very narrow band of frequencies (see Sec. 4.1).

E.1 The Experimental System

The design of the isotropic periodic waveguide system is as follows. The termination waveguide is 1.2 m long and is loaded with a 1.0 m long, gently tapered anechoic fiberglass wedge. The periodic waveguide has the following dimensions: The design of the isotropic periodic waveguide system is as follows. The termination waveguide is 1.2 m long and is loaded with a 1.0 m long, gently tapered anechoic fiberglass wedge. The periodic waveguide has the following dimensions:

$$
\begin{array}{llll}
\text{waveguide period:} & h & = & .1\ \text{m} \\
\text{side branch depth:} & d & = & 38.1\ \text{mm} \quad (1\text{-}1/2\ \text{in.}) \\
\text{side branch width:} & l & = & 9.5\ \text{mm} \quad (3/8\ \text{in.}) \\
\text{waveguide height:} & b & = & 25.4\ \text{mm} \quad (1\ \text{in.}) \\
\text{waveguide width:} & a & = & 38.1\ \text{mm} \quad (1\text{-}1/2\ \text{in.})
\end{array}
$$

The dimensions were chosen such that a scatterer resonance stopband occurs roughly midway between the π and the 2π Bragg stopbands without overlap. Such a stopband structure allows the two species of stopbands to be experimentally investigated independently of one another. For the chosen dimensions, the π and 2π stopbands are expected to occur at roughly 1.7 and 3.4 kHz, respectively, with the intervening scatterer resonance stopband at roughly 2.2 kHz.

The anisotropic waveguide system is simply the isotropic waveguide system with selected side branches filled or half filled. Every third side branch is fit with an aluminum insert that completely fills it, and those to one side of the filled side branches are fit with half filling inserts. The period of the resultant waveguide is tripled ($h = .1\text{m} \rightarrow h = .3\text{m}$), and the scatterers become composed of an uneven pair of side branches of depths 38.1 mm (1-1/2 in.) and 19.1 mm (3/4 in.) set 0.1 m apart. For the cited dimensions, we expect the π, 2π, and 3π Bragg stopbands to occur at roughly 570, 1140, and 1700 Hz, respectively.

E.1.1 Periodic Waveguide Construction

The periodic waveguide is essentially a rectangular duct with one wall removed and replaced by a piece of near-square stock with slots cut periodically across the width. The duct is a section of 38.10 mm x 69.85 mm (1-1/2 in. x 2-3/4 in., i.d.) rectangular extruded aluminum tubing with one of the walls milled off, forming a rectangular channel. Slots 38.10 mm (1-1/2 in.) deep and 9.52 mm (3/8 in.) wide were milled across the narrow width of 38.10 mm x 50.80 mm (1-1/2 in. x 2 in.) aluminum stock at 0.1 m intervals. The rectangular channel is fit over the slotted stock in such a manner that there remains an open 25.40 mm x 38.10 mm (1 in. x 1-1/2 in.) rectangular tube over the slotted stock. To ensure a good seal between the duct and the slotted sections, a piece of 31.75 mm (1-1/4 in.) square aluminum tubing is placed on either side of the duct (below the area that forms the waveguide) and through-bolted to act as a clamp and force the duct walls into the sides of the slotted stock. In order to further seal the joint between the duct and the slotted stock, vacuum grease was applied to the sides of the slotted stock prior to assembly. A rectangular U-shaped piece of aluminum is fit over the driven end of the waveguide and screwed into the slotted stock to act as a mounting flange for the driver. The assembled waveguide is shown in Fig. E.1.
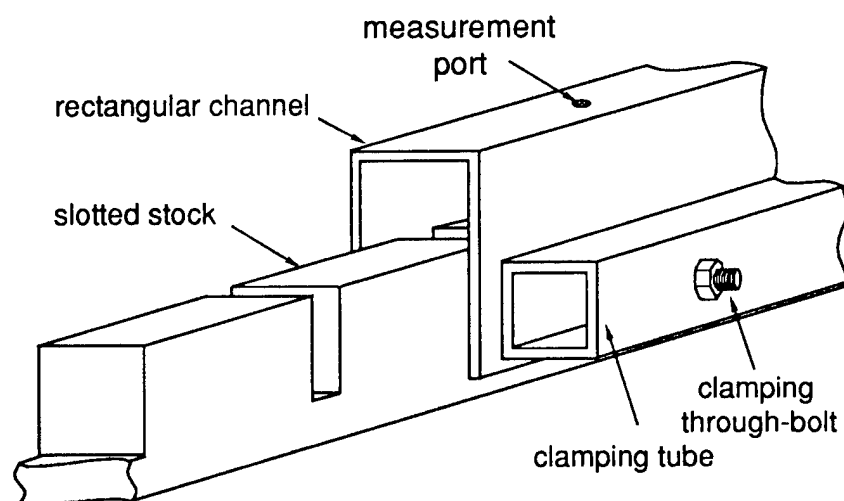
Figure E.1: The assembly of the periodic waveguide.

The measurement ports are 9.53 mm (3/8 in.) diameter holes drilled

along the center of the side of the duct opposite the slotted stock (the top). The holes are located midway between side branches, at the center of each cell. When not in use, the ports are fit with cylindrical delrin plugs which form a flush surface on the waveguide interior. When in use, the port can accomodate either a 1/4 in. microphone or a probe tube clamping jig. The microphones are fit with a sleeve that holds the active face (the condenser membrane) flush with the waveguide interior (see Fig. E.2(a)). The probe tube clamping jig is an aluminum block with a cylindrical protrusion that, like the port plugs, forms a flush waveguide interior surface. The block is drilled to accomodate a probe tube set at an angle to the waveguide wall normal (see Fig. E.2(b)).

(a)   (b)
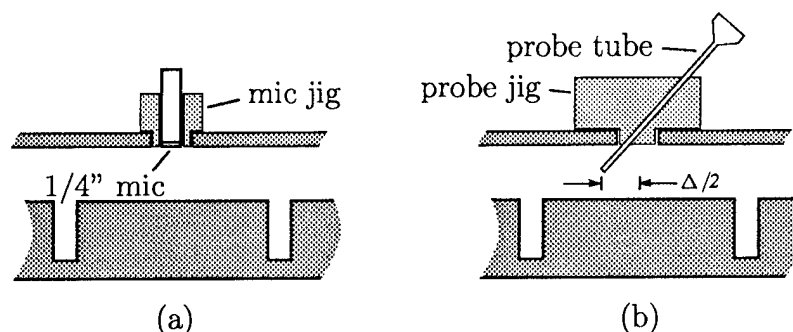
Figure E.2: The two field measurement configurations. In (a) the microphone is mounted flush with the interior surface of the waveguide, and in (b) a probe tube is used to probe the field in the volume of the field.

AS-94-788

E.1.2 The Experimental Setup and the Acquisition of Data

The experimental setup is diagrammed in Fig. E.3. At the heart of the setup is the Mac II microcomputer, which runs National Instruments' Lab-VIEW, a data acquisition/analysis/display software package. The computer and instrumentation are linked via a National Instruments NB-DMA-8-G interface board and GPIB bus. The signal source is in some cases a Hewlett-Packard 3325A frequency synthesizer and in others a Wavetek 275 arbitrary function generator. These sources, under computer control, send a signal to a Hafler P500 audio range power amplifier, which in turn drives a JBL 2485J

compression driver. The resultant acoustic signal is picked up by a Brüel and Kjær 4136 1/4 in. condenser microphone (with its associated preamplifier and bias power supply, the Brüel and Kjær 2619 and 2804, respectively) and routed to either a Sony-Tektronix RTD 710A digitizer or a Hewlett-Packard 35660A dynamic signal analyzer. In some instances, two microphones and two channel digitization is used, and in some instances the 1/4 in. microphone is replaced by a Brüel and Kjær 4133 1/2 in. microphone in a Brüel and Kjær UA 0040 1.9 mm (.075 in., o.d.) probe tube.
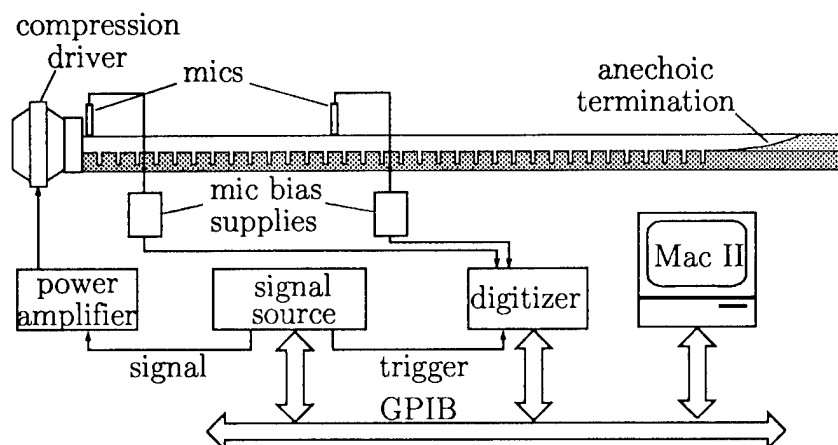
Figure E.3: The experimental setup.

AS-94-789

E.2 The Dispersion and g/f Measurements

The two parameters that characterize a linear, time-harmonic Bloch wave function are the Bloch wave number q and the relative component wave amplitude g/f. The technique used to extract values of these parameters from a set of measurements is the standard method in which the data set is fit to a theoretical model in the least-squares sense (numerical recipes). The acoustic pressure is measured at several locations in the waveguide and the Bloch wave parameters are extracted from the data set using two different least-squares approaches. One approach is used for the isotropic periodic waveguide and the other for the anisotropic waveguide. For the isotropic periodic waveguide case, it turns out that we are able justify the use of a simple progressive Bloch wave

model in the least-square fit procedure. In the case of the anisotropic periodic waveguide, however, we must use the full compound Bloch wave model. The key difference in the waveguides that necessitates the different approaches is their lengths. While both waveguides have the same *physical* length, their lengths in terms of *number of cells* differ by a factor of three. We can justify using a progressive wave model for the relatively long (48 cycle) isotropic waveguide, but not for the relatively short (16 cycle) anisotropic waveguide.

For the dispersion measurement in the isotropic waveguide, microphones are placed in the reference port (the port in the cell nearest the driver) and in one of the downstream ports. The computer is then prompted to begin a data acquisition algorithm that measures the amplitude and phase of the wavefield at the downstream port relative to those at the reference port for a specified set of frequencies. This process is repeated for 22 downstream ports at intervals of $2h$ (i.e., measurements were made in every other cell). For the g/f measurement in the isotropic waveguide, one microphone is placed in the reference port and a probe tube microphone is placed in a clamping jig in one of the downstream ports such that the field point being sampled is *upstream* of the cell center by 15 mm. After the data acquisition algorithm is run with the microphones in that configuration, the probe tube jig is rotated 180° so that the field point being sampled is 15 mm *downstream* of the cell center. The algorithm is then rerun with the microphones in the new configuration. This process is repeated for eight downstream ports at intervals of $2h$. For the anisotropic waveguide, the measurement procedure is identical to that for the g/f measurement in the isotropic waveguide, though data are collected at intervals of h at 10 downstream ports.

The function of the data acquisition algorithm is to measure and store values of the relative amplitude and phase of the signals at the two channels of the digitizer for a specified set of frequencies. The algorithm works as follows. For any particular frequency, the digitizer sampling rate is set such that there are roughly 300 samples/cycle. Upon completion of the acquisition and transfer of the data, the two data vectors (one associated with each channel) are resampled using a linearly interpolating resample algorithm. The resampling is such that exactly one cycle of the waveform occupies a 256-bin time series vector. When each time series is Fourier transformed, then, the complex number

in the fundamental frequency bin is the complex amplitude of the signal. The complex ratio of the downstream amplitude to the reference amplitude (i.e., the relative amplitude) is then calculated and stored.

E.2.1 The Isotropic Periodic Waveguide

Although the Bloch wave field is compound, we may justify the use of a progressive wave model in the least squares procedure because the influence of the backward traveling wave is small. The presence of the backward traveling wave causes spatial oscillations in the measured values of q and g/f that are averaged out in the least squares procedure. Consider first the measurement of the Bloch wave number q. The acoustic pressure at the center of the nth cell in a compound Bloch wave field is

$$p(nh) = Ae^{jnqh} + R_B Ae^{j(2N-n)qh},$$

where N is the number of cycles in the periodic waveguide, and R_B is the Bloch wave reflection coefficient at the termination (at $z = Nh$). Whereas the phase of a progressive field increases linearly with distance in the direction of propagation, the backward traveling wave causes the phase to oscillate periodically about a linear increase. Likewise, the exponential decay associated with the amplitude of a progressive wave takes on periodic oscillations about the exponential decay in the presence of a counter propagating wave. The *net* amplitude decay, however, is still exponential and the *net* phase advance is still linear. Therefore, over a large enough number of cycles of the periodic perturbation the amplitude and phase will average out to essentially exponential decay and linear increase, respectively. A linear regression of the sampled Bloch wave phase against distance effectively filters out the oscillations and retains only the linearly increasing component. The result of the regression is therefore a good measure of $\text{Re}\{q\}$. Likewise, a linear regression of the logarithm of the sampled Bloch wave amplitude against distance should be a good measure of $\text{Im}\{q\}$. These linear regressions are simply least-squares fits of the measurements to a progressive wave model.

In order for our "oscillation averaging" scheme to be valid we have two requirements: (1), the magnitude of the oscillations must be relatively small,

and (2), we must have a relatively large number of these small oscillations over which to average. For the isotropic periodic waveguide, $R_B = -g/f$ (ref), and the field may be expressed

$$p(nh) = Ae^{jnqh}\left[1 - |g/f|e^{-2(N-n)q_i h}e^{j[2(N-n)q_r h + \phi]}\right], \qquad (E.1)$$

where $q = q_r + jq_i$ and $g/f = |g/f|e^{j\phi}$. The second term in the square brackets in Eq. E.1 represents the influence of the backward traveling Bloch wave on the otherwise progressive Bloch wave field. The magnitude of the second term is $|g/f|e^{-2(N-n)q_i h}$, which we want to be somewhat smaller than one. Because we always have $e^{-2(N-n)q_i h} < 1$, and $|g/f|$ is small compared to one away from stopbands, our first requirement is met as long as we are not near a stopband frequency. In and near the stopbands, $|g/f| \simeq 1$, but q_i is relatively large. If $2(N-n)q_i h > \sim 2$, then again our first requirement is met. This will hold as long as our measurement interval ends some substantial number of waveguide cycles (say, ~ 10) from the termination. This is also a requirement we can meet as our waveguide is 48 cycles in length. We can end the measurement interval sufficiently far from the termination that the influence of the backward traveling Bloch wave is always small, yet still have a measurement interval that is large enough that we can average over a relatively large number of oscillations.

A similar argument is used to justify the use of a progressive field model in the measurement of g/f. Where in a progressive Bloch wave field the relative amplitude of the component waves is g/f in all cells of the waveguide, there is a periodic deviation from g/f in the compound Bloch wave case. Again, the oscillations can be averaged out provided they are of relatively small amplitude and we have a sufficiently large number of oscillations over which to average.

In order to obtain sufficient information to determine the complex amplitudes of the components of a compound conventional wave field, the field must be measured at more than one point in each cell. If the acoustic pressure field in the nth cell of the periodic waveguide is $p(z) = C_n^{(+)}e^{jkz_n} + C_n^{(-)}e^{-jkz_n}$, then acoustic pressure measurements at $z = nh - \triangle/2$ and $z = nh + \triangle/2$, where$\triangle < h - l$, are given by

$$\begin{bmatrix} p(nh - \triangle/2) \\ p(nh + \triangle/2) \end{bmatrix} = \begin{bmatrix} e^{-jk\triangle/2} & e^{jk\triangle/2} \\ e^{jk\triangle/2} & e^{-jk\triangle/2} \end{bmatrix} \begin{bmatrix} C_n^{(+)} \\ C_n^{(-)} \end{bmatrix}, \qquad (E.2)$$

where $z_n = z - nh$. Inversion of Eq. E.2 yields

$$\begin{bmatrix} C_n^{(+)} \\ C_n^{(-)} \end{bmatrix} = \frac{-1}{2j\sin(k\triangle)} \begin{bmatrix} e^{-jk\triangle/2} & -e^{jk\triangle/2} \\ -e^{jk\triangle/2} & e^{-jk\triangle/2} \end{bmatrix} \begin{bmatrix} p(nh - \triangle/2) \\ p(nh + \triangle/2) \end{bmatrix},$$ (E.3)

or

$$C_n^{(-)}/C_n^{(+)} = \frac{p(nh + \triangle/2)/p(nh - \triangle/2) - e^{jk\triangle}}{1 - p(nh + \triangle/2)/p(nh - \triangle/2)e^{jk\triangle}}.$$ (E.4)

If the Bloch wave field being measured were progressive, then each value of $C_n^{(-)}/C_n^{(+)}$ calculated from a pair of pressure measurements in the nth cell would be a good measure of g/f. The field, however, is compound, and the theoretical value of the amplitude ratio in the nth cell is

$$C_n^{(-)}/C_n^{(+)} = \frac{g/f + R_B e^{2jq(N-n)h}}{1 + R_B g/f e^{2jq(N-n)h}} = \frac{g/f[1 - e^{2jq(N-n)h}]}{1 - (g/f)^2 e^{2jq(N-n)h}}.$$

By the same argument used earlier, if our measurement interval does not include the region of the waveguide near the termination, then $|(g/f)^2 e^{2jq(N-n)h}| \ll 1$ at all frequencies, and the standing wave ratio becomes

$$C_n^{(-)}/C_n^{(+)} \simeq g/f \left[1 - e^{2jq(N-n)h} + (g/f)^2 e^{2jq(N-n)h} - (g/f)^2 e^{4j(N-n)h}\right].$$

Upon averaging over the first several cells, the contributions of the oscillatory terms (which are small compared to one) approach zero, and

$$C^{(-)}/C^{(+)} = (1/n)\sum_n C_n^{(-)}/C_n^{(+)}$$

is a good measure of g/f.

E.2.2   The Anisotropic Periodic Waveguide

While the justifications for the use of a progressive Bloch wave model are valid for the isotropic periodic waveguide, the same cannot be said of the anisotropic waveguide. The reasons are manifold. As was shown in the last section, the use of a progressive wave model is valid provided (1), the amplitude of the backward traveling Bloch wave is small, and (2), the measurement interval is large. Where in the isotropic case we have $|R_B| < 1$ at all frequencies, in the anisotropic case $|R_B|$ may be arbitrarily large. Because the waveguide is only

16 cycles in length, we cannot have both a large unmeasured interval (to allow the reflected Bloch wave to decay) and a large measured interval (to average out the oscillations). We therefore use the full least-squares procedure with a compound Bloch wave model.

The least-squares procedure is outlined as follows. We begin with a set of n_m measurements of the complex acoustic pressure amplitude. The measured pressure amplitude at the ith measurement location is $\bar{p}_i$, and the corresponding theoretical value based on the model is p_i. The measure of error in the theoretical description of the field is taken to be

$$\chi^2 = \sum_{i=1}^{n_m} |p_i - \bar{p}_i|^2.$$

The theoretical value of the pressure amplitude p_i, and therefore χ^2 as well, is dependent upon the values of the various parameters (such as $\text{Re}\{q^{(-)}\}$ or $\text{Im}\{g/f^{(+)}\}$) that appear in the model. The set of parameter values for which χ^2 is a minimum are those for which the model fits the data in the least-square sense. These values of the parameters are considered to be the best estimates of their values.

The minimization of χ^2 with respect to the values of the parameters is the problem to be solved. If n_p is the number of real parameters that appear in the model, then we say that ζ_i is the ith such parameter, and the vector $\vec{\zeta}$ is the collection of all n_p parameters. We can express the dependence of χ^2 on the parameters in the functional sense $\chi^2 = \chi^2(\vec{\zeta})$ and think of χ^2 as being a scalar function in an n_p dimensional parameter space. The set of parameter values $\vec{\zeta}_{\text{min}}$ for which $\chi^2(\vec{\zeta})$ is a minimum is that for which the best fit to the data has been achieved. In other words, we seek $\vec{\zeta}_{\text{min}}$ such that

$$\left.\frac{\partial \chi^2}{\partial \zeta_i}\right|_{\vec{\zeta}=\vec{\zeta}_{\text{min}}} = 0 \quad \text{and} \quad \left.\frac{\partial^2 \chi^2}{\partial \zeta_i^2}\right|_{\vec{\zeta}=\vec{\zeta}_{\text{min}}} > 0$$

for all $i = 1 \cdots n_p$.

The procedure used to find the value of the parameter vector $\vec{\zeta}$ for which χ^2 is a minimum is not the most elegant (num. rec.), but is quite straightforward and certainly effective. The algorithm begins with a seeded set of parameter values and, holding all but a single parameter constant, finds the

value of the variable parameter for which χ^2 is minimum. The value of the parameter corresponding to the minimum is taken as the updated value of the parameter and the procedure is repeated for each parameter in the set. When χ^2 has been minimized with respect to each parameter, then every component of the parameter vector $\vec{\zeta}$ has been updated. The entire cycle is repeated until it is verified that, to within a reasonable tolerance, an absolute minimum has been found.

While the least squares fit approach appears to be an ideal means for the simultaneous extraction of numerous parameter values from an arbitrary set of measurements, the procedure is likely to become unstable if it is implemented blindly. There are three fundamental stability problems. The first of these problems stems from a lack of information in the data with respect to one or more of the parameters. Consider the case wherein we allow all ten parameters (the real and imaginary parts of $q^{(+)}$, $q^{(-)}$, $g/f^{(+)}$, $g/f^{(-)}$, and R_B) to vary. In the stopbands the forward traveling Bloch wave is rapidly attenuated and essentially no backward traveling Bloch wave is excited at the termination. The field, therefore, contains very little information with respect to $q^{(-)}$ and $g/f^{(-)}$. Field measurements, owing to their inherently limited dynamic range, may contain no information whatsoever with respect to these parameters and, as might be expected, the minimization algorithm becomes unstable. This stablility problem may be solved by performing two experiments instead of one. In the first of the two, the experiment is simply performed as described earlier. We have strong excitation of the forward traveling Bloch wave and the presence of information in the data regarding $q^{(+)}$ and $g/f^{(+)}$ is ensured. The periodic waveguide is then reversed and the experiment repeated. This ensures the strong excitation of the backward traveling Bloch wave and therefore the strong representation of information with respect to $q^{(-)}$ and $g/f^{(-)}$ in the data.

The second stability problem occurs if the model has only a very weak dependence on the value of a varying parameter, such as $g/f^{(-)}$ in the preceding example. As a result of the rapidly decaying field, large changes in the value of $g/f^{(-)}$ have very little effect on the resultant value of χ^2. The algorithm may find extremely unrealistic values of the parameter to optimize the fit to the measurement taken nearest the termination. This problem is easily side

stepped by fixing the problematic parameters at their theoretical values. Such an approach is viable because, as a result of the first stability problem, we must perform separate experiments to gather forward and backward traveling Bloch wave data.

The third stability problem is simply the inherent instability of a computationally practical minimum search algorithm when the measurement set is finite and the dimensionality of the parameter space is large. To contend with this problem, the data from both experiments described above is analyzed in two stages. In the first stage of the forward traveling Bloch wave experiment, only $q^{(+)}$ and R_B (i.e., four real parameters) are allowed to vary; and the other six are fixed at their theoretical values. In the second stage $q^{(+)}$ is held fixed at its measured value, $q^{(-)}$ and $g/f^{(-)}$ are held at their theoretical values, and $g/f^{(+)}$ and R_B are allowed to vary. The same approach is used in the backward traveling Bloch wave experiment to detemine $q^{(-)}$ and $g/f^{(-)}$.

E.3 The Bloch Wave Pulse Measurements

The Bloch wave pulse measurements are made in the isotropic periodic waveguide system with a section of uniform waveguide inserted between the driver the and periodic waveguide. The narrowband pulse is therefore introduced into the uniform waveguide, where it propagates as a conventional wave pulse. This pulse is then incident upon the periodic waveguide, in which a Bloch wave pulse is excited. The reason for the section of uniform waveguide is to delay the incidence of the train of reflected pulses. The pulse that is incident upon the periodic waveguide is partially reflected back to the driver, where it is again reflected back towards the periodic waveguide. When the driver is loaded directly onto the periodic waveguide, these reflected pulses arrive immediately, and the resultant Bloch wave pulse is smeared. An alternative perspective is that the throat of the driver behaves roughly like a length of uniform waveguide and therefore acts as a resonant tank, the frequency response of which colors the spectrum of the transmitted Bloch wave pulse. With the uniform waveguide inserted, the transmitted Bloch wave pulse is colored only by the Bloch wave transmission coefficient which, for narrowband pulses, causes much less severe coloration than the resonant tank.

The acoustic pressure associated with the Bloch wave pulses are measured using the microphone in the flush mounted configuration (see Fig. E.2). The signal from the microphone is digitized and the data vector transferred to the computer. In order to measure the time of arrival of the pulse peak, which is the basis of the group velocity measurement, the envelope of the pulse must be detected (i.e., the pulse must be AM demodulated). In order to measure the frequency shift and frequency ramp rate of the pulse, the local frequency associated with the pulse must be found (i.e., the pulse must be FM demodulated). The objective of the pulse data analysis is therefore the AM/FM demodulation of the pulse time series.

In order to AM/FM demodulate the pulse time series, a property of the Fourier transform is exploited. Consider the real signal $f(t)$ with Fourier transform $F(\omega)$. The signal is a narrowband pulse that is both amplitude and phase (or, equivalently, frequency) modulated and is therefore expressed

$$f(t) = A(t)\cos[\omega_0 t + \phi(t)],$$

where $A(t)$ and $\phi(t)$ are real. The goal is to find a straightforward method of extraction of the magnitude of the pulse envelope function $|A(t)|$ and the local frequency $\omega_0 + \dot{\phi}(t)$. The pulse spectrum is given by

$$F(\omega) = \frac{1}{2}\int_{-\infty}^{\infty} A(t)e^{j\phi(t)}e^{j(\omega+\omega_0)t}dt + \frac{1}{2}\int_{-\infty}^{\infty} A(t)e^{-j\phi(t)}e^{j(\omega-\omega_0)t}dt$$

$$= \frac{1}{2}\Lambda(\omega - \omega_0) + \frac{1}{2}\Lambda^*(\omega + \omega_0),$$

where

$$\Lambda(\omega) = \int_{-\infty}^{\infty} A(t)e^{-j\phi(t)}dt$$

is the modulation spectrum.

Consider now the truncated pulse spectrum

$$
\begin{aligned}
F_t(\omega) &= 2F(\omega)H(\omega) \\
&= H(\omega)\left\{\Lambda(\omega - \omega_0) + \Lambda^*(\omega + \omega_0)\right\},
\end{aligned}
\tag{E.5}
$$

where $H(\omega)$ is the Heaviside or unit step function. If the pulse is of sufficiently narrow bandwidth (i.e., neither the amplitude nor the frequency modulation

is too strong), then the half spectrum $\Lambda(\omega - \omega_0)$ is nonzero only for positive frequencies and we have

$$F_t(\omega) = \Lambda(\omega - \omega_0).$$

The signal associated with the truncated spectrum is given by

$$\begin{aligned}
f_a(t) &= \frac{1}{2\pi} \int_{-\infty}^{\infty} F_t(\omega) e^{-j\omega t} d\omega \\
&= \frac{1}{2\pi} \int_{-\infty}^{\infty} \Lambda(\omega - \omega_0) e^{-j\omega t} d\omega \\
&= A(t) e^{-j[\omega_0 t + \phi(t)]},
\end{aligned}$$

which is referred to here as the "augmented" signal. Note first that $f(t) = \mathrm{Re}\{f_a(t)\}$. In other words, in the preceding process we have simply augmented the real signal $f(t)$ with a nonzero imaginary part. The imaginary part is at each instant in time in phase quadrature with the real part. Owing to this augmentation, the amplitude and phase modulation of the signal may be found simply by calculation of the magnitude and phase of the augmented signal. The magnitude is simply

$$|f_a(t)| = |A(t)|,$$

which is the pulse envelope, and the phase is simply

$$\angle f_a(t) = -[\omega_0 t + \phi(t)]. \tag{E.6}$$

The local frequency of the pulse may be found simply by differentiation of Eq. E.6 with respect to time (see Eq. 5.42):

$$\omega_1(t) = -\frac{\partial}{\partial t}[\angle f_a(t)] = \omega_0 + \dot{\phi}(t).$$

This method of envelope and local frequency detection is extremely straightforward to implement. If we have a digitized signal, we simply perform a discrete Fourier transform on the time series vector and set the values that occupy the negative frequency bins of the resultant discrete spectrum to zero. We then inverse transform this truncated frequency spectrum vector to result in the augmented time series. The magnitude of this time series is the pulse envelope and the derivative of its phase is the local frequency.

BIBLIOGRAPHY

J. D. Achenbach and M. Kitahara, "Harmonic Waves in a Solid with a Periodic Distribution of Spherical Cavities," *J. Acoust. Soc. Am.* **81**, 595-598 (1987).

S. A. Akhmanov, G. A. Lyakhov, O. V. Rudenko, and V. I. Shmal'gauzen, "Parametric interaction of acoustic waves in periodically inhomogeneous media," *Sov. Tech. Phys. Lett.* **1**, 283-284 (1975).

M. J. Anderson and P. G. Vaidya, "Thermoviscous Effects on Finite Amplitude Sound Propagation in a Rectangular Waveguide," *J. Acoust. Soc. Am.* **90**, 1056-1067 (1991).

G. Arfken, *Mathematical Methods for Physicists* (Academic Press, Inc., New York, 1985).

D. Bai and J. B. Keller, "Sound Waves in a Periodic Medium Containing Rigid Spheres," *J. Acoust. Soc. Am.* **82**, 1436-1441 (1987).

T. G. Barnes and B. R. Kirkwood, "Passbands for Acoustic Transmission in an Idealized Drill String," *J. Acoust. Soc. Am.* **51**, 1606-1608 (1972).

D. T. Bell and R. C. M. Li, "Surface Acoustic Wave Resonators," *Proc. IEEE* **64**, 711-721 (1976).

R. T. Beyer, *Nonlinear Acoustics* (Naval Sea Systems Command, 1974).

F. Bloch, "Der Quantenmechanik Electronishen," *Z. Phyzik* **52**, 555 (1928).

N. Bloembergen and A. J. Seivers, "Nonlinear Optical Properties of Periodic Laminar Structures," *Appl. Phys. Lett.* **17**, 483-485 (1970).

C. E. Bradley, "Acoustic Bloch Wave Propagation in a Periodic Waveguide," M.S. thesis, The University of Texas at Austin, 1990. Also issued as Technical Report ARL-TR-91-19, Applied Research Laboratories, The University of Texas at Austin (July 1991).

L. M. Brekhovskikh, *Waves in Layered Media*, 2nd ed. (Academic, New York, 1980).

L. Brillouin, *Wave Propagation in Periodic Structures* (McGraw-Hill Book Co., Inc., New York, 1946).

R. E. Collin, *Field Theory of Guided Waves* (McGraw-Hill Book Co., Inc., New York, 1960).

P. G. Drazin, *Nonlinear Systems* (Cambridge University Press, Cambridge, 1992).

D. S. Drumheller, "Acoustical Properties of Drill Strings," *J. Acoust. Soc. Am.* **85**, 1048-1064 (1989).

C. Elachi, "Waves in Active and Passive Periodic Structures: A Review," *Proc. IEEE* **64**, 1666-1698 (1976).

D. C. Flanders, H. Kogelnik, R. V. Schmidt, and C. V. Shank "Grating Filter for Thin Film Optical Waveguides," *Appl. Phys. Lett.* **24**, 194-196 (1974).

J. Goodman, *An Introduction to Fourier Optics* (McGraw-Hill Book Co., Inc., San Francisco, 1968).

M. F. Hamilton and J. A. TenCate, "Sum and Difference Frequency Generation due to Noncollinear Wave Interaction in a Rectangular Duct," *J. Acoust. Soc. Am.* **81**, 1703-1712 (1987).

A. Hessel, "General Characteristics of Traveling-Wave Antennas," in *Antenna Theory*, Part 2, R. E. Collin and F. J. Zucker, Eds. (McGraw-Hill Book Co., Inc., New York, 1969).

C. O. Hines, "Electromagnetic Energy Density and Flux," *Can. J. Phys.* **30**, 123-129 (1952).

E. L. Ince, *Ordinary Differential Equations* (Dover, New York, 1956).

J. D. Jackson, *Classical Electrodynamics* (John Wiley and Sons, Inc., New York, 1975).

A. Jeffrey and T. Kawahara, *Asymptotic Methods in Nonlinear Wave Theory* (Pitman Publishing, Inc., London, 1982).

C. Kittel, *Introduction to Solid State Physics*, 6th ed. (John Wiley and Sons, Inc., New York, 1986).

H. Kogelnik and C. V. Shank, "Stimulated Emmision in a Periodic Structure," *Appl. Phys. Lett.* **18**, 152-154 (1971).

A. Korpel, "A Frequency Approach to Nonlinear Dispersive Waves," *J. Acoust. Soc. Am.* **67**, 1954-1958 (1980).

L. D. Landau and E. M. Lifshitz, *Fluid Mechanics*, 2nd ed. (Pergamon Press, New York, 1987).

E. P. Lanina, O. V. Rudenko, and V. I. Shmal'gauzen, "Acoustic interactions in media with weak periodic inhomogeneities," *Sov. Phys. Acoust.* **24**, 314-317 (1978).

J. Lighthill, *Waves in Fluids*, 2nd paperback ed. (Cambridge University Press, Cambridge, 1980).

P. M. Morse, *Vibration and Sound*, 1st paperback ed. (American Institute of Physics for the Acoustical Society of America, 1976).

P. M. Morse and K. U. Ingard, *Theoretical Acoustics*, 1st paperback ed. (Princeton University Press, 1986).

A. H. Nayfeh, "Sound Waves in a Two Dimensional Duct with Sinusoidal Walls," *J. Acoust. Soc. Am.* **56**, 768-770 (1974).

A. H. Nayfeh, "Acoustic Waves in Ducts with Sinusoidally Perturbed Walls and Mean Flow," *J. Acoust. Soc. Am.* **57**, 1036-1039 (1975).

J. Naze Tjotta and S. Tjotta, "Interaction of Sound Waves. Part I: Basic Equations and Plane Waves," *J. Acoust. Soc. Am.* **82**, 1425-1428 (1987).

A. Nusayr, "Propagation in Rectangular Ducts with Sinusoidal Undulations," *J. Acoust. Soc. Am.* **67**, 1472-1476 (1980).

A. D. Pierce, *Acoustics: an Introduction to its Physical Principles and Applications* (McGraw-Hill Book Co., Inc., New York, 1981).

S. Ramo, J. R. Whinnery, and T. Van Duzer, *Fields and Waves in Communication Electronics* (McGraw-Hill Book Co., Inc., New York, 1965).

S. A. Rybak, "Plane wave scattering by small periodic irregularities," *Sov. Phys. Acoust.* **11**, 72-74 (1965).

R. F. Salant, "Acoustic Propagation in Waveguides with Sinusoidal Walls," *J. Acoust. Soc. Am.* **53**, 504-507 (1973).

J. C. Samuels, "On Propagation of Waves in Slightly Rough Ducts," *J. Acoust. Soc. Am.* **31**, 319-325 (1958).

E. Skudrzyk, *The Foundations of Acoustics* (Springer-Verlag, Wein, 1971).

J. C. Slater, "The Design of Linear Accelerators," *Revs. Modern Phys.* **20**, 473-518 (1948).

J. C. Slater, *Microwave Electronics* (D. Van Nostrand Co., Inc., New York, 1950).

C. L. Tang and P. B. Bey, "Phase Matching in Second-Harmonic Generation Using Artificial Periodic Structures," *IEEE J. Quantum Electronics* QE-9, 9-17 (1973).

R. H. Tancrell, "Analytic Design of Surface Wave Bandpass Filters," *IEEE Trans. Sonics Ultrason.* SU-21, 12-22 (1974).

P. J. Westervelt, "Parametric Acoustic Array," *J. Acoust. Soc. Am.* **35**, 535-537 (1963).

G. B. Whitham, *Linear and Nonlinear Waves* (John Wiley and Sons, Inc., New York, 1974).

DISTRIBUTION LIST FOR
ARL-TR-94-10
UNDER CONTRACT N00014-89-J-1109

Copy No.

1   DEFENSE ADVANCED RESEARCH
     PROJECTS AGENCY
    TECHNICAL LIBRARY
    3701 NORTH FAIRFAX DR
    ARLINGTON VA 22203-1714

2-3   DR LOGAN HARGROVE
    OFFICE OF NAVAL RESEARCH
    ONR 331
    800 NORTH QUINCY STREET
    ARLINGTON VA 22217-5660

4-5   DTIC-OCC DEFENSE TECHNICAL
     INFORMATION CENTER
    8725 JOHN J KINGMAN ROAD SUITE 0944
    FORT BELVOIR VA 22060-6218

298 only*   ADMINISTRATIVE GRANTS OFFICER
    OFFICE OF NAVAL RESEARCH
    SAN DIEGO REGIONAL OFFICE
    4520 EXECUTIVE DRIVE SUITE 300
    SAN DIEGO CA 92121-3019
    Mail 1 copy of Form 298 only

6   DIRECTOR NAVAL RESEARCH LABORATORY
    ATTN CODE 2667
    4555 OVERLOOK AVENUE SW
    WASHINGTON DC 20375-5326

7   J D ACHENBACH
    CENTER FOR ENGINEERING AND
     FAILURE PREVENTION
    NORTHWESTERN UNIVERSITY
    2137 NORTH SHERIDAN ROAD
    EVANSTON IL 60208-3020

8   R E APFEL
    DEPARTMENT OF ENGINEERING
    YALE UNIVERSITY
    MASON LABORATORY
    9 MILL HOUSE AVENUE
    NEW HAVEN CT 06520

9   A A ATCHLEY
10   S L GARRETT
11   T H HOFLER
12   R M KEOLIAN
13   A LARRAZA
    DEPARTMENT OF PHYSICS
    NAVAL POSTGRADUATE SCHOOL
    MONTEREY CA 93943-5000

14   H E BASS
15   M A BREAZEALE
16   B C DENARDO
17   R RASPET
    DEPARTMENT OF PHYSICS AND ASTRONOMY
    UNIVERSITY OF MISSISSIPPI
    UNIVERSITY MS 38677

Copy No.

18   H O BERKTAY
19   V F HUMPHREY
    SCHOOL OF PHYSICS
    UNIVERSITY OF BATH
    CLAVERTON DOWN
    BATH BA2 7AY
    UNITED KINGDOM

20   Y H BERTHELOT
21   J H GINSBERG
22   P H ROGERS
    SCHOOL OF MECHANICAL ENGINEERING
    GEORGIA INSTITUTE OF TECHNOLOGY
    ATLANTA GA 30332

23   M M BILGUTAY
    DEPARTMENT OF ELECTRICAL AND
     COMPUTER ENGINEERING
    DREXEL UNIVERSITY
    32ND AND CHESTNUT STREET
    PHILADELPHIA PA 19104

24   L BJORNO
    INDUSTRIAL ACOUSTICS LABORATORY
    THE TECHNICAL UNIVERSITY OF DENMARK
    BUILDING 352
    DK-2800 LYNGBY
    DENMARK

25   C E BRADLEY
26   R M WHITE
    BERKELEY SENSOR AND ACTUATOR CENTER
    497 CORY HALL
    DEPARTMENT OF ELECTRICAL ENGINEERING
     AND COMPUTER SCIENCE
    UNIVERSITY OF CALIFORNIA BERKELEY
    BERKELEY CA 94720

27   F D COTARAS
28   TECHNICAL LIBRARY
    DEFENCE RESEARCH ESTABLISHMENT ATLANTIC
    PO BOX 1012
    DARTMOUTH NOVA SCOTIA B2Y 3Z7
    CANADA

29   D G CRIGHTON
    DEPARTMENT OF APPLIED
     MATHEMATICS AND THEORETICAL PHYSICS
    CAMBRIDGE UNIVERSITY
    SILVER STREET
    CAMBRIDGE CB3 9EW
    UNITED KINGDOM

Copy No.

30 M R BAILEY
31 R O CLEVELAND
32 L A CRUM
33 K L WILLIAMS
APPLIED PHYSICS LABORATORY
UNIVERSITY OF WASHINGTON
1013 NE 40TH STREET
SEATTLE WA 98105-6698

34 D S DRUMHELLER
SANDIA NATIONAL LABORATORIES
GEOTHERMAL RESEARCH DIVISION
ALBUQUERQUE NM 87185

35 E C EVERBACH
DEPARTMENT OF ENGINEERING
SWARTHMORE COLLEGE
SWARTHMORE PA 19801-1397

36 D L GARDNER
37 G W SWIFT
38 JAMES A TENCATE
LOS ALAMOS NATIONAL LABORATORY
MAIL STOP K764
LOS ALAMOS NM 87545

39 T KAMAKURA
THE UNIVERSITY OF ELECTROCOMMUNICATIONS
1-5-1 CHOFUGAOKA
CHOFU-SHI
TOKYO
JAPAN

40 M S KORMAN
US NAVAL ACADEMY
PHYSICS DEPARTMENT
ANNAPOLIS MD 21403

41 W LAUTERBORN
INSTITUT FUR ANGEWANDTE PHYSIK
TECHNISCHE HOCHSCHULE
DARMSTADT
SCHLOSGARTENSTR 7 D-6100
DARMSTADT
GERMANY

42 M LEVY
DEPARTMENT OF PHYSICS
UNIVERSITY OF WISCONSIN
-MILWAUKEE
MILWAUKEE WI 53201

43 B LIPKENS
MACROSONIX CORPORATION
1054 TECHNOLOGY PARK DRIVE
GLEN ALLEN VA 23060

44 J A MANN
DEPARTMENT OF ENGINEERING
SCIENCE AND MECHANICS
IOWA STATE UNIVERSITY
AMES IA 50011

Copy No.

45 P L MARSTON
DEPARTMENT OF PHYSICS
WASHINGTON STATE UNIVERSITY
PULLMAN WA 99164-2814

46 W G MAYER
PHYSICS DEPARTMENT
GEORGETOWN UNIVERSITY
WASHINGTON DC 20057

47 J D MAYNARD
THE PENNSYLVANIA STATE
UNIVERSITY
PHYSICS DEPARTMENT
UNIVERSITY PARK PA 16802

48 B E MCDONALD
NAVAL RESEARCH LABORATORY
PO BOX 8337
ORLANDO FL 32858

49 C L MORFEY
INSTITUTE OF SOUND AND VIBRATION
RESEARCH
UNIVERSITY OF SOUTHAMPTON
SOUTHAMPTON S09 5NH
UNITED KINGDOM

50 A NAKAMURA
DEPARTMENT OF TECHNOLOGY
FUKUI INSTITUTE OF TECHNOLOGY
3-6-1 GAKUEN
FUKUI 910
JAPAN

51 R E PACKARD
DEPARTMENT OF PHYSICS
UNIVERSITY OF CALIFORNIA AT
BERKELEY
BERKELEY CA 94720

52 A D PIERCE
DEPARTMENT OF AEROSPACE AND
MECHANICAL ENGINEERING
BOSTON UNIVERSITY
110 CUMMINGTON ST
BOSTON MA 02215

53 A PROSPERETTI
DEPARTMENT OF MECHANICAL
ENGINEERING
JOHNS HOPKINS UNIVERSITY
BALTIMORE MD 21218

54 C F QUATE
W W HANSEN LABORATORY OF PHYSICS
STANFORD UNIVERSITY
STANFORD CA 94305-4085

<u>Copy No.</u>

55 W H SACHSE
    THEORETICAL AND APPLIED
     MECHANICS
    CORNELL UNIVERSITY
    ITHACA NY 14853-1503

56 M A SCHOENBERG
    SCHLUMBERGER CAMBRIDGE
     RESEARCH
    SEISMIC DEPARTMENT
    HIGH CROSS
    MADINGLEY ROAD
    CAMBRIDGE CB3 OEL
    ENGLAND

57 V W SPARROW
    GRADUATE PROGRAM IN ACOUSTICS
    THE PENNSYLVANIA STATE UNIVERSITY
    UNIVERSITY PARK PA 16802

58 S TJOTTA
59 J NAZE-TJOTTA
    DEPARTMENT OF MATHEMATICS
    UNIVERSITY OF BERGEN
    N-5014 BERGEN-U
    NORWAY

60 P G VAIDYA
    DEPARTMENT OF MECHANICAL AND
     MATERIALS ENGINEERING
    WASHINGTON STATE UNIVERSITY
    THURSTON HALL
    PULLMAN WA 99154-2920

61 Y WATANABE
    FACULTY OF ENGINEERING
    DOSHISHA UNIVERSITY
    IMADEGAWA KARASUMA
    KYOTO 602
    JAPAN

62 W M WRIGHT
    DEPARTMENT OF PHYSICS
    KALAMAZOO COLLEGE
    KALAMAZOO MI 49007

63 A BEDFORD (ASE/EM:UT)

64 D T BLACKSTOCK (ARL:UT)

65 I J BUSCH-VISHNIAC (ME:UT)

66 T A GRIFFY (PHYS:UT)

67 M F HAMILTON (ME:UT)

68 E L HIXSON (ECE:UT)

69 T G MUIR (ARL:UT)

70 ARL:UT LIBRARY

<u>Copy No.</u>

71-90   RESERVE, SPACE AND GEOPHYSICS GROUP